



TECHNICAL REPORT

No. 3/83

Volume 2

The Advanced Sodium Receiver
(ASR)

- Topic Reports -

prepared by the Contracting Companies

Agip Nucleare, Milano

and

Franco Tosi Industriale, Legnano

IEA- OPERATING AGENT
DEUTSCHE FORSCHUNGS- UND VERSUCHSANSTALT
FÜR LUFT-UND RAUMFAHRT e.V.

23.2446

VOL 2

OPERATING AGENT

Deutsche Forschungs- und Versuchsanstalt für Luft- und Raumfahrt e.V. (DFVLR)
Linder Höhe, D - 5000 Köln 90; Tel.: D - 2203-6011; Tx: D - 8 874 433 (dfv d)
Apartado 649, Almeria, Spain; Tel.: E - 51-36.51.89; Tx: E - 78 893 (dfv e)

(Dr. W. von Kries)
(W. Grasse, Project Manager)

INTERNATIONAL TEST AND EVALUATION TEAM

Apartado 649, Almeria, Spain; Tel.: E - 51-36.51.89; Tx: E - 78 893 (dfv e)

(C. S. Selvage)

PLANT OPERATION AUTHORITY

Cia. Sevillana de Electricidad S. A.

Apartado 21, Tabernas, Prov. Almeria, Spain; Tel.: E - 51-36.51.89; Tx: E - 78 893 (dfv e) (F. Ruiz Munoz)

SSPS TECHNICAL REPORT No. 3/83

The Advanced Sodium Receiver

(ASR)

- Topic Reports -

Volume 2

by

the Contracting Companies

Agip Nucleare, Milano

and

Franco Tosi Industriale, Legnano

Italy

Prepared for

IEA - OPERATING AGENT DFVLR, Köln

IEA ALMERIA PROJECT
ADVANCED SODIUM RECEIVER (ASR)
TOPIC REPORTS

C O N T E N T S

VOLUME 1

- Topic Report Nr. 1 Incident Flux Distribution
Topic Report Nr. 2 Absorber Thermal Analysis
Topic Report Nr. 3 Tube Panel Stress Analysis
Topic Report Nr. 4 Dynamic Model
Topic Report Nr. 5 Final Design of ASR Temperature Control System

VOLUME 2

- Topic Report Nr. 6 Operating Conditions to be considered in the Lifetime Analysis
Topic Report Nr. 7 Tube Panel Final Stress Analysis
Topic Report Nr. 8 Final Evaluation of Receiver Thermal State
Topic Report Nr. 9 Receiver Piping System Stress Analysis
Topic Report Nr. 10 Receiver Structure Analysis
Topic Report Nr. 11 DDC Final Configuration
Topic Report Nr. 12 Receiver Headers Stress Analysis
Topic Report Nr. 13 Tube-stirrup Supporting Plate Connection Analysis
Topic Report Nr. 14 Final Workshop Acceptance Procedure

IEA ALMERIA PROJECT

ADVANCED SODIUM RECEIVER

ASR

Operating conditions to be considered in
the lifetime analysis

Topic Report No. 6

Revision 0

March 1982

Prepared by: ENEL

FRANCO TOSI

SNAMPROGETTI

Contents

1. Definition of transient behaviour events for ASR lifetime analysis

Introduction

1.1. Incident peak flux distribution during the year

- 1.1.1. Receiver operating hours during the year
- 1.1.2. Peak heat flux distribution during the year
- 1.1.3. Receiver operating hours at peak flux value between F1 and F2
- 1.1.4. Lifetime analysis flux levels

1.2. Transients definition

- 1.2.1. Normal operating conditions
 - 1.2.1.1. Morning hot start-up
 - 1.2.1.1.1. Number of events
 - 1.2.1.2. Overnight shutdown
 - 1.2.1.2.1. Number of events
 - 1.2.1.3. Cold start up
 - 1.2.1.3.1. Number of events
 - 1.2.1.4. Clouds passage
 - 1.2.1.4.1. Number and kind of transient
- 1.2.2. Upset operating conditions
 - 1.2.2.1. Loss of control in the receiver control circuit

- 1.2.2.1.1. Failure of the control system of the pump in case of 100% reinsolation
 - 1.2.2.1.1.1. Number of events
 - 1.2.2.1.2. Failure of the control system of sodium pump in case of shading of the field
 - 1.2.2.1.2.1. Number of events
- 1.2.2.2. Loss of sodium supply due to electrical failure of sodium pump drive
 - 1.2.2.2.1. Number of events
- 1.2.3. Faulted conditions
 - 1.2.3.1. Blocking of sodium pump

1. OPERATING CONDITIONS TO BE CONSIDERED IN THE
LIFETIME ANALYSIS

INTRODUCTION

This report has been prepared for the assesment of the operating conditions to be used in the lifetime analysis of the receiver.

The content is based on the Progress Report No. 10 - Nov. 1981 and the raccomandations collected during the "Ad Hoc Working Group" meeting held in Almeria in November 1981.

1.1. INCIDENT PEAK FLUX DISTRIBUTION DURING THE YEAR

1.1.1. Receiver operating hours during the year

The number of hours of ASR operation during the year H_y has been assumed by considering:

- . The insolation model proposed by Interatom in the C.R.S Document No. 1510 which considers for the site of Tabernas in a typical year:
 - 38 COVER DAYS (no energy is collected by receiver due to persistent cloudness)
 - 145 CLOUDY DAYS

The resulting number of sunny hours with this model is approximately 3000.

- Annual availability of beam radiation greater than 300 W/M^2 reported in "Tabernas meteo data analysis based on evaluated data prepared by the SSPS - O.A. (by Belgonucleaire, June 1981)".

The estimated total value of hours of beam radiation greater than 300 W/M^2 during 1978-80 is 3116.

In accordance with these values and taking into account the purposes of the following analysis, the number of

$$H_y = 3000 \text{ hours per year}$$

of ASR operating time has been assumed as a reasonable basis for ASR lifetime evaluation.

1.1.2. Peak heat flux distribution during the year

The incident peak flux on the receiver absorber changes during the day and raises its maximum at noon. This noon peak value changes during the year too, ranging from 100 W/CM^2 (W.S) to 138 W/CM^2 (EQ).

Fig. 1.1.2/1 shows the behaviour of the incident peak flux on the ASR for the days:

- 21 March (21 September)
- 21 June
- 21 December

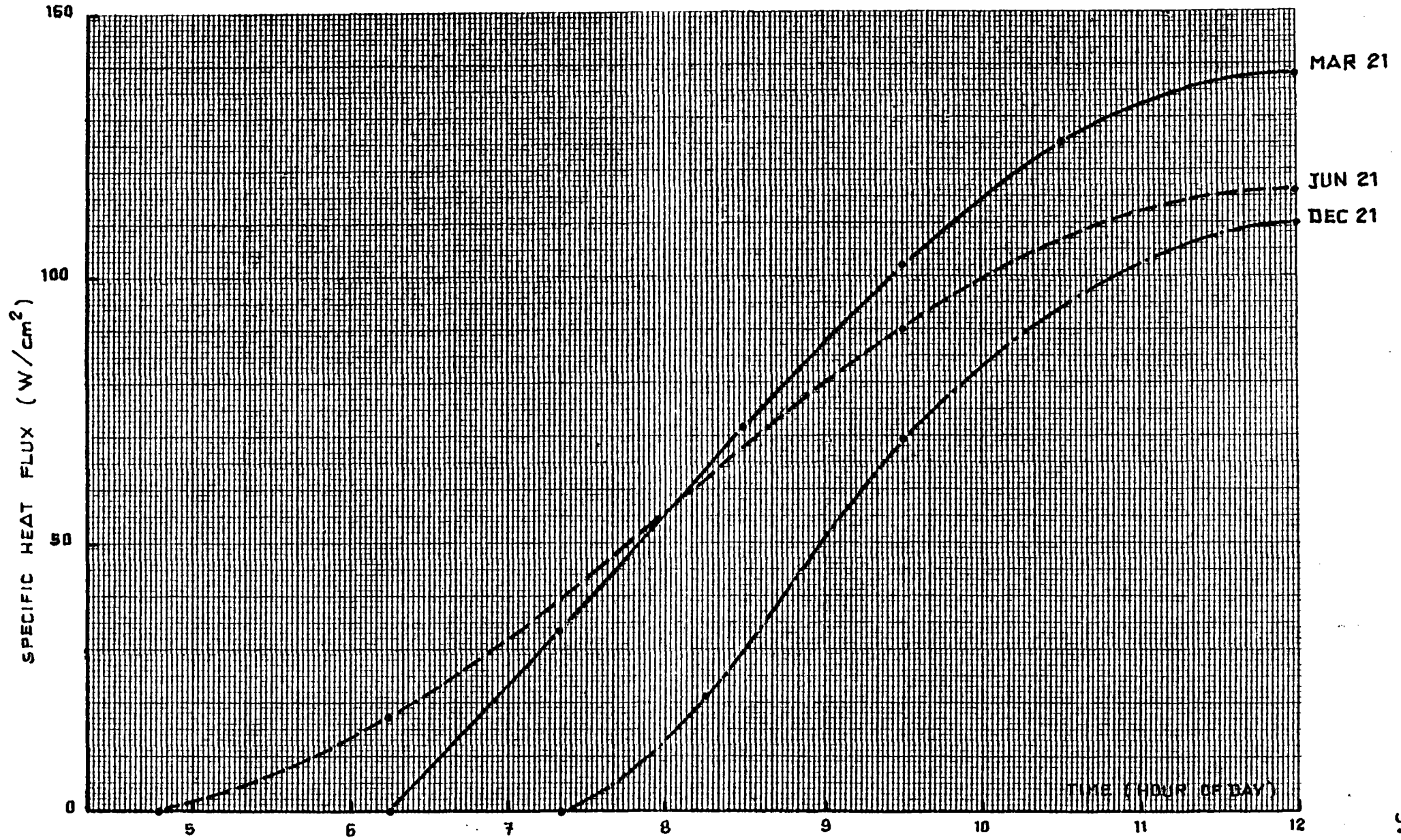


FIG. 1.1.2/1 - INCIDENT PEAK HEAT FLUX BEHAVIOUR ON THE ASR TUBES FOR THREE TYPICAL DAYS

1.1.3. Receiver operating hours at peak flux value between F1 and F2

By analysing curves as those shown in fig. 1.1.2/1, it is possible to estimate the hours per year of permanence of peak flux on the receiver between two values F1 and F2. This evaluation has been performed in steps of 10 W/CM² from 0 to 140 W/CM² (13 steps).

The operating hours per year at peak flux value between F1 and F2, $hy(F1, F2)$, is obtained according to:

$$hy(F1, F2) = \sum_{m=1}^{12} \left(\text{daily time at peak flux between F1 and F2} \right)_m \times x \times (N_m - N_{cm}) \times r$$

N_m Number of days in the month m

N_{cm} Number of cover days in the month m

r 0.75 . This factor takes into account the reduction of hy due to cloudness of the "cloudy days" (partially cover). (*)

Table 1.1.3/1 shows the results of the analysis.

(*) The total hours of operation, if we account only for the cover days (38 in one year), would be about 4000. The estimated value of effective operating hours accounting for both cover day and cloudy days are about 3000 (see § 1.1.1.). The r - value is obtained as $3000/4000 = 0.75$.

F1 - F2	hy (f)	P (f)
(w/cm ²)	hours per year	(%)
130 - 140	188	6.2
120 - 130	281	9.3
110 - 120	352	11.7
100 - 110	320	10.6
90 - 100	228	7.6
80 - 90	228	7.6
70 - 80	206	6.8
60 - 70	206	6.8
50 - 60	182	6.1
40 - 50	182	6.1
30 - 40	195	6.5
20 - 30	217	7.2
10 - 20	225	7.5

Table 1.1.3/1 - Operating hours per year at peak flux value between F1 and F2

Fig. 1.1.3/1 shows the probability density function of the specific incident heat flux on the receiver adsorber.

1.1.4. Lifetime analysis flux levels

To simplify lifetime analysis calculations the receiver operating hours per year are splitted in 6 discrete levels of incident peak flux according to the probability function of fig. 1.1.3/1.

Table 1.1.4/1 gives the yearly number of operating hours corresponding to the incident peak flux levels.

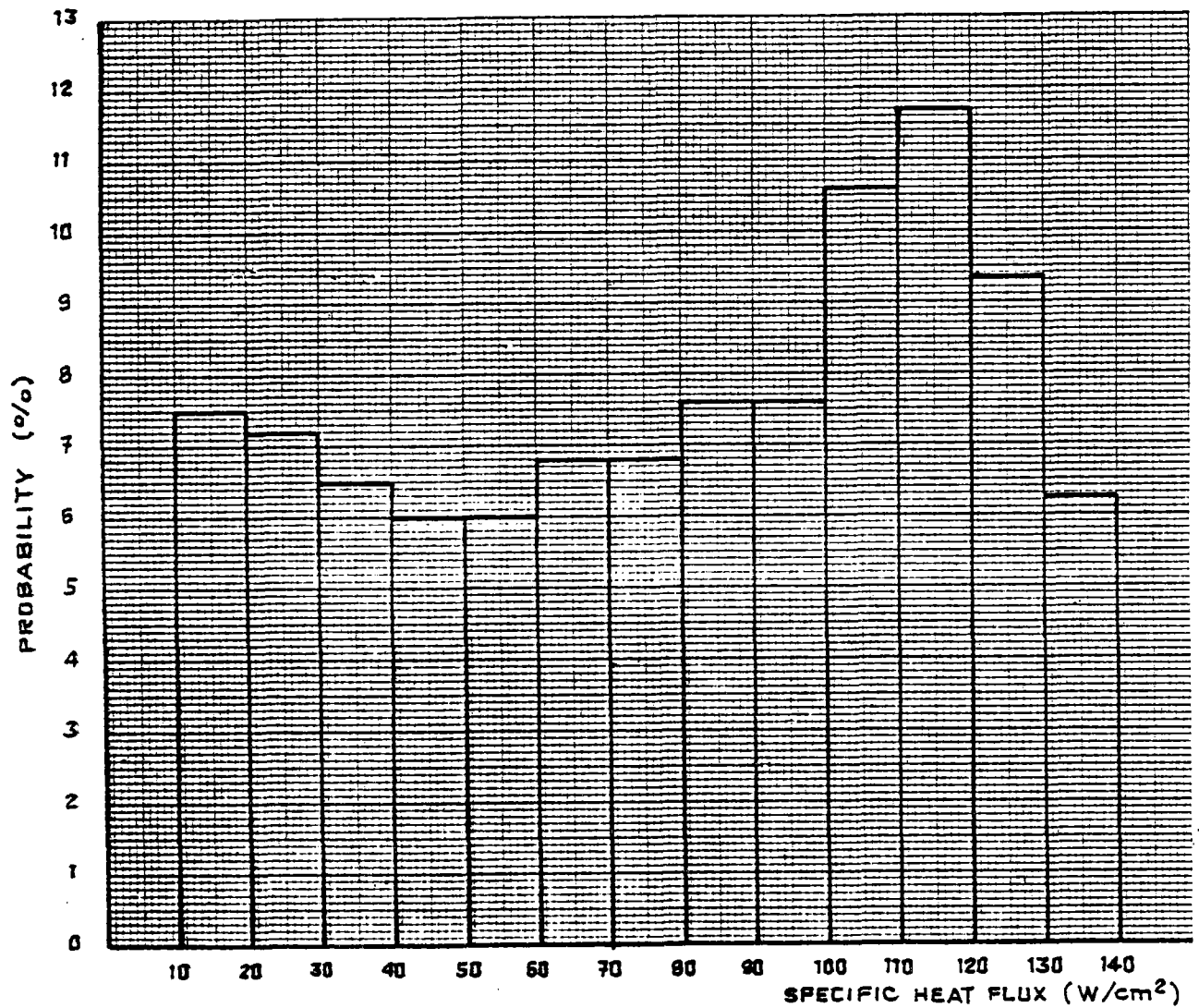


FIG. 1.1.3/1 _ PROBABILITY DENSITY FUNCTION OF THE SPECIFIC PEAK INCIDENT HEAT FLUX ON THE RECEIVER TUBES IN A TYPICAL YEAR

	Flux level (*) (W/CM ²)	Operating hours per year	Probability (%)
I	130 (120 + 140)	469	15.5
II	110 (100 + 120)	672	22.3
III	90 (80 + 100)	456	15.2
IV	70 (60 + 80)	412	13.6
V	50 (40 + 60)	364	12.2
VI	25 (10 + 40)	637	21.2
		$\Sigma = 3010$	$\Sigma = 100$

(*) Mean value of the incident peak flux variation in the level

Table 1.1.4/1 - Incident peak flux levels for lifetime analysis

1.2. TRANSIENTS DEFINITION

Hereafter all the events considered in the ASR lifetime analysis are listed subdivided in three categories corresponding to normal upset and faulted operating conditions:

- Normal operating conditions
 - . Morning hot start-up
 - . Overnight shutdown
 - . Cold start-up
 - . Clouds passage

- Upset operating conditions
 - . Loss of control in the receiver control system
 - a) failure of the control system of the pump in case of 100% reinsolation (flowrate at 10%)
 - b) failure of the control system of the pump in case of shading of the field (flowrate at 100%).
 - . Loss of sodium supply due to electrical failure of sodium pump drive.

- Faulted conditions
 - . Blocking of sodium pump

1.2.1. Normal operating conditions

1.2.1.1. Morning hot start-up

During nighttime the ASR doors are closed and hot sodium is provided to maintain the temperature of the receiver at about 270 °C to prevent freezing in the receiver.

Circulation is from cold storage to receiver than back to cold storage.

At beginning of a hot start-up the ASR will be at uniform temperature of approximately 270 °C.

The receiver will be started as soon as the expected receiver thermal losses at the rated working temperature will be less than the calculated absorbed power of ASR.

At this time of the day and for the meteorological conditions of the moment ASR will require a sodium flow rate Q_s to reach the rated outlet conditions.

After opening the receiver doors the flowrate will be increased from the nighttime value to the calculated Q_s value.

After performing this operations, heliostats will be focused in groups on the receiver unit.

During this phase sodium will be circulated in the hot bypass line from cold storage to receiver and back to cold storage. As soon as the rated receiver outlet temperature is raised, the receiver starts to produce hot sodium to be discharged in the hot storage. Automatic control is commanded to adjust flow rate to the power as soon as possible.

1.2.1.1.1. Number of events

277 per year.

The value has been obtained starting from the 327 operating days (365 - Number of cover days) according to Interatom Document N. 1510, by subtracting 15 days in which a cold start-up has been considered.

1.2.1.2. Overnight shutdown

As the insolation level decreases, the point is approached where reduced flux on the receiver no longer permits rated output conditions.

The flow rate will be adjusted by the automatic control as long as possible. When the flowrate decreases to the minimum, the control will pass to the operator. The flow path of the sodium will be changed from the hot storage line to the hot bypass line. Heliostats will be

brought in stowed position group by group and receiver doors closed.

1.2.1.2.1. Number of events

327 per year (see also point 1.2.1.1.1.).

1.2.1.3. Cold start up

This operation is performed for the first start-up of the receiver and after a draining.

The receiver is at ambient temperature and filled with argon. Non radiated pipes will be heated up by electrical trace heating whereas receiver tube bundles are heated by a limited number of heliostats from ambient temperature up to about 270 °C.

Once the loop is filled with sodium and the circulation through the hot bypass is actuated, the operation is the same as a hot start up.

1.2.1.3.1. Number of events

50 per year.

1.2.1.4. Clouds passage

During a cloud passage the receiver will remain in normal operation and the automatic control system will adjust the flowrate to the flux level according to the shading-reinsolation sequence.

However if the direct solar flux goes below the flux level required to attain the rated sodium outlet temperature, the receiver tube bundles temperatures will begin to decrease.

By maintaining the flowrate at a minimum value of 10% the receiver tube bundles will lose their temperature profiled in about 5' after which a uniform temperature level of approximately 270 °C is reached. For shading time less than 5' the receiver will be ready to restart and the heliostats will be kept in tracking position.

After this time, operator will begin the defocalization of the heliostats, which will turn in groups to stand-by or stowed position according to the prevision made by operator about the duration of the cloud passage. With heliostats in stowed position, ASR doors will be closed.

Start-up after a passing cloud cover period longer than 5' will follow the hot start-up procedure.

1.2.1.4.1. Number and kind of transient

Cloud passage numbers per year are reported in table 1.2.1.4.1/1. They are splitted in kinds of transients taking into account the following points:

1) Cloud velocity

Cloud velocities of 10, 23 and 50 Km/h are considered; the corresponding measured shading time of the whole field is reported in the following table:

Cloud velocity (km/h)	Time shading (sec)
10	54
23	24
50	11

(Source: actual measurements over the receiver area transmitted in the letter od 21/08/81 by Kastl-IA)

TYPE	CLOUD VELOCITY (Km/h)		
	10	23	50
	t_s (sec)		
	54	24	11

a	1		1000	1000	1000
	2		1000	1000	1000
	3		150	150	25
			2150	2150	2025

TABLE 1.2.1.4.1/1 — CLOUD PASSAGE TRANSIENTS (PER YEAR)
 (P = PEAK INCIDENT FLUX
 Σ EVENTS = 6050)

2) Shading-reinsolation sequence

3 types of sequences are supposed:

- 1) shading and prompt reinsolation
- 2) shading over a period of 5 minutes and succeeding reinsolation
- 3) shading for long time (>5 minutes) and succeeding reinsolation.

The events number for transients of type a/2 and a/3 at cloud velocity of 50 km/h are quite unlikely because persistent cloudness (shading for long time) has a low frequency of occurrence in a day with high wind. (Letter of Kastl-IA of 21/08/81)

3) Level of peak incident flux before cloud passage

Each kind of cloudness is assumed to have an uniform probability of occurrence during the day and the year. So the level of incident peak flux P before cloud passage is distributed along the year according to the 6 levels of probability of specific heat flux reported in table 1.1.4/1.

1.2.2. Upset operating conditions

1.2.2.1. Loss of control in the receiver control circuit

1.2.2.1.1. Failure of the control system of the pump in case of 100% reinsolation

At the moment of reinsolation, control system fails and the through put sticks at 10%.

Corrective actions are the following:

- heliostat defocusing
- flow rate increased by safety action
- switch over to manual control.

1.2.2.1.1.1. Number of events

6 events of this type are supposed to occur in a year taking into account the incident peak flux distribution during the year (table 1.1.4/1).

The total numbers of events may be splitted in the following manner:

Peak heat flux (W/cm ²)	No. of events
130	0.5
110	0.7
90	0.5
70	0.4
50	0.4
25	0.5

1.2.2.1.2. Failure of the control system of sodium pump in case of shading of the field

At the moment of field shading for a cloud passage, control system fails and the through put sticks at 100%.

Corrective action:

- switch over to manual control

1.2.2.1.2.1. Number of events

6 events of this type are supposed to occur in a year. Total number of events may be splitted as in section 1.2.2.1.1.1.

1.2.2.2. Loss of sodium supply due to electrical failure of sodium pump drive

Sodium pump slows down with a flowrate decay presented in section 1.5.2. of the Progress Report No. 11.

Corrective action:

- heliostat field emergency shutdown.

1.2.2.2.1. Number of events

6 per year, splitted as follows:

Peak heat flux (w/cm ²)	Nr. of events
130	0.96
110	1.32
90	0.90
70	0.84
50	0.72
25	1.26

1.2.3. Faulted conditions1.2.3.1. Blocking of sodium pump

This type of incident is not expected to occur. It is postulated because its consequences would include the potential for the release of significant amounts of sodium to the ambient.

If this incident occurs, sodium pump stops running immediately. Heliostat field emergency shutdown prevents receiver tube bundles temperatures to exceed safety limits.

IEA ALMERIA PROJECT

ADVANCED SODIUM RECEIVER

ASR

Tube panel final stress analysis

Topic Report No. 7

Revision 0

July 1982

Prepared by: ENEL

FRANCO TOSI

AGIP NUCLEARE

INDEX

Abstract

1. Forward

2. Tube panel elastic stress analysis

2.1. Analysis limits

2.2. Description of structure and its boundary conditions

2.3. Thermal load basic data

2.4. Mechanical load basic data

2.5. Material basic data

2.6. Hypothesis and calculation method

2.7. Results

3. Code stress limits compliance

3.1. Analysis limits

3.2. Operating conditions

3.3. Stress table following ASME criteria

3.4. Bursting analysis

- 3.5. Shake down analysis
 - 3.6. Ratcheting analysis
 - 4. Panel tube inelastic stress analysis
 - 4.1. Considerations about the inelastic analysis
 - 4.2. Approach methodology
 - 4.3. Structure definition and boundary conditions
 - 4.4. Material properties
 - 4.5. Temperature distributions
 - 4.6. Full size tube analysis by means of "pipe type elements"
 - 4.7. Generalized plain strain tube analysis
 - 4.8. Creep evaluation
 - 5. Creep-fatigue interaction analysis
 - 5.1. Effect of the daily cycling
 - 5.2. Effect of the clouds passage
 - 5.3. Effect of the operational incidents
 - 5.4. Creep damage evaluation
 - 5.5. Lifetime evaluation
 - 6. Conclusion
- Appendix 1 : Mechanical characteristics of tube material
- Appendix 2 : Considerations and comparison between elastic and inelastic creep-fatigue analysis

ABSTRACT

The main contents of this report are:

- 1) Detailed elastic stress analysis of the most stressed tube due to thermal heat flux and mechanical loads. The analysis is based on the final panel configuration.
- 2) Compliance analysis of the tube stresses with the code limits and in accordance to the contract.
No mention to the creep fatigue analysis.
- 3) Inelastic stress analysis due to thermal heat flux and mechanical loads.
- 4) Compliance analysis with the code limits with reference to the creep-fatigue phenomena.

1. FORWARD

The object of this report is the description of the final panel stress analysis based on the final receiver configuration and dimensions.

Therefore this report updates and replaces the Topic Report no. 3 released in March 1981.

2. TUBE PANEL ELASTIC STRESS ANALYSIS

2.1. Analysis limits

The analysis regards the hottest tube, subject to thermal flux conditions and to stationary mechanical load, corresponding to max. loads.

We have assumed that attainment of these conditions is so slow as not to cause any overstresses; therefore the considered stress condition is also the most severe one.

2.2. Description of structure and its boundary conditions

The structure under consideration is the receiver tube ($D_e = 14$ mm, $t_{\text{thn}} = 1$ mm), restrained in the rectilinear portion by means of stirrup supports, clamped in the upper header connection point and built in the lower header connection point.

With reference to the clamped point, a displacement has been imposed in order to take into account the differential expansions between the panel tube and the downcomer that are respectively

$$\Delta l_{\text{panel tube}} = 40.65 \text{ mm}$$

$$\Delta l_{\text{downcomer}} = 33.94 \text{ mm}$$

In fig. 1 are shown the 3 shapes of tube, alternately assembled. By the experience of previous calculations only shape A will be later on analyzed.

2.3. Thermal load basic data

The receiver flux map used as a basis for these calculations is the equinox noon heat flux map reported in Topic Report No. 1 in fig. 2.7.

Fig. 2 shows the trend of the absorbed flux and the sodium temperature along the tube length.

These data are assumed as a basis for the thermal calculation of section 2.6.

2.4. Mechanical load basic data

The mechanical loads which act on the structure are:

- tube and sodium weight (0,424 kg/m);
- internal pressure (6,11 kg/cm²);
- wind load at full power operation (50 km/h);
- two horizontal directions hearthquake statically applied with an acceleration of 4 m/s² in both directions.

2.5. Material basic data

The receiver tube material is SANDVIK Alloy 3R60 corresponding to the ASTM 316L type.

The material features have been taken from the manufacturer's documentation.

In the Appendix 1 the material is completely specified.

2.6. Hypothesis and calculation method

On the basis of the outside flux conditions and internal sodium temperature data given in Section 2.3, we have determined, by means of a finite elements calculation program (FLHE of the BERSAFE series), the temperature field on every point of the section.

This calculation has been performed on a certain number of sections, with the purpose of determining the complete temperatures field on the tube.

In fig. 3 is shown the 2-D mesh used in these thermal calculations and in the plain strain analysis too.

In the assumption of linear elastic behaviour of the material, the stress condition has been determined by means of superimposition of 3 effects:

- 1) stresses due to internal pressure;
- 2) self equilibrating stresses in every section, due to the non-linear portion of the temperature distribution on the section;
- 3) stresses due to partial restraint of expansion and deflections on the tube, due to the linear portion of temperature;
- 4) stresses due to weight, wind and earthquake.

Stresses at point 1) can easily be determined by formulas.

Stresses at point 2) can be found by imposing the non linear temperature field previously determined on a generalized plain strain model discretized as shown in fig. 3, with SAP V structural analysis code.

Stresses at point 3) and 4) are determined by a flexibility calculation using a beam element discretization, whose loading condition consists in the previously found linear temperature distribution and in the corresponding mechanical loads.

In fig. 4, 5, 6 are shown the meshes and the deformed shapes due to the thermal loads, the weight and the sun of them respectively.

2.7. Results

In Table 1 are shown the axial and shear forces and moment in the tube restrain points. The tube rotation in the stirrup zones are reported as well.

An evaluation has been carried out about the stresses arising from the friction forces in the stirrup devices: an increase of less than 1% of the total stress in the most stressed section has to be expected. Therefore this effect will be neglected in the foregoing considerations.

In Table 2 are shown all the stress components obtained in the most stressed structure point (the outer point of max flux on the most radiated section).

Pressure stresses are of little importance; stresses due to non linear temperature distribution in the section are considerable, and cannot be reduced because they are not influenced by boundary conditions.

Stresses due to partial expansion restraint have been reduced by suitable disposition and number of boundaries, in compliance with other functional requirements.

Stresses due to the earthquake are very low and are obtained by the application of a static horizontal acceleration of 4 m/sec^2 . In Table 2 are reported the values of the maximum heat flux section.

The maximum earthquake stress is located at lower header-tube connection and a bending value of 0.48 kg/mm² is reached. It must be noted that this section has no other important loads.

3. CODE STRESS LIMITS COMPLIANCE

3.1. Analysis limits

In compliance with Contract Section A-7.1, since the tube is a sodium containing component, the design has been carried out by the following criteria:

- a) Primary membrane stress is limited to prevent bursting, according to par. UG-27, Asme Section VIII, Division 1.
- b) An extension of the shakedown limit is imposed on primary and secondary stresses, to prevent noticeable distortions, that is: $P_L + P_B + Q \leq 3 S_m$, according to par. 4-134, Appendix A, Asme Section VIII, Division 2.
- c) To satisfy the distortion limits by using an elastic analysis, and particularly to limit the inelastic strain amount that can occur during the service life of the component, Test No. 3, par. T-1324, Appendix T, Code Case N-47-17 has been applied.

3.2. Operating conditions

The trend of the principals parameters during the daily cycle (referred to 21 March and to the hottest section of the tube) is reported in fig. 7.

These data are:

- . metal wall average temperature on the hottest radial section of the tube;
- . sodium temperature;
- . absorbed heat flux.

3.3. Stress table following ASME criteria

In Table 2 are shown the stresses with their classification according ASME criteria.

With a large conservatisme, the effects of non linear temperature distribution on the cross section of the tube have been classified as secondary stresses Q.

Actually, part or all the stresses due to that non-linearity, since doesn't produce any distortion, could be classified as F, by definitions in 3213.11 and 3213.13(b)(2), Code Case N-47-17.

3.4. Bursting analysis

The joint efficiency E, requested in UG-27, Asme Section VIII, Division 1, is equal to 1.

The allowable stress value S_m is determined conservatively corresponding with the maximum metal wall-avera

ged temperature on the hottest cross section (see table 3).

3.5. Shake down analysis

The S_m value is taken as average of the two S_m values at maximum and minimum cycle temperature, as it results from Note (1), fig. 4-130.1, Appendix 4, Asme Section VIII, Division 2, because all secondary stress is a thermal stress (see Table 3).

3.6. Ratcheting analysis

We have excluded the presence of "Elastic follow-up", by which the thermal stresses due to linear temperature distribution on the tube cross section, responsible of the strain, would be classified as P_L for purpose of Test No. 3, T-1324, Code Case N-47-17. Such assumption is justified in the following points:

- a) The possible plasticity doesn't affect the total tube cross section but only a portion; therefore the plastic portion cannot reach noticeable strains, because of the internal restrains caused by the elastic core of the section.
- b) The thermal stress distribution along the tube length has a quite smooth trend without picks in the most stressed section.

The step by step procedure proposed by par. T-1321 and T-1324 in the Appendix T of Code Case N-47-17 has been followed and the results are shown in Table 4.

Non axisymmetric loads has been included as axisymmetric loads, and the curves of fig. T-1324-1 has been used, according with T-1324(a), Appendix T, Code Case N-47-17.

4. PANEL TUBE INELASTIC STRESS ANALYSIS

4.1. Considerations about the inelastic analysis

The reasons for which an inelastic analysis has been carried out in the evaluation of the panel tubes of the ASR must be found in the impossibility to reach the requested number of operating cycles by a strict application of the Code Case N-47-17 creep-fatigue in teraction based on an elastic stress analysis. A deeper knowledge on the behaviour of the tube and on the possibility to support high heat fluxes is requested as well.

The results we have obtained by the inelastic approach show the large conservatism that is contained in the Code Case elastic creep-fatigue analysis.

No problems have to be expected therefore from the point of view of the creep-fatigue interaction that is the most important failure mechanism of a central receiver with high thermal fluxes.

4.2. Approach methodology

The inelastic analysis has been carried out by means of the F.E. MARC Code. A first approach, in order to check the mesh, has been run in elastic hypothesis

giving results in a very good agreement with those obtained by SAP V. All the thermal fields used are obtained from the thermo-hydraulic analysis reported in the Topic Report No. 2. An interpolation method has been implemented in order to obtain wall temperatures at any position.

A second calculation in inelastic conditions has been carried out with "tube type elements" in order to approach the problem step by step and to obtain the behaviour of the whole tube. Due to the fact that the applied loads are essentially "strain controlled", we found out a good agreement between the strain obtained with this elasto-plastic analysis and the strain deduced with the Hook law starting from the stresses elastically evaluated.

As last approach, a generalized plain strain finite element model has been implemented after considering quite impracticable from the point of view of calculation times and costs a 3D analysis; it is to be noted that such a model gives an overestimation of the stresses and strains because the actual rotation of the tube cross section is not allowed by the used model.

4.3. Structure definition and boundary conditions

The model used in the inelastic analysis is very similar to that used for the elastic analysis.

The only difference consists in the fact that the clamped end and the built in one are exchanged each other: due to the quite complete symmetry of the system we consider the results from the inelastic analysis as representative of the actual situation.

4.4. Material properties

Tube material is s.s. AISI 316 L and, where possible, we make use of the average characteristic values from supplier (see Appendix 1, Annex 1).

The stress-strain relation at 20 °C is presented in Table 5. The temperature influence is considered and correction coefficient $R(T)$ evaluated at $\Delta \epsilon$ intervals of 0.002.

Table 6 shows $R(T)$ and $\Delta R(T)/\Delta T$ values as a function of temperature; in fig. 8 is represented the $\sigma - \epsilon$ plotting.

As regards as the instantaneous thermal expansion coefficient, two different sets of values are used:

- $\alpha_1(T)$ is obtained from mean values and applied to computations concerning the overall behaviour of the tube.
- $\alpha_2(T)$ is taken from ASME and applied in the most stressed section strain range evaluation.

At high temperature $\alpha_2(T)$ is greater than $\alpha_1(T)$ (see Table 6) and in such a way the safety limits of the approach are increased.

4.5. Temperature distributions

The following assumptions, referring to the hottest tube, are utilized as starting point:

- the non-irradiated tube wall temperature equals so dium temperature (inlet 450 °C, outlet 544 °C);
- along the irradiated length, sodium bulk temperature, together with internal and external tube wall maximum temperature values are known in 25 axial positions from the tube panel thermal analysis;
- at the maximum flux tube section a temperature map with 648 computed points is built and used to obtain elastic stress evaluation.

In order to get a good flexibility, in connection with the use of different elements and meshes, an inter

polation method is implemented to compute temperatures anywhere in the tube wall.

First the 25 axial values are interpolated using expansion formulas as:

$$T(z) = G(0) + G(1)\theta + \sum_1^{20} G(i+1) \sin \left[(i+1)\theta \right]$$

with $\theta = z \frac{\pi}{L}$, $L = 2850$ mm

Therefore the internal and external circumferential profiles are expanded into a modified Fourier series as follow:

$$T_{\text{ext}}(\theta) = A(0) + A(1)\theta + \sum_1^5 \left\{ A(i+1) \cos \left[(i+1)\theta \right] + B(i+1) \sin \left[(i+1)\theta \right] \right\}$$

$$T_{\text{int}}(\theta) = D(0) + D(1)\theta + \sum_1^5 \left\{ D(i+1) \cos \left[(i+1)\theta \right] + E(i+1) \sin \left[(i+1)\theta \right] \right\}$$

With the following hypothesis:

- temperature profile shape independent on the section;
- linear temperature behaviour across the tube wall thickness at the same angular position;

temperature can be obtained, as a function of coordinates, anywhere in the tube wall.

In order to analyze the thermal cycling, the following steps can be identified:

- a) Trace heating phase and sodium filling.

The tube temperature, from 20 °C (ambient temperature) increases up to 270 °C uniformly.

- b) Power increases from starting condition to one fifth of the design level.

Sodium temperature axial profile is augmented step by step and reaches the steady state nominal profile (inlet 450 °C, outlet 544 °C). Tube wall temperatures depend on impinging flux level.

- c) Power increases up to design power and then decreases to one fifth again.

The nominal sodium temperature axial profile is maintained, while temperature differences in the tube wall increase (or decrease) following the incident flux.

- d) Power decreases from one fifth to shut down level.

Sodium axial temperature profile (and metal temperature)

tures) from nominal profiles reaches the constant value of 270 °C.

- e) Sodium emptying and tube cooling.
Temperature from 270 °C to 20 °C.

Step d) and e) are bypassed during computations.

4.6. Full size tube analysis by means of "pipe type elements"

The approach to the whole tube has been carried out in order to:

- evaluate the overall behaviour of the structure;
- compute the support loads;
- locate the most critical section.

The geometric scheme of the structure is shown in fig. 9. The top of the tube is fixed, while the bottom end is sliding. The differential expansion between the panel tube and the downcomer has been considered as well in the same way used for the elastic calculations. The intermediate supports are sliding hinges; 47 pipe elements are used with 2 nodes each.

The element (the reference number of the element in MARC library is 14) is a hollow circular cylinder and takes into account plasticization. Axially 3 control planes are available with 16 control points around

circumference, 6 degrees of freedom each node (rotations and displacements). The wall mean temperatures (between internal and external values) are assigned to the points, so that the average behaviour for tube fibres is obtained.

Only the first temperature increase, from 20 °C to maximum, is simulated step by step, following the criteria of par. 4.4. and with temperature step less than 10 °C.

From the MARC computations the following results are obtained:

- During pre-heating phase with axially uniform temperature (from 20 °C up to 270 °C), the most stressed sections coincide with the extreme supports (maximum stress 1.5 kg/mm^2). The two sections, where at full power the peak flux (element 23, section 3) and the peak temperature (element 24, section 2) are located, in this condition show small stresses (about 0.5 kg/mm^2).
- When one fifth of incident power is reached, the maximum stress along Z are:

Top support section	2.6 kg/mm^2
Bottom support section	2.23 kg/mm^2

Element 23, section 3	-1.99 kg/mm ²
Element 24, section 2	-1.62 kg/mm ²

- At maximum power condition, the stresses and strains around the tube circumference are shown for the 4 mentioned sections in Table 7.
- The support loads for the different power levels are summarized in Table 8.
- Output data analysis confirms that the worst tube section is where the maximum temperature difference (or maximum flux) is located and shows that stresses are mainly connected with temperature gradients. This section is placed close to 1690 mm from the lower header axis.
- The local curvature in the worst section is towards the hot tube side and very small (about $1.21 \cdot 10^{-5}$).

4.7. Generalized plain strain tube analysis

In order to perform further computations, the most irradiated tube section has been chosen and the generalized plain strain model has been applied stressing the following points:

- the structure is free to expand axially; the differential thermal expansion between tube and downcomer

is taken up by brackets flexibility with negligible axial effect on the tube;

- tube sections keep plain and therefore an overstimulation of the stresses has to be expected;
- analysis can be limited to a slice placed at worst section height;
- because of geometrical and thermal symmetry, only one half of the ring is examined.

Under these hypothesis a distorted quadrilateral finite element with plastic description capability has been applied (no. 29 of MARC library). In addition to the 8 nodes for the conventional biquadratic representation of plain strain (in x-y plane) two additional bulk nodes (common to all the sections) express average Z displacement and x and y rotations.

The half ring is subdivided circumferentially into 24 sectors, radially the tube thickness into 3 layers, so 72 elements are required and the nodes amount to 273.

Thermal cycling is carried out to compute the maximum strain range; after three times up to maximum power and down, stabilization is reached.

In order to save CPU time, only situations with considerable flux incident on the tube are computed, as stresses are mainly produced by temperature gradients. So cycling can be limited and a minimum temperature of 495 °C considered. This approximation is checked and a transient until the lower temperature (270 °C) performed.

The resulting strain is $479 \cdot 10^{-4}$, to compare with the value of $4.35 \cdot 10^{-3}$ obtained stopping at 495 °C.

From MARC output examination it appears that the most stressed point in the section is located where the maximum temperature is reached.

In order to visualize the section status when maximum temperatures are first reached, plotting is presented for the equivalent stress (fig. 10) and the equivalent plastic strain (fig. 11).

Fig. 12 shows, represented on the equivalent stress-strain plane, the most stressed point status during thermal cycling; it appears that stabilisation is reached after two cycle.

The performed analysis proves that, when stabilization is reached and the hypothesized conditions (thermal

load and material characteristics) take place, the most critical point strain range is $14.2 \cdot 10^{-4}$.

4.8. Creep evaluation

In the previous plastic analysis the relaxation effect on the strain range was neglected because of its very small amount.

In fact, in the hypothesis of adding the relaxation effect at the end of the first cycling with a sustained time of 12 hours at the maximum stress/temperature level without stress relaxation (very conservative assumption because the primary creep is stress dependent with an exponent greater than 4) we obtain (with reference to the creep model suggested by CEA Report "Behavior in fatigue relaxation of a high creep resistance 316L SS"):

$$\sigma = 95.1 \text{ N/mm}^2$$

$$t = 12 \text{ hrs}$$

$$\epsilon_{\text{prim}} = 5.69 \cdot 10^{-14} \times \sigma^{4.31} \times t^{0.467} = 6.1 \cdot 10^{-5}$$

$$\epsilon_{\text{sec}} = \dot{\epsilon} t = \left(\frac{95.1}{663} \right)^{10.15} \times 12 = 3.3 \cdot 10^{-8}$$

and therefore the relaxation effect gives influence only on the third significant digit of the strain range.

5. CREEP-FATIGUE INTERACTION ANALYSIS

This part of the report deals with the lifetime analysis of the most irradiated section of the panel tube.

The analysis is carried out following T 1400 procedure reported in Code Case N-47-17 with reference to inelastic calculations.

The events that will be taken into account in this analysis are reported in Topic Report No. 6 and can be summarized as follow:

- . Effect of the daily cycling
- . Effect of the cloud passage
- . Failure of the control system of the pump in case of 100% re-insolation with 10% of sodium flowrate
- . Failure of the control system of the pump in case of shading of the field with 100% of sodium flowrate
- . Loss of sodium supply due to electrical failure of the sodium pump drive

The probability concepts reported in the Topic Report No. 6 have been applied to all the transient considered. In order to obtain the equivalent strain range

at different heat fluxes, the following linearization has been assumed:

$$\left[\Delta \varepsilon \right]_{\phi} = \left[\Delta \varepsilon \right]_{\phi = 125} \times \frac{\phi}{125}$$

As consequence of the small thermal tube inertia, the slope of the thermal shocks caused by the transients aforementioned has no practical impact on the tube stresses. A certain amount of calculation has been carried out in order to check this assumption and an increase of the stresses (elastically calculated) of 2.5% with respect of the steady state ones has been recognized for a flux ramp of $125 \text{ W/cm}^2/\text{sec}$.

5.1. Effect of the daily cycling

The start up and the shutdown events do not cause overstresses compared with the normal operating conditions due to the smoothness of the transient and the low thermal tube inertia.

With reference to the cold start-ups, they were considered in the same way of the hot start-ups; conservatively the cold start-ups were elevated as following shutdown from the maximum flux level.

The curves T 1420 of the Code Case N-47-17 were considered as basis for the allowable cycles evaluation.

The total daily cycling damage is 3.2% as shown in more detail in Table 9.

5.2. Effect of the clouds passage

For the reasons reported at point 5 of the report all the foreseen cloud passage types can be considered as identical and therefore the total events number is 63250 in 10 years. As shown in a more detailed form in Table 10, the total cloud passage damage is 7.3%.

5.3. Effect of the operational incidents

Again for the same reasons reported at point 5, the incidents itself can be considered as a normal daily cycling except the different temperature level.

The following damages for the foreseen events were obtained:

- 1) Failure of the control system of the pump in case of 100% reinsolation with 10% of sodium flowrate:
 - . maximum metal temperature (assumed) 705 °C
 - . number of incidents 60
 - . fatigue damage 10^{-3}

2) Failure of the control system of the pump in case of shading of the field with 100% sodium flowrate:

. maximum metal temperature	596 °C
. number of incidents	60
. fatigue damage	$4.6 \cdot 10^{-4}$

3) Loss of sodium supply due to electrical failure of the sodium pump drive:

. maximum metal temperature	610 °C
. number of incidents	60
. fatigue damage	$4.6 \cdot 10^{-3}$

TOTAL INCIDENTS FATIGUE DAMAGE: $1.92 \cdot 10^{-3}$

5.4. Creep damage evaluation

In order to simplify the analysis, conservatively the maximum stress evaluated by the inelastic calculations as $\sigma = 111.2 \text{ N/mm}^2$ is considered constant during all the day and the year.

The component operating life is assumed as 30000 hrs during the 10 years life on the receiver corresponding to 2730 "reference day" with 11 operating hours.

A splitted damage has been carried out for different time intervals at different average cross section

temperatures as shown in Table 11 and a total creep damage of 5.1% has been obtained.

5.5. Lifetime evaluation

In Table 12 it is shown the representative point in the plane fatigue damage-creep damage as requested by Code Case N-47-17. As can be seen all the operating conditions foreseen in Topic Report No. 6 can be withstood by the receiver.

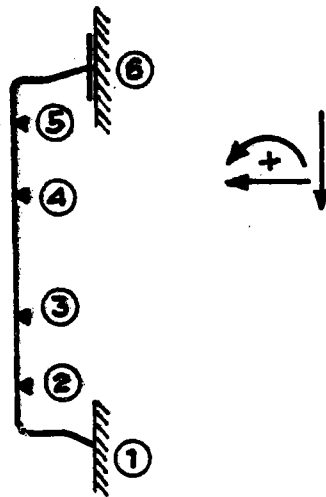
Extrapolating the results and within the hypothesis of identical operating conditions over the year, a life of 45.3 years has to be expected for the component.

6. CONCLUSIONS

All test are complied, particularly the tube is prevented against the creep-fatigue interaction which is the most dangerous failure mechanism for the component under examination.

The available margin of safety evaluated by the lifetime analysis allows to foresee that the component can withstands all the prescribed operating conditions.

POSITION	AXIAL FORCE Kg	SHEAR FORCE Kg	MOMENT Kgmm	ROTATION rad
1	3.98	- 2.51	- 818	
2		- 1.31		- 0.0105
3		- 1.83		0.00972
4		0.06		- 0.0071
5		- 1.63		0.00954
6	2.71	0.93	250	



N.B. All the quantities are referred to the tube

— TABLE 1 —

Stresses in the most stressed point on the cross section, corresponding to the highest metal temperature during the daily cycling.

Loads	Axial	Circumf.	Radial	Classif.
Weight	0.06	0.	0.	P _m
Pressure	0.17	0.34	0.	P _m
Restraints	-9.54	0.	0.	Q
Thermal	-14.49	-9.27	0.	Q
Wind	negligible	0.	0.	-
Earthquake	0.06	0.	0.	P _m

Highest metal temperature in a point of cross section:

$$T_{\max} = 596 \text{ } ^\circ\text{C}$$

BURSTING ANALYSIS

Maximum metal wall-averaged temperature on the hottest hoop section	$T_{\max_{h.s.}} = 566 \text{ }^\circ\text{C}$
Maximum allowable stress at $T_{\max_{h.s.}}$	$S_m = 7.62 \text{ Kp/mm}^2$
Minimum required thickness of shell	t
Design pressure	$P = 0.0611 \text{ Kp/mm}^2$
Inside radius of shell	$R = 12 \text{ mm}$

$$\text{Circumferential stress: } t = \frac{PR}{S-0.6P} = \frac{0.0611 \times 12}{7.62-0.6 \times 0.0611} = 0.10 \text{ mm}$$

$$\text{Longitudinal stress : } t = \frac{PR}{2S+0.4P} = \frac{0.0611 \times 12}{2 \times 7.62+0.4 \times 0.0611} = 0.05 \text{ mm}$$

The actual tube tickness is: $t_a = 1 \text{ mm}$

SHAKE DOWN ANALYSIS

Highest metal temperature in a point of the cross section	$T_{\max} = 596 \text{ }^\circ\text{C}$
Lowest metal temperature in a point of the cross section	$T_{\min} = 270 \text{ }^\circ\text{C}$
Allowable stress at T_{\max}	$S_m(T_{\max}) = 7.48 \text{ Kp/mm}^2$
Allowable stress at T_{\min}	$S_m(T_{\min}) = 9.84 \text{ Kp/mm}^2$
Allowable stress for the shake down analysis	$S_m = 8.66 \text{ Kp/mm}^2$

$$P_L + P_B + Q = 14.49 + 9.54 - 0.17 - 0.06 =$$

$$= 23.80 \text{ Kp/mm}^2 < 3 S_m = 3 \times 8.66 = 25.98 \text{ Kp/mm}^2$$

REATCHETING ANALYSIS

Maximum metal wall-averaged temperature
on the hottest hoop section $T_{\max} = 566 \text{ }^{\circ}\text{C}$
 Minimum metal wall-averaged temperature $T_{\min} = 270 \text{ }^{\circ}\text{C}$
 Yield strength at T_{\min} $S_y = 8.45 \text{ Kp/mm}^2$

$$X = \left(P_L + \frac{P_b}{K_T} \right) \div S_y ; \quad Y = \frac{(Q_R)_{\max}}{S_y} ;$$

$$K_T = 1 + K_S \left(1 - \frac{P_L}{S_t} \right) \approx 1 + K_S^{(*)} ; \quad K_S = \alpha (K - 1) ;$$

$K = 1.27$ (from ASME Section III, Appendix A, Table A-9221(a)-1);

$$\alpha = 0.5 ; \quad K_S = 0.5(1.27 - 1) = 0.135 ;$$

P_L	P_b	Q_R	K_T	X	Y	Z	ζ_c
0.34	0.	24.03	1.135	0.04	2.84	0.114	1.20

$$\zeta_c = 1.25 Z S_y$$

Entering the isochronous stress-strain curves at temperature $566 \text{ }^{\circ}\text{C}$, and for any time, by ζ_c , we read no significant strain, % due to creep.

(*) Smallness of $\frac{P_L}{S_T}$ justifies this position.

Strain	Stress ₂ kg/mm ²
0.	0.
$0.666 \cdot 10^{-3}$	13.333
$1 \cdot 10^{-3}$	15.9
$2 \cdot 10^{-3}$	18.65
$3 \cdot 10^{-3}$	20.
$11.3 \cdot 10^{-3}$	24.

- TABLE 5 -

$T / ^\circ\text{C}$	$R(T)$	$\Delta R / \Delta T \cdot 10^{-3}$	$\alpha^1 \cdot 10^{-6}$	$\alpha^2 \cdot 10^{-6}$
20	1	-1.563	15.2	14.3
100	0.875	-1.250		
120				15.43
150			17.8	
200	0.750	-1.002		
230				17.98
250			18.4	
300	0.649	-0.498		
350			18.6	
370				19.13
400	0.600	-0.500		
450			18.76	
480				19.96
500	0.55	-0.500		
550			19.16	
565				20.48
600	0.5			
620				20.80
650			20.24	

POINT	BOTTOM SUPPORT		TOP SUPPORT		ELEMENT 23, SECTION 3		ELEMENT 24, SECTION 2	
	σ_z	ϵ_{plast}	σ_z	ϵ_{plast}	σ_z	ϵ_{plast}	σ_z	ϵ_{plast}
5	-1.835	0.0	-2.074	0.0	-8.599	-4.49 E-4	-8.217	-2.513 E-4
6	-1.674	0.0	-1.945	0.0	-8.491	-3.56 E-4	-8.024	-1.808 E-4
7	-1.228	0.0	-1.510	0.0	-7.784	-1.16 E-4	-7.014	-9.506 E-6
8	-5.468 E-1	0.0	-8.345 E-1	0.0	-2.972	0.0	-1.704	0.0
9	1.57 E-1	0.0	0.0	0.0	3.374	0.0	3.45	0.0
10	6.96 E-1	0.0	7.02 E-1	0.0	4.649	0.0	4.25	0.0
11	1.099	0.0	1.33	0.0	4.235	0.0	3.65	0.0
12	1.365	0.0	1.76	0.0	3.95	0.0	3.24	0.0
13	1.455	0.0	1.94	0.0	3.86	0.0	3.11	0.0

- TABLE 7 -

Condition	Support n.1	n.2	n.3	n.4
AXIALLY UNIFORM	0.94542 kg	- 0.30517 kg	- 0.3051 kg	0.94542 kg
1/5 of FULL POWER	1.62141 kg	- 0.58288 kg	- 0.18865 kg	1.2234 kg
FULL POWER	- 0.49264	1.7587	- 4 E - 3	0.46081

- TABLE 8 -

DAILY CYCLING

Period	Days	Cover days	Working days	Incident flux W/cm ²	Absorbed flux W/cm ²	ΔE equivalent strain range 10 ⁻³	Allowable cycles M _D	Fatigue damage
Febr./April	890	120	770	138	125	1.42	79100	0.0097
May/July	920	40	880	116	103	1.17	250000	0.0035
Aug./Oct.	920	80	840	138	125	1.42	79100	0.0106
Nov./Jan.	920	140	780	110	98	1.11	354500	0.0022
						Hot start up:	total	0.0260
						Cold start up:	"	0.0060
							TOTAL	0.0320

- TABLE 9 -

CLOUD PASSAGES

Incident flux W/cm ²	Absorbed flux W/cm ²	$\Delta \epsilon$ strain range 10 ⁻³	Allowable cycles N _D	Flux level probability %	No. of events N	Fatigue damage N/N _D
120-140	116	1.14	297000	15.5	9803	0.0330
100-120	98	1.11	354500	22.3	14106	0.0398
80-100	80	0.91	>10 ⁶	15.2	9614	~0
60-80	62	0.70	>10 ⁶	13.6	8602	~0
40-60	44.5	0.51	>10 ⁶	12.2	7716	~0
10-40	22	0.21	>10 ⁶	21.2	13409	~0
Total					63250	0.0728

- TABLE 10 -

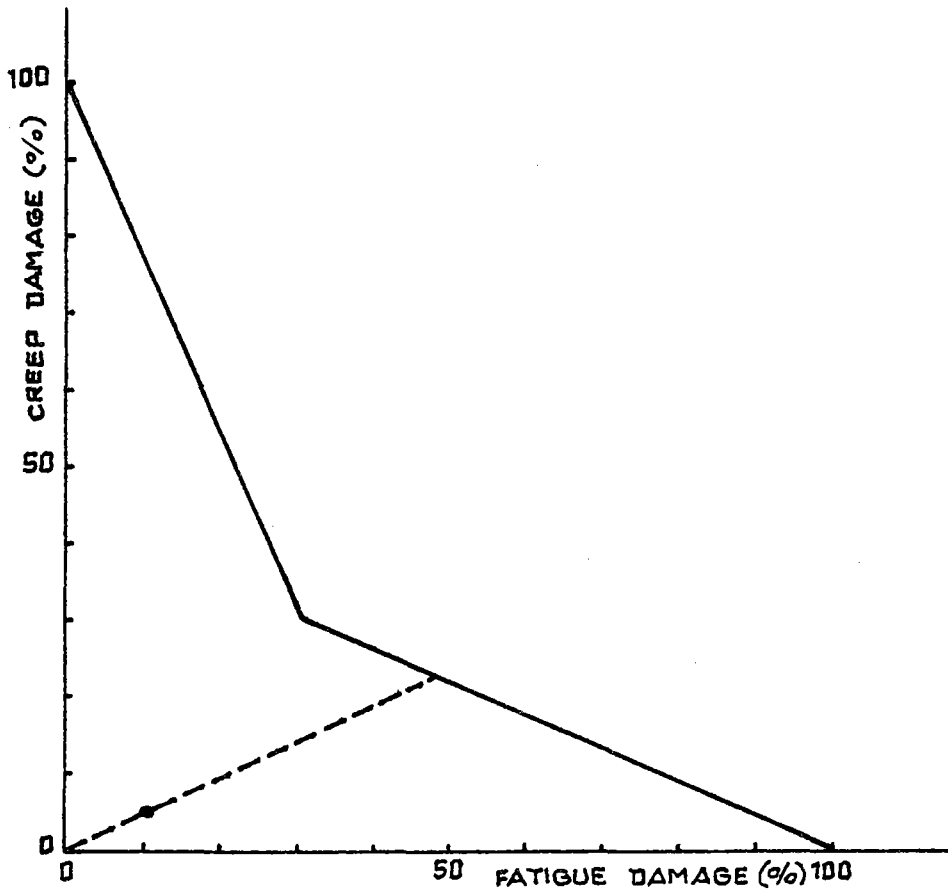
CREEP DAMAGE EVALUATION

Creep damage on an half cycle of a day				
Time interval	Interval length t	Temperat. $^{\circ}\text{C}$	Allowable time T_D	Damage t/T_D
6.30+7.1	0.75	510	$5 \cdot 10^7$	$1.5 \cdot 10^{-8}$
7.15+8	0.75	525	$6.5 \cdot 10^6$	$1.15 \cdot 10^{-7}$
8 + 9	1	540	$2 \cdot 10^6$	$5 \cdot 10^{-7}$
9 +10	1	555	$5 \cdot 10^5$	$2 \cdot 10^{-6}$
10+11	1	566	$3 \cdot 10^5$	$3.3 \cdot 10^{-6}$
11+12	1	566	$3 \cdot 10^5$	$3.3 \cdot 10^{-6}$
$\Sigma t/T_D$				$9.3 \cdot 10^{-6}$

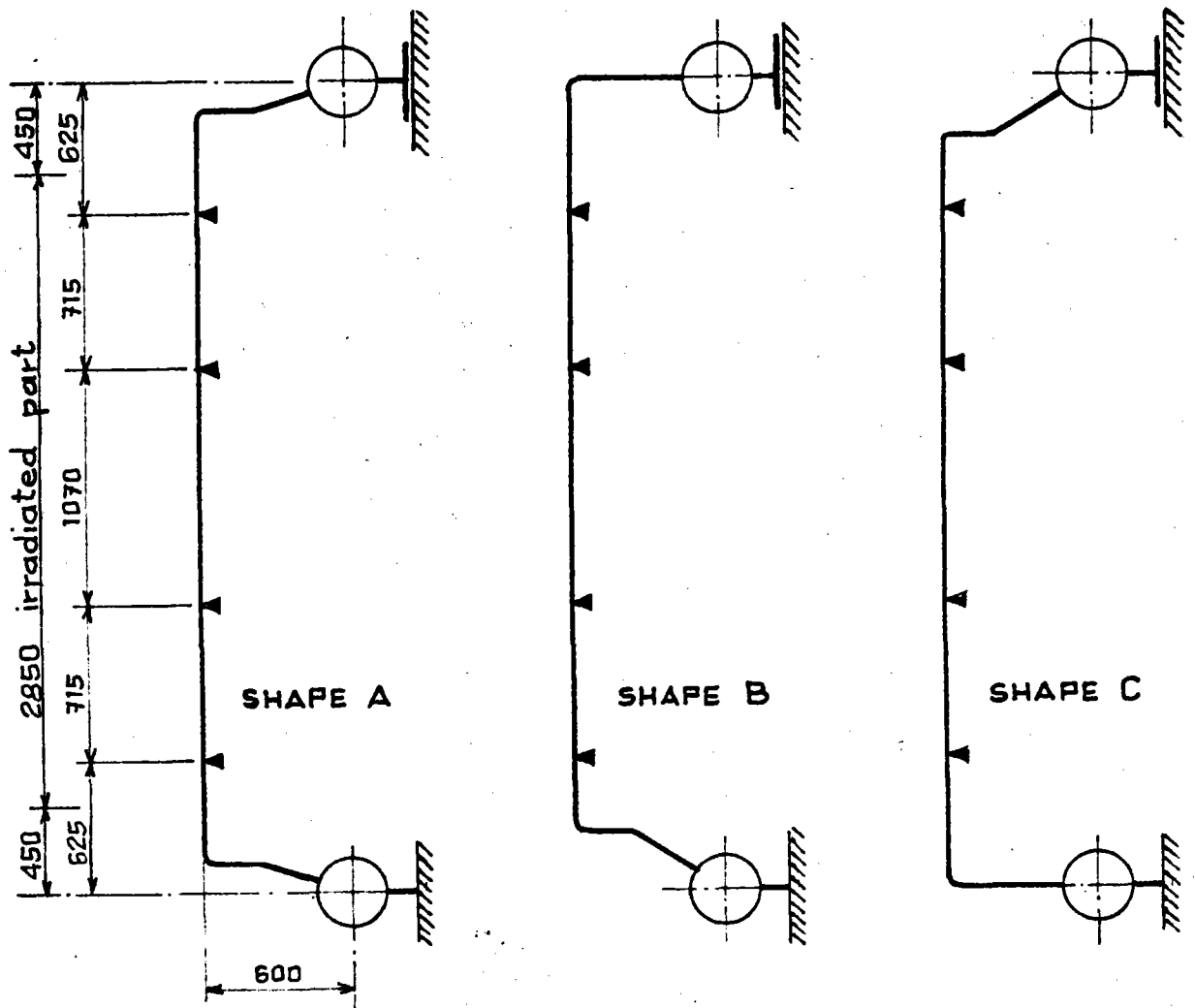
$$\text{Creep damage} = 2 \times 2730 \times 9.3 \cdot 10^{-6} = 5.08 \cdot 10^{-2}$$

CREEP-FATIGUE INTERACTION

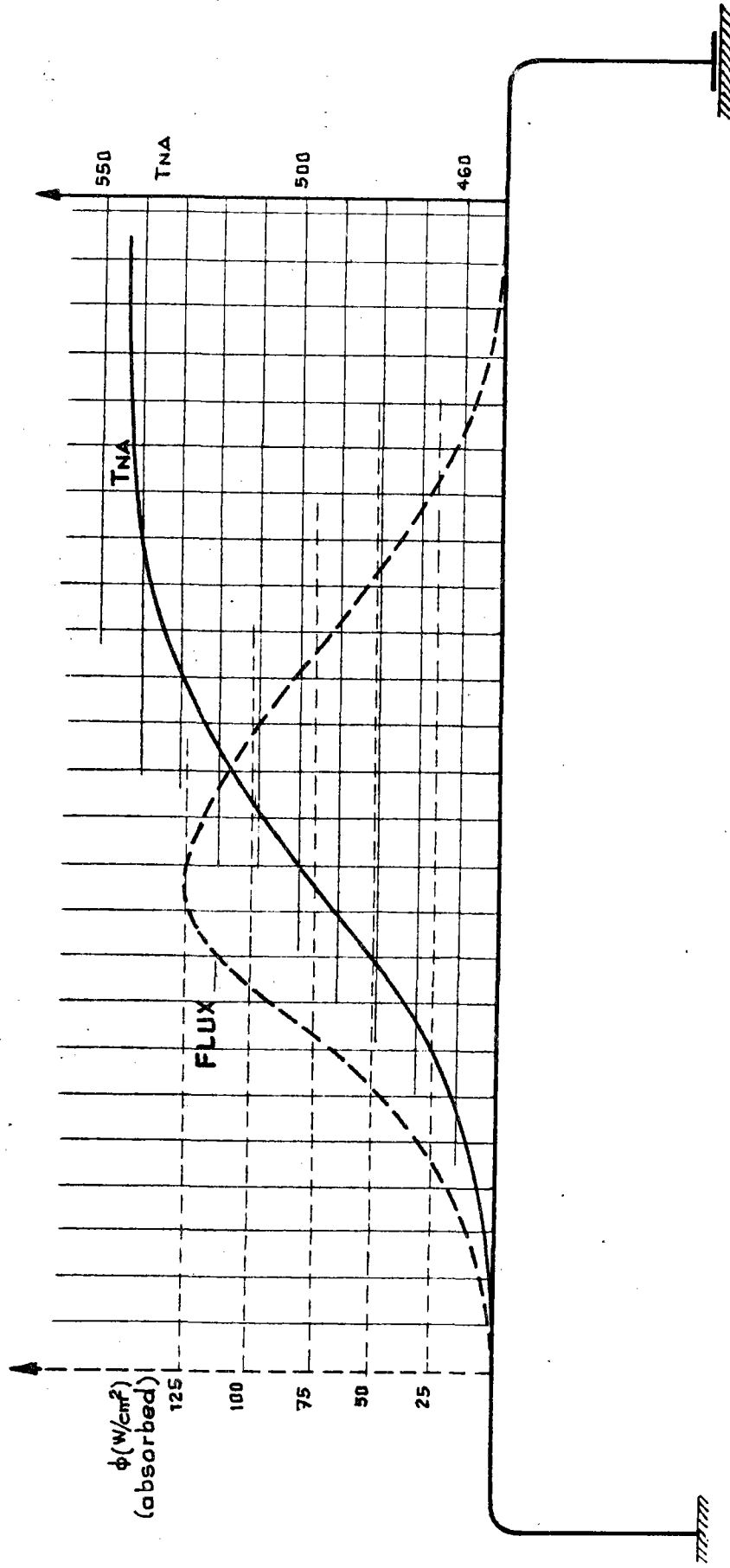
. Daily cycling fatigue damage	3.2 %
. Clouds passage fatigue damage	7.3 %
. Incidents fatigue damage	0.2 %
	<hr/>
TOTAL FATIGUE DAMAGE	10.7 %
TOTAL CREEP DAMAGE	5.08 %



— TABLE 12 —



— FIG. 1 —



— FIG. 2 —



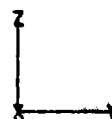
LEGNANO

*** 1/2 TUBO - ELEM. TIPO 4 ***

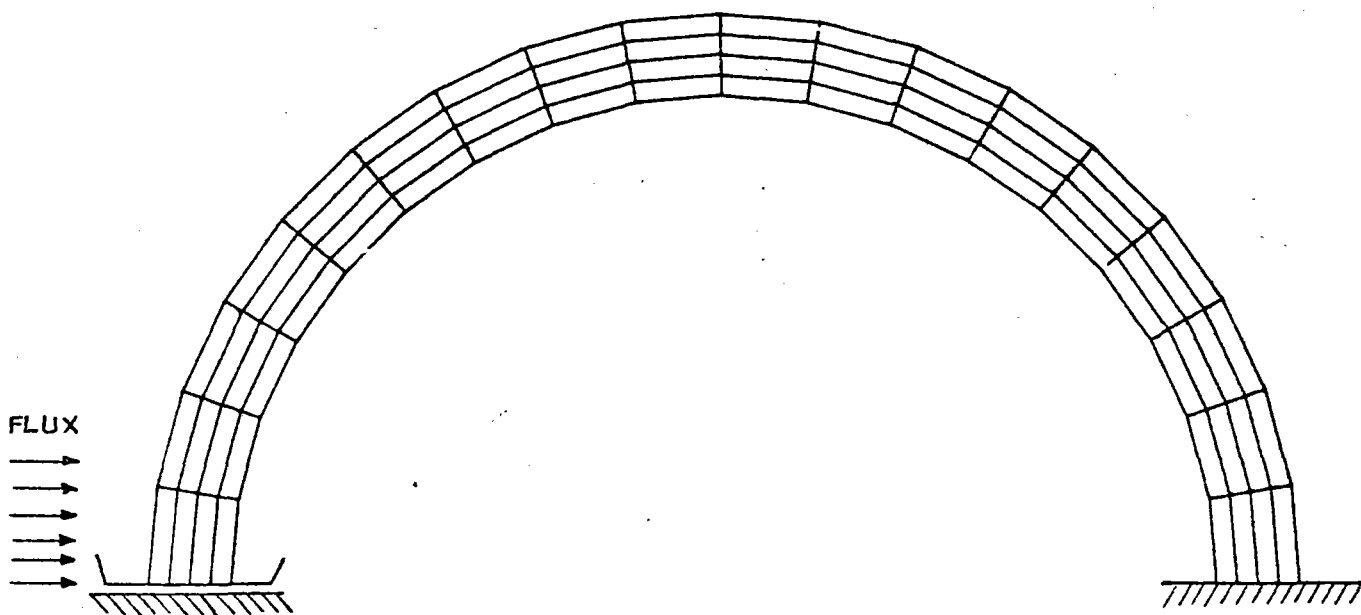
UNDEFORMED SHAPE

FEBRUARY 25, 1981 09:19:56

1 AXIS= 3 ALPHA= 0.00 BETA= 0.00



— FIG. 3 —





LEGNANO

ALMERIA-TUBO TIPO 1-VINC.DIS.8-COLLET.SUPER.MOBILE-INTERASSE COLLET=3750
 STATIC LOAD CASE 1
 JANUARY 28. 1982 12:25:25
 IAXIS= 1 ALPHA=0.00 BETA= 90.00
 DEFLECTION SCALE FACTOR= 0.63942 E-1

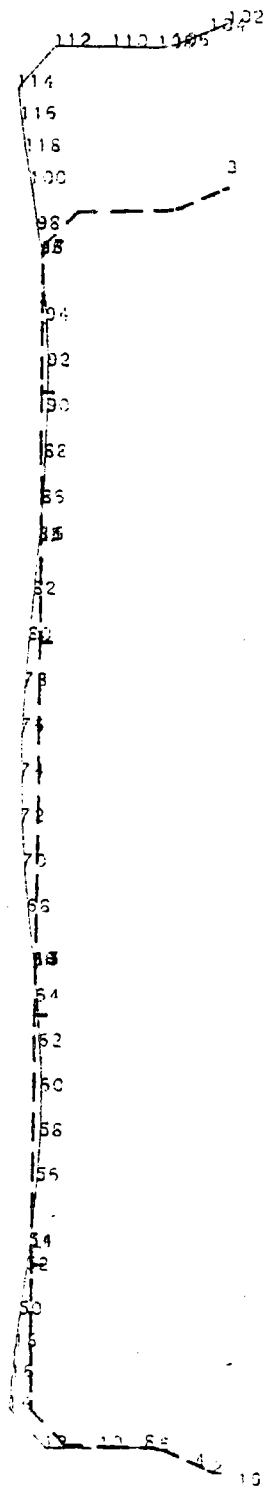
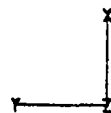


FIG. 4 - BEAM CALCULATION
Thermal load



LEGNANO

ALMERIA-TUBO TIPO 1-VINC.DIS.8-COLLET.SUPER.MOBILE-INTERASSE COLLET=3750
STATIC LOAD CASE 2
JANUARY 28. 1982 12:25:25
IAXIS= 1 ALPHA= 0.00 BETA= 90.00
DEFLECTION SCALE FACTOR= 2.2882

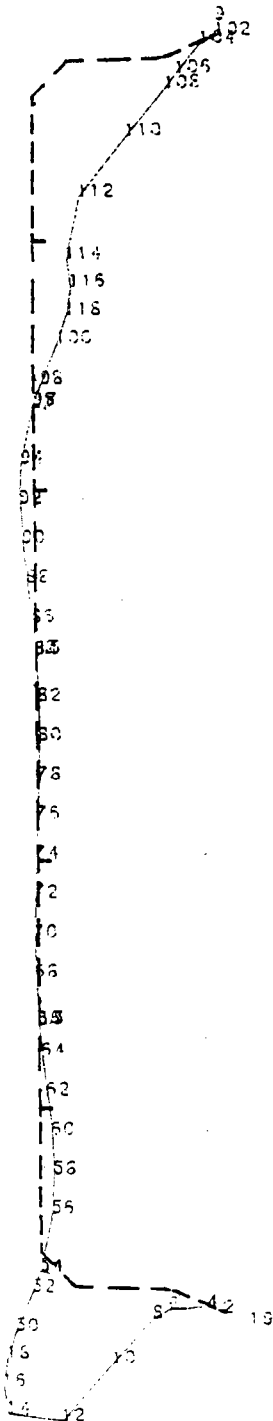
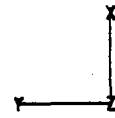


FIG. 5 - BEAM CALCULATION
Weight load



LEGNANO

ALMERIA-TUBO TIPO 1-VINC.DIS.8-COLLET.SUPER.MOBILE-INTERASSE COLLET=3750
STATIC LOAD CASE 3
JANUARY 28. 1982 12:25:25
IAXIS= 1 ALPHA= 0.00 BETA= 90.00
DEFLECTION SCALE FACTOR= 0.65056 E-1

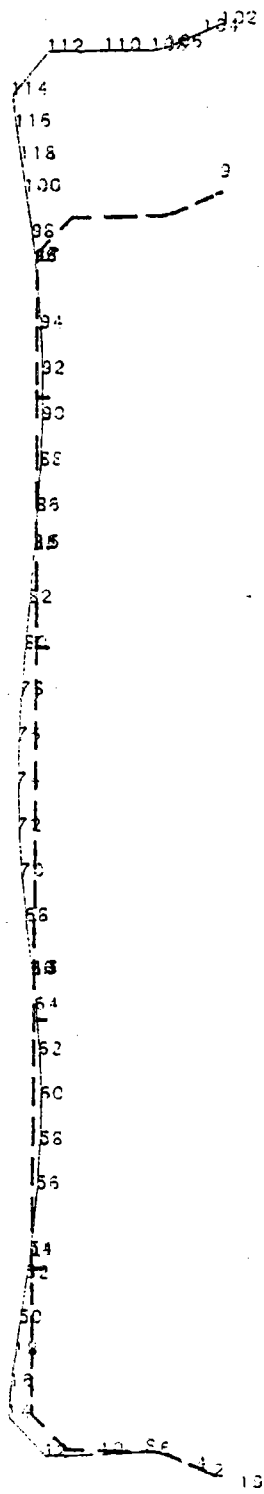
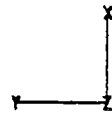
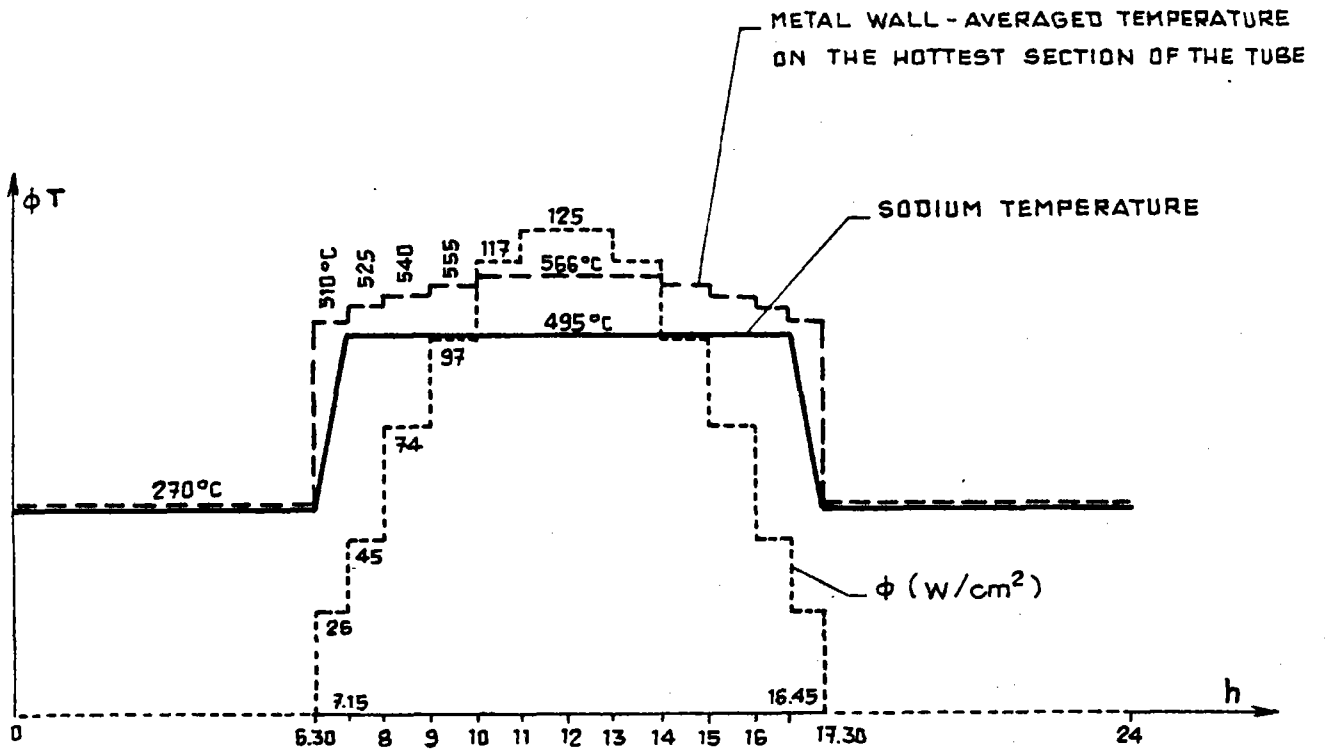
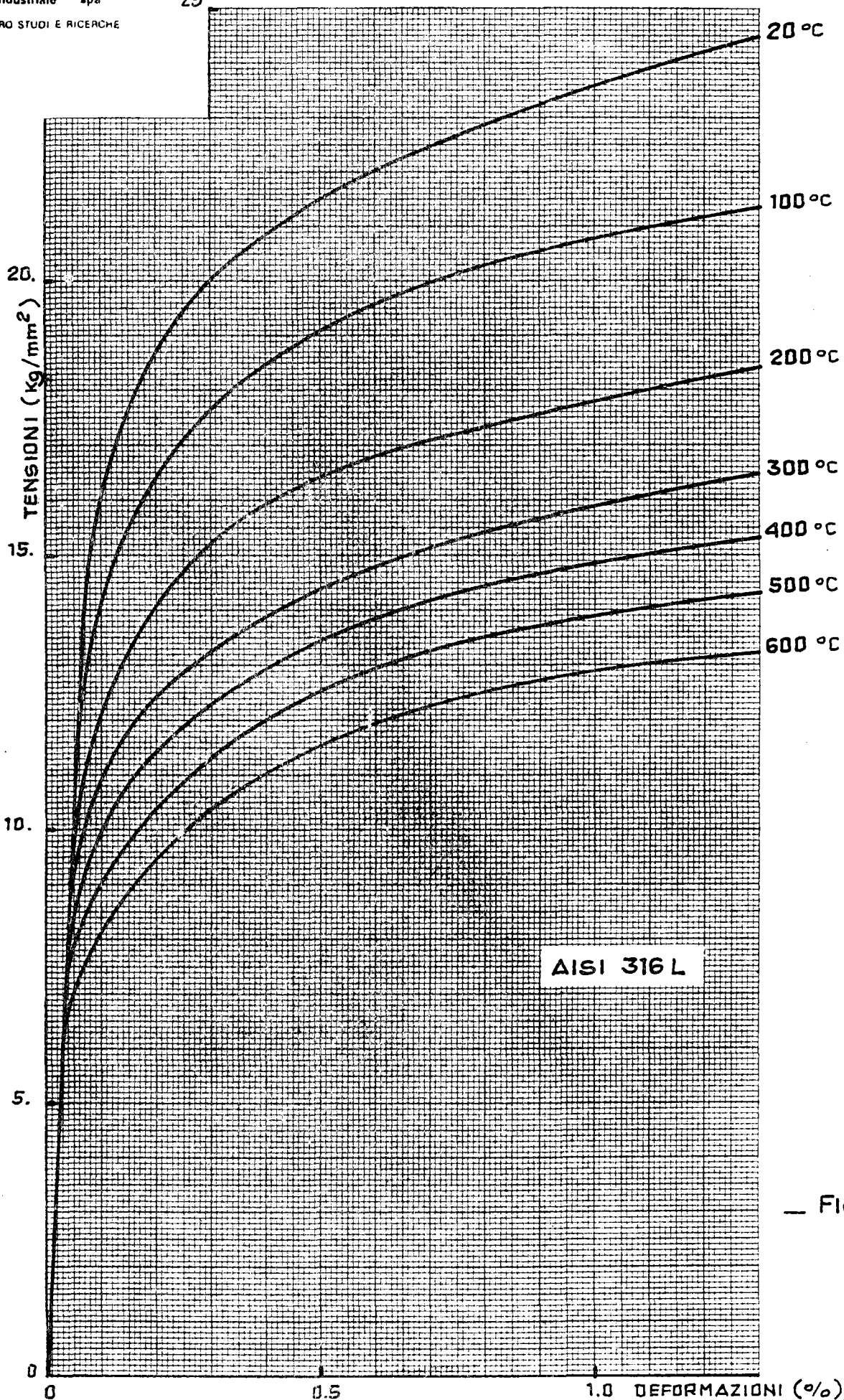


FIG. 6 - BEAM CALCULATION
Thermal and weight
load



— FIG. 7 —



— FIG. 8 —

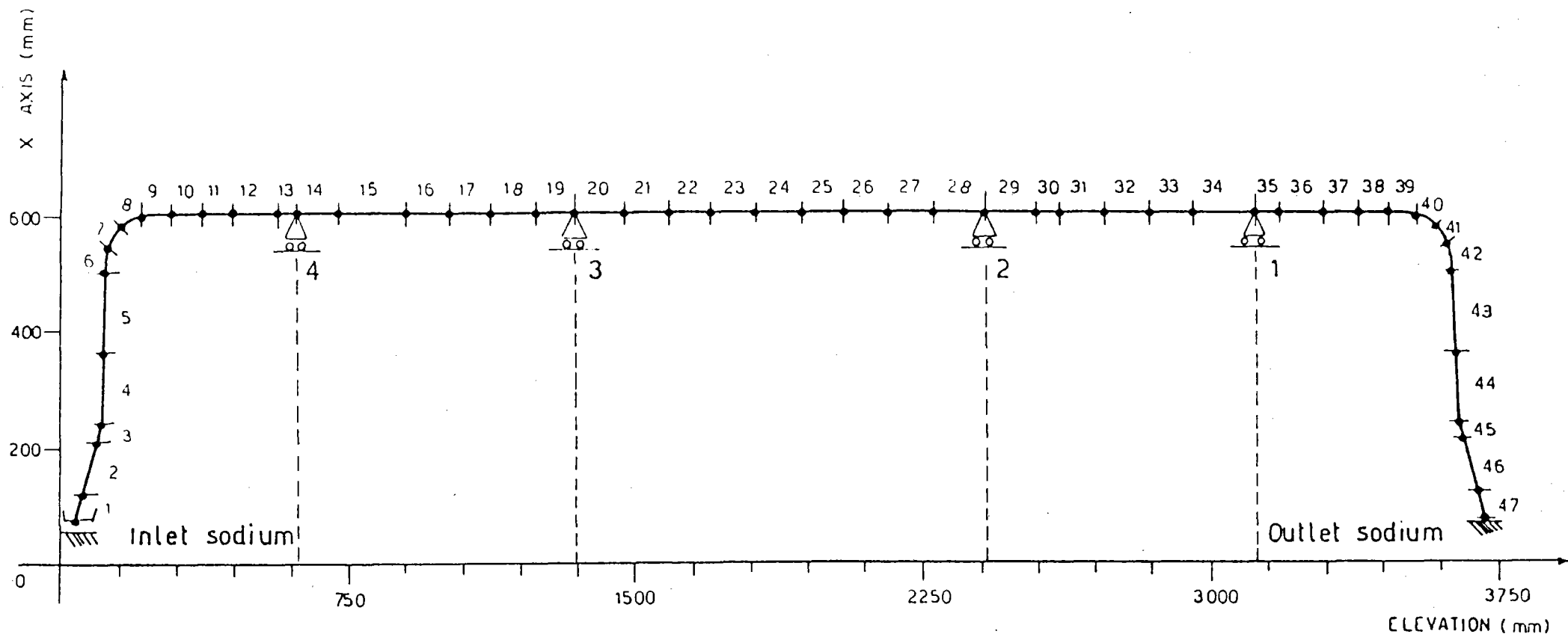
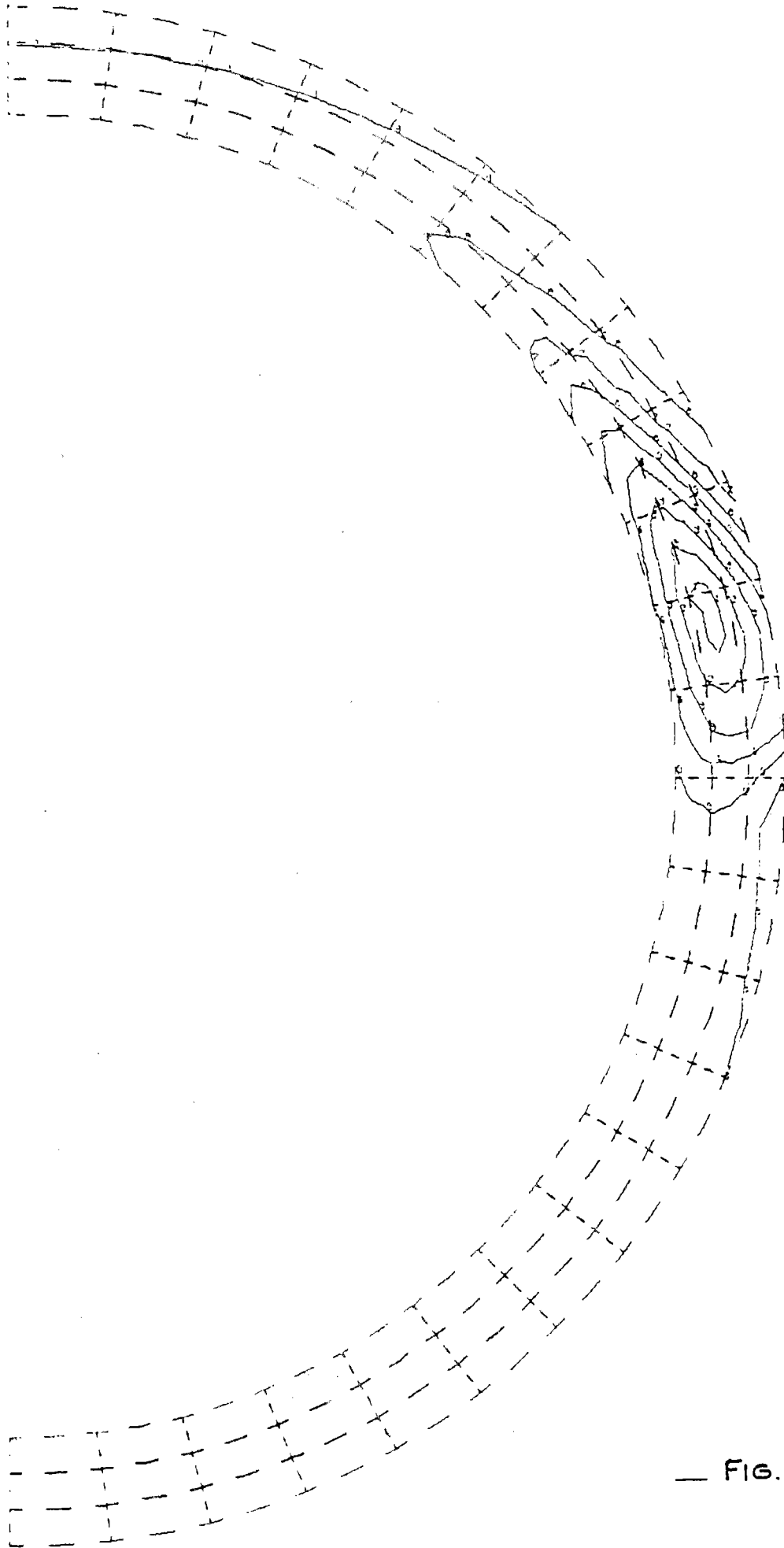


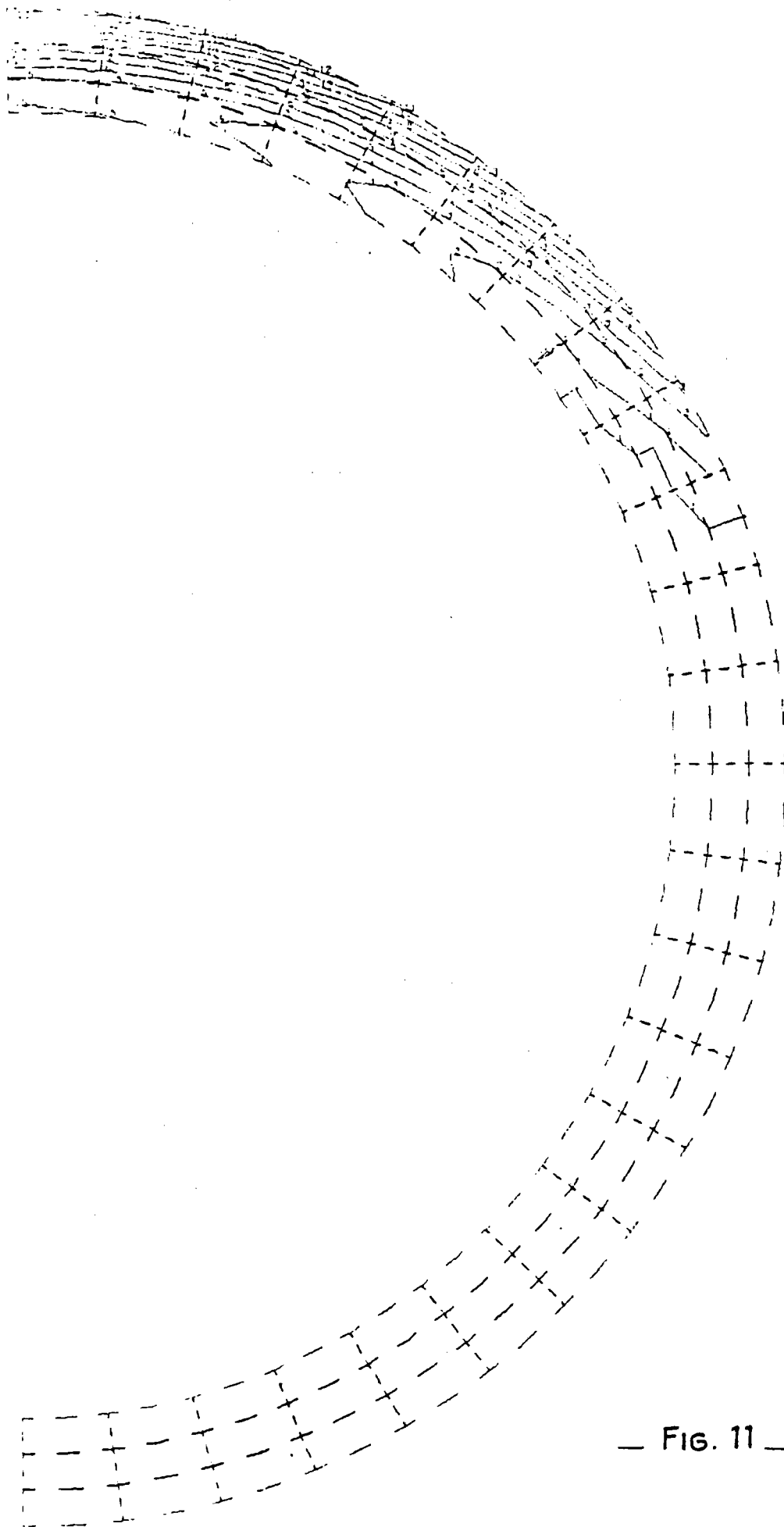
FIG. 9 - TUBE STRUCTURAL SHAPE

- 1 = 1. E.
- 2 = 2. E.
- 3 = 3. E.
- 4 = 4. E.
- 5 = 5. E.
- 6 = 6. E.
- 7 = 7. E.
- 8 = 8. E.
- 9 = 9. E.



— FIG. 10 —

- 1 = 0. E.
- 2 = 1. E-4
- 3 = 2. E-4
- 4 = 3. E-4
- 5 = 4. E-4
- 6 = 5. E-4
- 7 = 6. E-4
- 8 = 7. E-4
- 9 = 8. E-4
- 10 = 9. E-4
- 11 = 1. E-3
- 12 = 1.10E-3
- 13 = 1.20E-3
- 14 = 1.30E-3



— FIG. 11 —

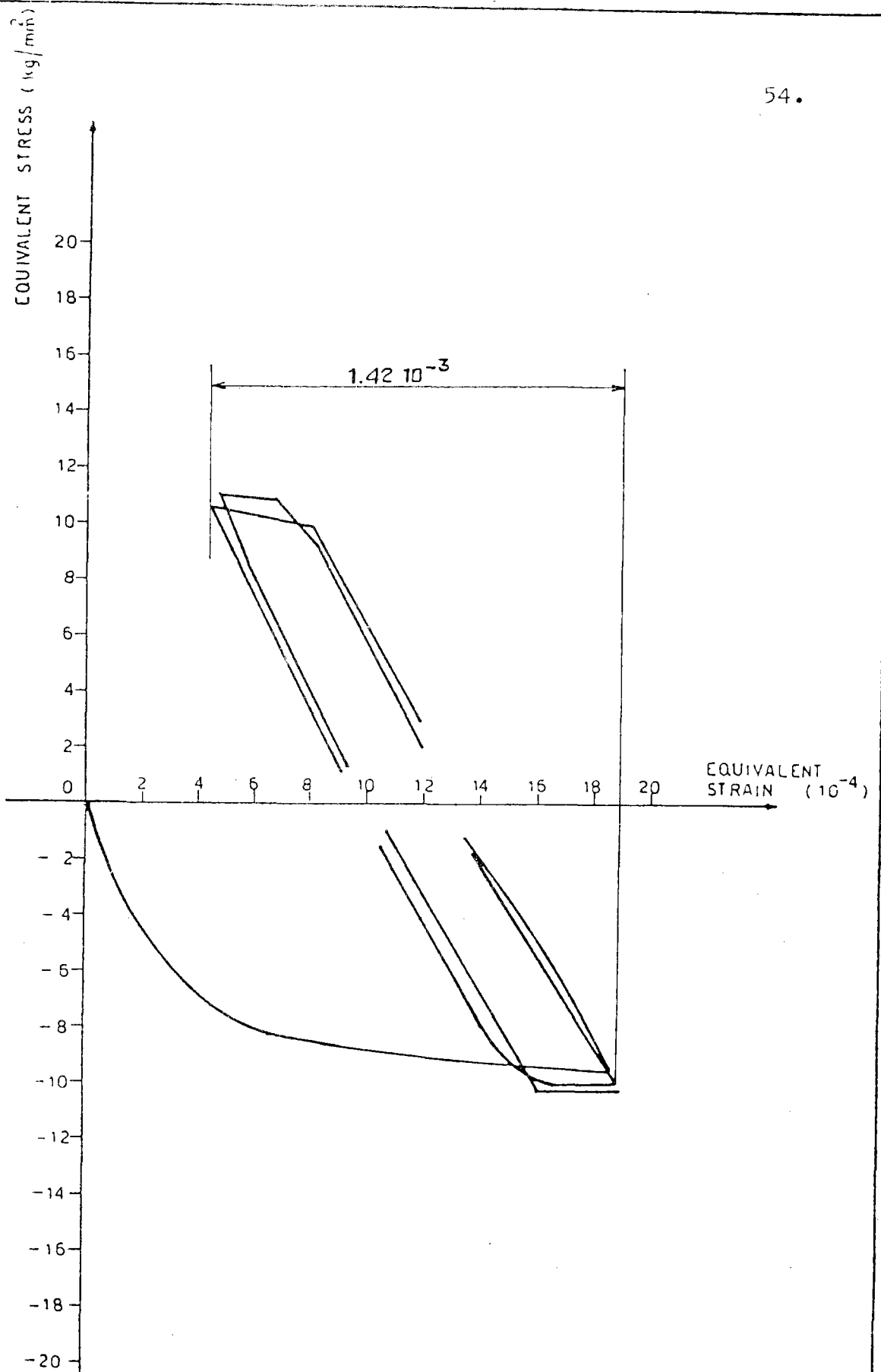


FIG. 12 - STRESS - STRAIN DIAGRAM

APPENDIX 1Mechanical characteristics of
tube material

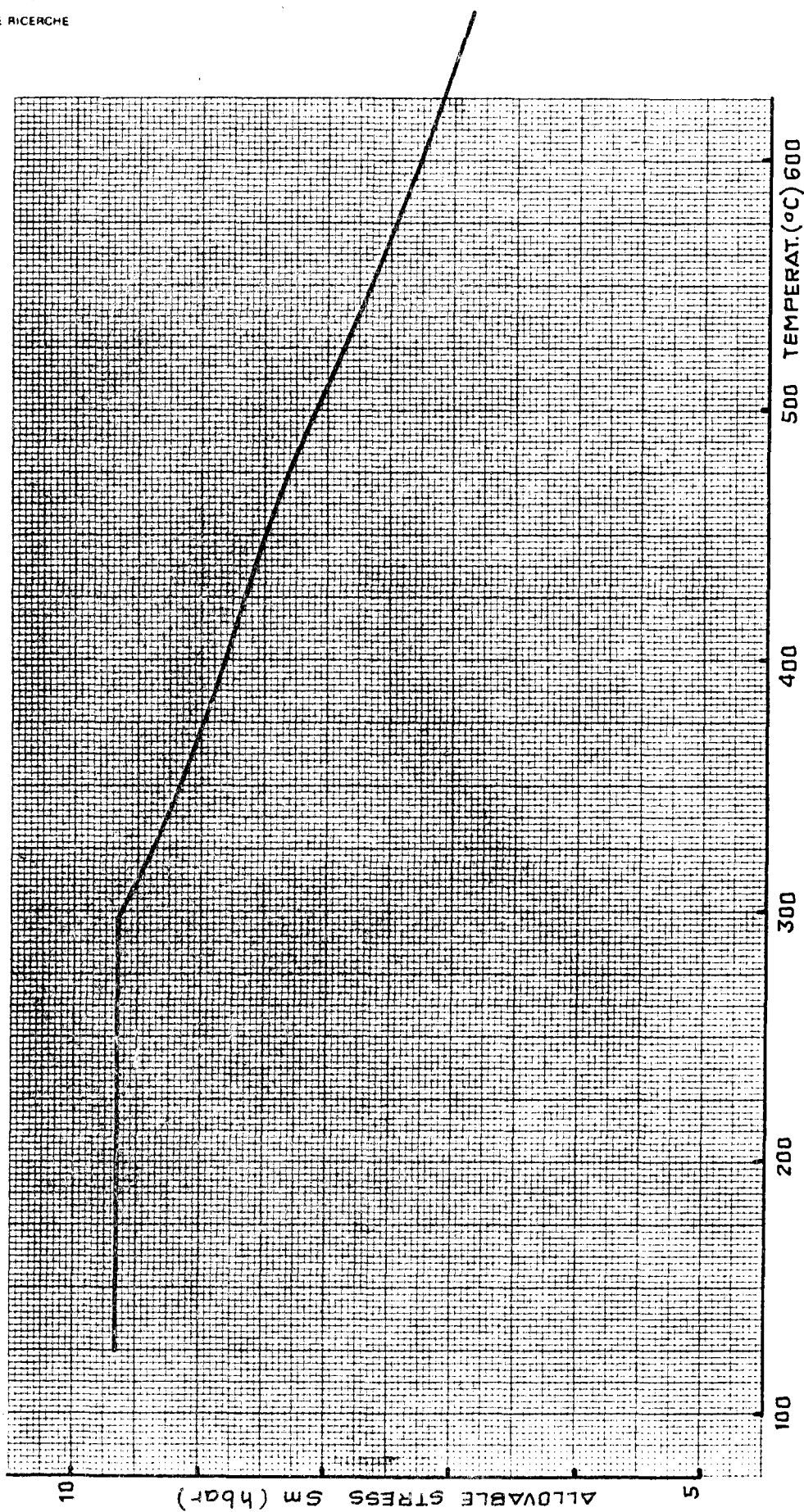
In the thermoelastic calculations the following assumptions are made:

- . density: the values are assumed from physical properties in the SANDVIK 3R60 fish reported in Annex 1;
- . thermal conductivity: as above;
- . specific heat capacity: as above;
- . instantaneous coefficient of thermal expansion: the values are assumed from Table I-14.8 of ASME Code Case N47-17;
- . modulus of elasticity: the values are assumed from SANDVIK 3R60 fish reported in Annex 1.

In the code compliance analysis the following assumptions are made:

- . yield strength: the values are assumed from fig. 1 in Annex 2;

- allowable stress S_m : the values are represented in fig. A1/1 as the minimum value between:
 - 1/3 of the tensile strength at temperature;
 - 90% of the yield strength at temperature but not exceed 2/3 of the specified minimum yield strength at room temperature;the yield and the tensile strength are deduced from fig. 1 and fig. 2 in Annex 2;
- fatigue curves: the values are assumed from fig. T-1420 1B of ASME Code Case N47-17;
- isochronous curves: the values are assumed from fig. T-1800-B of ASME Code Case N47-17;
- minimum time to rupture: the values are assumed at the lower bound of the curves represented in fig. 3 in Annex 2.



— FIG. A1/1 —

SANDVIK 3R60

ASTM type 316 L

Austenitic stainless ELC-steel

Sandvik · Sandviken · Sweden

SANDVIK

Tube

1,842 E

SANDVIK steel catalogue

FSI, September 1975

Cancels edition of September 1971

(1,8 E - 3R60)

SANDVIK 3R60 is a molybdenum-alloyed austenitic ELC-steel.

On request the material can also be supplied in a variant for the urea industry, Urea Grade, which has a guaranteed low ferrite content and meets the requirements in Huey-testing according to ASTM A262, practice C. This has been achieved by means of a well balanced chemical composition and an extremely low impurity content.

The steel is also delivered in a nitrogen-alloyed variant having higher strength, SANDVIK 3R69. See data sheet 1,846 E.

This data sheet gives information on mechanical properties, corrosion resistance and welding. For data on chipforming machining of SANDVIK 3R60 hollow bar, please refer to the data sheet 1,45 E - 3R60.

Chemical composition (nominal), %

C	Si	Mn	P	S	Cr	Ni	Mo
max			max	max			
0.030	0.6	1.7	0.030	0.030	17.5 ^a	13.5 ^b	2.7

^a Cr = 17% for welded tube and pipe; ^b Ni = 13% for welded tube and pipe

Specifications

ASTM A213, A249, A269, A312, A311

BS 3605

DIN 17440, 2463, 2464

Type of steel

ASTM	AISI	DIN	W.-Nr.	BS	SIS
TP316L		X 2 CrNiMo 18 12	1.4435	316S14	2353
MT316L	316L		(1.4404)	316S22	

AFNOR Z 2 CND 17.13

Forms of supply, finishes and dimensions

Seamless tube and pipe

Tube and pipe are supplied in the quench-annealed and white-pickled or in the bright-annealed condition. The latter alternative applies as a rule to small sizes. The principal size range can be seen from Figure 1, but also certain other sizes can be delivered on request.

Hollow bar

These tubes are supplied quench-annealed and white-pickled in the size range 32—250 mm (1.3—9.8 inch) O.D.

Welded tube and pipe

Longitudinally welded and calibrated

Tube and pipe are delivered quench-annealed and white-pickled or bright-annealed. In the range above 10 mm (0.4 inch) I.D. tube and pipe can be supplied internally bead rolled. The principal size range can be seen from Figure 2, but also certain other sizes can be delivered on request.

Longitudinally welded and cold-drawn

The tubes are supplied quench-annealed and white-pickled or bright-annealed with maximum O.D. = 87 mm (3.4 inch).

Wall thickness, mm (inch)

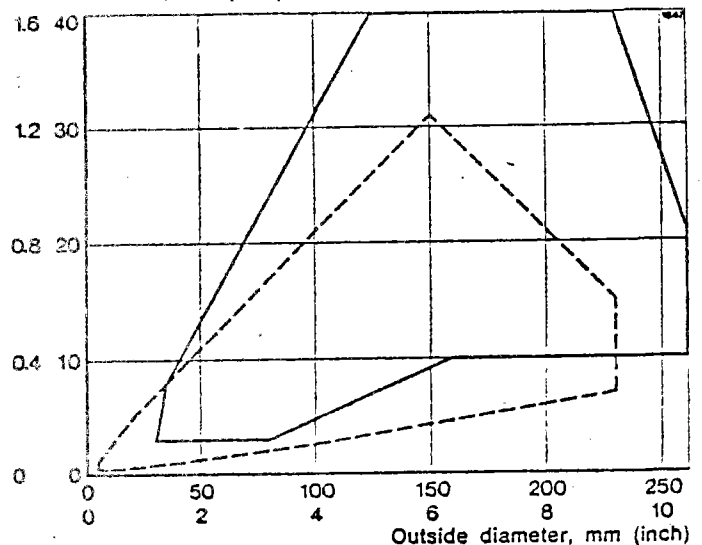


Figure 1 Size range for seamless tube and pipe

Solid line = hot-worked

Broken line = cold-worked

Wall thickness, mm (inch)

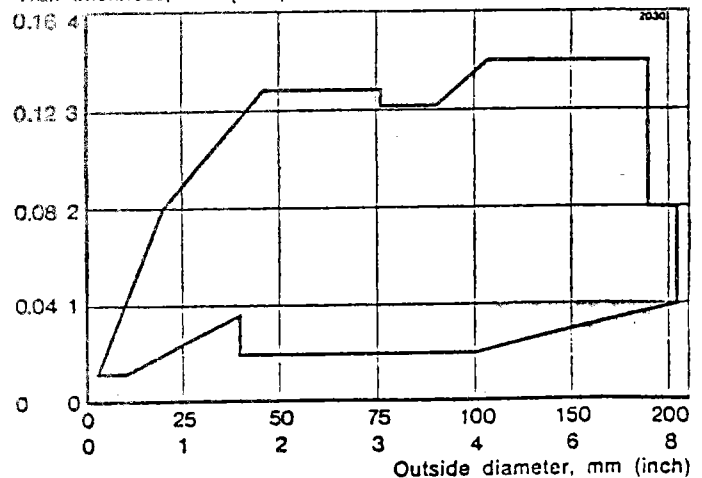


Figure 2 Size range for longitudinally welded, calibrated tube and pipe

indicated

Starting material is annealed and white-pickled sheet.

The size range of tube is:

outside diameter = 205—1200 mm (7.9—47 inch)

wall thickness = ≥ 2.5 mm (0.1 inch)

Pipe is made according to ANSI B36.10 and B36.19 in the following size range:

nominal pipe size = 3 1/2"—24"

wall thickness = Schedule 5—Schedule 80

Spiral-welded

Starting material is annealed and white-pickled strip.

Size range:

outside diameter = 90—508 mm (3.5—20 inch)

wall thickness = 1.5—5 mm (0.06—0.2 inch)

Pipe fittings

Fittings are available in SANDVIK 3R60 comprising butt-weld fittings according to ISO and ANSI standards, as well as SANDVIK couplings.

Sizes in stock

Seamless tube and pipe

Seamless tube and pipe are stocked in a large number of sizes according to ISO R1127, ISO R65 medium series and ANSI B36.19. See our brochure 1,10 E.

Hollow bar

Hollow bar are stocked in a large number of sizes.

Longitudinally welded tube and pipe

Longitudinally welded tube and pipe are stocked in sizes according to ISO R1127. See our brochure 1,10 E.

Fabricated tube and pipe

These types are stocked in frequent sizes.

Pipe fittings

Sandvik's pipe fittings are stocked in a large number of sizes and finishes. See our brochures 1,13 E, 1,14 E and 1,15 E.

Mechanical properties

At 20°C (68°F)

Metric units

Yield strength		Tensile strength		Elong. ^a	Hardness		
1.2% offset	1.0% offset			A5	Vickers		
N/mm ²	kg/mm ²	N/mm ²	kg/mm ²	N/mm ²	kg/mm ²		
min	min	min	min	%	nom.		
95	20	235	24	500—650	51—66	45	150

^aA5 corresponds to $5.65\sqrt{S_0}$

The impact energy at -60°C is min 157 J, 16.0 kgm, and the transition temperature (transition from ductile to brittle fracture) is lower than -200°C.

English units

Yield strength		Tensile strength		Elong. ^a	Hardness		
1.2% offset	1.0% offset			A5	Vickers		
psi	ksi	N/mm ²	ksi	%	nom.		
min	min	min	min	min	nom.		
95	28	235	34	500—650	73—94	45	150

The impact energy at -75°F is min 157 J, 116 ft-lb, and the transition temperature (transition from ductile to brittle fracture) is lower than -330°F.

At high temperatures

Temperature		Yield strength			1.0% offset		
		0.2% offset					
°C	°F	N/mm ²	kg/mm ²	ksi	N/mm ²	kg/mm ²	ksi
		min	min	min	min	min	min
100	210	172	17.5	24.9	206	21.0	29.9
200	390	147	15.0	21.3	177	18.0	25.6
300	570	128	13.0	18.5	157	16.0	22.8
400	750	118	12.0	17.1	147	15.0	21.3
500	930	108	11.0	15.6	137	14.0	19.9
600	1110	98	10.0	14.2	128	13.0	18.5

Physical properties

Density

8.0 g/cm³, 0.29 lb/in³

Thermal conductivity

Temperature		W/m · °C	kcal/m · h · °C	Btu/ft · h · °F
°C	°F			
20	68	15	13	9
100	210	16	14	9.5
300	570	19	16	10.5
500	930	21	18	12
700	1290	23	20	13.5

Specific heat capacity, mean values

Temperature		J/kg · °C	kcal/kg · °C	Btu/lb · °F
°C	°F			
50—100	120—210	500	0.12	0.12
600—700	1110—1290	630	0.15	0.15

Thermal expansion, mean values (x10⁻⁶)

Temperature		Per °C	Per °F
°C	°F		
20—100	68—210	16.0	8.9
20—200	68—390	17.0	9.5
20—300	68—570	17.5	9.7
20—400	68—750	17.8	9.9
20—500	68—930	18.0	10.0
20—600	68—1110	18.2	10.1
20—700	68—1290	18.5	10.3

Modulus of elasticity

Temperature		N/mm ²	kg/mm ²	ksi
°C	°F			
20	68	200 000	20 000	28 500
400	750	170 000	17 000	24 000
600	1110	150 000	15 000	19 000

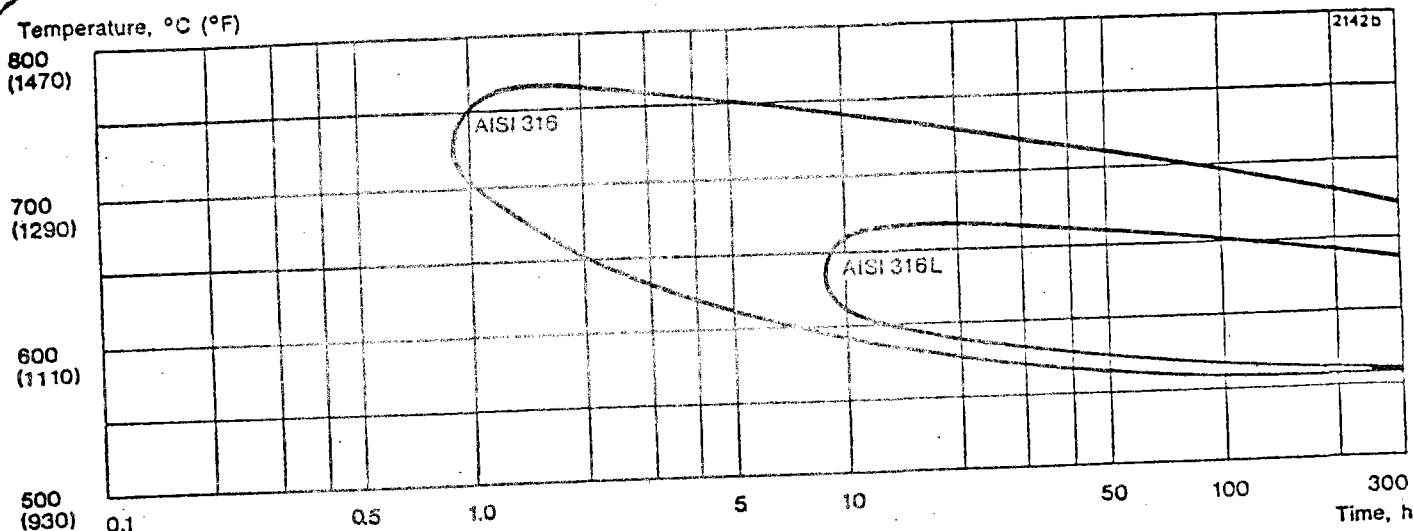


Figure 3 TTC-diagram for SANDVIK 3R60 (AISI 316L) and AISI 316.

Corrosion resistance

General corrosion

SANDVIK 3R60 has good resistance to

organic acids, e.g. citric, lactic, formic, tartaric and acetic acids, at high concentrations and temperatures

inorganic acids, e.g. boric, phosphoric, nitric and sulphurous acids, at moderate concentrations and temperatures. The steel can also be used in sulphuric acid at low temperature and concentrations below 10% or above 90%

salts, e.g. sulphates, sulphides and sulphites

solutions of carbamate in urea processes.

SANDVIK 3R60 is unsuitable for use in hydrochloric acid.

Pitting

Resistance to pitting improves with increasing molybdenum content and SANDVIK 3R60, containing about 2.7% of molybdenum, has substantially higher resistance to pitting than steels of the 18/8 type.

Intergranular corrosion

Thanks to its low carbon content SANDVIK 3R60 has better resistance to intergranular corrosion than steels of type AISI 316.

The TTC-diagram — Figure 3 — shows the results of corrosion testing for 24 hours in boiling Strauss-solution (12% sulphuric acid, 6% copper sulphate). As can be seen in the diagram the resistance to grain boundary attacks is much better for SANDVIK 3R60 than for a corresponding steel with higher carbon content (AISI 316). This is of course an advantage in complicated welding operations.

Stress corrosion cracking

Austenitic steels are susceptible to stress corrosion cracking. This may occur at temperatures above about 70°C (160°F), if the steel is subjected to tensile stresses and at the same time comes into contact with certain solutions, particularly those containing chlorides. Such service conditions should therefore be avoided. Also when plants are shut down the conditions must be considered, as the condensates which are then formed can develop a chloride content that leads to both stress corrosion cracking and pitting.

Mechanical stresses are set up e.g. in bending or welding. Therefore, the risk of stress corrosion cracking can be reduced by stress relieving bends and welds.

Where good resistance to stress corrosion cracking is required, the choice should be another stainless steel, e.g. a ferritic or a ferritic-austenitic steel or a material of high nickel content.

Heat treatment

Stress relieving

850—950°C (1560—1740°F), 10—15 minutes, cooling in air

Quench annealing

1050—1100°C (1930—2010°F), 5—20 minutes, rapid cooling in air or water.

Welding

The weldability of SANDVIK 3R60 is good. Suitable fusion-welding methods are manual metal-arc welding with coated electrodes or gas-shielded arc welding, with the TIG and MIG methods as first choice. No preheating is required in normal cases, and as a rule post-weld heat treatment is not necessary.

Since the material has low thermal conductivity and high thermal expansion, welding must be carried out with a low heat input and with welding plans well thought out in advance, so that the deformation of the welded joint can be kept under control. If, despite these precautions, it is foreseen that the residual stresses might impair the functioning of the structure, we recommend that the entire structure be stress-relieved.

As filler material for gas-shielded arc welding we recommend wire of SANDVIK grades 2R61 (AWS ER 316L), 3RS63 (AWS ER 316L Si) or, when a ferrite-free weld metal is desired, SANDVIK 3RS69 (AWS ER 316L Si). In manual metal-arc welding we recommend coated electrodes of type ESAB OK 63.30, SMIT Arosta 316L, PHILIPS RS 316 or OERLIKON Inox BWL. In the urea industry filler metal of the type 19Cr/15Ni/MnMo, e.g. SANDVIK 3RM69, is often used for welds in contact with the process solution.

Bending

Annealing after cold bending is not normally necessary, but this point must be decided with regard to the degree of bending and the operating conditions. Heat treatment, if any, should take the form of stress relieving or quench annealing, see these headings.

Hot bending is carried out at 1100—850°C (2010—1560°F) and should be followed by quench annealing.

ANNEX 2

The annex hereafter consists of a part of the
SANDVIK document No. K0605/3.

Date 1977-11-21	DOSSIER DE CARACTERISATION	Reg. No.	Page
Prepared by TRH/Andersson		Page 1/4	
Approved by TR/Gullberg / <i>HP</i>		Spec. No. Rev. 4	
		Supersedes 1977-10-19	

TOSI COMMANDE 77/383

TUBES SANS SOUDURE SANDVIK 3R60 (TYPE 316L)

SANDVIK COMMANDE: 345-47566, 47567

DOCUMENTATION NO: K 0605/3

1.5 Structure micrographique

- grosseur du grain: 3-7 avec la possibilité de fournir tubes avec grosseur du grain 8.

2. CARACTERISTIQUES MECANIQUES

Les caractéristiques mécaniques pour SANDVIK 3R60 à la température ambiante (20°C) sont indiquées dans paragraphe 2.1 et pour températures élevées dans paragraphe 2.2.

Toutes les valeurs représentent des valeurs minimales que nous pouvons garantir.

- 2.1 $R \geq 490$ MPa
 $E_{0,2\%} \geq 172$ MPa
 $A5 \geq 40$ %

- 2.2 Les valeurs minimales aux températures élevées que nous pouvons garantir sont indiquées en fig. 1 - limite élastique et en fig. 2 - résistance à la traction. Interpolation entre 500 et 600°C donne les valeurs minimales suivantes à 550°C

- $R \geq 378$ MPa
 $E_{0,2\%} \geq 85$ MPa

2.3 Fluage

4 coulées différentes de SANDVIK 3R60 ont été soumises à des essais de fluage à 550°C, 600°C et 700°C.

Fig. 3 indique les contraintes conduisant à la rupture. A la température de 550°C une extrapolation jusqu'à 100.000 heures donne la valeur 165 MPa pour la contrainte moyenne conduisant à la rupture.

Fig. 4 indique les contraintes donnant 1 % d'élongation en t heures pour température T. Les valeurs représentent des valeurs moyennes.

3. TENUE A LA CORROSION VIS A VIS DU FLUIDE

La tenue à la corrosion vis à vis du sodium en contact à 550°C est très bonne.

- Références:
- Faisceau tubulaire des échangeurs intermédiaires de Phénix.
 - G.A. WHITLOW, J.C. CWYNAR, S.L. SCHROCK - "Sodium corrosion behavior of alloys for fast reactor application" - Proceedings Symp, Detroit, Michigan, Oct 19-20, 1971
 - E. BERKEY, G.A. WHITLOW - "Microstructural and compositional changes in sodium exposed stainless steel by scanning electron microscopy"-id-
 - P.A. BACUE, L.J. CHAMPEIX, E.T. HONNORAT - "Compositionnal changes in austenitic steels after corrosion in sodium at 700°C" -id-
 - A. LAFON - "Compatibilité d'aciers austenitiques avec le sodium dynamique à 700°C" - "Quelques aspects métallurgiques" - R. STRS 029 - Fév. 73 -

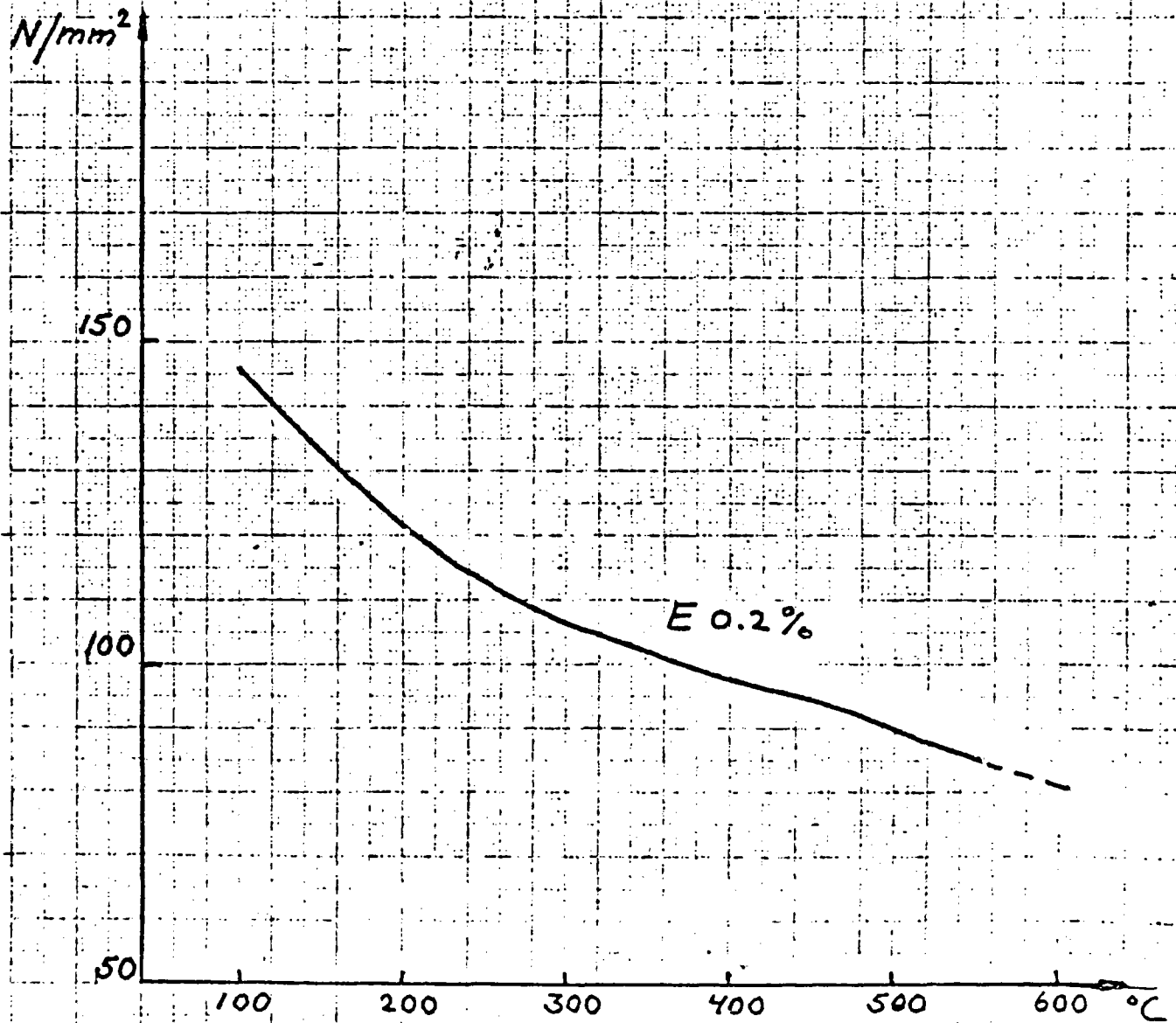
4. SOUDAGE

Le SANDVIK 3R60 a une bonne soudabilité. Pour tubes avec une épaisseur de paroi de 1 mm on recommande soudage automatique ou manuel selon la méthode TIG. Comme métal d'apport on recommande du fil en SANDVIK 2R61 (AWS ER 316L), 3RS63 (AWS ER 316L Si) ou quand le métal déposé ne doit pas contenir de ferrite, 3RS69 (AWS ER 316L Si).

SANDVIK 3R60

Fig. 1

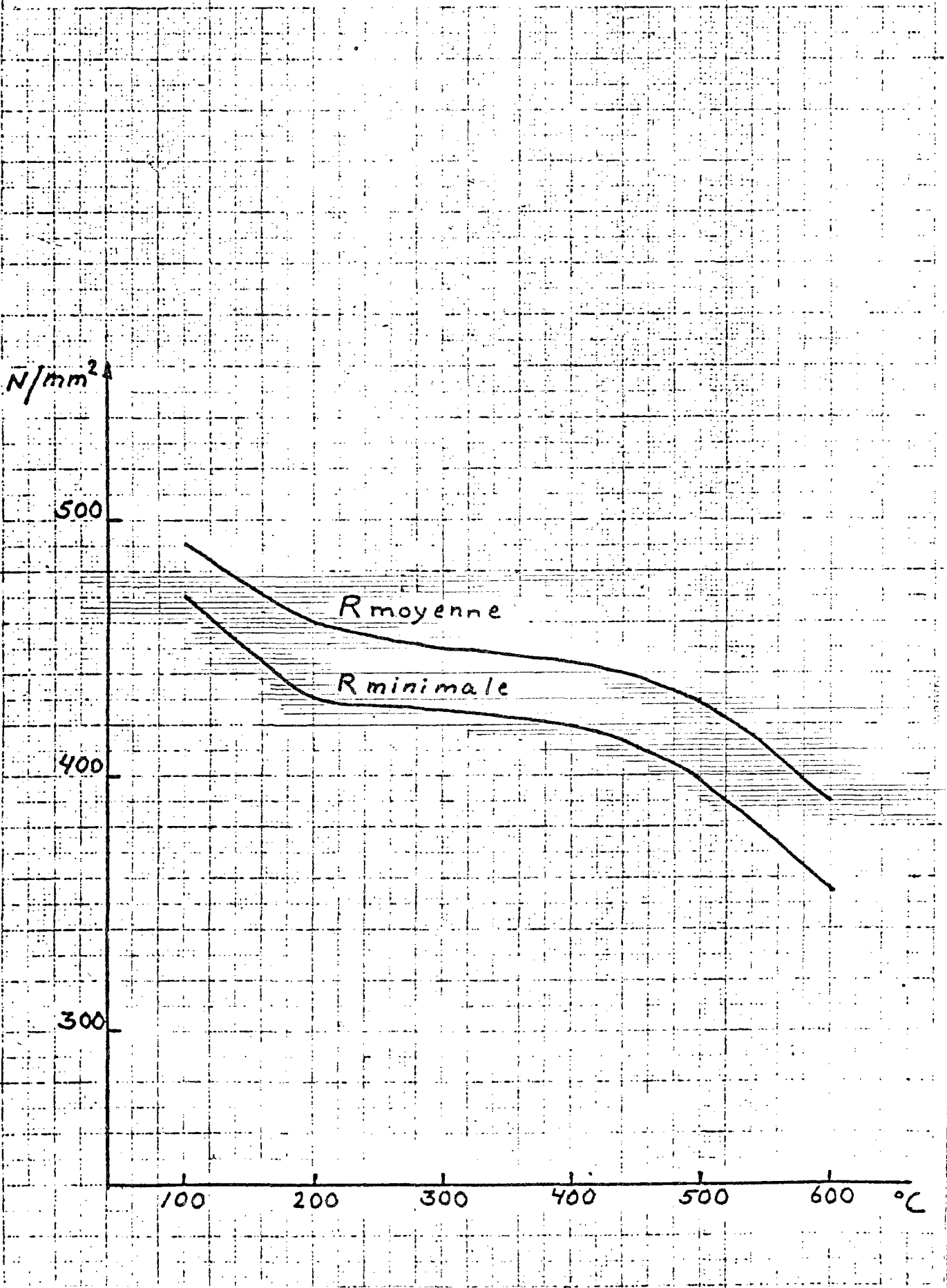
Limite élastique



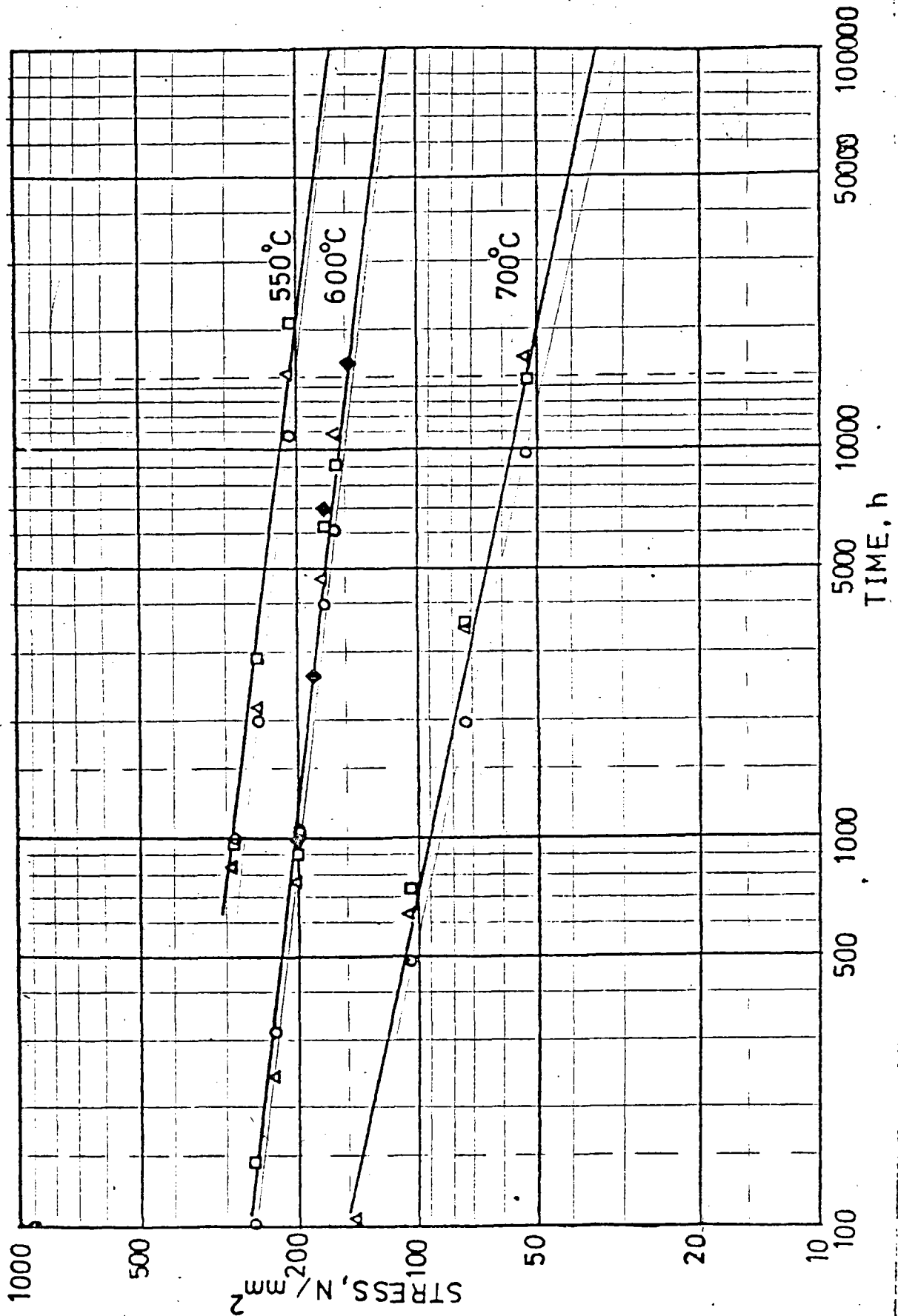
SANDVIK 3R60

Fig. 2

Résistance à la traction



SANDVIK 3R60
Contraintes conduisant à la
rupture



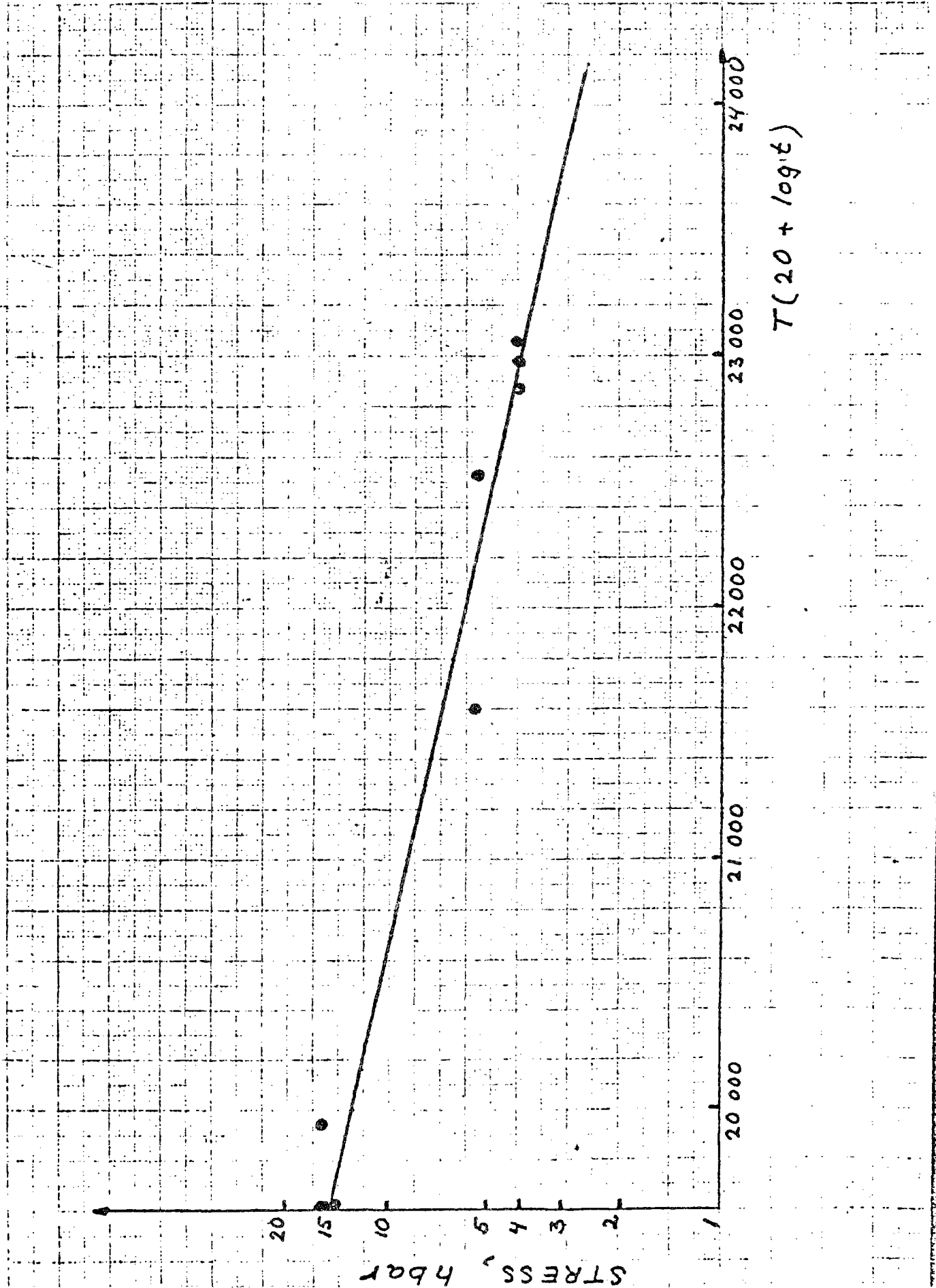
1330-10A

101
S&S
LIFE

SANDVIK 3R60

Fig. 4

Contraintes donnant 1 % d'élongation
en t heures pour température T.



A P P E N D I X 2

Considerations and comparison between elastic and inelastic creep-fatigue analysis

The considerations reported in this appendix will mainly concern the possibility of using an elastic analysis in order to obtain the strain range to enter T1420 fatigue curves of ASME Code Case.

A strict application of the Code philosophy would request to use the T1430 curves when an elastic analysis is followed; on the other hand the actual stress status of the tube is essentially strain controlled because the primary stresses are about 1.5% of the total stress in the case of ASR and therefore, as suggested by the work carried out by Foster Wheeler "An Interim Structural Design Standard for Solar Energy Applications", it might be reasonable to consider the elastically strain range to enter T1420 curves as well.

With reference to stress table no. 2 of the report the following stress component due to weight, pressure restraints and thermal gradient are considered at the operating conditions:

$$\tilde{\sigma}_z = -23.8 \text{ kg/mm}^2$$

$$\tilde{\sigma}_r = 0$$

$$\tilde{\sigma}_\theta = -8.33 \text{ kg/mm}^2$$

$$t = 596 \text{ }^\circ\text{C}$$

$$E = 15260 \text{ kg/mm}^2$$

According to equation no. 8 in T1432 Code Case N47-17 we obtain

$$\epsilon_m = \epsilon_{LC} + \frac{1}{E} S_{SC} = \sim 0 + \frac{23.8}{15260} = 1.56 \cdot 10^{-3}$$

and therefore because of $K = 1$

$$\epsilon_t = 1.56 \cdot 10^{-3}$$

This value is 9.8% greater than the inelastically evaluated strain range and therefore a reasonable safety margin is contained in this approach of the problem.

Considering a status with no loads as "reference one", the Foster Wheeler approach for the strain range evaluation starting from elastically calculated stresses would give:

$$\epsilon_{r0} = 0$$

$$\epsilon_{z0} = 0$$

$$\varepsilon_{\theta 0} = 0$$

$$\varepsilon_{r1} = \frac{1}{15260} \left[0 - 0.3 (-23.8 - 8.33) \right] = 0.63 \cdot 10^{-3}$$

$$\varepsilon_{z1} = \frac{1}{15260} \left[-23.8 - 0.3 (0 - 8.33) \right] = -1.39 \cdot 10^{-3}$$

$$\varepsilon_{\theta 1} = \frac{1}{15260} \left[-8.33 - 0.3 (0 - 23.8) \right] = -0.08 \cdot 10^{-3}$$

$$\Delta \varepsilon_r = \varepsilon_{r1} - \varepsilon_{r0} = 0.63 \cdot 10^{-3}$$

$$\Delta \varepsilon_z = \varepsilon_{z1} - \varepsilon_{z0} = -1.39 \cdot 10^{-3}$$

$$\Delta \varepsilon_{\theta} = \varepsilon_{\theta 1} - \varepsilon_{\theta 0} = -0.08 \cdot 10^{-3}$$

$$\varepsilon_t = \frac{\sqrt{2}}{3} \sqrt{(\Delta \varepsilon_r - \Delta \varepsilon_z)^2 + (\Delta \varepsilon_r - \Delta \varepsilon_{\theta})^2 + (\Delta \varepsilon_z - \Delta \varepsilon_{\theta})^2} = 1.18 \cdot 10^{-3}$$

This value, obtained by applying the Van Mises criterion is 17% smaller than the inelastically evaluated

strain range and therefore a little underestimation of the strain is connected.

Coming back to the strain range evaluation by the Code Case approach essentially based on Tresca yielding criterion and starting from elastically calculated stresses we can conclude that an elastic approach seems to be reasonable as well because a safety margin is still contained in the evaluated strain range.

This margin, if the curves T1420 were applied, would lead to a life reduction (with respect to the inelastically evaluated one) of about 37%; any way always acceptable within the operating conditions and lifetime specified for the ASR.

IEA ALMERIA PROJECT

ADVANCED SODIUM RECEIVER

ASR

Final Evaluation of Receiver Thermal State

Topic Report No. 8

Revision 0

November 1982

Prepared by: ENEL

FRANCO TOSI

AGIP NUCLEARE

CONTENTS

Introduction

1. Tube-supporting plate connection analysis
2. Stirrup system supporting beam thermal analysis
3. Backwall thermal analysis
4. Incident heat flux distribution on the backwall

Appendix A

Appendix B

INTRODUCTION

The scope of this report is to describe the significant results of the thermal analysis performed for the ASR absorber back-structure.

In ASR project, in order to allow lateral thermal expansion of tubes and panels, gaps are provided between tubes in addition to manufacture tolerances: so there are some parts of ASR which are impinged by concentrated solar flux entering through these gaps. Consequently an accurate control of the gaps between tubes of the receiver is requested so to keep the solar flux leakage through them as little as possible not to cause overheating of structures behind tubes.

The critical parts of the absorber back-structure are shown in the map of fig. 1 and are the objects of the reported thermal analysis:

- Detail 1 Tube-supporting plate connection
- Detail 2 Stirrup system supporting beam
- Detail 3 Tube bundle backwall

1. TUBE-SUPPORTING PLATE CONNECTION ANALYSIS

1.1. Object

The object of this section is the evaluation of temperature distribution of the plate connecting the absorber tubes three by three with a restraining function.

See detail 1 of the map of figure 1.

1.2. Gap

As already mentioned, in order to allow lateral thermal growth of the absorber without causing any additional load on the tubes, a suitable gap between tubes has been provided.

In fig. 2a and 2b the details of the stirrup supporting system and assembly in panel structure are shown.

Two gap situations have to be considered for stirrup-plate thermal evaluation:

- A) Gap between tubes connected by the same plate. A gap at 0.2 mm (*) has been considered taking into account:
- nominal design value of the tube center to center distance;

(*) Manufacture of the 3-tube groups has confirmed the caution of this value, assumed for verification analysis purpose.

- tube diametral tolerance (± 0.1 mm).

B) Gap between tubes of different plates.

In this case the gap value is greater than the previous one, but the flux entering through this gap strikes only on a little part of the plate side which has the contour shaped in such a way to minimize entering radiation capture.

From figure 2b it can be noted that a gap of 1.4 mm between each of the 5 panels has been prescribed by design during receiver panels assembly. During receiver operation this gap will be reduced by panel thermal expansion.

However taking into account:

- critical transient condition, such as sudden return of insolation after a period of shadow;
 - dimensional and manufacturing tolerances;
- a maximum gap of 2 mm has been assumed for plate thermal analysis in the case of a B-gap.

1.3. Heat flux

An incident peak value of heat flux on the absorber of 138 W/cm^2 has been assumed, based on the solar flux map at design point.

To determine the solar direct flux distribution on the stirrup plate an heliostat field beam angle of 80° has been assumed and, in this angle, the normalized solar flux distribution has been approximated by cosine law. Heat fluxes at various distances from the gap have been calculated by integrating within the view angle at the field and accounting for incoming ray direction with respect to surface position.

The validity of these assumptions in heat flux distribution evaluation has been checked by a complete analysis of the flux through the tube-gap by using Helios computer program (see section 4).

The followed procedure overestimates the incident flux peak values and permits an high computer time saving. Heat flux distribution on the lower face of the plate is reported in fig. 3 and 4 for gap A and B respectively.

1.4. Analysis model

A 2 mm thickness strip of the stirrup plate has been considered connected to a portion of tube of 12 mm height, wetted by sodium, as shown in fig. 5.

All the cut edges of the tube-strip system of fig. 5 were assumed adiabatic (no conduction heat transfer to the adjacent material). Under the assumption on flux and

gap symmetry, analysis has been limited to one half of the tube and strip system. Equilibrium temperature distribution was evaluated using the finite element computer code FLHE.

1.5. Analysis data list

Hereafter the significant analysis data for detail 1 are reported:

Geometry

Plate thickness (mm)	2
Tube O.D. (mm)	14
Tube thickness (mm)	1

Material

Tube - plate	AISI 316 L (Sandvik catalogue 1,842E - 3 R 60)
--------------------	--

Heat flux

Incident peak value on the tube (W/cm^2)	138
Flux distribution on the tube irradiated side	cosine low
Flux distribution on the plate	see fig. 3-4

Thermal input data

Inside tube sodium temperature ($^{\circ}C$) ..	495
Inside tube sodium convection coeff. ($W/m^2/C$)	36000 (Skupinski correlation for Na velocity of 1.8 m/sec)

Tube absorption efficiency	0.9 (IR, refl., conv losses included)
Plate radiation losses	none
Plate convection losses	none
Plate solar absorptance	0.8 (assumed)

Gap

A - type (mm)	0.2
B - type (mm)	2

1.6. Results for 0.2 mm gap (type A)1.6.1. Temperature distribution in tube - plate connection

Fig. 6 reports the code plot for the temperature distribution in the tube thickness and in the lower surface of the strip.

Temperature increases in the plate moving from the tube connection to the free end of the strip, where the strip temperature reaches its maximum of 543 °C: this zone receives less thermal input by solar entering flux but is more distant from sodium heat sink which is the only way to drain heat from the plate.

The plate temperature is always well under the maximum temperature in the system of 595 °C, reached in the front of the tube.

1.6.2. Thermal gradient in the plate thickness

During ASR operation, the tube bending requires rotation of the plate.

Due to the fact that the plate receives solar heat flux only from the lower surface, a thermal gradient in the plate thickness may exist causing a curvature of the plate with consequent reduction of the design allowed rotation angle.

An evaluation of this thermal gradient has been carried out taking into account also a different convection loss coefficient in the upper and lower surfaces of the plate. A thermal gradient less than 5° C has been obtained. This value is quite negligible with respect to the curvature effect (*).

1.7. Results for 2 mm lateral gap (type B)

As previously reported in section 1.2, the contour shape of the plate is very effective in reducing incident heat flux, in spite of a critical gap width such as 2 mm.

(*) Considering the analyzed plate strip as a free beam fixed at one end a thermal gradient in the thickness of more than 70 °C would be required to produce a rotation of 1° of the beam in correspondence of the pin hole.

Fig. 4 show the incident heat flux distribution on the lower face and in the lateral surface of the plate (incident peak value on the absorber: 138 W/cm^2).

The calculated values of incident heat flux are of the same magnitude of those obtained for gap A analysis. Considering the results of the section 1.6, the heat flux values of fig. 4 have been judged acceptable without any further investigation.

1.8. Different axial expansion of tubes connected by the same plate

Taking into account transversal flux gradient on the absorber, maximum temperature difference between tubes connected by the same plate is about $3 \text{ }^\circ\text{C}$. However the adjacent tubes of different panels, owing to their different metal temperature, are interested by a radiative heat exchange which causes temperature differences between tubes of the same plate (the extreme plates of each panel). The effect of this heat exchange is most effective between tubes of the 5th and 3rd panels which have a mean temperature difference of $137 \text{ }^\circ\text{C}$. Analysis is reported in App. A.

Sodium temperature at the outlet of the extreme tube of the 3rd panel is about $13 \text{ }^\circ\text{C}$ higher than those of the two other tubes connected together.

The effect of this extreme tubes heat exchange has been taken into account in plate design giving more flexibility to the 8 extreme plates of each panel by making cuts in the plates between the tube-plate connection weldings.

2. STIRRUP SYSTEM SUPPORTING BEAM THERMAL ANALYSIS

2.1. Object

Object of this section is the detail n. 2 of the map of fig. 1. See fig. 2a and 2b for relative detailed assembly drawing.

2.2. Gap

With reference to fig. 2b the nominal gap between each 3-tube group is 0.3 mm.

Taking into account dimensional and manufacturing tolerances a gap value of 1.2 mm (*) has been assumed for the thermal verification of the stirrup supporting beam.

2.3. Heat flux

The peak flux of 138 W/cm^2 is assumed to be positioned on the receiver absorber in correspondence of a stirrup supporting beam (**).

(*) This value has been obtained by adding in the worst way all the design tolerances.

(**) The Helios design map (P.R. N° 8, pag. 6) shows a maximum flux value in correspondence of the tube supports less than 100 W/cm^2 .

Heat flux distribution on the analysed support system has been evaluated according to section 1.3. No screen effect of the tube connected plate has been considered.

In fig. 7 the incident heat flux significant maps are shown.

2.4. Analysis model

In fig. 8 the beam mesh geometry is shown. All the cut edges of the beam have been considered adiabatic.

Under the assumption on heat flux and gap symmetry only one half on the beam has been analysed.

2.5. Analysis data list

The significant data for detail 2 analysis are:

Geometry

Upper and lower plate thickness (mm).. 5

C-beam thickness (mm) 10

Material AISI 304 L

Heat flux

Incident peak value on the
absorber (W/cm^2) 138

Heat flux distribution fig. 7

Thermal input data

Solar absorptance	0.8	(1)
I.R. emissivity	0.65	(2)
Convection power losses	none	
<u>Gap (mm)</u>	1.2	

2.6. Results

Fig. 9 show temperature distribution on the most significant surfaces of the beam. Surface identification letters are shown in fig. 8. The maximum temperature in the system is reached in sections GG'H'H and CC'D'D and is about 580 °C.

The temperature difference DT between the upper and lower plate of the beam end, which are differently irradiated by the entering solar heat flux, has been verified as regards to the possible thermal displacement of the stirrup pin.

(1) Assumed value for brown, after heating, stainless steel. The irradiated surfaces of the supporting beam are painted with white Pyromark series 2500. The painting reflectance has not been taken into account in the following thermal verification analysis.

(2) W.H. Mc Adams - Heat Transmission - 3rd Edition

A deformation analysis of the supporting beam, subjected to a constant DT between upper and lower plate for its whole length has been performed with the following results:

beam end deflection: 0.005 mm per DT degree

beam end rotation : 0.0013 rotation degree per DT degree

From the plots of fig. 9 it can be noted that the performed analysis shows:

- upper plate temperature in correspondence
of the pin hole ~ 550 °C
- lower plate temperature in correspondence
of the pin hole ~ 540 °C

The obtained deflection and rotation values guarantee for good thermal stability of the beam well over the calculated DT of about 10 °C: so this analysis has not been furtherly implemented.

3. BACKWALL THERMAL ANALYSIS

3.1. In the back of the tube bundle a double shield of mullite, high refractory Alumina based material, protects the back structure from the entering radiation.

See item 3 of the map of fig. 1 and the drawing of fig. 10 for detailed backwall thermal shield concept.

Each interstice between the mullite shield and the stirrup supporting beams and between the tube panels are closed with ceramic fiber felt. Object of this section is the evaluation of thermal performance of the backwall.

3.2. Gap

Because of the uncertainty to evaluate the gap width far from the tube restraints under high flux condition, it is necessary to investigate a sufficiently wide range of values of gap width to gain more confidence in the capability of the backwall to withstand high flux density.

So a gap width ranging from 1 to 3 mm has been analysed.

3.3. Analysis model

Hereafter the most important points of the model are reported:

- Maximum equilibrium temperature for the examined cases has been calculated by a finite element approach.
- No conduction occurs in the axial direction of the backwall.
- The gap width is assumed constant in the axial direction (2 D model).
- The same gap width is considered present between each tube of the panel.
- Thermal conductivity of ceramic fiber has been used to perform calculation because the mullite conductivity is one order of magnitude greater.
- No air convection losses occur.

3.4. Analysis data list

The significant data for backwall analysis are:

Geometry

Setback distance (mm)	0 + 50 (*)
Gap width (mm)	1 + 3

(*) Backwall setback selected value: 45 mm

Heat flux

Incident peak value on the
 tube (W/cm^2) 150
 Incident peak value on the backwall .. see fig. 11

Thermal data

Solar absorptance 0.3 (*)+ 0.8
 IR emissivity 0.7 (*)
 Radiation heat sink temperature ($^{\circ}\text{C}$).. 495 $^{\circ}\text{C}$
 Thermal conductivity Kaowool blanket
 (8 pcf)
 Convection power losses none

3.5. Results

Fig. 12 show the influence of the setback distance on the maximum backwall temperature taking into account the solar absorptance uncertainty range.

The calculated temperature peaks are well withstood by mullite thermal barriers over the entire analysis ranges: mullite refractoriness is 1850 $^{\circ}\text{C}$.

Also the use of ceramic fiber to close each interstices between stirrup supporting beams and mullite shields, so as the junctions of the five panels, is adequate taking into account a chosen setback distance of 45 mm for ASR backwall.

(*) Experimentally checked values for kaowool blanket reported in: EPRI ER-629 - Project 377-1 Final Report January 1978.

4. INCIDENT HEAT FLUX DISTRIBUTION ON THE BACKWALL

A complete analysis of the solar flux through the tube gap by using Helios computer program is carried out.

As Helios considers only plane window and disregards aperture thickness, overlay C is modified and a testing on each reflected ray introduced to verify if the ray path is intercepted by the tubes. If the reflected sun ray strikes on the tube wall, owing to the high absorptivity of the paint layer, the assumption is made that no reflection of radiation on the backwall occurs. On the contrary if the ray passes through the tubes, it gives an incident heat flux contribution to the backwall.

Calculated heat flux distribution and peak values on the backwall are shown in the graphs of fig. 13 and 14, considering a tube axis - backwall distance of 60 mm (set back value of 53 mm).

In fig. 15 a comparison is made between two calculations of heat flux distribution carried out with two different assumptions about heliostats aiming strategy:

- single aiming point
- 3 aiming points

with a gap width of 8 mm.

All the referred results are obtained considering:

- incident peak value on the tubes: 129 W/cm^2 (*)
- only one gap present that contributes to the heat flux distribution on the backwall (no - overlapping).

In Appendix B some analytical details of the Helios code modification are reported.

(*) Incident heat flux value on the target center according to heat flux design map (P.R. N° 8, pag. 6).

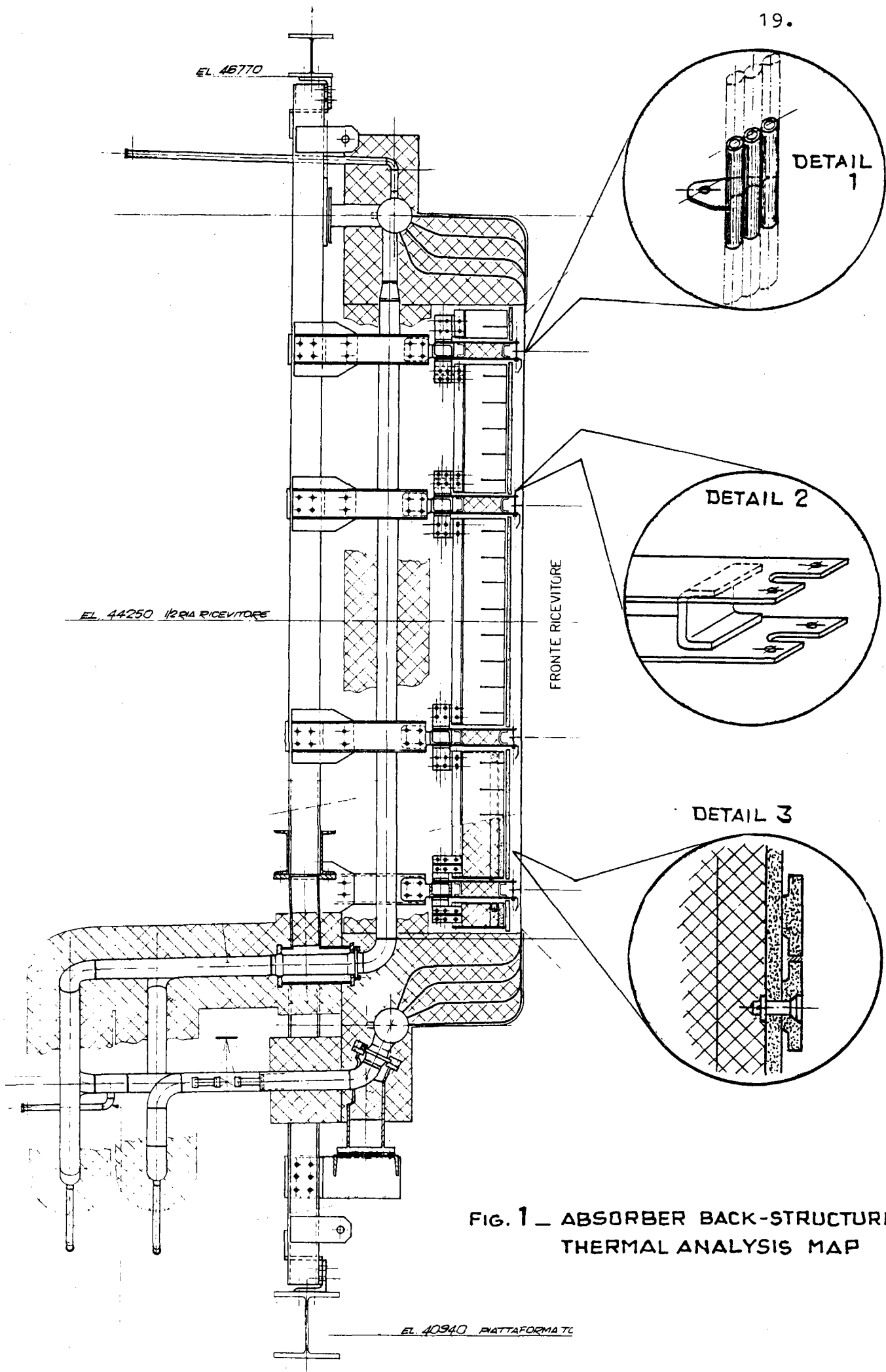


FIG. 1 - ABSORBER BACK-STRUCTURE
THERMAL ANALYSIS MAP

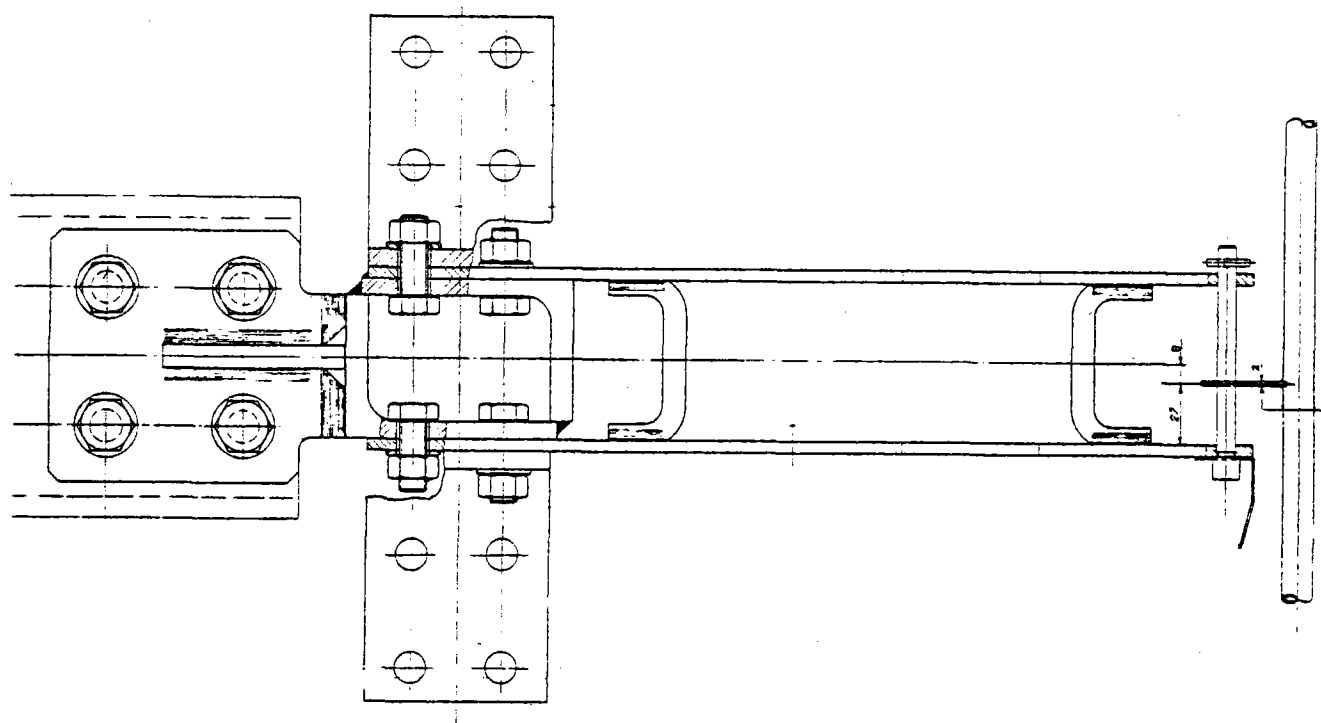
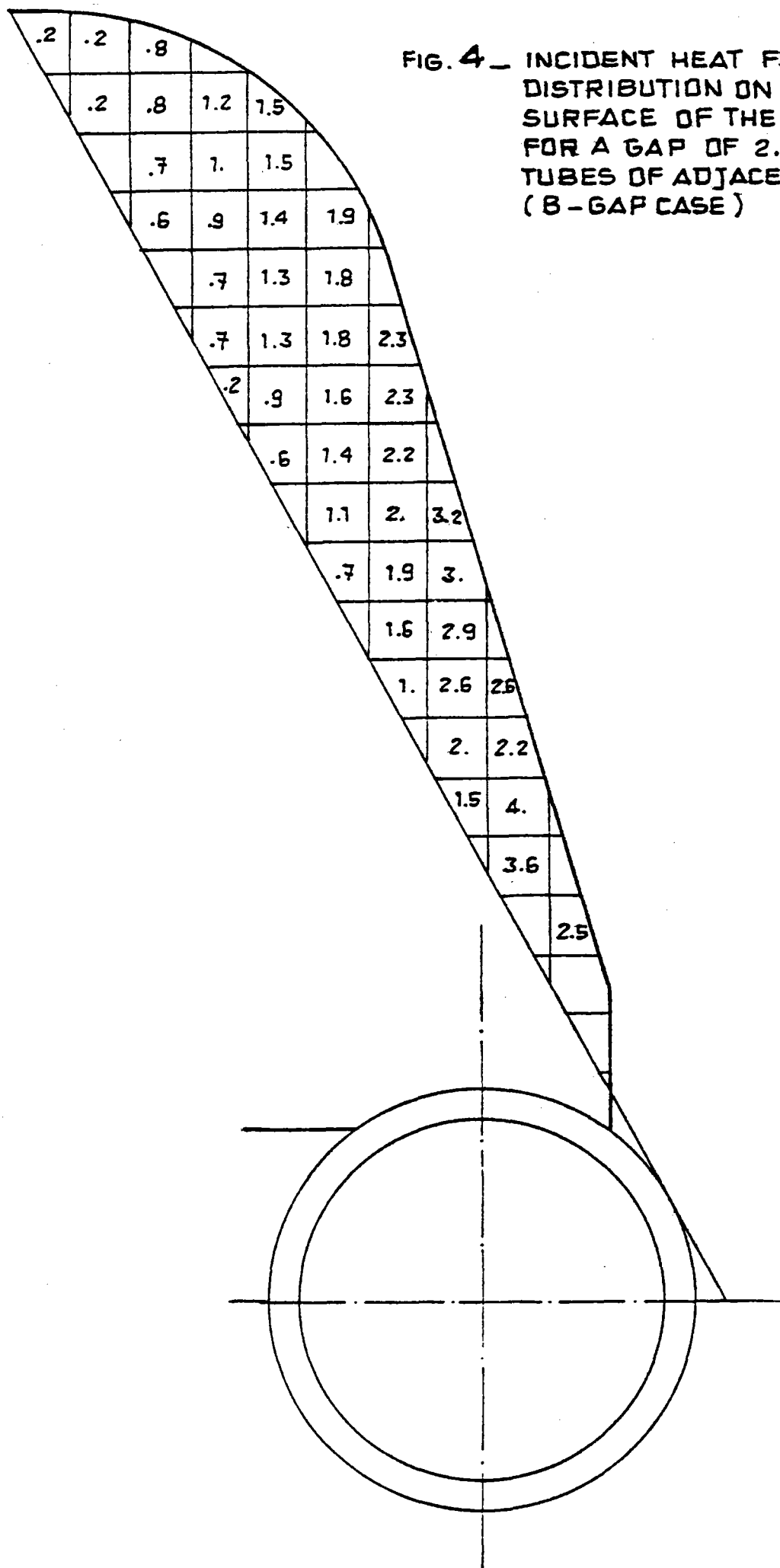
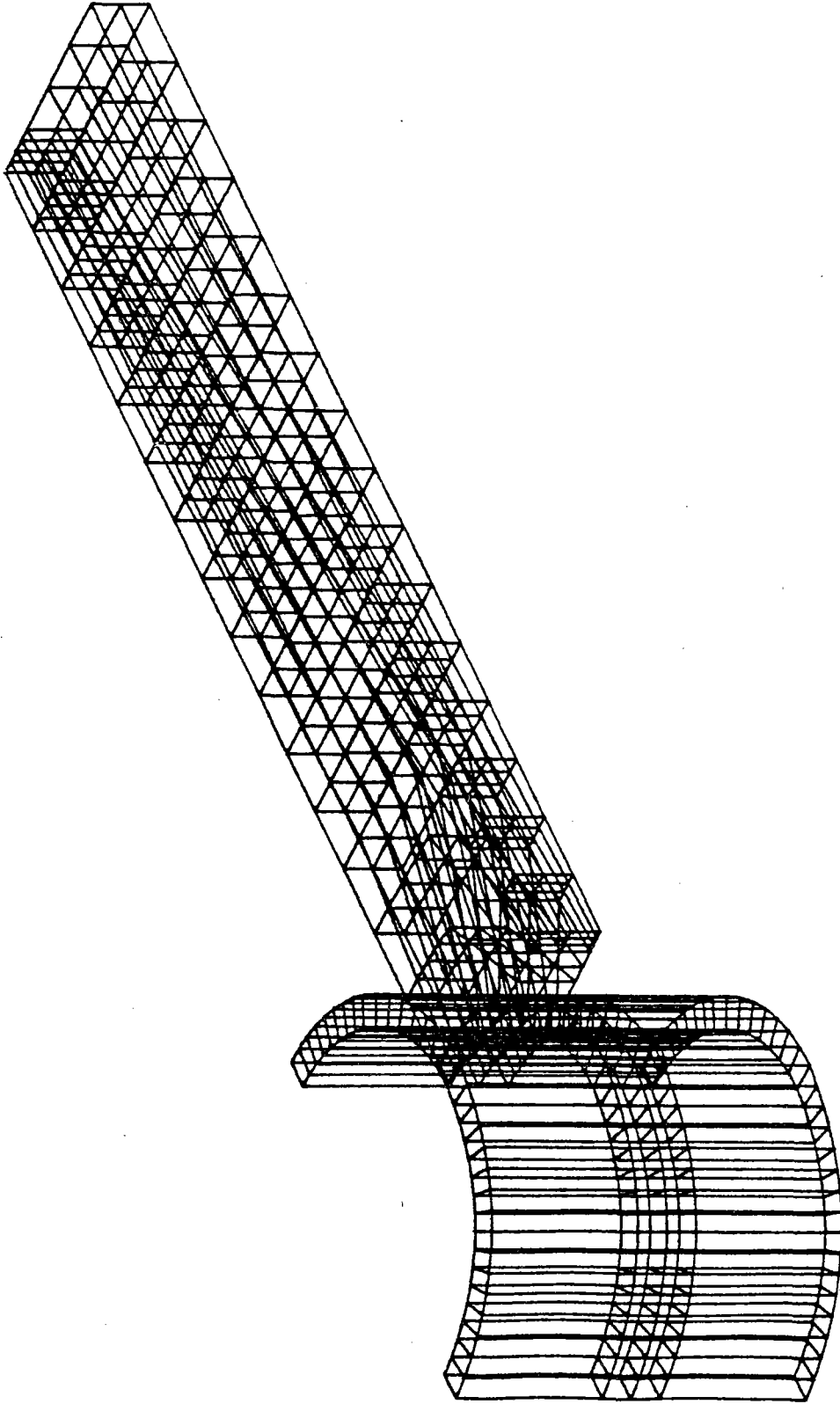


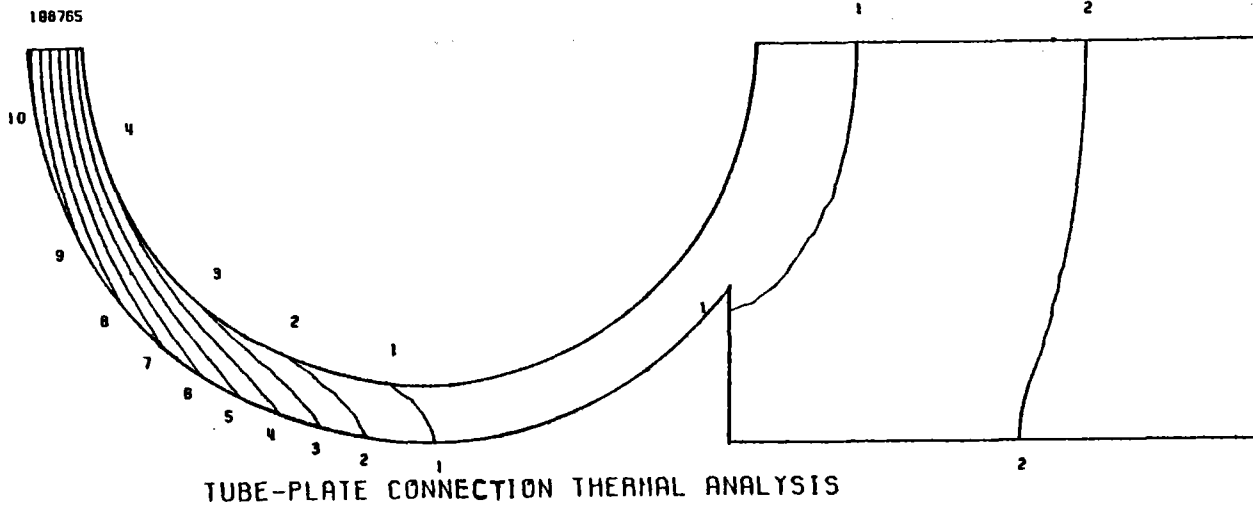
FIG. 2A _STIRRUP SUPPORTING SYSTEM



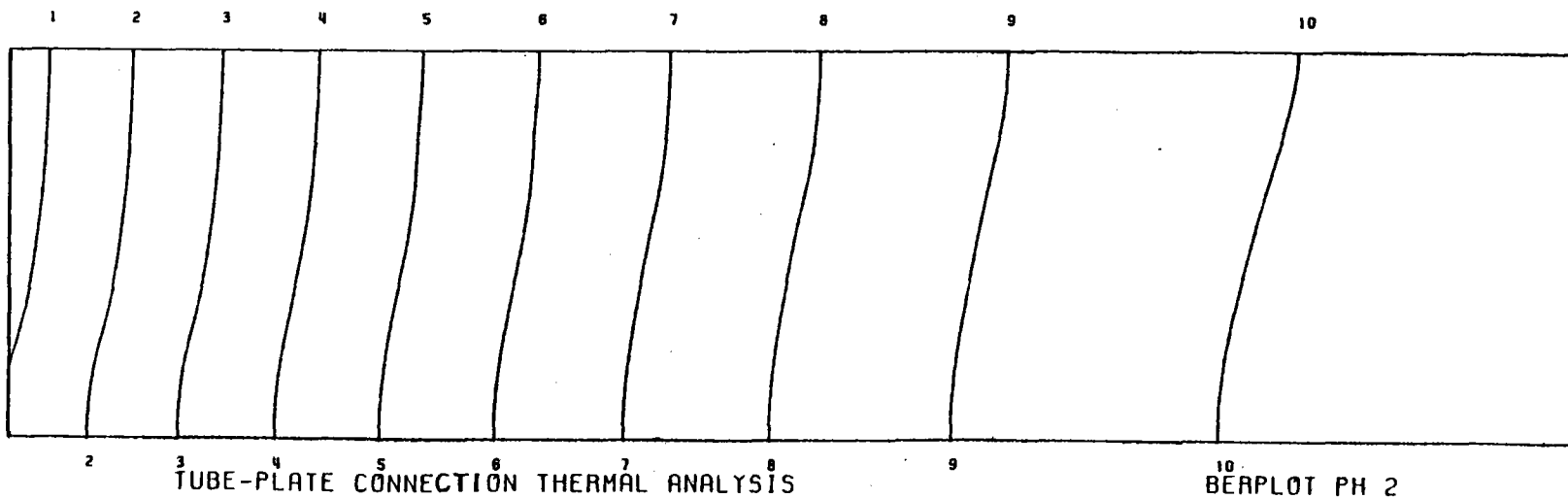


PLOT OF COMPONENT 1 - MESH PLOT 0.0 30.0 45.0 60.0

FIG. 5 -- TUBE - PLATE CONNECTION THERMAL ANALYSIS: 3D MESH PLOT



KEY	
1	0.500448E3
2	0.511049E3
3	0.521649E3
4	0.532248E3
5	0.542849E3
6	0.553449E3
7	0.564049E3
8	0.574649E3
9	0.585249E3
10	0.595850E3



KEY	
1	0.518739E3
2	0.521418E3
3	0.524098E3
4	0.526778E3
5	0.529458E3
6	0.532138E3
7	0.534817E3
8	0.537497E3
9	0.540177E3
10	0.542856E3

FIG. 6 — TEMPERATURE DISTRIBUTION IN THE TUBE THICKNESS AND IN THE LOWER SURFACE OF THE STRIP FOR 0.2mm GAP

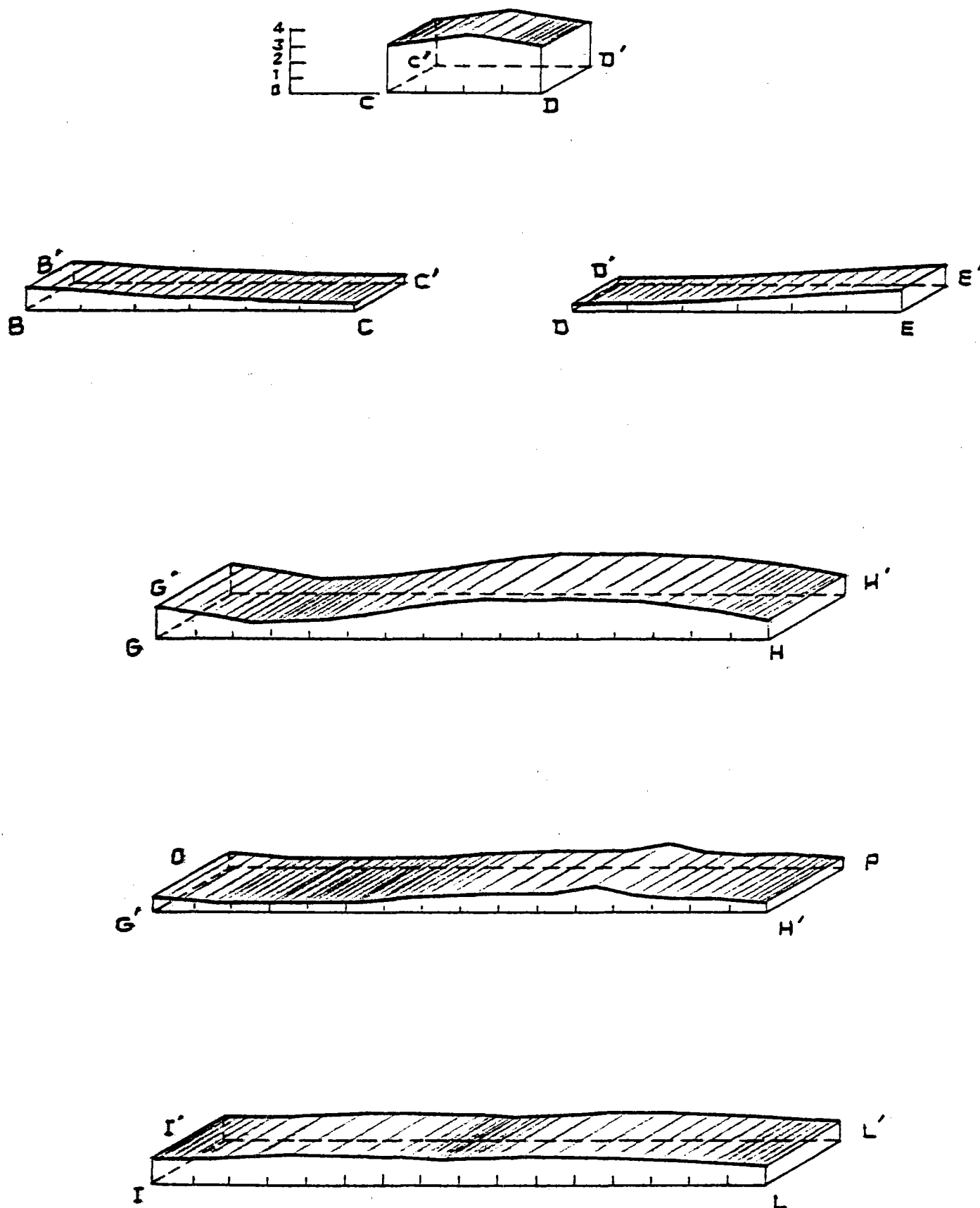


FIG. 7 - INCIDENT HEAT FLUX ON THE MOST SIGNIFICANT SURFACES OF THE STIRRUP SYSTEM SUPPORTING BEAM (SEE FIG. 8 FOR SURFACES IDENTIFICATION LETTERS)

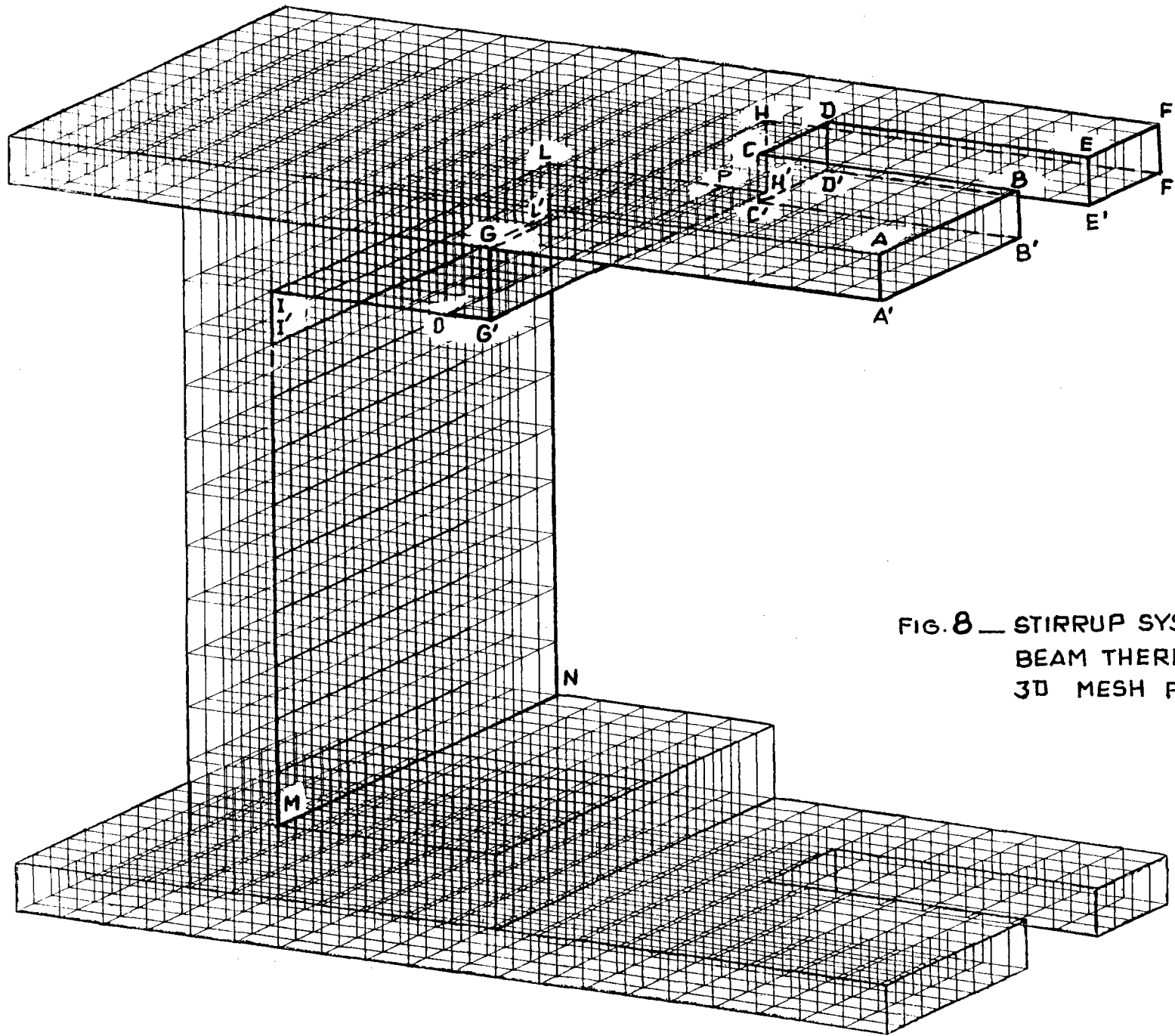
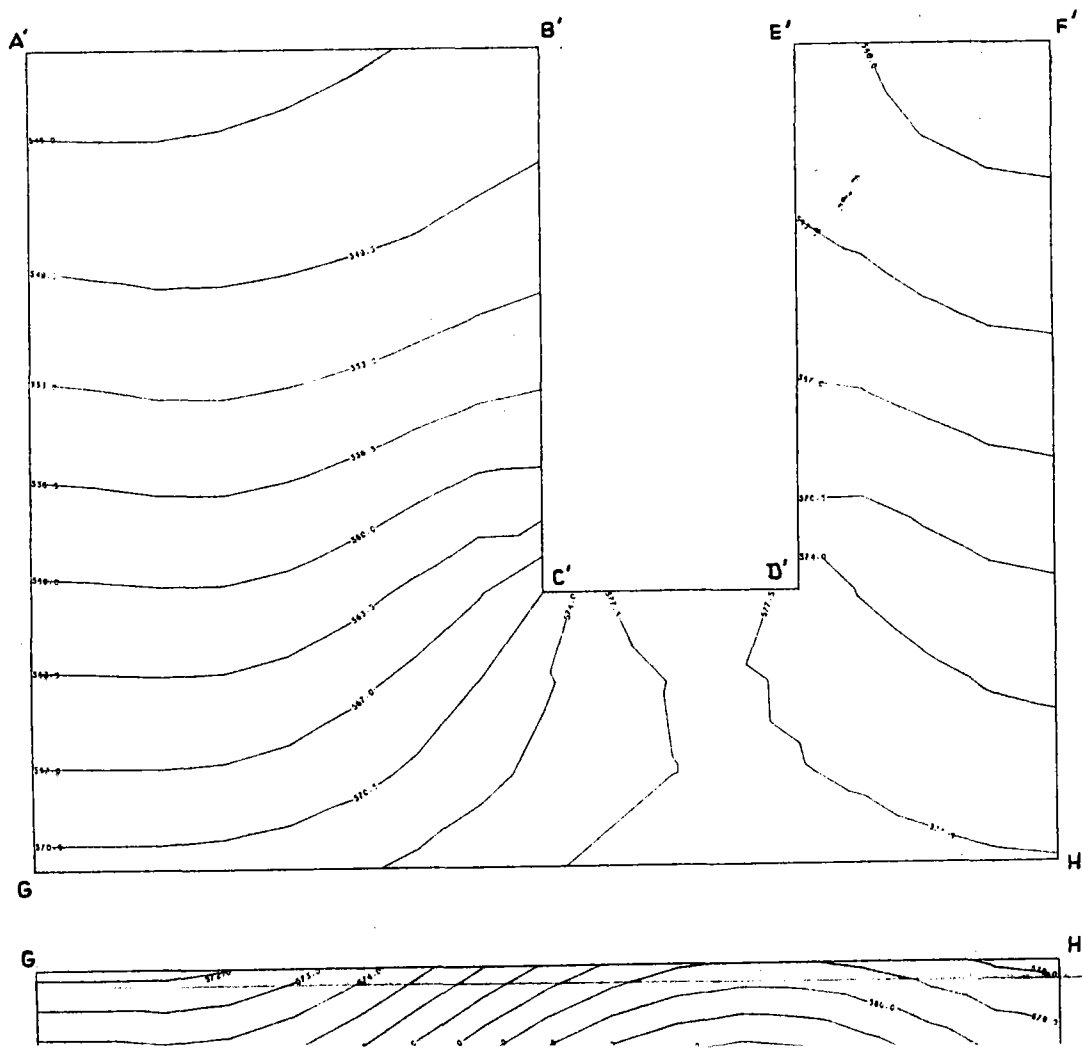
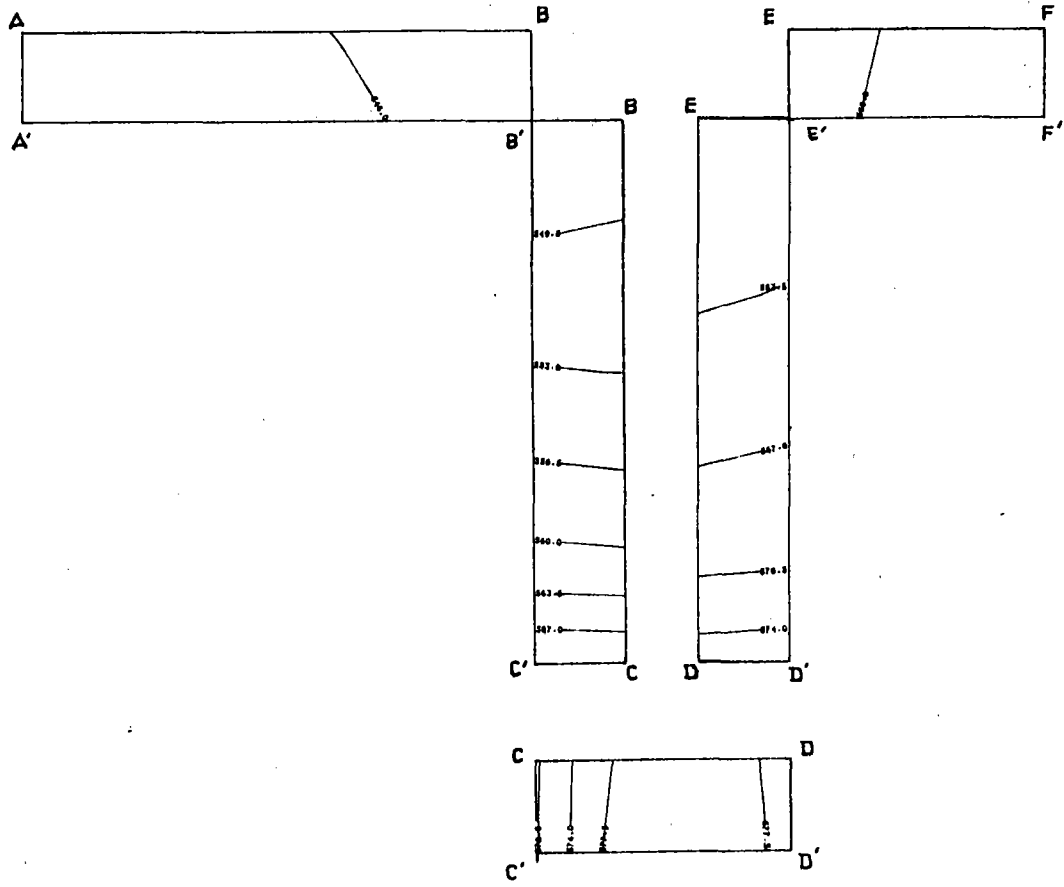
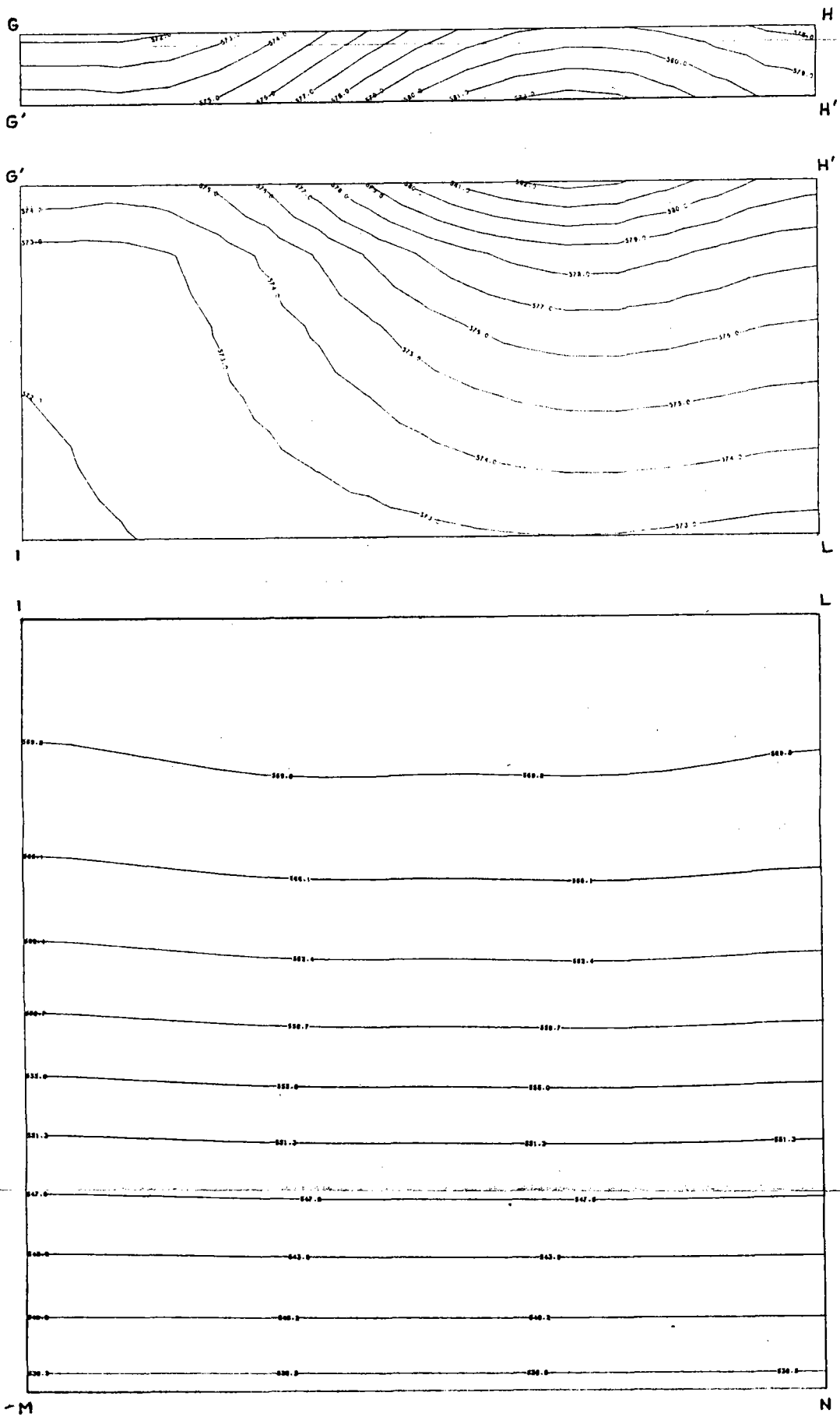


FIG. 8 — STIRRUP SYSTEM SUPPORTING
BEAM THERMAL ANALYSIS:
3D MESH PLOT





STIRRUP SYSTEM SUPPORTING BEAM THERMAL ANALYSIS

FIG. 9 TEMPERATURE DISTRIBUTION IN THE MOST SIGNIFICANT SECTIONS OF THE STIRRUP SYSTEM SUPPORTING BEAM

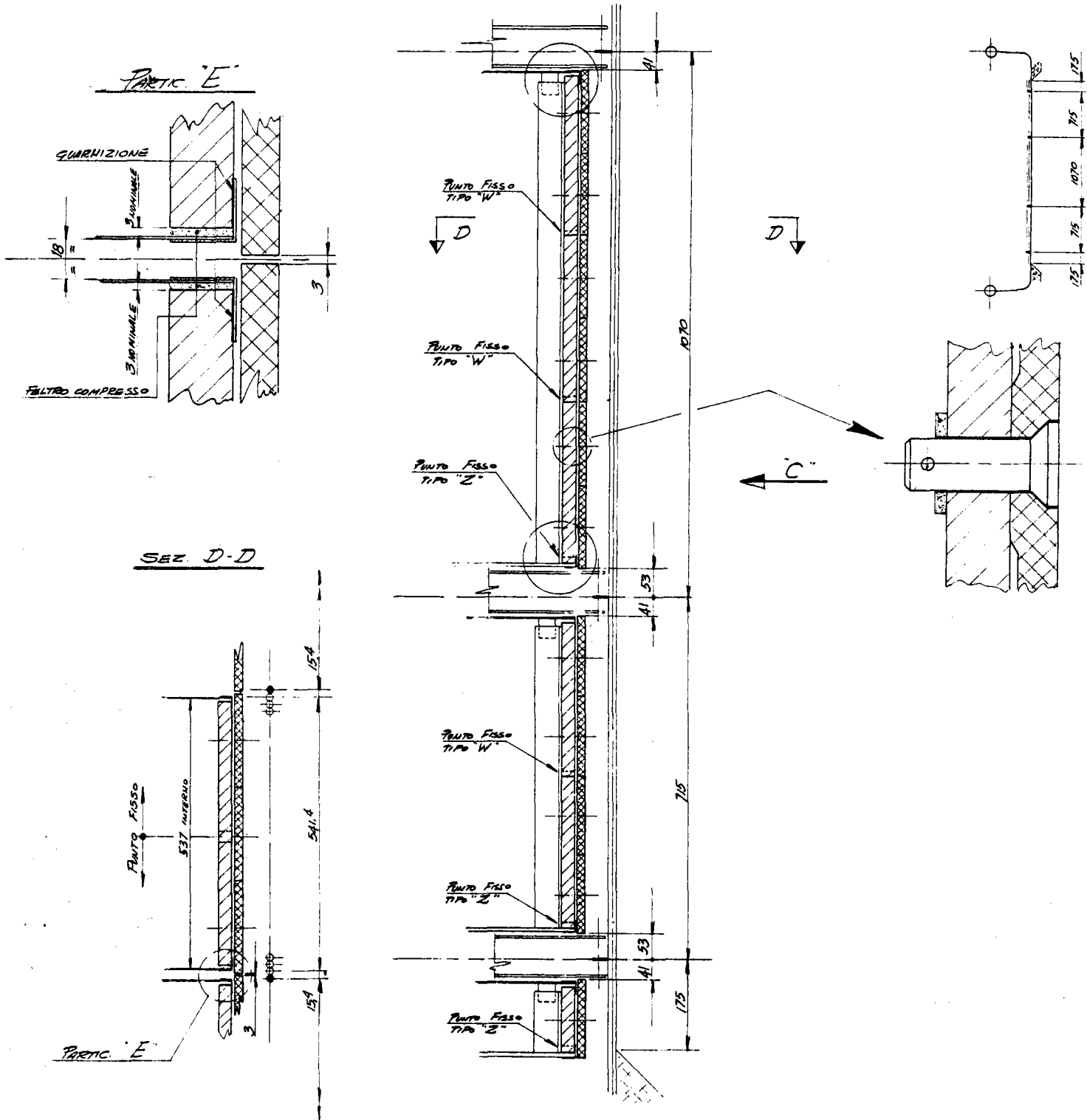
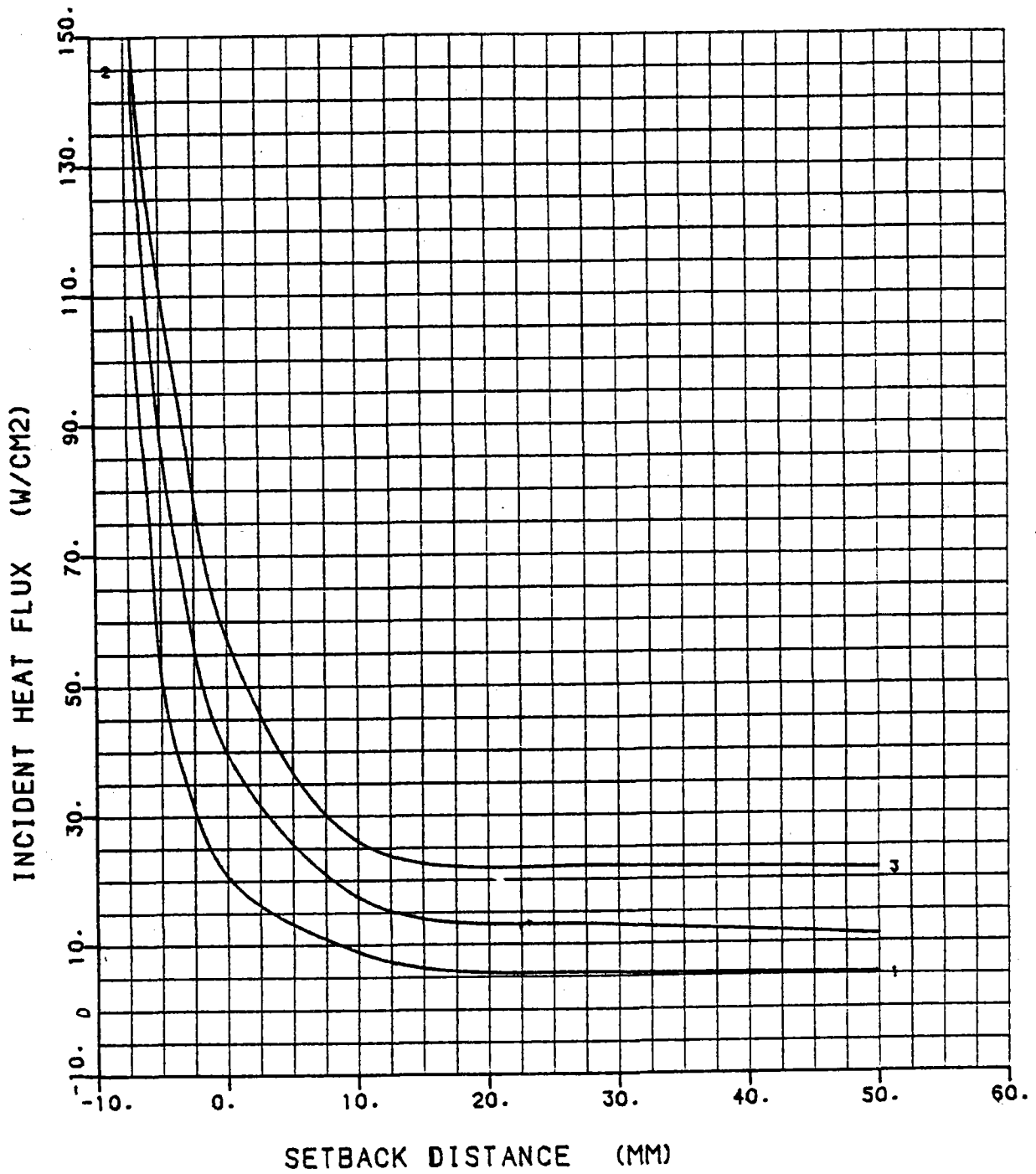


FIG. 10 - BACKWALL THERMAL SHIELD CONCEPT

INCIDENT HEAT FLUX VS SETBACK DISTANCE
AND GAP WIDTH



CURVA 1/ GAP WIDTH = 1. MM
CURVA 2/ GAP WIDTH = 2. MM
CURVA 3/ GAP WIDTH = 3. MM

— FIG. 11 —

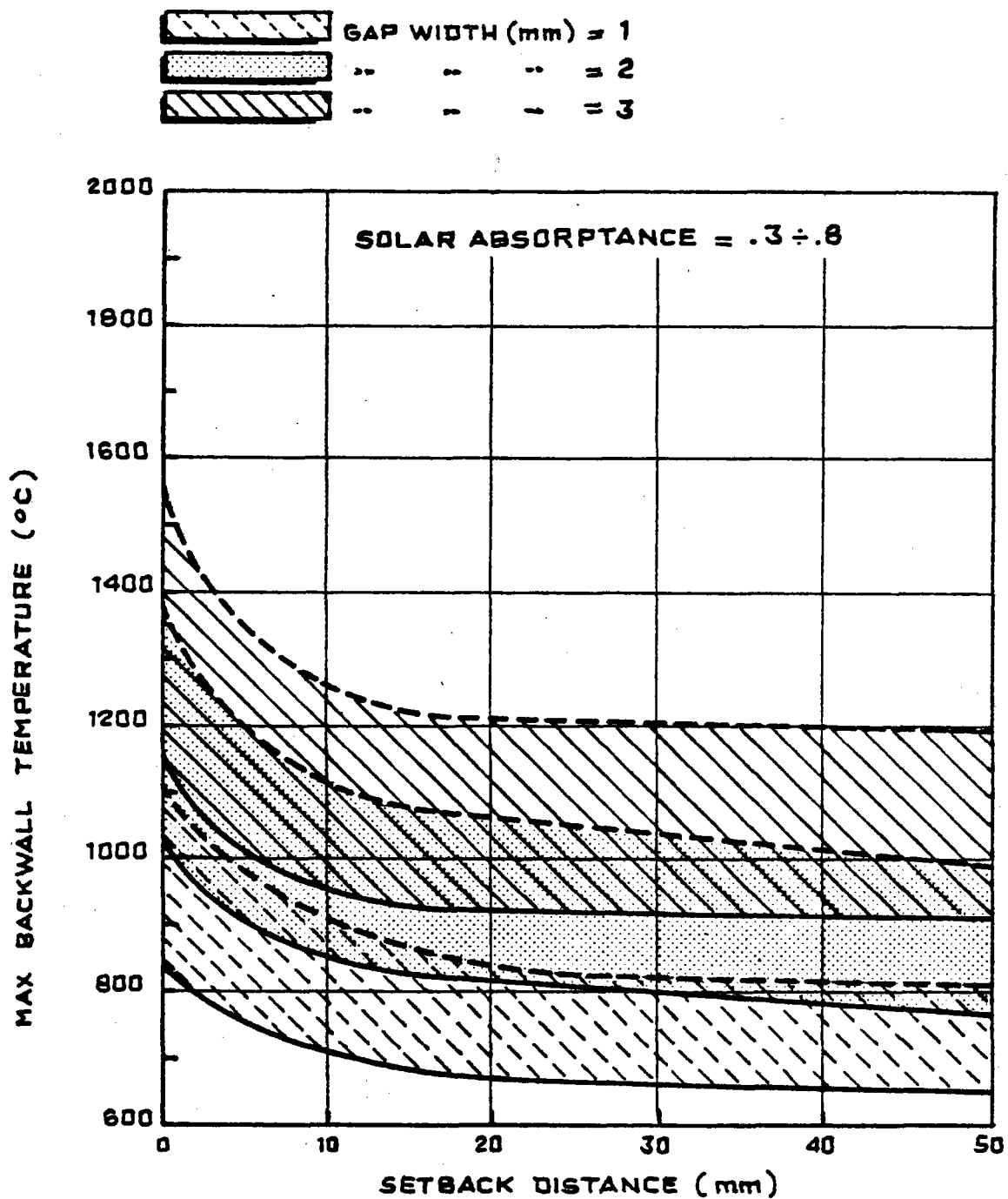


FIG. 12_ INFLUENCE OF SETBACK DISTANCE ON
MAXIMUM BACKWALL TEMPERATURE

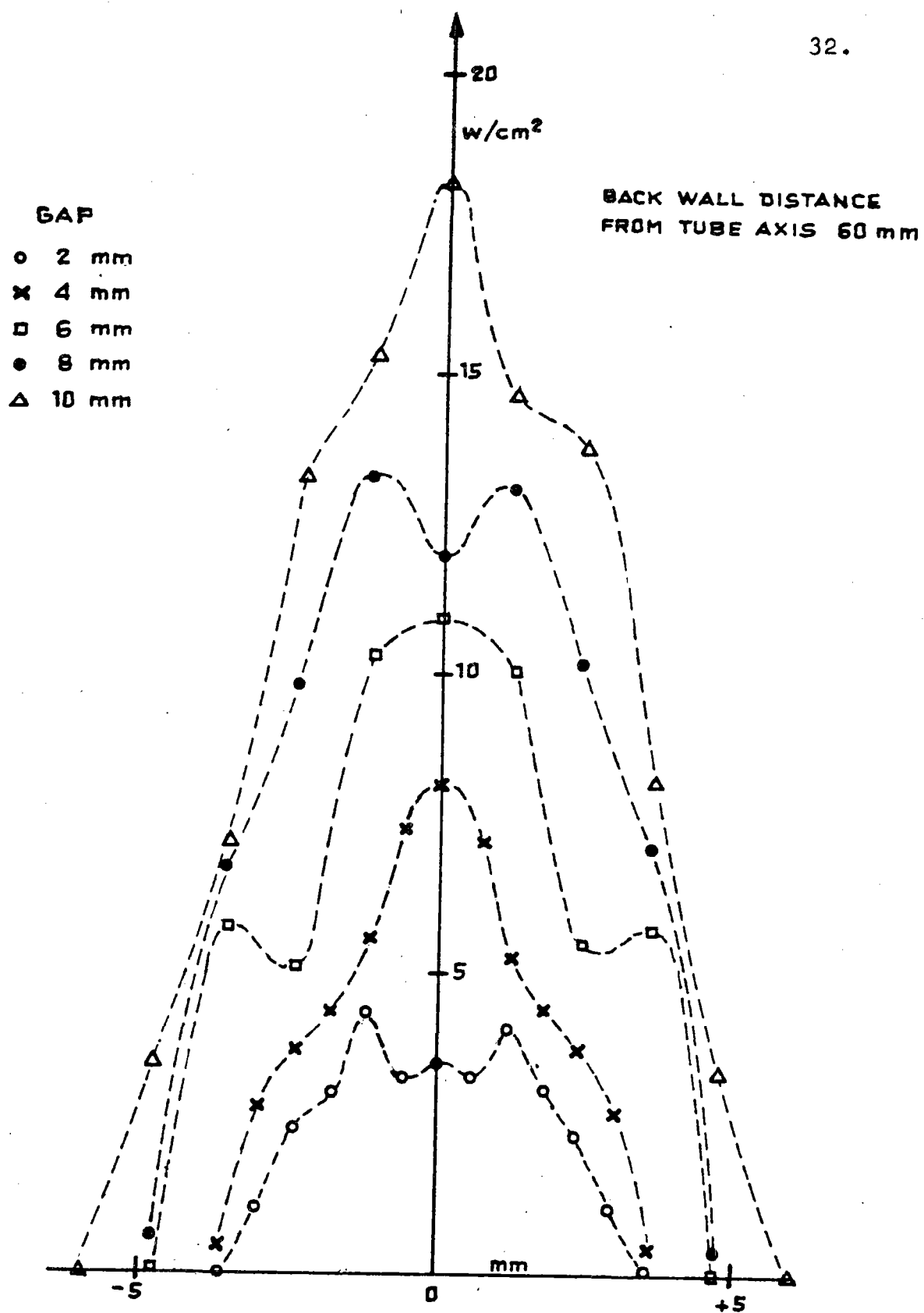


FIG. 13 — SOLAR FLUX THROUGH THE GAP

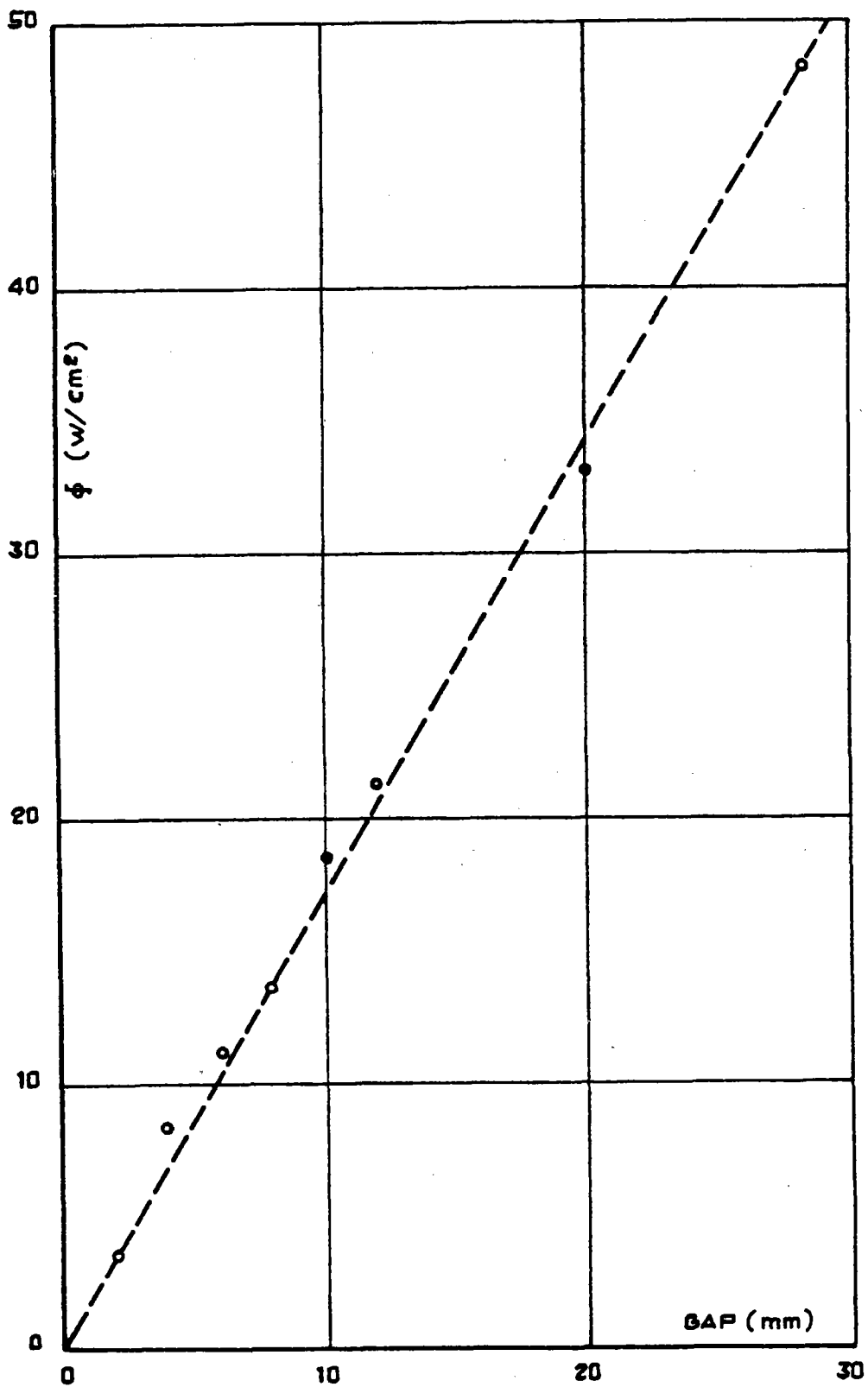


FIG. 14 - BACKWALL FLUX VS GAP

- X SINGLE AIMING POINT
● 3 AIMING POINTS

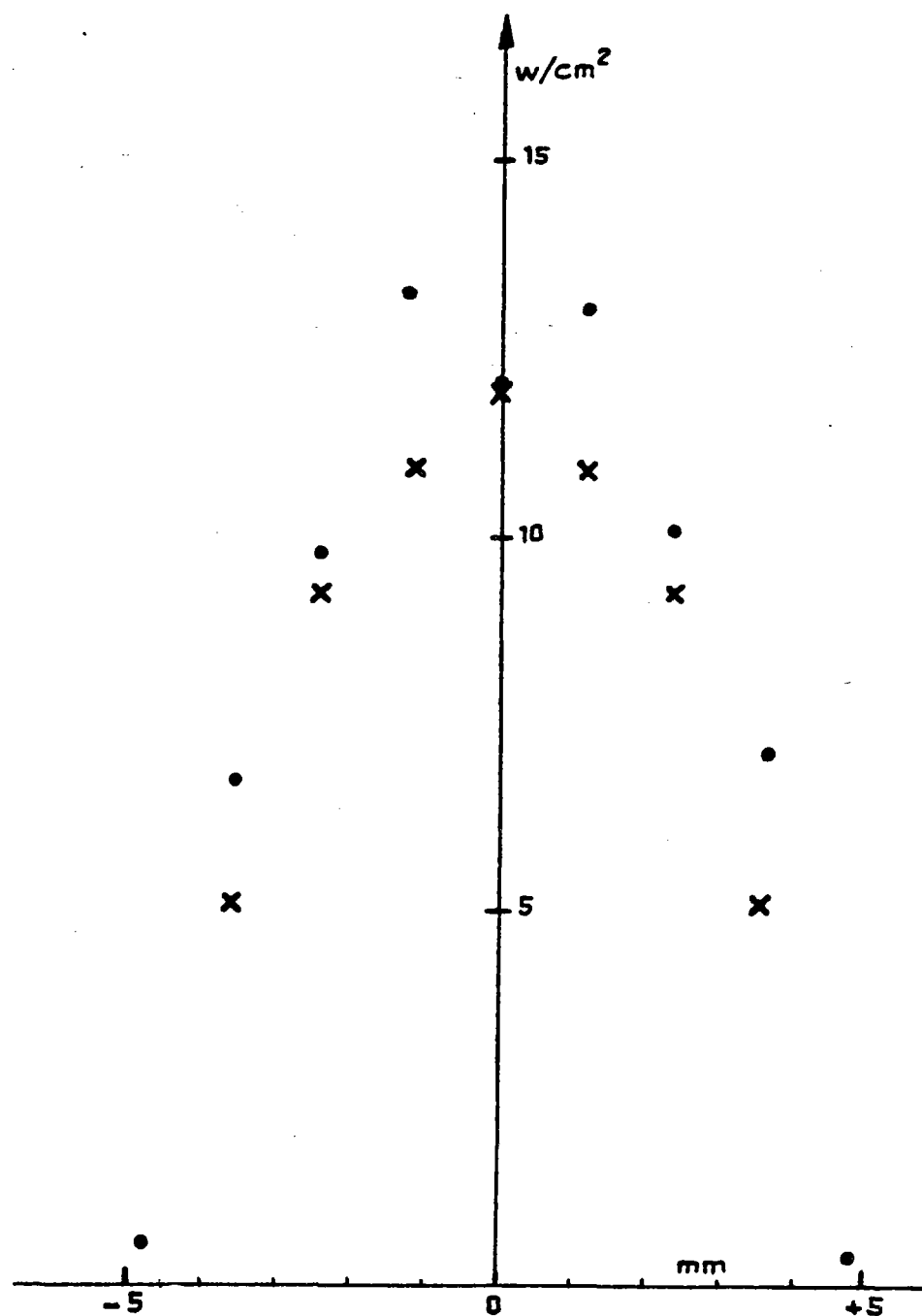


FIG. 15 - SINGLE AIMING - 3 AIMING COMPARISON
(GAP = 8 mm)

A P P E N D I X A

RADIATION EXCHANGE BETWEEN THE EXTREME TUBES OF
EACH PANEL

By numbering all the absorber tubes from 1 to 195 starting from the coldest panel, the extreme tubes of each panel and the relative mean external wall temperature T_w are reported in the following sketch:

	□ 1	□ 4	□ 5	□ 3	□ 2
tube n°	→ 39	↓ 40 ↓ 78	↓ 79 ↓ 117	↓ 118 ↓ 156	↓ 157
T_w	→ 305	417 442	510 510	373 348	325

The temperature difference between the extreme tubes of the 5 panels are:

$$\Delta T_{1-4} \quad 112 \text{ } ^\circ\text{C}$$

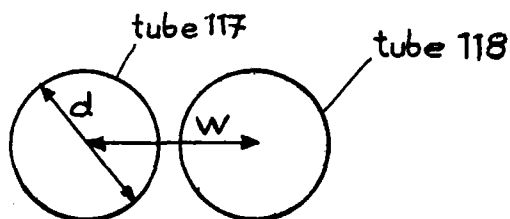
$$\Delta T_{4-5} \quad 68 \text{ } ^\circ\text{C}$$

$$\Delta T_{5-3} \quad 137 \text{ } ^\circ\text{C}$$

$$\Delta T_{3-2} \quad 23 \text{ } ^\circ\text{C}$$

The maximum temperature difference is between the 5th and 3rd panels (tube n. 117 and 118).

Hereafter the calculation is reported to evaluate the outlet sodium temperature increase ΔT_N in the tube 118 due to the radiation heat exchange with the tube 117. This calculation refers to a partial load of the receiver of 10%.



h = tube length effective for radiation exchange

$$Q_{12} = A_1 \cdot F_{12} \cdot \sigma (T_1^4 - T_2^4)$$

$$A_1 = h \times \pi \times d = 3.52 \times \pi \times 0.014 = 0.155 \text{ m}^2$$

$$F_{12} = \frac{1}{\pi d} \left(d \sin^{-1} \frac{d}{w} + \sqrt{w^2 - d^2} - w \right) \quad \text{for } w = d$$

$$F_{12} = \frac{\pi - 2}{2\pi} = 0.18$$

σ = Stefan · Boltzmann constant

$$T_1 = T_{W(117)} + 273 = 783 \text{ }^\circ\text{K}$$

$$T_2 = T_{W(118)} + 273 = 646 \text{ }^\circ\text{K}$$

$$Q_{12} = 0.155 \times 0.18 \times 5.73 \cdot 10^{-8} (783^4 - 646^4) = 323 \text{ W}$$

ΔT_N = outlet sodium temperature increase in tube 118
due to the radiation heat exchange with tube 117.

\dot{m}_{10} = flow rate at 10% partial load per tube =
= $0.73 / 39 = 0.0187$ kg/sec

$C_p = 1290$ J/kg \cdot $^{\circ}\text{C}$ ($T = 353$ $^{\circ}\text{C}$)

$\Delta T_N = 323 / (0.0187 \times 1290) = 13.4$ $^{\circ}\text{C}$

A P P E N D I X B

Evaluation of heat flux distribution on the backwall by using Helios computer code.

To evaluate if the mirror element S gives a contribution to the heat flux incident on the backwall point T, the following check on the ray path has been added to the code.

With reference to fig. B/1 the condition has been imposed to the ray that it must not interfere with the two cylindrical surfaces representing the tubes with the vertical axes containing the points C1 and C2 respectively.

This means that the ray-line ST must pass at a distance \overline{AB} from the two tube vertical axes:

$$\overline{AB} \geq D/2$$

The distance \overline{AB} results:

$$\overline{AB} = \left| \pm \frac{(\frac{D}{2} + Y_s) \cos \alpha - (\pm \frac{P}{2} + X_s) \cos \beta}{\sqrt{\cos^2 \alpha + \cos^2 \beta}} \right|$$

with $\cos \alpha$ and $\cos \beta$ the direction cosines of the line TS with respect to X and Y axes.

If $\overline{AB} \geq D/2$ the intensity of the considered ray gives a contribution to the analysed backwall point T.

To calculate the incident flux on the backwall the cosine effect has to be taken into account:

$$\cos \theta = \vec{n}_T \cdot \vec{r}$$

where:

$$\vec{r} = \cos \alpha \vec{i} + \cos \beta \vec{j} + \cos \gamma \vec{k}$$

The versor \vec{n}_T (interception plane normal) has to be assigned to the code as input data:

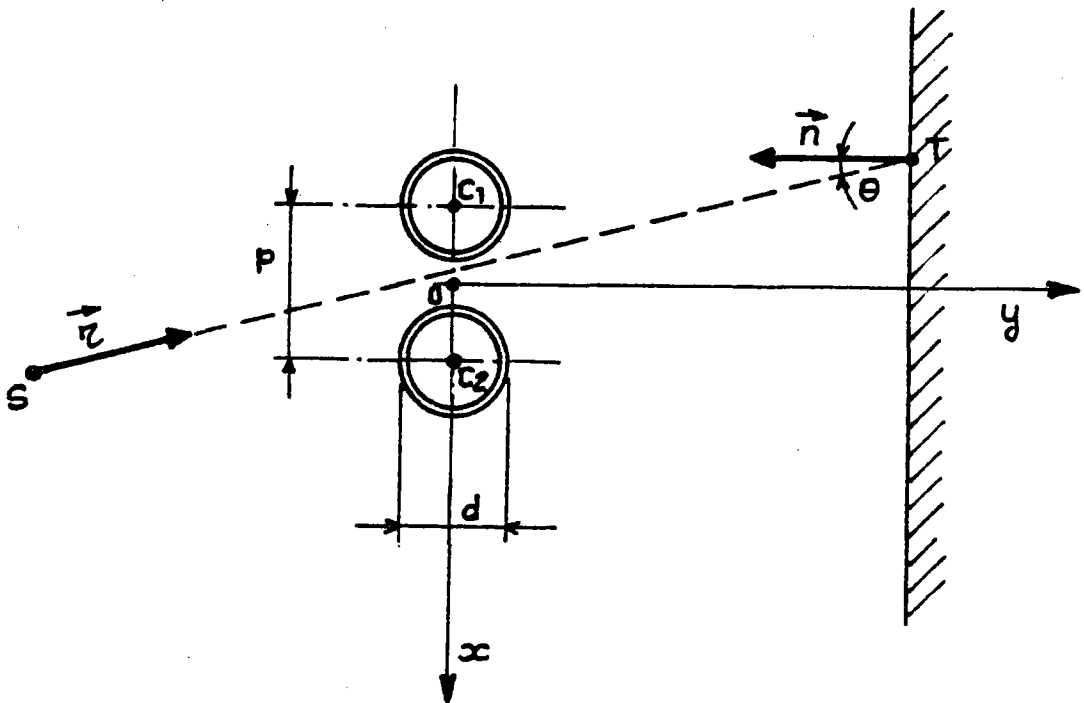
$$\vec{n}_T = a \vec{i} + b \vec{j} + c \vec{k}$$

So one may write:

$$\cos \theta = a \cos \alpha + b \cos \beta + c \cos \gamma$$

At this point the intensity in T is given by:

$$I_{\alpha, \beta, \gamma} = R (\cos \alpha, \cos \beta, \cos \gamma) \cdot \cos \theta$$



$$C_1 \left(-\frac{p}{2} ; -\frac{d}{2} \right)$$

$$C_2 \left(+\frac{p}{2} ; -\frac{d}{2} \right)$$

$$T (x_T, y_T, z_T)$$

$$S (x_S, y_S, z_S)$$

— FIG. B/1 —

IEA ALMERIA PROJECT

ADVANCED SODIUM RECEIVER

ASR

Receiver piping system stress analysis

Topic Report No. 9

Revision 0

November 1982

Prepared by: ENEL

FRANCO TOSI

AGIP NUCLEARE

CONTENTS

1. Abstract
2. Piping system description with limit of supply
3. Design and operating conditions
 - 3.1. Design data
 - 3.2. Operating data
 - 3.2.1. Transient operating conditions
 - 3.2.2. Temperature gradient distribution in transient conditions
 - 3.3. Material basic data
4. General description of pipe supports and restraints
 - 4.1. Variable and constant spring hanger supports
 - 4.2. Restraints
5. Piping flexibility analysis
 - 5.1. Analysis method

5.2. Piping system structural analysis

5.2.1. Weight analysis

5.2.2. Thermal expansion analysis

5.2.3. Earthquake analysis

6. Piping flexibility results and compliance analysis

6.1. Codes and rules used

6.2. Piping flexibility results

6.3. Compliance analysis with NB3600

6.4. Compliance analysis with Code Case N47-17-3600

6.4.1. Operating conditions

6.4.2. Considerations about the analysis

6.4.3. Compliance with design loads

6.4.4. Compliance with service loads

Appendix 1

1. ABSTRACT

The goal of this report is to investigate about the mechanical stability of the ASR piping system consisting of the connecting pipes between panels and of the draining and vent pipes.

A geometrical description of the system is carried out as well as the definition of all the operating conditions.

After words a flexibility analysis, by means of the computer code SAP V, is reported and finally a compliance analysis based on ASME Code is contained.

2. PIPING SYSTEM DESCRIPTION WITH LIMIT OF SUPPLY

The piping system considered in the following analysis is shown in fig. 2./1. The system consists of:

- LEG 1 - Inlet leg.; locations 1 through 2, 3 (fig. 2./2)
- LEG 2 - Outlet leg., locations 4 through 5, 6, 7, 8 (fig. 2./3)
- LEG 3 - Crossover from 1st to 2nd panel, locations 9 through 10, 11, 12, 13, 14, 15 (fig. 2./4)
- LEG 4 - Crossover from 2nd to 3th panel, locations 16 through 17, 18, 19, 20, 21, 22 (fig. 2./5)
- LEG 5 - Crossover from 3th to 4th panel, locations 23 through 24, 25, 26, 27, 28, 29 (fig. 2./6)
- LEG 6 - Crossover from 4th to 5th panel, locations 30 through 31, 32, 33, 34, 35, 36 (fig. 2./7)
- LEG 7 - Draining leg., locations 22 through 37, 29, 36, 15, 4 (fig. 2./8)
- LEG 8 - Overflow leg., locations 16 through 38, 23, 8, 30, 9, 39, 40, 41 (fig. 2./9)

The limits of supply are at the locations 1, 5, 41 above the valves and 4 (comprehensive of 3"½ x 2" butt welding TEE).

For the analysis the inlet, outlet and overflow legs above 33895 mm level up to the platform level have been

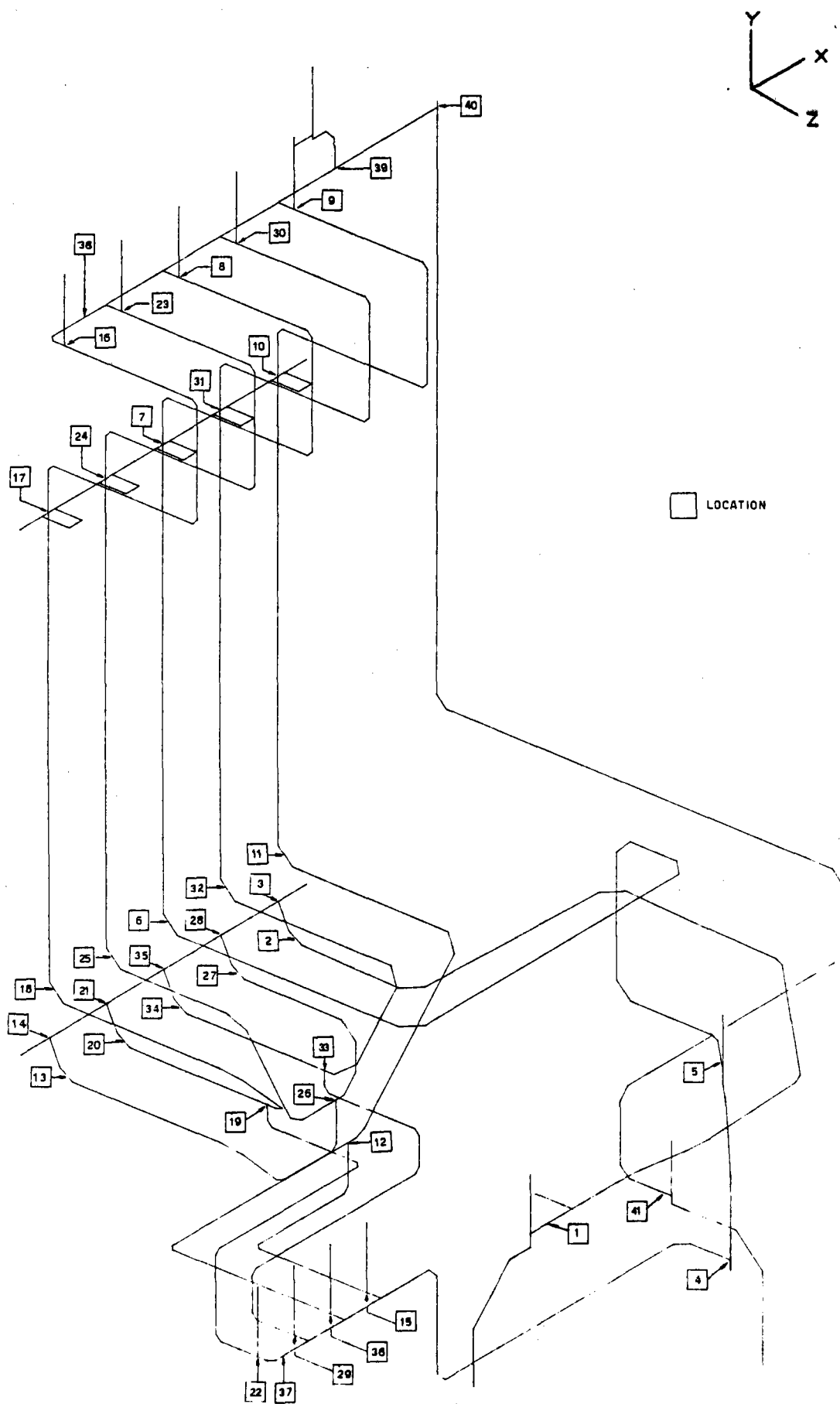
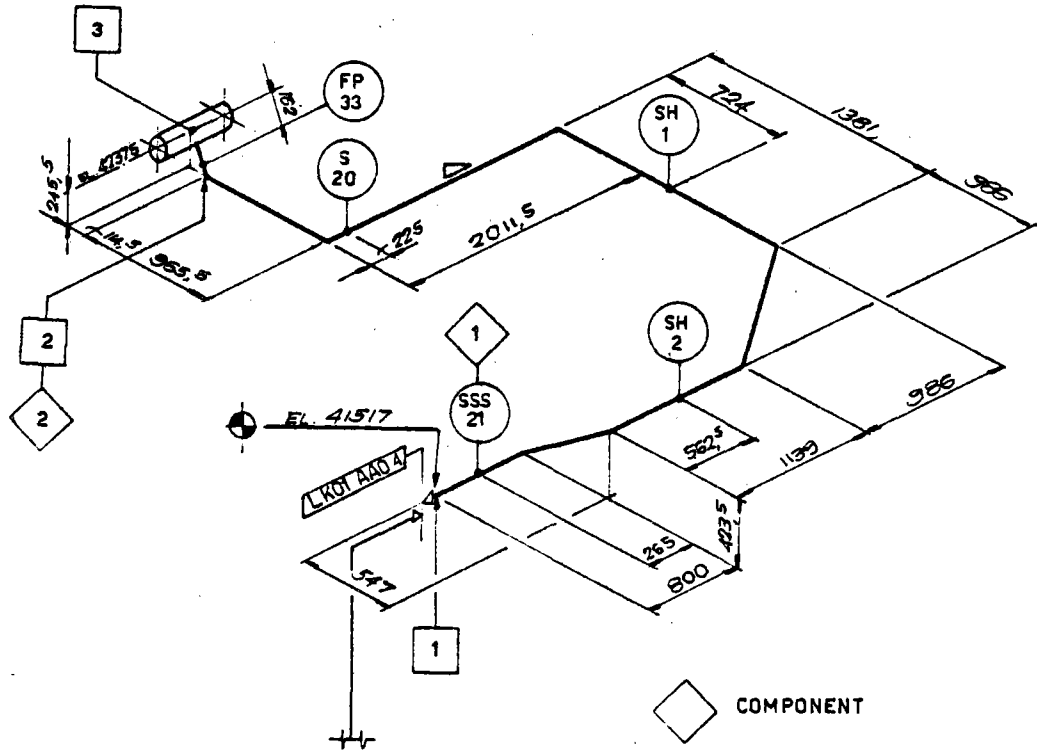






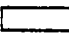



FIG. 2 /1

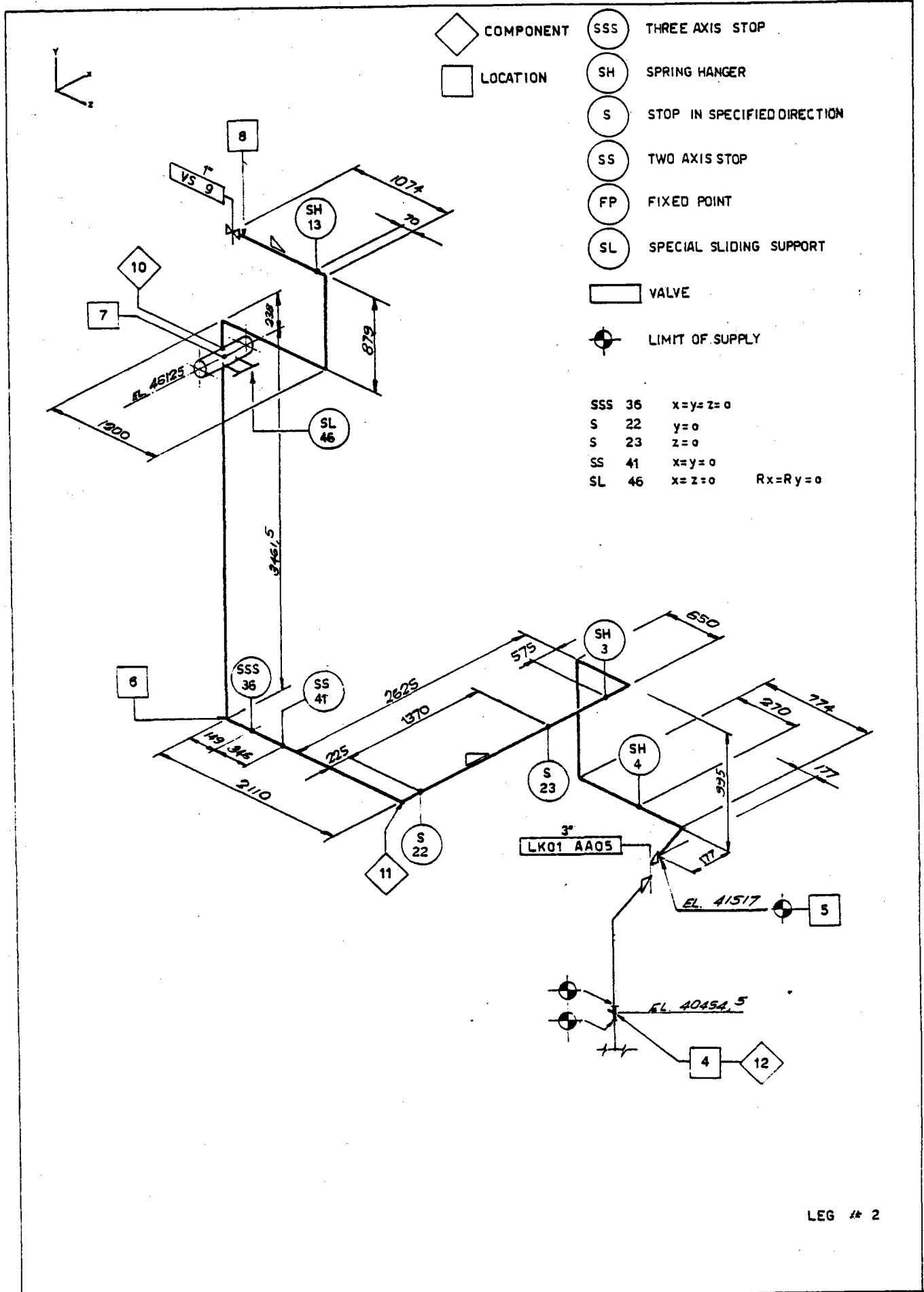


-  COMPONENT
-  LOCATION
-  SPRING HANGER
-  STOP IN SPECIFIED DIRECTION
-  THREE AXIS STOP
-  FIXED POINT
-  VALVE
-  LIMIT OF SUPPLY

S 20 y=0
 SSS 21 x=y=z=0

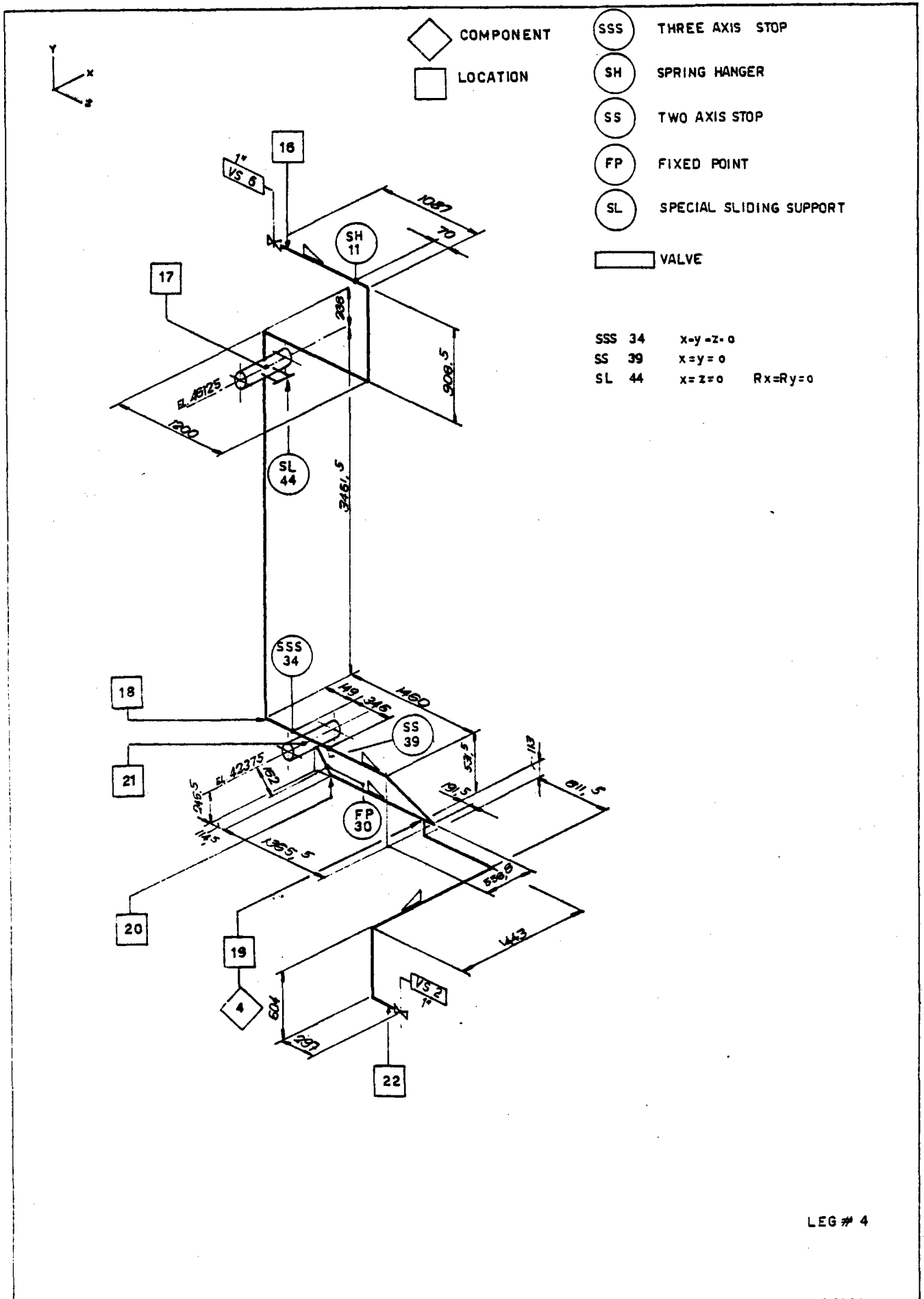
LEG # 1

FIG. 2. /2



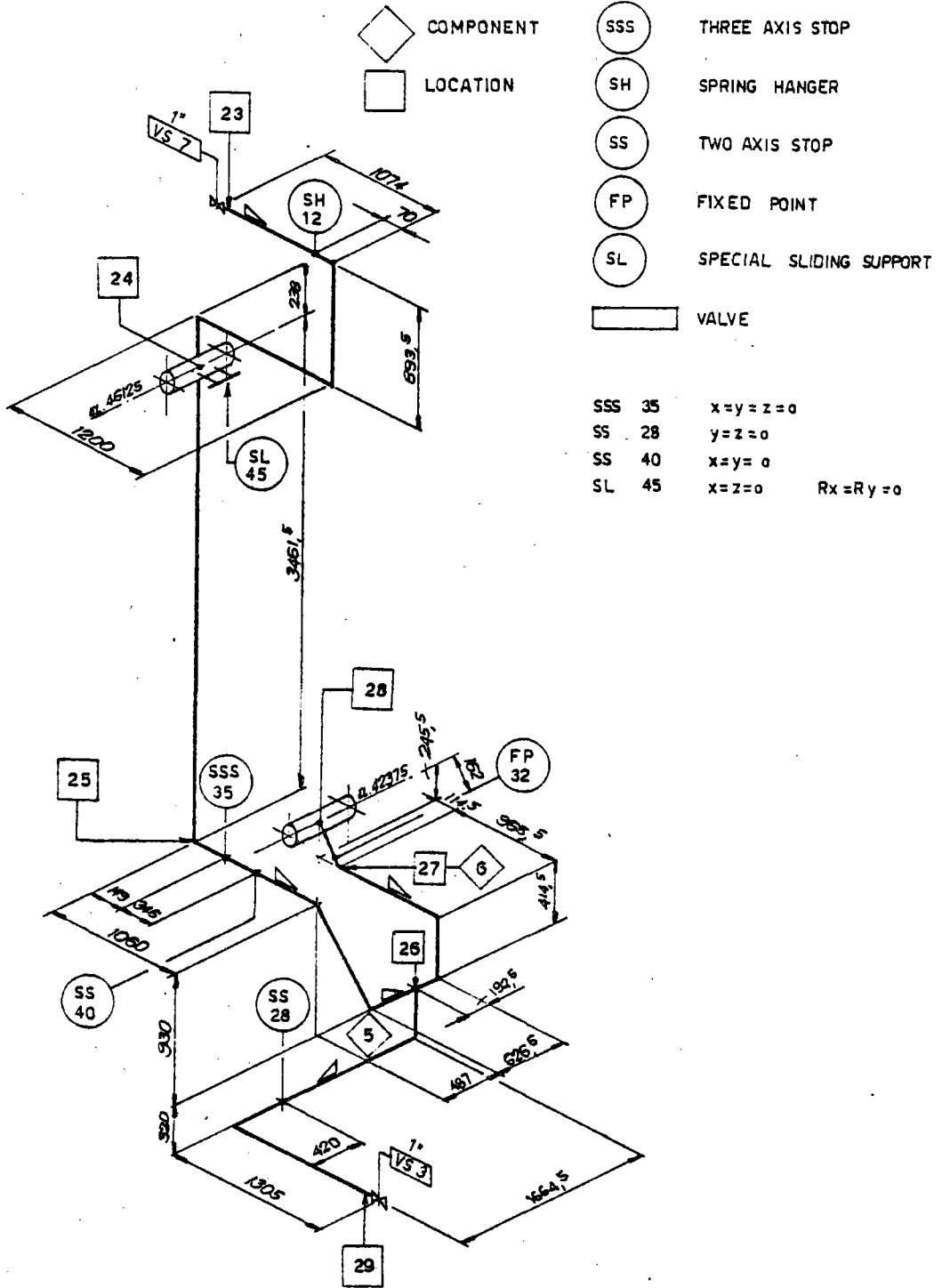
LEG # 2

FIG. 2. /3



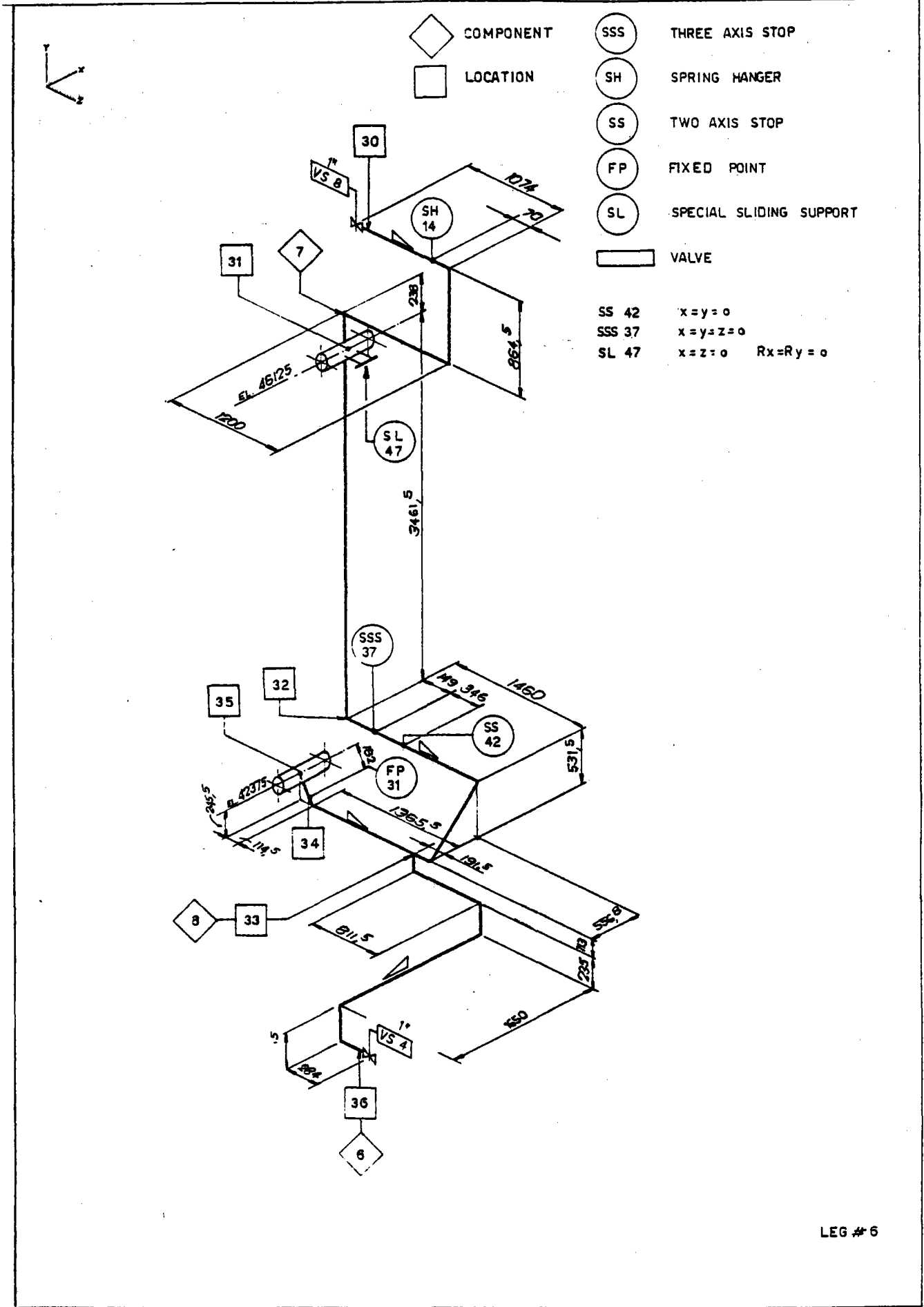
LEG # 4

FIG. 2. /5



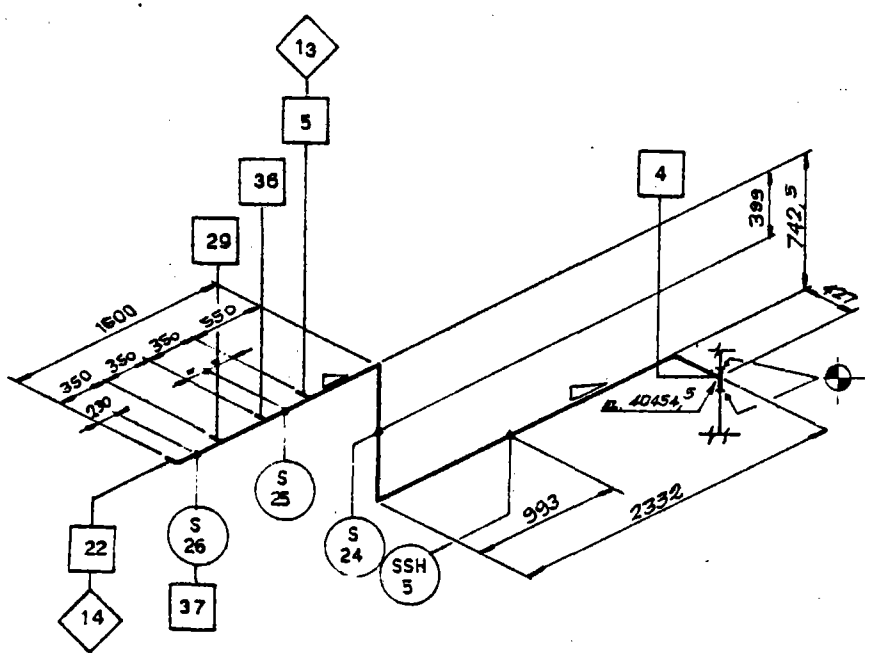
LEG # 5






FIG. 2. /6



LEG #6

FIG. 2. /7

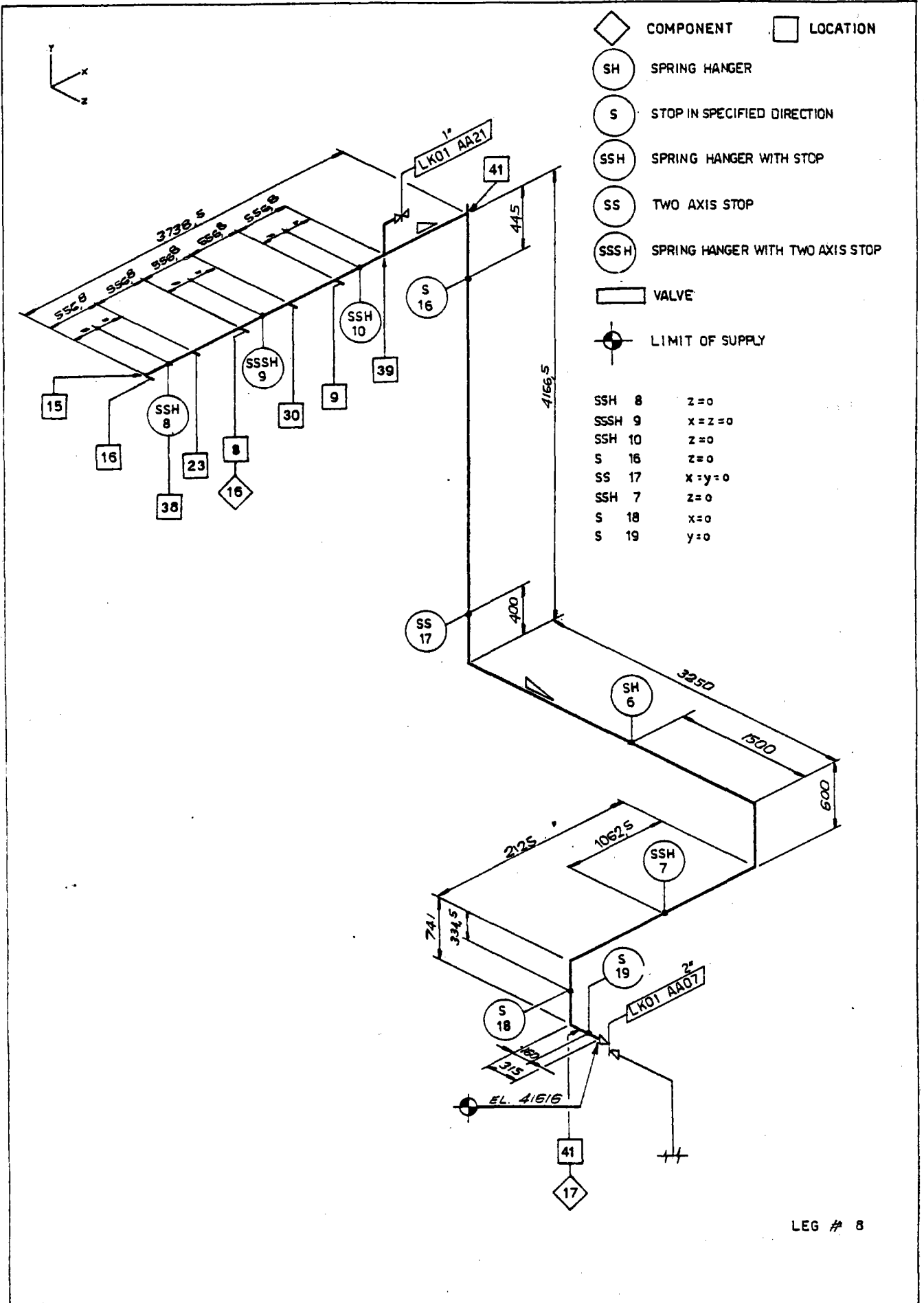


-  COMPONENT
-  LOCATION
-  STOP IN SPECIFIED DIRECTION
-  SPRING HANGER WITH STOP
-  LIMIT OF SUPPLY

S	24	x = 0
S	25	y = 0
S	26	y = 0
SSH	5	z = 0

LEG #7

FIG. 2. 18



LEG # 8

FIG. 2. /9

considered as well. No effects from the panel tubes have been kept into account.

Hereafter a brief description of the different legs is reported with indications about diameters, thickness, bend radius etc.

LEG 1

From location 1 to location 2 $Do = 88.9$ mm, $Th. = 3.05$ mm and $R = 114.3$ mm

At location 2 BEND with $Do = 88.9$, $Th. = 5.49$, $R = 114.3$

At location 3 $Do = 162$, $Th. = 7$

LEG 2

At location 4 TEE $Do = 88.9 * 88.9 * 60.3$, $Th. = 3.05 * 3.05 * 2.77$

From 5 to 6 $Do = 88.9$, $Th. = 3.05$ and $R = 114.3$

At location 6 BEND with $Do = 88.9$, $Th. = 5.49$ and $R = 114.3$

From 6 to 7 straight pipe with $Do = 88.9$, $Th. = 5.49$ except near by the location 7 where there are a reducer $88.9 - 73$ and a nozzle $Do = 73$, $Th. = 5.19$

At location 7 there are two branch connections: the first with $Do = 162 * 162 * 73$, $Th. = 5 * 5 * 5.19$ and the second with $Do = 33.4$, $Th. = 2.77$ and $R = 38.1$

LEG 3

From location 9 to 10 Do = 33.4, Th. = 2.77 and R = 38.1

At location 10 there are two branch connections: the first with Do = 162 * 162 * 334, Th. = 5 * 5 * 2.77 and the second with Do = 162 * 162 * 73, Th. = 5 * 5 * 5.19

From 10 to 11 pipe with Do = 88.9, Th. = 5.49 except near by the location 10 where there are a nozzle Do = 73, Th. = 5.19 and a reducer 88.9 - 73

At location 11 BEND with Do = 88.9, Th. = 5.49 and R = 114.3

From 11 through 12, 13 Do = 88.9, Th. = 3.05, R = 114.3

At 12 a branch connection is inserted with Do = 88.9 * 88.9 * 33.4, Th. = 5.49 * 5.59 * 2.77

From 12 to 15 straight and bend with Do = 88.9, Th. = 2.77, R = 38.1

LEG 4

The dimensions (diameter, thickness and bend radius) of this LEG are the same of LEG 3 in the correspondent locations.

LEG 5

As above.

LEG 6

As above.

LEG 7

From location 22 to 27 Do = 33.4, Th. = 2.77, R = 38.1

At location 37 reducer 60.3 to 33.4, Th. = 2.77

From 37 through 29, 36, 15, 4 Do = 60.3, Th. = 2.77,
R = 76.2

At locations 29, 36 and 15 TEES are inserted with
Do = 60.3 * 60.3 * 33.4 and Th. = 2.77

LEG 8

From location 16 to 38 Do = 33.4, Th. = 2.77, R = 38.1

At location 38 reducer 60.3 to 33.4, Th. = 2.77

From 38 through 23, 8, 30, 9, 39, 40, 41 Do = 60.3,
Th. = 2.77 and R = 76.2

At location 23, 8, 30, 9, 39 TEES are inserted with
Do = 60.3 * 60.3 * 33.4, Th. = 2.77

At location 40 TEE is inserted with Do = 60.3*60.3*60.3,
Th. = 2.77

3. DESIGN AND OPERATING CONDITIONS

3.1. DESIGN DATA

The following design data have been used in the analysis:

- design pressure 6 bar
- design temperature 530 °C
- design mechanical loads
 - a) weight of the piping system with insulation and sodium
 - b) earthquake statically considered with 0.4 g acceleration in the horizontal plane and 0.2 g acceleration in vertical direction as specified in Interatom letter dated 18/2/1982

3.2. OPERATING DATA

During the normal steady state operating conditions of the piping system the following data have been assumed:

- operating pressure 6. bar
- operating temperature:

LEG 1	270 °C
LEG 2	530 °C
LEG 3	290 °C
LEG 4	320 °C
LEG 5	380 °C
LEG 6	450 °C
LEG 7	250 °C
LEG 8	200 °C

3.2.1. Transient operating conditions

The normal operating conditions include the following transients:

cold start up	500 times
hot start up	2770 times
total cloud passage	63250 times

Conservatively the earthquake has been considered as normal operating condition and a number of 10 events has been assumed.

In order to make the analysis simpler, the cloud passages have been considered as shut down followed by hot start up; an upper bound of 70000 cold start up-shut down have been assumed with certain exceptions for those cases in which the compliance with the fatigue couldn't be achieved: in those cases a more accurate splitting up in different cycles has been carried out.

3.2.2. Temperature gradient distribution in transient conditions

The temperature variation through out the pipe axis (T_a and T_b) is generally low and its effect is assumed to be negligible.

The temperature gradients terms ΔT_1 and ΔT_2 across the wall thickness have been assumed to be $\Delta T_1 = 25 \text{ }^\circ\text{C}$,

4. GENERAL DESCRIPTION OF PIPE SUPPORTS AND RESTRAINTS

4.1. VARIABLE AND CONSTANT SPRING HANGER SUPPORTS

After selecting the possible locations of spring hangers, the reaction forces have been calculated due to weight of pipe lines.

The types of chosen spring hangers allow displacements due to thermal expansions in hot conditions.

We took into account the ineffectiveness of the constant load supports during the earthquake as well.

The piping support locations are showed in figure 2./2 + 2./9.

4.2. RESTRAINTS

The location and direction of the restraints (fixed points, stops, hangers etc.) have been determined by a preliminary analysis with free pipe system in hot condition.

In fig. 2./2 + 2./9 the restraints distribution of the piping system is shown.

5. PIPING FLEXIBILITY ANALYSIS

5.1. ANALYSIS METHOD

For the calculation of the axial and shear forces, torsional and bending moments acting on the piping system, the computer code SAP V has been used.

The considered element types are: Pipe elements, Boundary elements and Beam elements.

Pipe elements represent a straight segment (TANGENT) or a circularly curved segment (BEND). The element is described by two nodes; every node has six degrees of freedom (x, y, z displacements and Rx, Ry, Rz rotations).

The member stiffness matrices take into account the specific bending, torsional, axial and shearing deformations for straight pipes, elbows, tees etc. according to NB 3686 of ASME Code Section III.

The output for a pipe element consists of forces and moments acting in the cross section at the end of the member and at the midpoint of the arc in bend elements.

Boundary elements are defined by a single axis through a specified nodal point and by a linear extensional stiffness along the axis. This element is used to constraint

nodal displacements to specified values and to compute support reactions in the desired direction.

Beam elements are defined by two nodes as pipe element. Torsion, bending in two axis, axial and shearing deformations are considered. Section geometrical properties are defined by: cross sectional area, shear area in the two axis of the section, torsional inertia.

The output consists of forces and moments acting on the member cross section at the position of two nodes.

5.2. PIPING SYSTEM STRUCTURAL ANALYSIS

The goal of the following analysis consists in the determination of forces and moments at selected points of the piping system. The moment due to thermal, weight and earthquake loads are separately calculated in order to evaluate the contribution to the stresses in each component of the piping system.

At each location the piping system analysis gives a set of three orthogonal moments, and forces.

Five load conditions have been considered and presented in the following.

5.2.1. Weight analysis

A weight loading analysis has been carried out by applying 1 "g" downward acceleration. For this analysis the complete piping system is considered as filled of sodium, with insulation and stainless steel jacket ($T_h = 0.4$ mm).

Valves weight and spring hanger reactions are considered as well.

5.2.2. Thermal expansion analysis

The thermal expansion analysis has been performed by applying to the piping system temperature distribution defined in the operating conditions (see point 3.2.) starting from ambient temperature assumed as 20 °C.

5.2.3. Earthquake analysis

The effects of earthquake have been simulated by a static analysis, applying one at a time the specified acceleration (see point 3.1.) in the three global directions.

The earthquake forces and moment have been considered, in the combination with the other loads, without algebraic sign.

6. PIPING FLEXIBILITY RESULTS AND COMPLIANCE ANALYSIS

6.1. CODES AND RULES USED

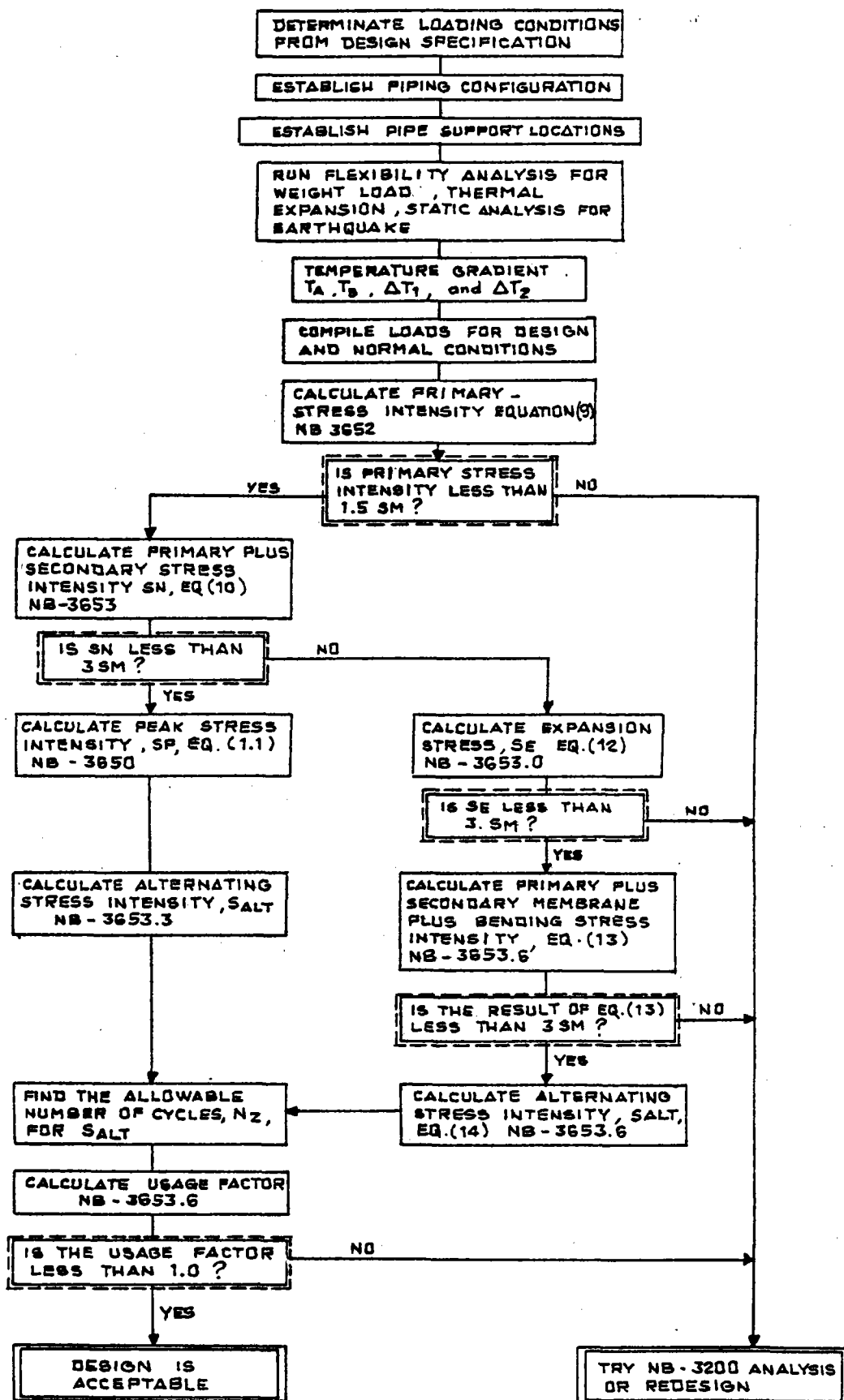
For the piping system analysis the compliance with stress limits has been investigated according to ASME Code Sect. III, Subsection NB3600 "Piping Design" (1980 issue). For legs 2 and 6 whose operating temperature are greater than 427 °C (800 °F) an extension of the Code have been carried out; in this case the allowable stress limits have been deduced from Appendix 1 for high temperatures and the fatigue curves T1420 contained in Code Case N47-17; a reduction factor of 5 in the cycles number has been applied.

In table 6.1./1 the flow chart of the design and compliance analysis procedure related to NB3600 is reported.

In addition, for leg 2 only, that well exceeds 427 °C as operating temperature, a compliance analysis following Code Case N47-17-3600 has been carried out.

6.2. PIPING FLEXIBILITY RESULTS

In the following the results of the flexibility analysis are reported. The forces and moments are referred to the most important points of the receiver, that is



FLOW CHART OF DESIGN AND ANALYSIS PROCEDURE

at the low header position and at the down comer fixed point position; in addition the results are reported for different meaning ful locations of the piping system.

The values are splitted according to the different type of load that is

- dead weight
- expantion
- earthquake in x direction
- earthquake in y direction
- earthquake in z direction

In fig. 6.2./1 + 6.2./5 the deformation shape of the piping system is reported for the different loads. In table 6.2./1 + 6.2./5 the forces and moment are reported as well; it is to be noted that all forces and moment are reported referred to local coordinated in which the x direction is tangent to the tube axis.

6.3. COMPLIANCE ANALYSIS WITH NB3600

As referred at point 6.1. an analysis following NB3600 has been carried out over 427 °C (800 °F) as well. In the following tables 6.3./1 + 6.3./8, for each leg, a compliance analysis for the most stressed and/or meaning ful locations or components is reported.

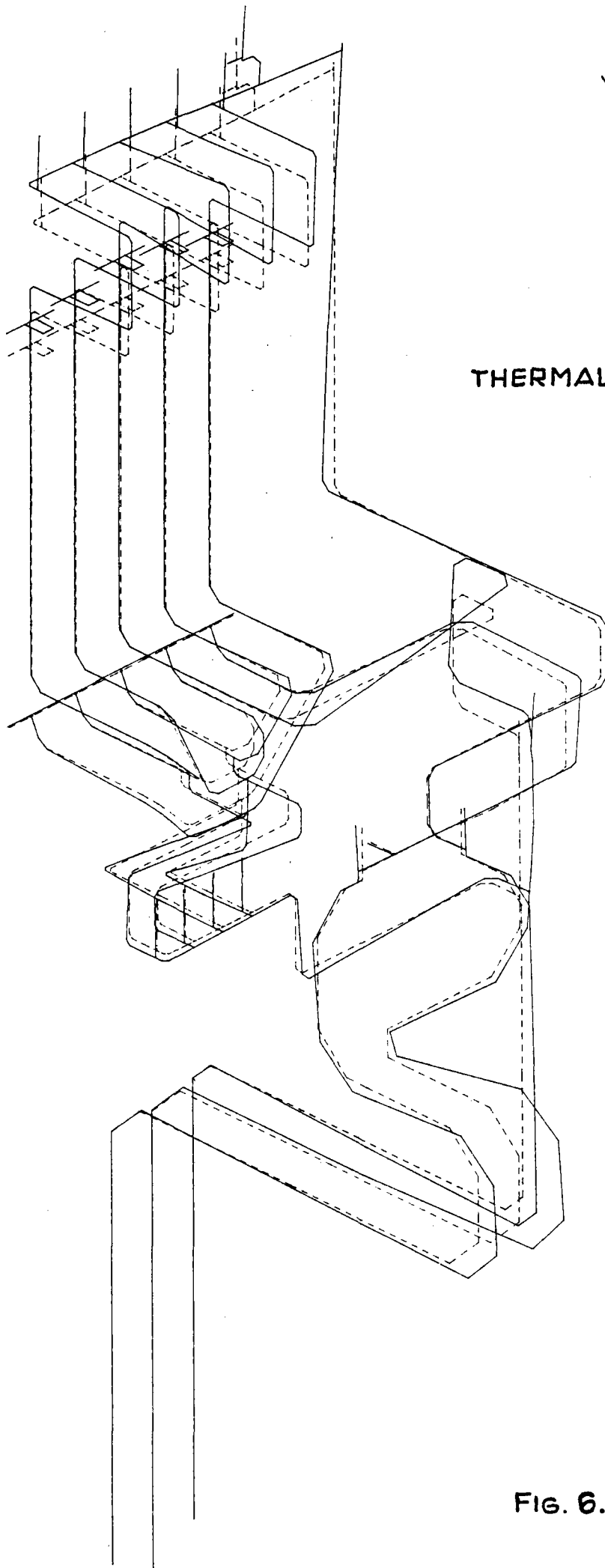


FIG. 6.2/1

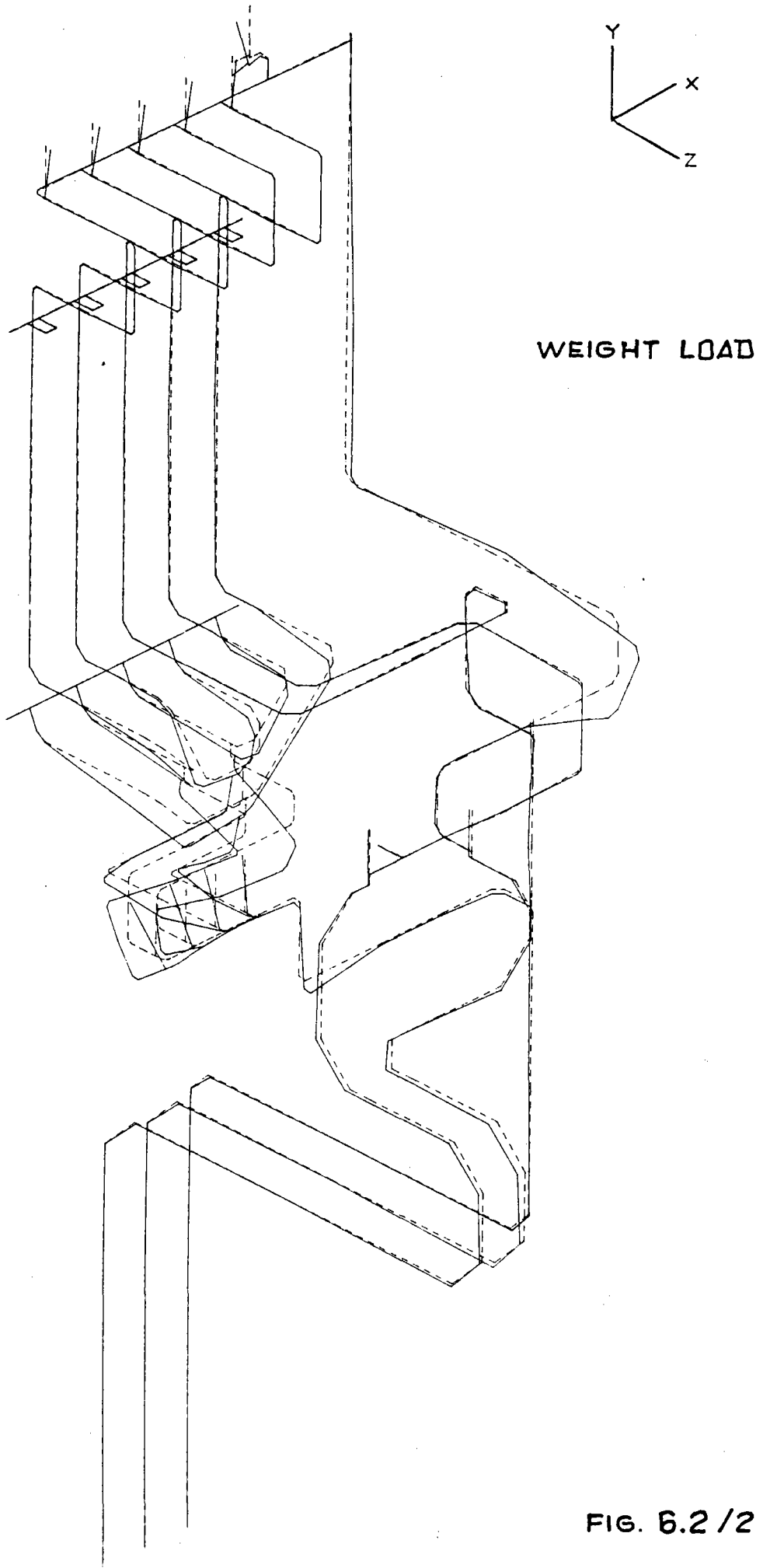
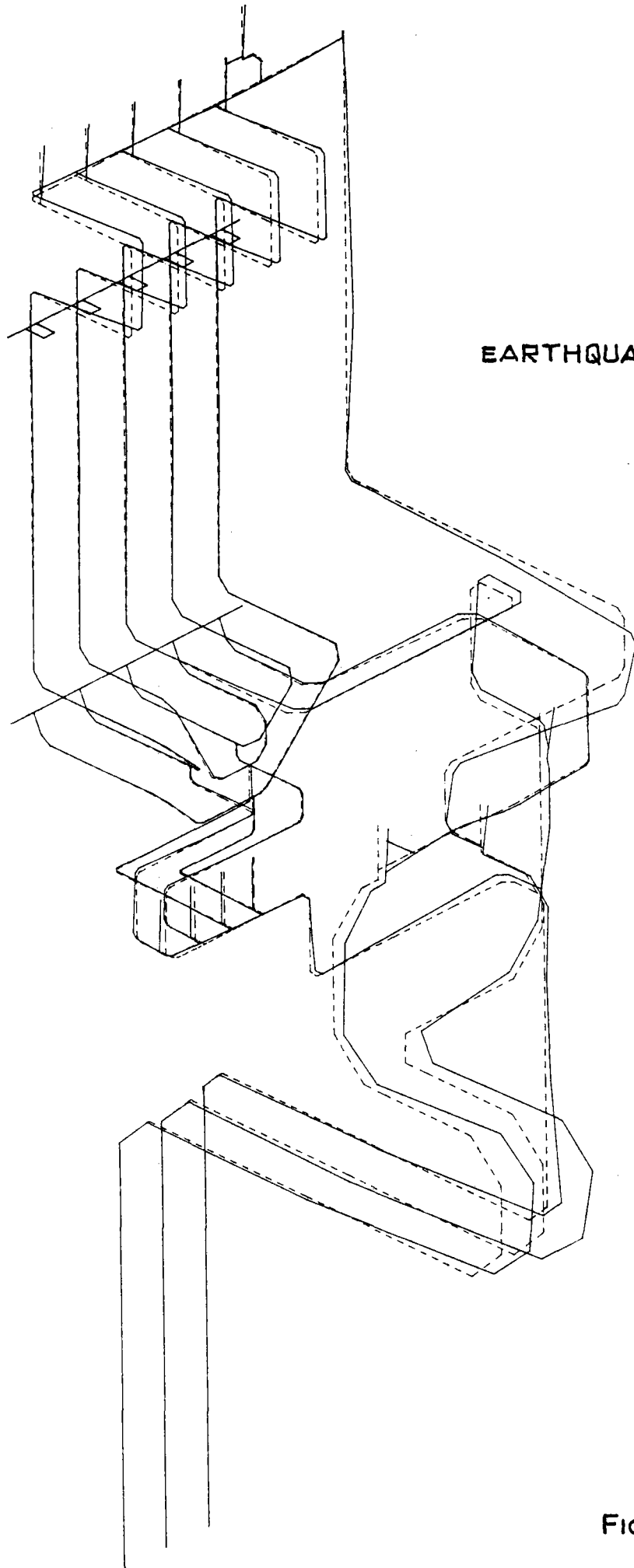
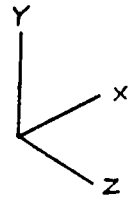


FIG. 6.2 / 2



EARTHQUAKE - X LOAD

FIG. 6.2/3



EARTHQUAKE -Z LOAD

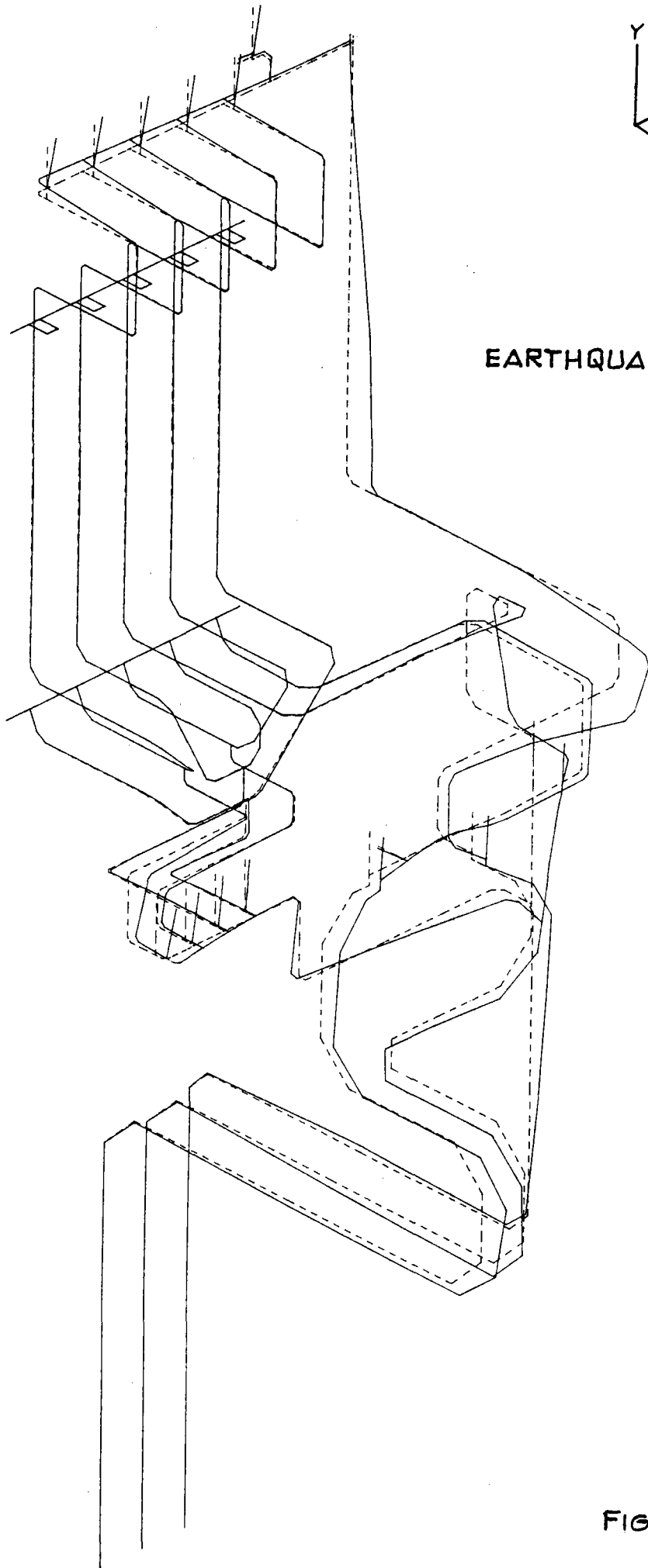
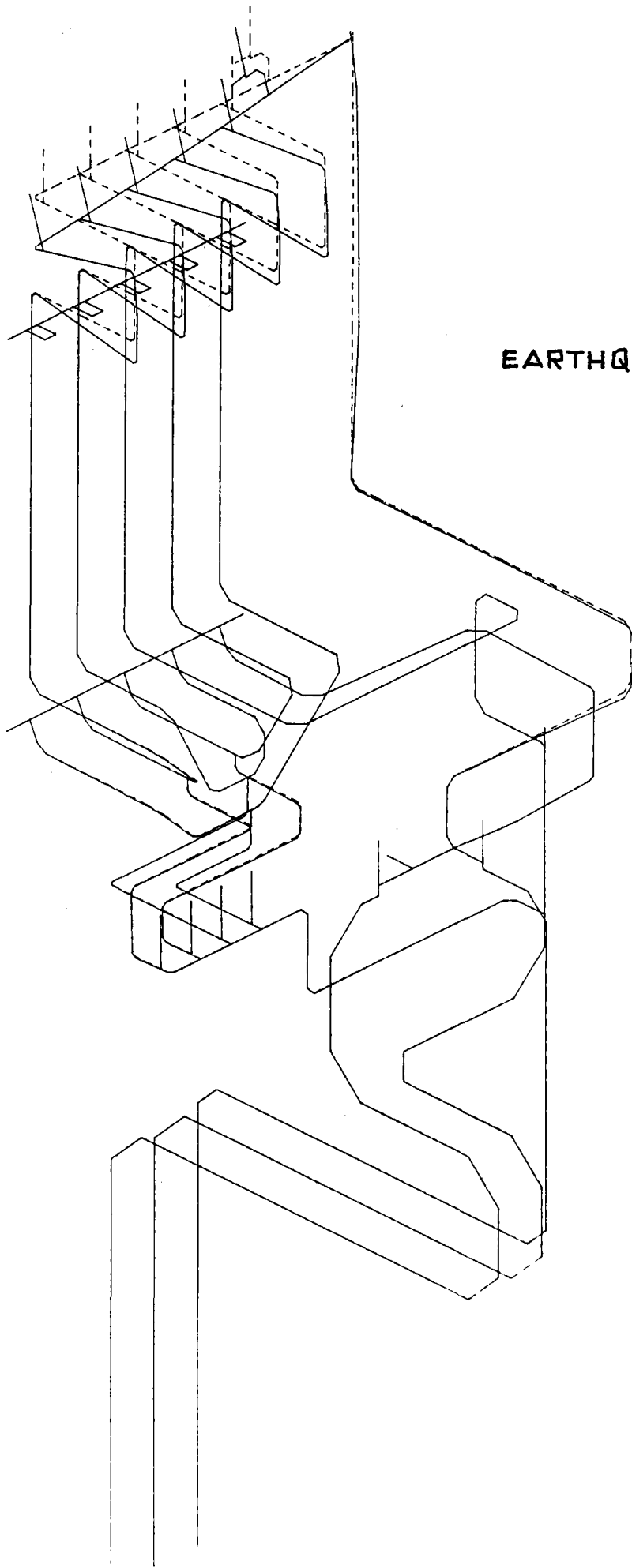
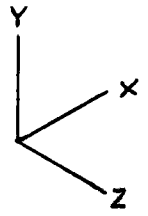


FIG. 6.2/4



EARTHQUAKE -Y LOAD

FIG. 6.2/5

FORCES AND MOMENTS FOR THERMAL LOAD

LEG	LOCATION (see fig. 2.1/1+9)	FORCE (kg)			MOMENT (kg·mm)		
		F _x	F _y	F _z	M _x	M _y	M _z
1	F.P. 33	-7.	14.	-4.	-15090.	-8078.	1383.
	1	-3.7	-1.	16.	10574.	-12422.	978.
	2	The forces and moments are the same of F.P. 33					
2	SSS 36	-0.8	9.	3.6	12085.	-133.	243.
	SS 41	-22.	18.	101.	12085.	33358.	-5712.
	10	N.R.					
	11	N.R.					
	12	N.R.					
3	F.P. 29	6.4	22.8	73.	59453.	53101.	-24028.
	SSS 38	0.	0.	3.4	12378.	-466.	-36.
	SS 43	1.3	-58.	215.8	12378.	70981.	19159.
	3	N.R.					
4	F.P. 30	20.3	31.7	-38.5	-31735.	-13449.	-30790.
	SSS 34	-0.2	-5.2	0.4	289.	329.	684.
	SS 39	18.6	-81.4	-105.	-2020.	-34402.	27637.
	4	N.R.					
5	F.P. 32	45.3	36.7	-95.	-50457.	-62019.	-51572.
	SSS 35	-0.2	-0.6	0.2	179.	420.	211.
	SS 40	8.	-93.5	-147.5	-19485.	-48411.	31185.
	5	-116.2	12.3	8.	6741.	17881.	41201.
	6	The forces and moments are the same of F.P. 32					
6	F.P. 31	29.	44.4	50.5	41245.	16325.	-43954.
	SSS 37	-0.2	6.5	0.7	2794.	-399.	-825.
	SS 42	22.3	-128.3	163.2	2794.	53632.	41634.
	7	-6.5	0.3	-0.6	-436.	377.	4223.
	8	N.R.					
	9	-5.7	5.6	-14.5	-618.	-342.	241.
7	13	N.R.					
	14	-0.8	-11.	-12.1	-4434.	6268.	-1721.
8	15	-1.7	1.5	-5.2	-4411.	-1382.	1127.
	16	N.R.					
	17	1.5	1.6	0.	1382.	-724.	772.

N.R. - The forces and moments of these components are not reported for table simplicity reasons.

FORCES AND MOMENTS FOR WEIGHT LOAD

LEG	LOCATION (see fig. 2.1/1+9)	FORCE (kg)			MOMENT (kg. mm)		
		F _x	F _y	F _z	M _x	M _y	M _z
1	F.P. 33	14.	6.	0.	-375.	841.	-997.
	1	0.	-8.3	0.	-345.	432.	-2676.
	2	The forces and moments are the same of F.P. 33					
2	SSS 36	-2.	156.	0.	-769.	-6.	-19870.
	SS 41	2.2	-34.7	-0.4	-769.	-150.	-6544.
	10	N.R.					
	11	N.R.					
3	F.P. 29	63.4	25.5	-12.	-13066.	-7092.	-58998.
	SSS 38	-2.6	156.4	1.8	6367.	174.	-18543.
	SS 43	4.5	143.	-45.	6367.	-14718.	-64225.
	3	N.R.					
4	F.P. 30	29.	34.6	1.7	3921.	6398.	-27226.
	SSS 34	-2.4	156.	0.	5.	7.	-19079.
	SS 39	17.4	70.	-2.7	-5592.	-898.	-40395.
	4	N.R.					
5	F.P. 32	45.6	22.6	10.5	6269.	8810.	-33158.
	SSS 35	-2.3	156.3	0.	-2.	-29.	-19324.
	SS 40	2.4	37.6	11.6	-4963.	3831.	-29930.
	5	15.	-5.8	2.4	2550.	-24.	-1004.
	6	The forces and moments are the same of F.P. 32					
6	F.P. 31	30.9	34.5	-4.	-5725.	-8933.	-30072.
	SSS 37	-2.4	156.5	1.4	5071.	38.	-19044.
	SS 42	18.3	75.6	3.	5071.	1119.	-42241.
	7	-5.	-1.6	0.	-35.	-15.	475.
	8	N.R.					
7	9	0.1	13.4	1.1	2010.	377.	-1736.
	13	N.R.					
8	14	-4.	5.6	-0.8	158.	-5090.	-1241.
	15	0.	1.8	-23.9	-127.	-848.	-89.
8	16	N.R.					
	17	-0.9	4.9	0.5	-689.	-272.	1502.

N.R. - The forces and moments of these components are not reported for table simplicity reasons.

FORCES AND MOMENTS FOR EARTHQUAKE IN X GLOBAL DIRECTION

LEG	LOCATION (see fig. 2.1/1+9)	FORCE (kg)			MOMENT (kg·mm)		
		F _x	F _y	F _z	M _x	M _y	M _z
1	F.P. 33	-6.6	1.	-34.	-25925.	-12693.	104.
	1	43.6	0.	4.	-2312.	-3092.	-13783.
	2	The forces and moments are the same of F.P. 33					
2	SSS 36	0.	0.	26.	4973.	3076.	-37.
	SS 41	20.	-10.	239.	4973.	81431.	3236.
	10	N.R.					
	11	N.R.					
	12	N.R.					
3	F.P. 29	8.	-4.	-27.4	-17027.	-10178.	-6024.
	SSS 38	0.	0.4	26.7	6797.	3539.	-168.
	SS 43	-4.7	-12.9	64.5	6797.	24132.	4099.
	3	N.R.					
4	F.P. 30	-5.6	7.3	-18.5	-10032.	-8467.	3063.
	SSS 34	0.	-1.6	29.1	15499.	3647.	256.
	SS 39	7.9	0.	42.5	2714.	16960.	247.
	4	N.R.					
5	F.P. 32	-14.6	-2.6	-26.6	-12808.	-11680.	13297.
	SSS 35	0.	-0.8	29.3	15622.	3715.	211.
	SS 40	5.6	10.2	28.1	5027.	12275.	-3155.
	5	14.3	-8.4	5.6	39.	713.	-2697.
	6	The forces and moments are the same of F.P. 32					
6	F.P. 31	1.9	-6.	-15.5	-7459.	-5568.	-822.
	SSS 37	0.	0.2	26.3	5293.	3594.	30.
	SS 42	-5.9	7.6	38.7	5293.	15658.	-2481.
	7	-0.2	0.	4.5	3025.	19.	111.
	8	N.R.					
	9	0.4	-0.7	8.4	1199.	1461.	173.
7	13	N.R.					
	14	5.4	-5.7	-117.	-4881.	6583.	-3711.
8	15	-15.9	0.2	-1.6	-1137.	2089.	6107.
	16	N.R.					
	17	0.8	-3.2	-11.1	4856.	-3205.	2493.

N.R. - The forces and moments of these components are not reported for table simplicity reasons.

FORCES AND MOMENTS FOR EARTHQUAKE IN Z GLOBAL DIRECTION

LEG	LOCATION (see fig. 2.1/1+9)	FORCE (kg)			MOMENT (kg.mm)			
		F _x	F _y	F _z	M _x	M _y	M _z	
1	F.P. 33	17.	-30.	-16.	251.	-7382.	-760.	
	1	-16.3	-4.7	43.3	8014.	-36091.	1524.	
	2	The forces and moments are the same of F.P. 33						
2	SSS 36	-23.7	0.4	0.	-446.	-46.	8124.	
	SS 41	-18.9	45.	17.	-446.	5575.	-6832.	
	10	N.R.						
	11		0.64	38.86	-12.55	-12065.	-988.	261.
	12	N.R.						
3	F.P. 29	13.3	-29.	-1.3	1617.	789.	7430.	
	SSS 38	-23.6	0.5	0.	-473.	8.	7869.	
	SS 43	27.	8.4	-5.2	-473.	-1710.	5097.	
	3	N.R.						
4	F.P. 30	13.4	-27.1	2.4	1091.	1638.	1208.	
	SSS 34	-23.7	0.	0.	-27.	4.	8062.	
	SS 39	15.	23.	-3.	-454.	-1014.	443.	
	4	N.R.						
5	F.P. 32	17.1	-22.6	3.9	798.	1863.	125.	
	SSS 35	-23.6	0.2	0.	-3.	10.	7920.	
	SS 40	13.9	9.5	-3.	-885.	-999.	4781.	
	5	-5.2	2.3	-5.6	-1709.	765.	222.	
	6	The forces and moments are the same of F.P. 32						
6	F.P. 31	11.7	-25.6	1.2	1065.	1747.	2748.	
	SSS 37	-23.6	0.5	-0.2	-534.	11.	7962.	
	SS 42	16.2	23.7	-4.5	-534.	-1491.	98.	
	7	-0.5	-4.	-0.3	-210.	33.	368.	
	8	N.R.						
	9	-4.5	-0.3	2.9	832.	1634.	57.	
7	13	N.R.						
	14	-0.8	-1.7	-1.5	6673.	-2681.	-2490.	
8	15	0.	-17.4	0.	-1073.	-153.	655.	
	16	N.R.						
	17	31.9	3.2	2.7	2660.	-4483.	-9824.	

N.R. - The forces and moments of these components are not reported for table simplicity reasons.

FORCES AND MOMENTS FOR EARTHQUAKE IN -Y GLOBAL DIRECTION

LEG	LOCATION (see fig. 2.1/1+9)	FORCE (kg)			MOMENT (kg·mm)		
		F _x	F _y	F _z	M _x	M _y	M _z
1	F.P. 33	2.8	1.3	0.	-78.	175.	-202.
	1	0.	-1.7	0.	-70.	88.	-549.
	2	The forces and moments are the same of F.P. 33					
2	SSS 36	0.	41.	0.	-125.	-8.	-5500.
	SS 41	0.4	-11.6	0.	-125.	-64.	-1297.
	10	N.R.					
	11		0.	4.2	-180.	558.	4.
	12	N.R.					
3	F.P. 29	13.	5.	-2.4	-2660.	-1441.	-12036.
	SSS 38	-0.4	38.3	0.4	1306.	22.	-4810.
	SS 43	0.9	26.	-9.	1306.	-2995.	-13097.
	3	N.R.					
4	F.P. 30	5.9	7.	0.3	799.	1299.	-5587.
	SSS 34	0.	44.7	0.	36.	-2.	-5590.
	SS 39	3.5	7.8	-0.6	-1135.	-198.	-8204.
	4	N.R.					
5	F.P. 32	9.3	4.6	2.1	1279.	1790.	-6780.
	SSS 35	0.	43.2	0.	27.	-13.	-5775.
	SS 40	0.5	2.	2.4	-1009.	772.	-6086.
	5	3.	-1.2	0.5	519.	-3.	-200.
	6	The forces and moments are the same of F.P. 32					
6	F.P. 31	6.3	7.	-0.8	-1163.	-1813.	-6148.
	SSS 37	-0.3	39.7	0.3	1041.	0.	-5145.
	SS 42	3.7	11.5	0.7	1041.	241.	-8599.
	7	-8.8	0.6	1.	735.	-336.	4998.
	8	N.R.					
	9	0.	2.7	0.2	410.	76.	-354.
7	13	N.R.					
	14	-0.8	1.1	-0.2	30.	-1045.	-258.
8	15	0.7	0.	3.4	3342.	1074.	-503.
	16	N.R.					
	17	0.	1.2	-0.3	621.	38.	694.

N.R. - The forces and moments of these components are not reported for table simplicity reasons.

TABLE 6.3./1LEG N° 1
=====- COMPONENT NUMBER 1 - Girth butt weld

EQ.(9) 3.038 < 11.865 Kg/mm²

EQ.(10) 5.575 < 27.73 Kg/mm²

EQ.(11) 20.805 Kg/mm²

SALT* = 15.042 KSI (')

NI > 10⁶ cycle

Cumulative damage = 0

Accepted

 (') Note: $SALT * = \left(\frac{S_p \cdot K_e}{2} \cdot 1.422333 \right) \cdot \frac{E \text{ TAB I 9.2}}{E \text{ COMPONENT}}$ in KSI

- COMPONENT NUMBER 2 - Butt welding elbow

EQ.(9) 1.294 < 11.865

EQ.(10) 2.723 < 23.73

EQ.(11) 15.884

SALT* = 11.485

NI > 10⁶ cycle

Cumulative damage = 0

Accepted

TABLE 6.3./2a

LEG N° 2
=====

- COMPONENT NUMBER 10 - Branch connection

EQ.(9) 7.288 < 11.865

EQ.(10) 24.273 > 23.73 not verified, try through EQ. 12, 13, 14

EQ.(12) 11.66 < 23.73

EQ.(13) 14.35 < 23.73

EQ.(14) : SALT = $K_e \frac{S_p}{2}$

$$K_e = 1. + \left[\frac{(1-n)}{n} (m-1) \right] (S_n/3S_m-1)$$

m and n values are taken m=1.7 , n=0.3

$$K_e = 1.038$$

EQ.(11 & 14) For the fatigue analysis standpoint a splitting in the operating conditions is necessary. The following cycles have been assumed:

- a) normal operating conditions with the maximum thermal expansion (20+530) and earthquake;
- b) cold start up with max. thermal expansion (20+530);
- c) hot start up with thermal expansion (270+530);
- d) type 1 cloud passage with thermal expansion (485+543);
- e) type 2 cloud passage with thermal expansion (338+530);
- f) type 3 cloud passage with thermal expansion (210+530).

For the cloud passage type see Topic Report N° 6 and 11; for transient d), e), f) a linearization between the Σ range and the cycle temperature difference has been assumed.

(LEG N° 2)

TABLE 6.3./2b

Load conditions	SP	K_e	SALT	ϵ_t	ND	n	n/ND
a	32.662	1.038	16.952	0.0021526	2200	10	0.0046
b	20.885	1.038	10.84	0.0013765	19500	500	0.0256
c	18.82	1.038	9.77	0.00124	37500	2770	0.0739
d				0.00028	$>10^6$	30000	~0.
e				0.00092	10^6	30000	0.03
f				0.00153	11200	3250	0.2902

$$\text{Total fatigue damage} = \sum_{i=1}^6 n_i/ND_i = 0.425 \text{ accepted}$$

- COMPONENT NUMBER 11 - Butt welding elbow

$$\text{EQ. (9)} \quad 6.71 < 11.865$$

$$\text{EQ. (10)} \quad 24.661 > 23.72 \text{ SN not verified, try through EQ 12, 13, 14}$$

$$\text{EQ. (12)} \quad 14.675 < 23.73$$

$$\text{EQ. (13)} \quad 11.02 < 23.73$$

$$K_e = 1.064$$

EQ. (11 & 14) The load conditions considered are the same used for component 10 excepted conditions c), d), e), f) for which an upper bound has been considered.

Load conditions	SP	K_e	SALT	ϵ_t	ND	n	n/ND
1	32.161	1.064	17.109	0.0021727	2100	10	0.0048
2	23.721	1.064	12.62	0.00160	8500	500	0.0588
3	15.23	1.064	8.1	0.001029	124000	66020	0.5324

$$\sum_{i=1}^3 n_i/ND_i = 0.596 \text{ accepted}$$

./.

(LEG N° 2)

TABLE 6.3./2c- COMPONENT NUMBER 12 - Butt welding tee

EQ.(9) $11.113 < 11.865$

EQ.(10) $16.342 < 23.73$

$K_e = 1$

The load conditions considered are the same of component 11.

Load conditions	SP	K_e	SALT	ϵ_t	ND	n	n/ND
1	26.291	1.	13.146	0.0016693	6800	10	0.0015
2	20.8	1.	10.4	0.0013206	25000	500	0.02
3	16.37	1.	8.185	0.001039	116000	66020	0.569

$$\sum_1^3 n/ND = 0.59 \quad \text{accepted}$$

TABLE 6.3./3LEG N° 3
=====- COMPONENT NUMBER 3 - Branch connection

EQ.(9) 7.3 < 11.865

EQ.(10) 17.88 < 23.73

EQ.(11) 25.792

SALT* = 18.752

NI > 10⁶ cycle

Cumulative damage = 0

Accepted

TABLE 6.3./4LEG N° 4- COMPONENT NUMBER 4 - Branch connection

EQ.(9) 9.9 < 11.865

EQ.(10) 23.683 < 23.73

EQ.(11) 32.054

SALT* = 23.568

NI > 10⁶ cycle

Cumulative damage = 0

Accepted

LEG N° 5- COMPONENT NUMBER 5 - Butt welding elbow

EQ.(9) 1.5 < 11.865

EQ.(10) 17.633 < 23.73

EQ.(11) 25.133

SALT * = 19.072

NI > 10⁶ cycle

Cumulative damage = 0

Accepted

- COMPONENT NUMBER 6 - Butt welding elbow

EQ.(9) 5.168 < 11.865

EQ.(10) 16.416 < 23.73

EQ.(11) 23.916

SALT * = 18.149

NI > 10⁶ cycle

Cumulative damage = 0

Accepted

TABLE 6.3./6

LEG N° 6
=====

- COMPONENT NUMBER 7 - Butt welding elbow

EQ.(9) 6.68 < 11.865

EQ.(10) 16.805 < 23.73

EQ.(11) 17.876

SALT * = 14.1

NI > 10⁶ cycle

Cumulative damage = 0

Accepted

- COMPONENT NUMBER 8 - Branch connection

EQ.(9) 6.3 < 11.865

EQ.(10) 13.227 < 23.73

EQ.(11) 21.147

SALT * = 16.68

NI > 10⁶ cycle

Cumulative damage = 0

Accepted

- COMPONENT NUMBER 9 - Girth butt weld

EQ.(9) 2.389 < 11.865

EQ.(10) 2.255 < 23.73

EQ.(11) 5.682

SALT * = 4.482

NI > 10⁶ cycle

Cumulative damage = 0

Accepted

TABLE 6.3./7LEG N° 7
=====- COMPONENT NUMBER 13 - Butt welding tee

EQ.(9) 5.091 < 11.865

EQ.(10) 10.094 < 23.73

EQ.(11) 18.

SALT * = 13.234

NI > 10⁶ cycle

Cumulative damage = 0

Accepted

- COMPONENT NUMBER 14 - Butt welding elbow

EQ.(9) 10.573 < 11.865

EQ.(10) 12.582 < 23.73

EQ.(11) 13.654

SALT * = 10.769

NI > 10⁶ cycle

Cumulative damage = 0

Accepted

TABLE 6.3./8

LEG N° 8
=====

- COMPONENT NUMBER 15 - Butt welding elbow

EQ.(9) 8.363 < 11.865

EQ.(10) 17.566 < 23.73

EQ.(11) 18.638

SALT * = 13.476

NI > 10⁶ cycle

Cumulative damage = 0

Accepted

- COMPONENT NUMBER 16 - Butt welding tee

EQ.(9) 8.01 < 11.865

EQ.(10) 18.579 < 23.73

EQ.(11) 28.528

SALT * = 20.626

NI > 10⁶ cycle

Cumulative damage = 0

Accepted

- COMPONENT NUMBER 17 - Girth butt weld

EQ.(9) 2.181 < 11.865

EQ.(10) 3.135 < 23.73

EQ.(11) 7.106

SALT * = 5.138

NI > 10⁶ cycle

Cumulative damage = 0

Accepted

The values have been obtained according to procedure illustrated in table 6.1./1. For the leg 2 (the hot one) the allowable stresses and cycles have been assumed following point 6.1.

6.4. COMPLIANCE ANALYSIS WITH CODE CASE N47-17-3600

As specified at point 6.1. of this report the aforementioned analysis has been carried out for leg 2 only which well exceeds 427 °C (800 °F). The most critical sections of the mentioned leg have been checked according to the Code Case and a detailed analysis is hereafter reported as example for the most stressed location corresponding to the butt welding elbow n° 11.

6.4.1. Operating conditions

The operating conditions for the aforementioned leg keep into account the dead weight, the pressure, the earthquake in the three directions as the most unfavorable composition with other loads and the stresses due to the thermal expansion between the following temperatures:

- a) cold start up 20 + 530
- b) hot start up 270 + 530

c) cloud transient type 1	485 + 543	} see Topic Report N° 6 and N° 11
d) cloud transient type 2	338 + 530	
e) cloud transient type 3	210 + 530	

The forces and moments are reported at point 6.2.; the thermal gradients in the thickness of the tube during transient conditions are reported at point 3.2. as well.

6.4.2. Considerations about the analysis

In the following analysis the stress index method has been applied with the following values:

$$\begin{array}{lll}
 B_1 = 0.5 & B_2 = 3.94 & B_3 = 1. \\
 C_1 = 1.3 & C_2 = 5.92 & C_3 = 0.5 \\
 K_1 = 1. & K_2 = 1. & K_3 = 1.
 \end{array}$$

From an analysis of the geometry of the considered leg (uniform pipe diameter and thickness, presence of a few butt welding elbows other than the considered one, absence of weaker points) and from considerations about the thermal expansion flexibility analysis showing a regular moment distribution on the pipe length, it can be desumed that the elastic follow up phenomenon is not to be expected; therefore, according to the Code, the thermal expansion stresses can be considered as secondary stresses.

6.4.3. Compliance with design loads

The design loads considered consist in pressure and the most unfavorable combination between dead weight and earthquake.

- Membrane stress

$$\frac{P D_o}{2t} + \frac{P}{2} + \frac{F}{A} = 1.01 < S_o = 7.82 \text{ kg/mm}^2 \text{ accepted}$$

- Bending stress

$$\frac{B_1 P D_o}{2t} + B_2 \frac{D_o M}{2I} + \frac{F}{A} = 6.79 < 1.5 S_o = 11.73 \text{ kg/mm}^2 \text{ accepted}$$

6.4.4. Compliance with service loads

The following definitions have to be considered:

$$P_m = P_L = \frac{P D_o}{2t} + \frac{P}{2} + \frac{F}{A}$$

$$(P_L + P_B) = B_1 \frac{P D_o}{2t} + B_2 \frac{D_o M}{2I} + \frac{F}{A}$$

$$(P_L + P_B + Q) = C_1 \frac{P D_o}{2t} + C_2 \frac{D_o M}{2I} + \frac{F}{A} + \frac{E \alpha}{2(1-\nu)} |\Delta T_1| +$$

$$+ C_3 E_{ab} |\alpha_a T_a - \alpha_b T_b|$$

$$Q = (P_L + P_B + Q) - (P_L + P_B)$$

$$(P_L + P_B + Q + F) = K_1 C_1 \frac{P D_0}{2t} + K_2 C_2 \frac{D O M}{2I} + \frac{F}{A} + K_3 \frac{E \alpha}{2(1-\nu)} |\Delta T_1| +$$

$$+ \frac{E \alpha}{1-\nu} |\Delta T_2| + K_3 C_3 E_{ab} |\alpha_a T_a - \alpha_b T_b|$$

$$F = (P_L + P_B + Q + F) - Q$$

$$K_t = 1 + [\alpha (K - 1)] (1 - P_L/S_t)$$

Considering pressure and the most unfavorable combination between dead weight and earthquake

- primary membrane stress

$$P_m = 1.01 < S_{mt} = 7.76 \text{ kg/mm}^2 \quad \text{accepted}$$

- primary membrane plus bending stress

$$(P_L + P_B) = 6.79 < 1.5 S_{mt} = 11.64 \text{ kg/mm}^2 \quad \text{accepted}$$

$$(P_L + P_B) = 6.79 < K_t S_t = 10.06 \text{ kg/mm}^2 \quad \text{accepted}$$

- time fraction requirements

$$\sum (t_i/t_{im}) \simeq 0$$

$$\sum (t_i/t_{ib}) \simeq 0$$

Considering the pressure, the maximum thermal expansion, the linearized part of the thermal gradient in the thickness of the tube and the most unfavorable combination between dead weight and earthquake

- primary and secondary stress

$$(P_L + P_B + Q) = 31.11 \text{ kg/mm}^2$$

- secondary stress

$$Q = 24.32 \text{ kg/mm}^2$$

- bending stress

$$P_B = 5.78 \text{ kg/mm}^2$$

- yielding strength of lower cycle temperature

$$S_y = 17.2 \text{ kg/mm}^2$$

- parameter $X = \frac{P_L + P_B / K_t}{S_y} = 0.36$

- parameter $Y = Q / S_y = 1.41$

And therefore for region S_1 of Bree diagram

$$Z = Y + 1 - 2 \sqrt{(1-X)Y} = 0.51$$

The corresponding creep stress to enter the isochronous curves is 15.59 KSI and the resultant strain after 30000 hours is

$$\epsilon = 0.17\% < 0.5\% \text{ (allowed for weld material) accepted}$$

With reference to creep-fatigue analysis a splitting in different operating conditions has been carried out.

a) Cold start up with normal operating conditions.

The loads are pressure dead weight and the maximum thermal expansion (20 + 530); the values of moment and forces are

$$M = 41370 \text{ kg mm}$$

$$F = 31.48 \text{ kg}$$

$$(P_L + P_B) = 4.31 \text{ kg/mm}^2$$

$$(P_L + P_B + Q) = 15.55 \text{ kg/mm}^2$$

$$(P_L + P_B + Q + F) = 15.55 \text{ kg/mm}^2$$

$$Q = 11.24$$

$$F = 0$$

$$\mathcal{E}_n = 0.00027 + 0.00071 = 0.00098$$

$$\mathcal{E}_c = 0$$

$$\mathcal{E}_F = 0$$

$$K = K_T = 1$$

$$\mathcal{E}_T = \mathcal{E}_n + \mathcal{E}_c + \mathcal{E}_F = 0.00098 \quad \omega \rightarrow N_D = 200000$$

$$\xi_a = \frac{500}{200000} = 0.0025$$

Considering as a bounding life of 30000 hours, the corresponding creep damage is

$$\xi_a' = \frac{30000}{200000} = 0.15$$

b) Hot start up with normal operating conditions.

The loads are pressure, dead weight and thermal expansion (270 + 530). By linearization between the ξ -range and the temperature difference

$$\xi_t = 0.0005$$

$$N_D = 10^6$$

$$\xi_b = \frac{2770}{>10^6} \approx 0$$

Again for a bounding life of 30000 hours, the corresponding creep damage is

$$\xi_b' = \frac{30000}{600000} = 0.05$$

c) Cloud passage type 1 operating conditions.

The loads are pressure, dead weight, linear and non linear thermal gradient in the tube thickness and thermal expansion (485 + 543)

$$\xi_T = 0.00068 \rightarrow N_D > 10^6 \quad \xi_c \approx 0$$

Negligible creep damage has to be expected and

therefore $\xi_c' \approx 0$

d) Cloud passage type 2 operating conditions.

The loads are pressure, dead weight, linear and non linear thermal gradient in the tube thickness and thermal expansion (338 + 530)

$$\epsilon_T = 0.00104 \mu \rightarrow N_D = 110000 \quad \xi_d = \frac{30000}{110000} = 0.273$$

Negligible creep damage has to be expected and

therefore $\xi_d' \approx 0$

e) Cloud passage type 3 operating conditions.

The loads are pressure, dead weight, linear and non linear thermal gradient in the tube thickness and thermal expansion (210 + 530)

$$\epsilon_T = 0.00119 \mu \rightarrow N_D = 43000 \quad \xi_e = \frac{3250}{43000} = 0.076$$

Negligible creep damage has to be expected and

therefore $\xi_e' \approx 0$

f) Earthquake after cold start up.

The loads are pressure, the most unfavorable combination between earthquake and dead weight and the maximum thermal expansion (20 + 530)

$$\epsilon_T = 0.00156 \mu \rightarrow N_D = 10000 \quad \epsilon_f = \frac{10}{10000} = 0.001$$

Negligible creep damage has to be expected and
therefore $\epsilon_f' \approx 0$

Concluding, the total fatigue damage is:

$$\epsilon = \epsilon_a + \epsilon_b + \epsilon_c + \epsilon_d + \epsilon_e + \epsilon_f = 0.352$$

and the total creep damage is:

$$\epsilon' = \epsilon_a' + \epsilon_b' + \epsilon_c' + \epsilon_d' + \epsilon_e' + \epsilon_f' = 0.2$$

Therefore the total fatigue-creep damage is

$$\epsilon_{\text{tot}} = \epsilon + \epsilon' = 0.552 < 1 \quad \text{acceptable}$$

APPENDIX 11. ALLOWABLE STRESS LIMITS FOR AISI 316 L

The following tables contain, as a function of the temperature, the values of allowable stresses that are used by Franco Tosi in design of stainless steel sodium component working of high temperature.

The definition of the term used is assumed according Code Case N47-17 sub. 3221.

1.1 Maximum allowable design stress intensity S_0

T (°C)	S_0 (N/mm ²)
20	107
100	105
200	96
300	95
400	86
500	80
600	72

1.2 Maximum time independent stress intensity S_m

T (°C)	S_m (N/mm ²)
20	115
100	115
200	107
300	94
400	85
500	80
600	72

1.3 Maximum temperature dependent stress intensity.

The value is tabulated for a working time of 30000 hours.

T (°C)	S_t (N/mm ²)
450	114
500	100
550	83
600	53

1.4 Maximum allowable value for general primary membrane stress intensity S_{mt}

The value is tabulated for a working time of 30000 h

T (°C)	S_{mt} (N/mm ²)
450	83
500	80
550	76
600	53

1.5 Yield strenght S_y

T (°C)	S_y (N/mm ²)
20	172
100	143
200	119
300	105
400	95
500	89
600	80

IEA ALMERIA PROJECT
ADVANCED SODIUM RECEIVER
ASR

Receiver Structure Analysis

Topic Report No. 10

Revision 0

December 1982

Prepared by: ENEL

FRANCO TOSI

AGIP NUCLEARE

CONTENTS

- Abstract
- 1. Panel frame analysis
 - 1.1. Analysis limits
 - 1.2. Single panel load analysis
 - 1.3. Structural calculation
 - 1.4. Material basic data
 - 1.5. Structure analysis results
 - 1.6. Principal connections analysis
- 2. Main frame analysis
 - 2.1. Analysis limits
 - 2.2. Main frame load analysis
 - 2.3. Material properties
 - 2.4. Structural calculation
 - 2.5. Structure analysis results
 - 2.6. Principal connections analysis

3. Sliding doors calculation

3.1. Analysis limits

3.2. Load analysis

3.3. Stress and displacements analysis

4. Conclusion

ABSTRACT

The main content of this report is related to the complete stress analysis of the receiver structure.

Three main parts have been recognized:

- . single panel structure
- . receiver main frame
- . sliding door system structure

For each substructure the geometric characteristics, the load sets, the stresses and the displacements have been carried out in order to check the stability and the operability of the component frame.

1. PANEL FRAME ANALYSIS

1.1. ANALYSIS LIMITS

The analysis hereafter reported is related to the single panel structure subjected to dead weight loads, wind loads, connecting pipes flexibility loads and earthquake loads.

In fig. 1.1/1 the structural scheme used in the analysis is reported.

In table 1.1/1 the restraints assumed for the different nodes are presented. It is to be noted that in all the internal junctions the beams have been considered as built in.

With reference to the "N" and "P" nodes (see fig. 1.1/1), although the structure schematization is not really equivalent to the actual one, the built in structure is realistic as far as no vertical load have been considered.

1.2. SINGLE PANEL LOAD ANALYSIS

In the structural analysis of the single panel frame the following loads have been considered:

CALCOLO DEFORMAZIONI TELAI0 PANNELLO
UNDEFORMED SHAPE

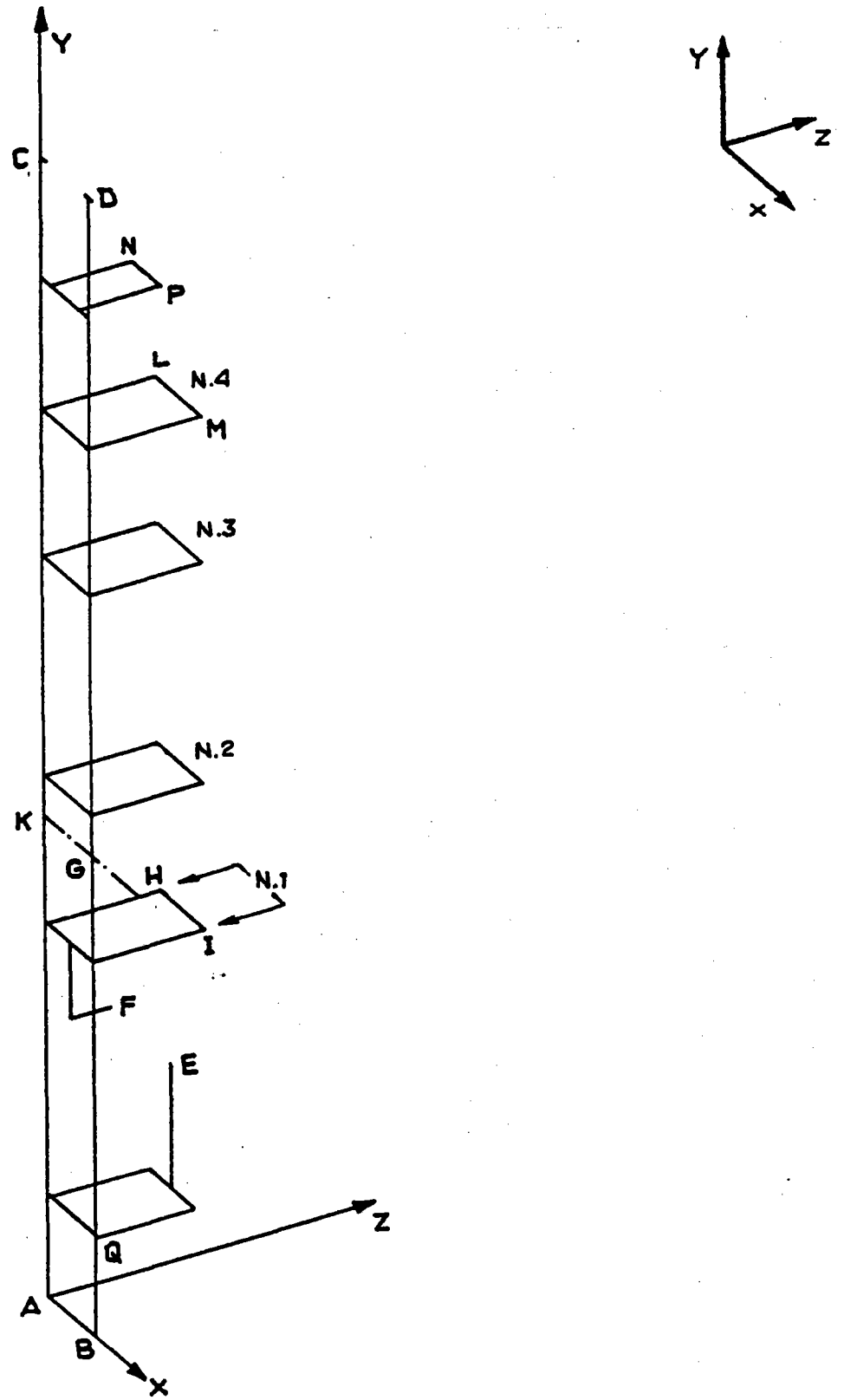


FIG. 1.1/1

SINGLE PANEL FRAME

Restraint conditions for the external nodes

Node	X displ.	Y displ.	Z displ.	X rot.	Y rot.	Z rot.
A	0	0	0	free	free	0
B	0	0	0	free	free	0
C	0	free	0	free	free	0
D	0	free	0	free	free	0
E	free	free	free	free	free	free
F	free	free	free	free	free	free
G	0	free	0	0	0	0
K	0	free	0	0	0	0

- a) dead weight of the structure;
- b) wind loads from wind pressure acting on the tube panel surface via stirrup system; the pressure considered is evaluated at the survival wind speed and the maximum operational wind speed in the case of opened door:

wind speed (Km/h)	150	50
corresponding pressure (Kg/m ²)	110	12
pressure at 44 m level (Kg/m ²)	166	18

- c) forces and moments, due to panel tubes, acting on lower and upper headers and on stirrup supporting system; these values are taken from Topic Report n° 7;
- d) connecting pipes flexibility loads evaluated following Topic Report n° 9. It has to be noted that the values used in the frame analysis are higher than those reported in Topic Report n° 9 because the aforementioned loads are related to a previous version of the piping flexibility analysis; for simplicity and conservatism those loads have been considered as actual;
- e) earthquake loads have been considered as static loads with a vertical acceleration of 0.2 g and with a horizontal one will an acceleration of 0.4 g according to Interatom letter dated 18/2/1982.

With reference to the operating conditions the following load sets have been considered in the frame analysis:

- load condition n° 1: . dead weight,
 - . forces and moments from the panel tubes,
 - . connecting pipes flexibility loads;
- load condition n° 2: wind loads at 150 and 50 Km/h wind speed;
- load condition n° 3: earthquake loads in x direction;
- load condition n° 4: earthquake loads in y direction;
- load condition n° 5: earthquake loads in z direction.

For the aforementioned load conditions in tables 1.2/1 + 1.2/5 forces and moments are presented at different mode locations of the frame (see fig. 1.1/1).

- Table 1.2/1 contains the loads acting on the lower header at point "E"; two contributions are considered: the first originated by the connecting pipes flexibility and the second originated by the panel tubes. It has to be noted that the load condition n° 2 is not applicable to the connecting pipes (first contribution) and the loads conditions n° 3 + 5 give negligible effects on the panel tubes (second contribution) and therefore on the structure.

LOWER HEADER LOADS

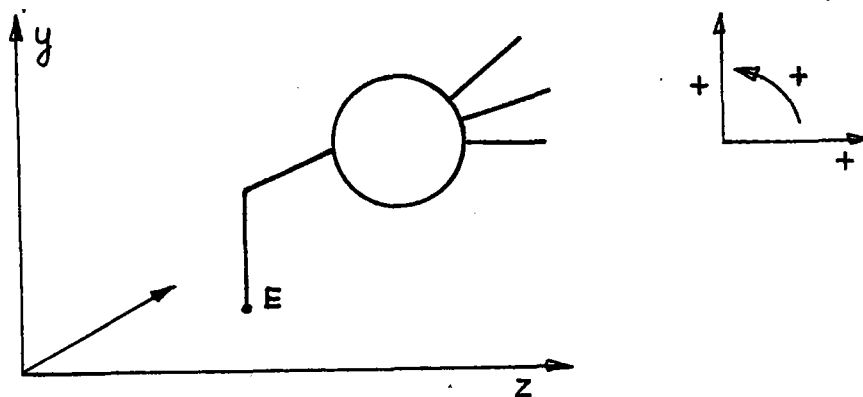
Node "E"

Moments and forces due to the connecting pipes flexibility

Load condition	F _x (Kg)	F _y (Kg)	F _z (Kg)	M _x (Kg mm)	M _y (Kg mm)	M _z (Kg mm)
1	68	-196	-147	-75800	-69700	-27800
2				not applicable		
3	34	6	9	5500	-25500	3400
4	-2	-16	0	-9900	2900	700
5	2	-2	34	-15400	1500	600

Moments and forces due to tube panel flexibility

Load condition	F _x (Kg)	F _y (Kg)	F _z (Kg)	M _x (Kg mm)	M _y (Kg mm)	M _z (Kg mm)
1	0	-97.89	-155.2	23972	0	0
2				not applicable		
3				negligible		
4				negligible		
5				negligible		



- TABLE 1.2/1 -

- Table 1.2/2 contains the loads acting at the down-comer fixed point (node "F"); at the location no effects are derived from load condition n° 2.
- Table 1.2/3 presents the loads acting on the upper header at point "N" and "P"; the same considerations as for point "E" are applicable.
- Table 1.2/4 is related to the wind loads on the stirrup supporting system for 150 and 50 Km/h wind speed. The 150 Km/h wind speed has been considered conservatively in the hypothesis of a failure of the door driving mechanism.
- Table 1.2/5 presents the load on the 4 cantilevers sustaining the stirrup systems. Three load contributions are taken into account: the first is the dead weight of the stirrup system itself, the second one is the dead weight of the "mullite" jacket boxes (see also table 1.2/6) and the third are the loads derived from the panel tubes.
Again the load condition n° 2 is not applicable to the first and second contribution and the load conditions n° 3+5 have negligible effects on the third contribution.
- Table 1.2/6 contains the weight evaluation of the mullite jacket box referred to the maximum span among cantilevers.

DOWNCORNER FIXED POINT

Node "F"

Moments and forces due to the connecting pipes flexibility

Load condition	F _x (Kg)	F _y (Kg)	F _z (Kg)	M _x (Kg mm)	M _y (Kg mm)	M _z (Kg mm)
1	-15	-217	7	-56400	72230	-22520
2			not applicable			
3	-65	6	6	470	26000	14530
4	3	-50	-2	-3000	-2760	-1410
5	2	0	-57	-15900	-450	570

- TABLE 1.2/2 -

UPPER HEADER LOADS

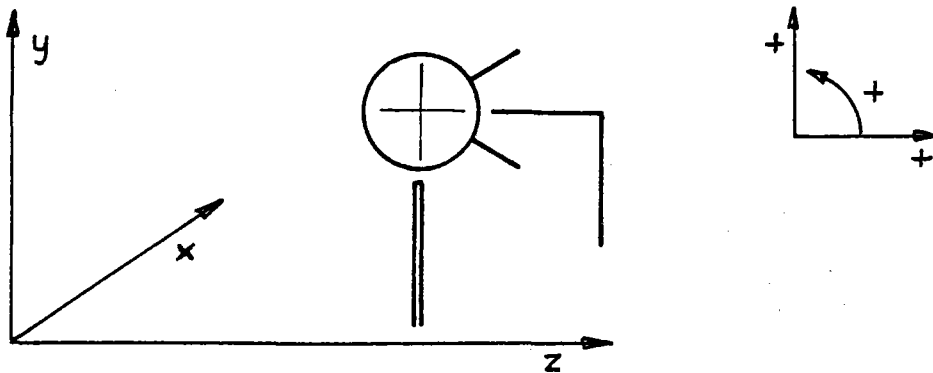
Nodes N and P

Moments and forces due to the connecting pipes flexibility

Load condition	F _x (Kg)	F _y (Kg)	F _z (Kg)	M _x (Kg mm)	M _y (Kg mm)	M _z (Kg mm)
1	0	36.27	-105.69	-12687	0	0
2			not applicable			
3			negligible			
4			negligible			
5			negligible			

Moments and forces due to downcomer

Load condition	F _x (Kg)	F _y (Kg)	F _z (Kg)	M _x (Kg mm)	M _y (Kg mm)	M _z (Kg mm)
1			negligible			
2			not applicable			
3			negligible			
4			negligible			
5	0	0	27	10000	0	0



- TABLE 1.2/3 -

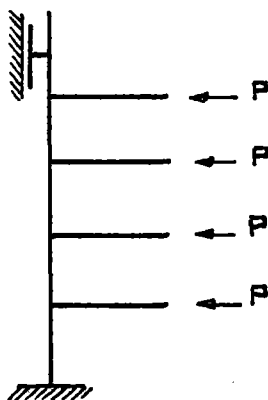
WIND LOAD ON THE TUBE PANEL

- Exposed surface $(3.75 \times 0.014) \times 39 = 2.04 \text{ m}^2$

considering a shape factor of 1.2, for the two wind speeds considered, the forces are:

- total force at $V = 150 \text{ Km/h}$ $F_{150} = 2.04 \times 1.2 \times 166 = 406 \text{ Kg}$
- total force at $V = 50 \text{ Km/h}$ $F_{50} = 2.04 \times 1.2 \times 18 = 44 \text{ Kg}$

for simplicity it has been assumed that each cantilever withstands one fourth of the total wind load



- force on a single support at $V = 150 \text{ Km/h}$ $f_{150} = 101.5 \text{ Kg}$
- force on a single support at $V = 50 \text{ Kg/h}$ $f_{50} = 11 \text{ Kg}$

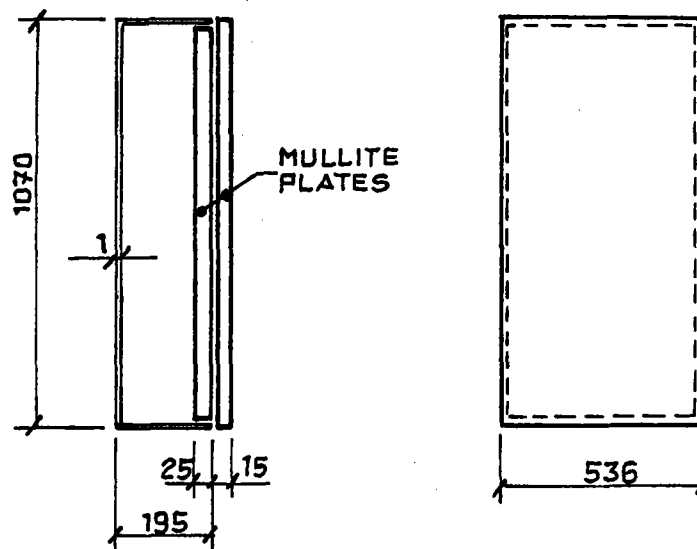
LOADS ON THE CANTILEVERS SUSTAINING THE STIRRUP SYSTEM

In order to simplify the table, the contributions of dead weight of the stirrup itself, the dead weight of the mullite jacket boxes and panel tubes loads have been summed up.

	Load condition	F _x (Kg)	F _y (Kg)	F _z (Kg)	M _x (Kg mm)	M _y (Kg mm)	M _z (Kg mm)
SUPPORT N. 1	1	0	-195	52	53500	0	0
	2	0	0	-102	0	0	0
	3	27	0	0	0	8000	0
	4	0	-14	0	4200	0	0
	5	0	0	27	10000	0	0
SUPPORT N. 2	1	0	-195	71	62500	0	0
	2	0	0	-102	0	0	0
	3	39	0	0	0	11700	0
	4	0	-20	0	6000	0	0
	5	0	0	39	20900	0	0
SUPPORT N. 3	1	0	-195	-2	53500	0	0
	2	0	0	-102	0	0	0
	3	27	0	0	0	8000	0
	4	0	-14	0	4200	0	0
	5	0	0	27	10000	0	0
SUPPORT N. 4	1	0	-165	63	53500	0	0
	2	0	0	-102	0	0	0
	3	27	0	0	0	8000	0
	4	0	-14	0	4200	0	0
	5	0	0	27	10000	0	0

- TABLE 1.2/5 -

MULLITE JACKET BOX WEIGHT EVALUATION



With reference to the largest box the following weight has been evaluated:

$$V_1 \approx 1.2 \text{ dm}^3$$

$$P_1 = V_1 \gamma_1 = 1.2 \times 8 \approx 9.6 \text{ Kg}$$

Insulation weight

$$V_{\text{ins}} \approx 100 \text{ dm}^3$$

$$P_2 \approx 100 \times 0.086 = 9.6 \text{ Kg}$$

Insulation plate weight

$$V_p = 23 \text{ dm}^3$$

$$P_3 = 23 \times 2.6 = 60 \text{ Kg}$$

$$P_{\text{tot}} = 9.6 + 9.6 + 60 + 15 = 95 \text{ Kg}$$

For the other jacket boxes, weights proportionally scaled down have been considered.

1.3. STRUCTURAL CALCULATION

The analysis of the panel frame has been carried out with the finite element SAP V code; the elements used are "beam elements".

The main goal of the design of the panel structure is a reasonable stiffness of the frame and the beam types have been chosen accordingly.

For the earthquake analysis, a static approach has been considered.

1.4. MATERIAL BASIC DATA

- Panel frame material:	FE 42 FN	
Yield strength	235 N/mm ²	
Ultimate strength	410+510 N/mm ²	
Ultimate elongation (%)	23	
Young's modulus	206000 N/mm ²	
- Bolts		
Class	8G (high strength)	
Screw type 8G	{ UNI 5727/65	
Nuts type 6S		UNI 5792/65
		UNI 5591/65
Yield strength	627 N/mm ²	
Ultimate strength	784+980 N/mm ²	
Ultimate elongation (%)	12	
Allowable shear strength	186 N/mm ²	
Allowable tensile strength	274 N/mm ²	

1.5. STRUCTURE ANALYSIS RESULTS

1.5.1. Node displacements

With reference to fig. 1.1/1, in table 1.5.1/1 the most meaningful node displacements have been reported.

For each location, the five loads conditions described at point 1.2. have been considered.

From the analysis of the results it can be noticed that no problem should arise for the regular operation of the component.

Taking into account the high stiffness requested by the frame design, negligible stresses have been found in the beams.

1.5.2. Panel boundary node loads

In order to evaluate the loads acting on the main receiver frame, in table 1.5.2/1 forces and moments are reported for the same different load conditions mentioned at point 1.2. at the boundary nodes of the panel.

NODE DISPLACEMENTS

	Load condition	DISPLACEMENTS (mm)			ROTATION (rad)		
		X	Y	Z	X	Y	Z
NODE H	1	-0.12	-0.20	-0.035	4.0 E-4	5.55E-5	-2.81E-5
	2	0.	-0.014	-0.012	2.52E-5	0.	0.
	3	0.080	0.017	0.020	-2.38E-5	8.87E-5	-5.20E-5
	4	6.67E-3	-0.020	-4.52E-3	3.72E-5	1.08E-6	-3.17E-6
	5	4.08E-3	9.23E-3	0.010	-5.31E-6	2.39E-6	-5.96E-6
NODE I	1	-0.12	-0.20	-0.062	4.15E-4	5.47E-5	-2.50E-5
	2	0.	-0.014	-0.012	2.52E-5	0.	0.
	3	0.080	-3.84E-3	-0.012	4.97E-7	0.80E-5	-5.20E-5
	4	6.67E-3	-0.021	-4.85E-3	3.86E-5	1.30E-6	-2.53E-6
	5	4.03E-3	6.84E-3	7.94E-3	-2.30E-6	8.03E-6	-5.96E-6
NODE L	1	-1.47E-3	-0.14	0.21	2.87E-4	-1.37E-7	-8.39E-6
	2	0.	-0.027	-0.22	4.98E-5	0.	0.
	3	0.87	0.012	0.24	-2.12E-5	1.23E-3	-6.05E-5
	4	3.16E-5	-0.016	0.016	2.62E-5	-2.90E-10	-1.50E-7
	5	6.18E-5	5.02E-3	0.14	1.57E-6	-1.04E-7	2.98E-7
NODE M	1	-1.47E-3	-0.15	0.21	2.87E-4	1.64E-7	-5.46E-6
	2	0.	-0.027	-0.22	4.98E-5	0.	0.
	3	0.87	-0.012	-0.24	2.12E-5	1.23E-3	-6.05E-5
	4	3.16E-5	-0.016	-0.016	2.62E-5	-2.82E-10	4.48E-7
	5	6.45E-5	5.14E-3	0.14	1.57E-6	1.03E-7	2.98E-7
NODE E	1	0.026	0.084	0.15	-9.087E-4	-2.32E-4	-6.56E-5
	2	0.	8.78E-3	-0.021	-1.83E-5	0.	0.
	3	0.13	-0.013	0.053	7.90E-5	1.87E-5	-6.42E-5
	4	-3.17E-3	2.61E-3	-0.034	-5.23E-5	1.65E-5	1.37E-5
	5	0.010	-0.022	0.078	8.12E-5	1.97E-5	1.27E-6
NODE F	1	0.75	0.36	0.69	-2.09E-3	4.08E-3	-8.05E-5
	2	0.	-4.79E-3	-0.020	2.52E-5	0.	0.
	3	4.89E-4	2.59E-4	0.14	-3.85E-4	7.98E-4	4.89E-6
	4	-0.023	-0.020	-0.36	1.00E-3	-1.26E-4	-2.23E-6
	5	1.92E-3	-0.050	-0.12	2.63E-4	1.07E-6	2.93E-6

- TABLE 1.5.1/1 -

PANEL BOUNDARY NODE LOADS

	Load condition	Fx (Kg)	Fy (Kg)	Fz (Kg)	Mx (Kg mm)	My (Kg mm)	Mz (Kg mm)
NODE A	1	-31.14	-661.5	-97.1			-8040
	2			-3.56			
	3	-41.66	76.64	27.05			-10390
	4		-115.40	-1.95			217
	5	-1.0	-1.35	30.62			-261
NODE B	1	-31.18	-859.	-11.45			-8045
	2			-3.56			
	3	-41.63	-64.64	-24.6			-10380
	4		-105.	-6.12			214.7
	5	-1.0		-20.72			-260
NODE C	1	-1.49	0.	28.19			294
	2			-33.5			
	3	-41.5		45.7			12670
	4			5.41			-4.87
	5			29.3			-12.86
NODE D	1	-1.54		28.19			304
	2			-33.58			
	3	-41.5		-45.76			12670
	4			5.41			-8
	5			29.30			-12.86
NODE K	1			122.	-78081	-396	-880
	2			-166.	47940		
	3			275.	-43890	722	-5854
	4				-10247	-16	-599
	5			89.	-32690	25	281
NODE G	1	-10		-128.	-148100	-237	-2892
	2			-166.	47940		
	3			-262.	52810	728	-5032
	4				-9514	-14	
	5			85.	-35240		

- TABLE 1.5.2/1 -

1.6. PRINCIPAL CONNECTIONS ANALYSIS

Hereafter the analysis of the connection between beams is reported. As example only two complete calculation are presented, the others having the same procedure. However no particular problems have to be expected at those points.

1.6.1. Connection between the principal column and the lower header support (node "Q")

The geometrical characteristics of the connection are reported in fig. 1.6.1/1. Having considered the joints between beams as built in, the analysis should demonstrate the bolts ability in withstanding moments. The detailed procedure methodology is reported in table 1.6.1/1.

The most unfavorable combination of the load conditions has been considered in this analysis taking into account that, for the particular connection, condition load n° 2 is not applicable. The numerical values are reported in table 1.6.1./2.

CONNECTION BETWEEN PRINCIPAL COLUMN AND LOWER HEADER SUPPORT : GEOMETRY

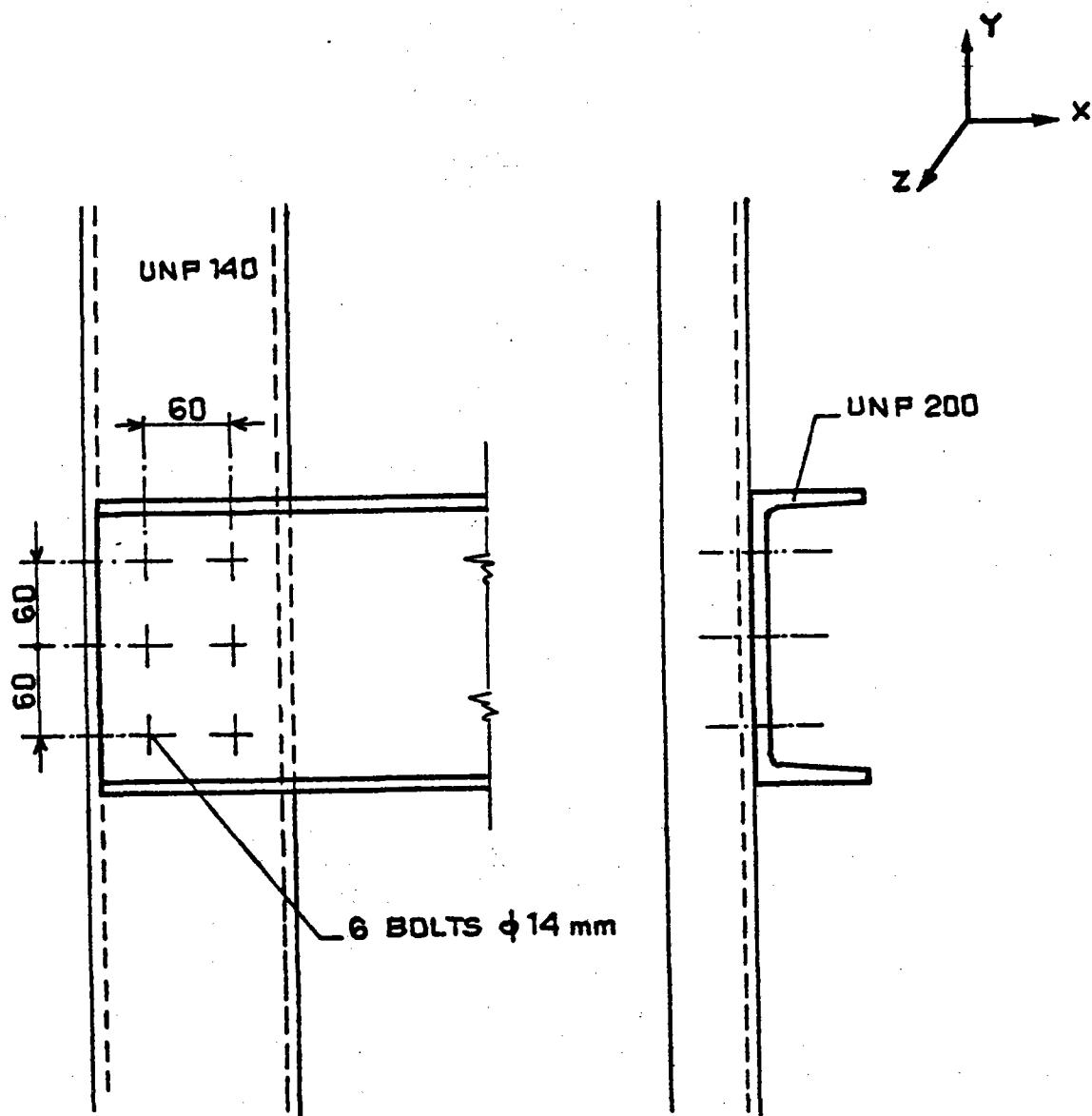


FIG. 1.6.1/1

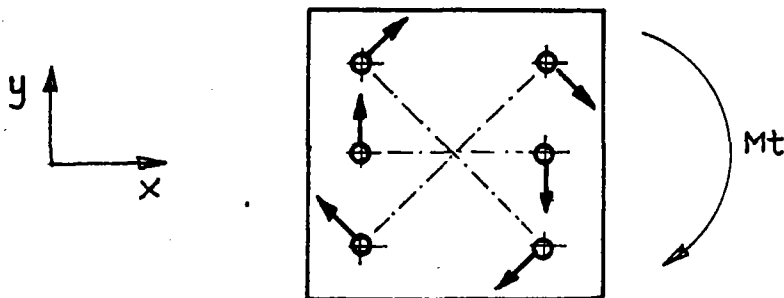
"COLUMN-LOWER HEADER SUPPORT" CONNECTION

ANALYSIS METHODOLOGY

- Single shear force acting on the bolts

$$V_t = \frac{M_t r_i}{\sum r_i^2}$$

M_t Torque moment
 r_i radius
 V_t Shear force on single bolt



- According to Italian Standard

$$\left(\frac{\tau}{\tau_{all}}\right)^2 + \left(\frac{\sigma}{\sigma_{all}}\right)^2 < 1$$

τ Shear stress
 τ_{all} Shear allowable stress
 σ Axial stress
 σ_{all} Axial allowable stress

- Maximum shear force allowable for a single bolt

$$N_t = \frac{1}{\gamma} \mu N_b$$

- Maximum shear force allowable for a single bolt in presence of axial forces

$$N_{tr} = N_t(1 - N/N_b)$$

where

N_{tr} Maximum shear force (by friction) trasmetted by each bolt in axial force presence
 N_t Maximum shear force (by friction) trasmetted by each bolt without axial force presence
 N Tensile force
 N_b Tensile force in the bolt
 γ Safety coefficient; assumed value 1.25
 μ Friction coefficient; assumed value 0.3

"COLUMN-LOWER HEADER SUPPORT" CONNECTION

CALCULATIONS

Total loads acting at the connection

Fx (Kg)	Fy (Kg)	Fz (Kg)	Mx (Kg mm)	My (Kg mm)	Mz (Kg mm)
439	-360	50	-22800	38025	-183480

$$V_t = 679 \text{ Kg}$$

$$V_{tx} = 588 \text{ Kg}$$

$$V_{ty} = 339.5 \text{ Kg}$$

$$V_{Fx} = 439/6 = 73 \text{ Kg}$$

$$V_{Fy} = 360/6 = 60 \text{ Kg}$$

$$V_{tot} = 772 \text{ Kg}$$

$$N_{tot} = 330 \text{ Kg}$$

Bolts ϕ 14 cross sectional area 115 mm²

$$\tau = 6.71$$

$$\sigma = 2.87$$

$$\left(\frac{6.71}{18.6}\right)^2 + \left(\frac{2.87}{27.4}\right)^2 = 0.14 < 1 \quad \text{accepted}$$

$$N_t = 1752 \text{ Kg}$$

$$N_{tr} = 1670 \text{ Kg} > V_{tot} = 772 \text{ Kg} \quad \text{accepted}$$

1.6.2. Connection between the principal column and the cantilevers supporting the stirrup system

The geometrical characteristics of the connection are reported in fig. 1.6.2/1. The analysis has been performed following table 1.6.1/1 and the detailed numerical values are reported in table 1.6.2/1.

The most unfavorable combination of load conditions has been considered.

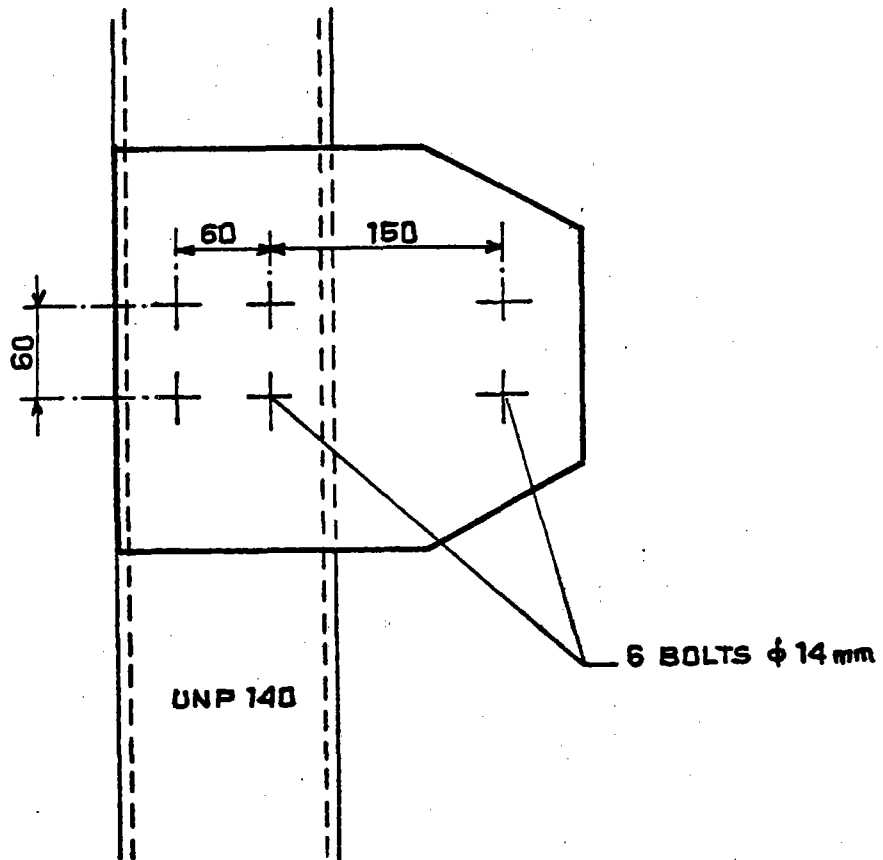
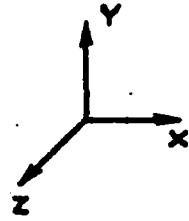


FIG. 1.6.2/1

"COLUMN-CANTILEVERS" CONNECTION

CALCULATIONS

Total loads acting at the connection

F _x (Kg)	F _y (Kg)	F _z (Kg)	M _x (Kg mm)	M _y (Kg mm)	M _z (Kg mm)
55	-107	20	16575		41700

$$V_t = 199 \text{ Kg}$$

$$V_{tx} = 30 \text{ Kg}$$

$$V_{ty} = 196 \text{ Kg}$$

$$V_{tot} = 311 \text{ Kg}$$

Bolts ϕ 14 cross sectional area 115 mm²

$$\tau = 311/115 = 2.71 \text{ Kg/mm}^2$$

$$\sigma = 0.73 \text{ Kg/mm}^2$$

$$\left(\frac{2.71}{18.6}\right)^2 + \left(\frac{0.73}{27.4}\right)^2 = 0.03 < 1 \quad \text{accepted}$$

$$N_t = 1272 \text{ Kg}$$

$$N_{tr} = 1252 \text{ Kg} > V_{tot} = 311 \quad \text{accepted}$$

2. MAIN FRAME ANALYSIS

2.1. ANALYSIS LIMITS

The analysis covers the main receiver frame subjected to dead weight loads, wind loads, earthquake loads and thermal expansion loads.

In fig. 2.1/1 the structural scheme used in the analysis is reported.

In table 2.1/1 the restraints assumed for the different nodes are presented. It is to be noted that in all the internal junctions the beams have been considered as built in.

2.2. MAIN FRAME LOAD ANALYSIS

In the structural analysis of the main frame the following loads have been considered.

a) Dead weight

- . Main frame elements
- . Outside casing and roof
- . Secondary elements (ribbed plates supporting beams etc.)
- . Panel frame
- . Sliding door

MAIN FRAME
STRUCTURAL SCHEME

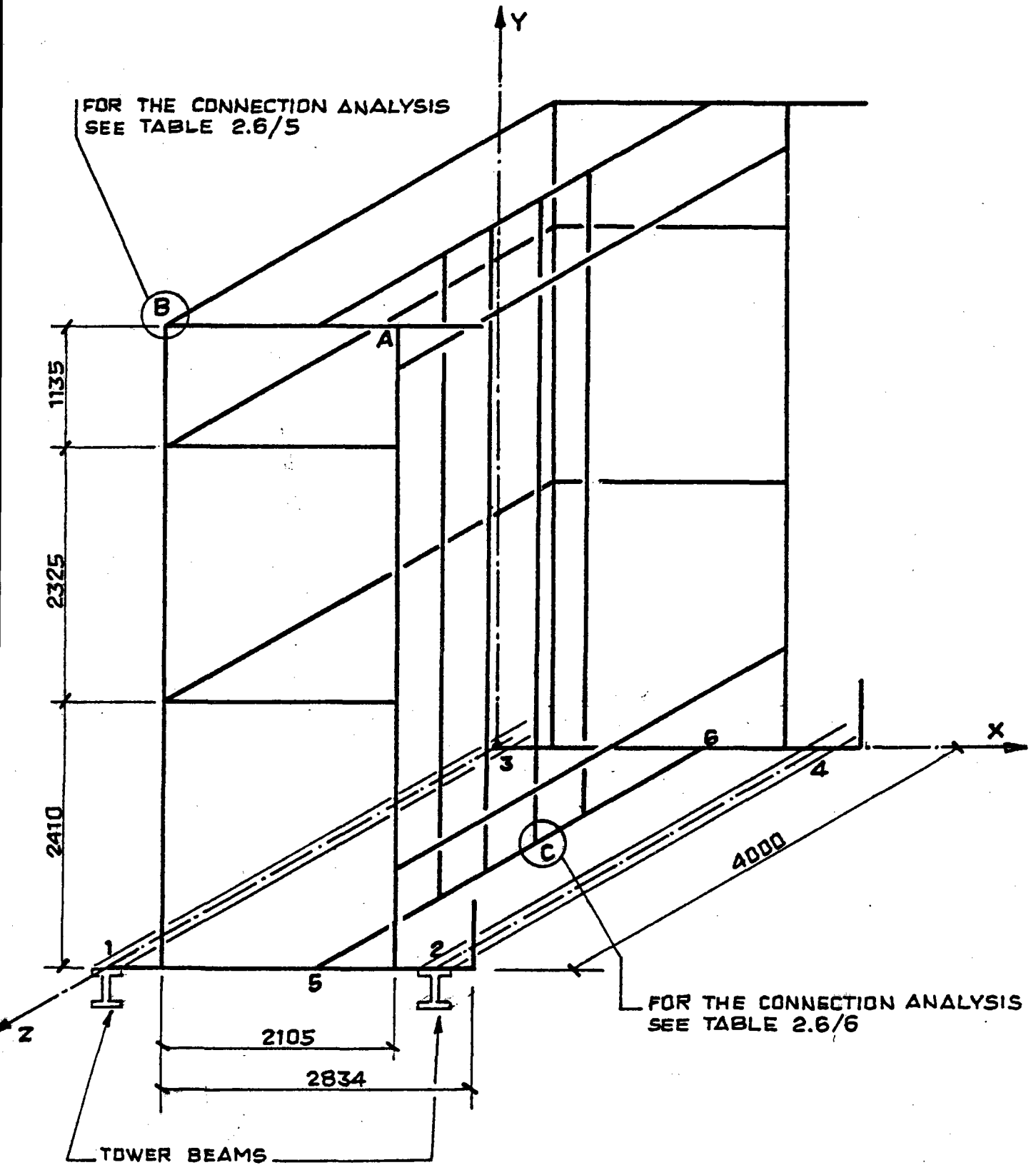


FIG. 2.1/1

MAIN FRAME
SUPPORT ANALYSIS

Restrain conditions for the external nodes

Node	Displacement			Rotation		
	X	Y	Z	X	Y	Z
1	0	0	0	free	free	free
2	free	0	0	free	free	free
3	0	0	0	free	free	free
4	free	0	0	free	free	free

All the other external nodes have been considered totally free.

- b) Wind loads from wind pressure acting on the outside walls, roof, sliding door and panel frame.

The pressure considered is evaluated at a wind speed of 50 e 150 Km/h.

	Wind speed (Km/h)	
	150	50
corresponding pressure (Kg/m ²)	110	12
pressure at 44 m level (Kg/m ²)	166	18

- c) Panel frame loads

The loads are taken from the previous panel frame analysis.

- d) Thermal expansion.

- e) Live load on the roof.

In the hypothesis that maximum wind (150 Km/h speed) and earthquake are not simultaneous loads and considering the maximum wind load more dangerous than horizontal earthquake effect, the maximum wind load has been assumed as horizontal design load.

In table 2.2/1 the principal load values acting on the frame are presented (see fig. 2.2/1 as well).

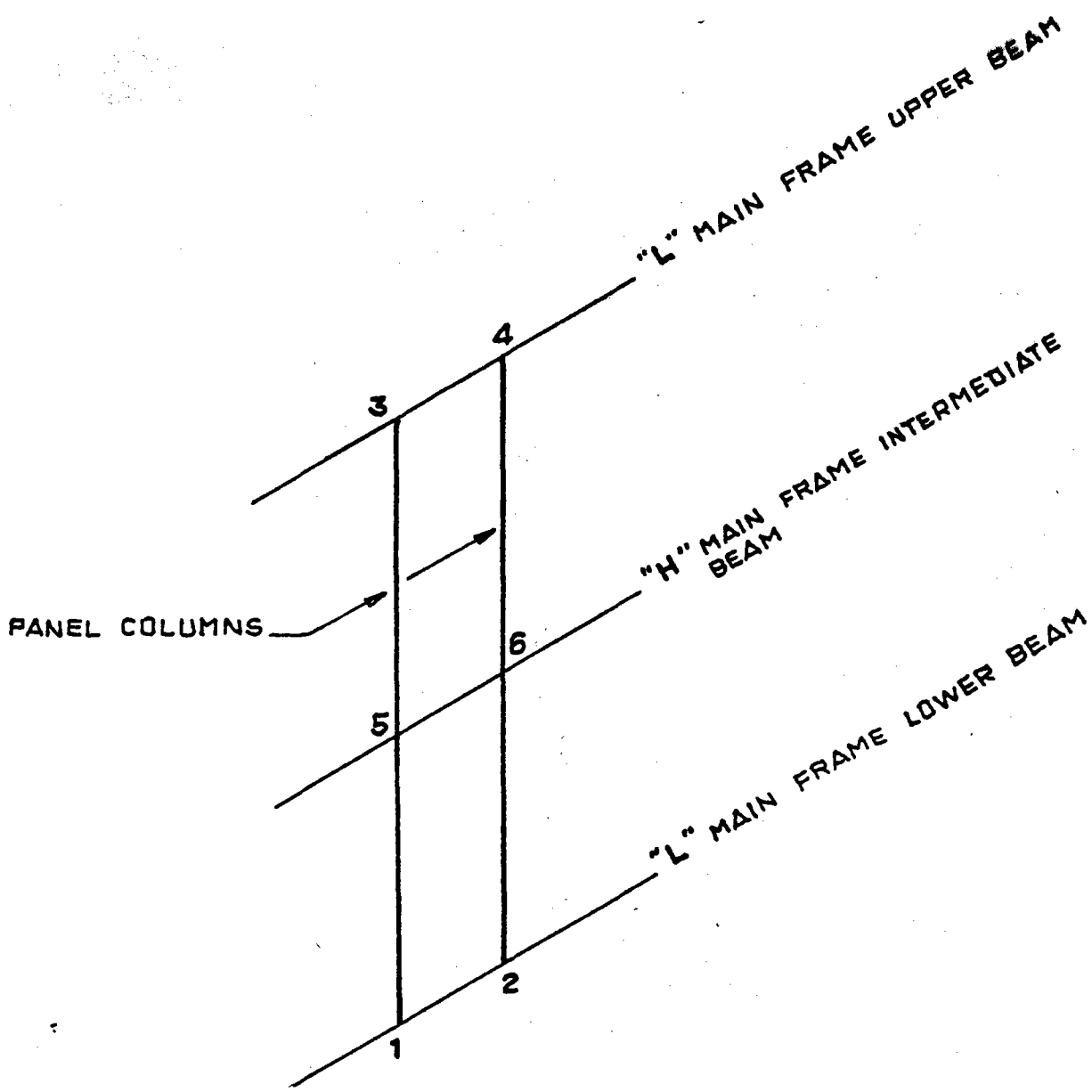


FIG. 2.2/1

LOAD DESCRIPTION

- . Dead load plus live load on the roof (vertical) ~ 300 Kg/m²
- . Outside casing load (vertical) 40 Kg/m²
- . Dead weight of the whole doors system (vertical) ~ 2300 Kg
- . Wind loads at two different wind speed (with a shape factor 1.2):
 - wind speed 50 Km/h 21.6 Kg/m²
 - wind speed 150 Km/h 199 Kg/m²
- . Single panel loads (see fig. 2.2/1; see also table 1.5.2/1):

	F _x (Kg)	F _y (Kg)	F _z (Kg)	M _x (Kg mm)	M _y (Kg mm)	M _z (Kg mm)
<u>NODE 1</u>						
1 dead load + thermal load	-97.1	-661.5	31.14	-8040		
2 wind load	-3.56					
<u>NODE 2</u>						
1	-11.45	-859	31.18	-8045		
2	-3.56					
<u>NODE 3</u>						
1	28.19		1.49	294		
2	-33.5					
<u>NODE 4</u>						
1	28.19		1.54	304		
2	-33.58					
<u>NODE 5</u>						
1	122			-880	-396	78081
2	-166					-47940
<u>NODE 6</u>						
1	-128			-2892	-237	148100
2	-166					-47940

- TABLE 2.2/1 -

The table 2.2/2 shows the description of the load conditions; the load combination is reported as well in table 2.2/3.

In table 2.2/2 the load condition n° 9 must be intended as a temperature difference between the beams 1-2, 3-4, 5-6 and the remaining part of the frame (see fig. 2.1/1).

2.3. MATERIAL PROPERTIES

The beams of the main frame of the receiver are manufactured in FE 37. The bolts used in the beam connections are in high strength material; all the characteristics are presented in table 2.3/1.

2.4. STRUCTURAL CALCULATION

The calculation has been carried out by means of the computer code ICES-STRUDL issued by M.I.T.

A spatial frame has been considered.

As in the panel frame analysis, again a particular care is used in order to avoid deformations that can affect the correct operation of the sliding door mechanism: therefore a particular stiffness is requested.

LOAD CONDITIONS

Load conditions n°:

- 1 live plus dead load
- 2 wind (150 Km/h) in the positive X direction with closed doors
- 3 wind (150 Km/h) in the negative X direction with closed doors
- 4 wind (150 Km/h) in the positive X direction with opened doors
- 5 wind (150 Km/h) in the positive X direction with opened doors
- 6 wind (150 Km/h) in the negative X direction with opened doors
- 7 wind (150 Km/h) in the negative Z direction
- 8 wind (150 Km/h) in the positive Z direction
- 9 difference in temperature ($\Delta t = 50 \text{ }^\circ\text{C}$)

LOAD COMBINATION

10th	Load condition 1 plus load condition 2
11th	L.C. 1 + L.C. 2 (scaled down to wind speed 50 Km/h)
12th	L.C. 1 + L.C. 3
13th	L.C. 1 + L.C. 3 (scaled down to wind speed 50 Km/h)
14th	L.C. 1 + L.C. 4
15th	L.C. 1 + L.C. 4 (scaled down to wind speed 50 Km/h)
16th	L.C. 1 + L.C. 5
17th	L.C. 1 + L.C. 5 (scaled down to wind speed 50 Km/h)
18th	L.C. 1 + L.C. 6
19th	L.C. 1 + L.C. 6 (scaled down to wind speed 50 Km/h)
20th	L.C. 1 + L.C. 7
21th	L.C. 1 + L.C. 7 (scaled down to wind speed 50 Km/h)
22th	L.C. 1 + L.C. 8
23th	L.C. 1 + L.C. 8 (scaled down to wind speed 50 Km/h)
24th	L.C. 1 + L.C. 9

MATERIAL PROPERTIES

Main frame material	FE 37
Yield strength	$\geq 235 \text{ N/mm}^2$
Allowable strength	156 N/mm^2
Allowable strength (at 150 Km/h wind speed)	176 N/mm^2
Ultimate strength	$362 + 470 \text{ N/mm}^2$
Ultimate elongation (%)	≥ 26

Bolts

Class 8G - High strength

Screw	type 8G	$\left\{ \begin{array}{l} \text{UNI 5727/65} \\ \text{UNI 5792/65} \\ \text{UNI 5591/65} \end{array} \right.$
Nuts	type 6S	
Allowable shear strength		186 N/mm^2
Allowable tensile strength		274 N/mm^2
Ultimate strength		$784+980 \text{ N/mm}^2$
Yield strength		627 N/mm^2

As mentioned at previous paragraph 2.2., the wind load at 150 Km/h speed has been considered a more dangerous horizontal load than earthquake; therefore only maximum speed wind load has been applied.

2.5. STRUCTURE ANALYSIS RESULTS

Considering the high stiffness requested to the structure, small stresses are found in the beam elements at each station.

In table 2.5/1 the displacements of the node "A" (see fig. 2.1/1), considered as the most meaningful, are presented for each load condition: as can be seen no problem can arise from the deformation of the structure that is as stiff as requested.

In table 2.5/2 the moments and forces at locations 1 + 4 (see fig. 2.1/1) connecting the receiver to the structure of the tower are reported; in this case the most unfavorable bound of load conditions has been applied.

2.6. PRINCIPAL CONNECTIONS ANALYSIS

The analysis of the beam connections has been carried out following European Recommendation (EKS) and Italian

NODE "A" DISPLACEMENTS

Load condition	DISPLACEMENTS (centimeters)			ROTATION (degrees)		
	X	Y	Z	X	Y	Z
1	0.02710	-0.01538	0.00231	-0.00340	0.02729	-0.00141
2	0.60205	-0.01638	-0.00117	0.00027	0.00532	-0.02360
3	-0.44647	0.00300	-0.00473	0.00030	0.01200	0.02789
4	0.22801	-0.01264	-0.00641	0.00038	0.01515	-0.00082
5	0.22565	-0.01270	0.02364	-0.00003	-0.03022	-0.00081
6	-0.43755	0.00335	0.00528	0.00098	-0.00775	0.02515
7	-0.04057	0.00577	-0.07578	0.02207	-0.11122	0.00133
8	0.03832	-0.00871	0.08944	-0.00743	0.09054	0.00022
9	0.04160	0.35576	0.18578	-0.00075	-0.27427	-0.00006
10	0.62915	-0.03176	0.00114	-0.00313	0.03261	-0.02501
11	0.09405	-0.01720	0.00218	-0.00337	0.02788	-0.00403
12	-0.41937	-0.01238	-0.00242	-0.00310	0.03929	0.02648
13	-0.02255	-0.01505	0.00178	-0.00337	0.02863	0.00169
14	0.25511	-0.02802	-0.00410	-0.00302	0.04244	-0.00223
15	0.05246	-0.01679	0.00159	-0.00336	0.02898	-0.00150
16	0.25275	-0.02808	0.02594	-0.00343	-0.00292	-0.00222
17	0.05219	-0.01679	0.00493	-0.00341	0.02393	-0.00150
18	-0.41045	-0.01203	0.00759	-0.00242	0.01954	0.02374
19	-0.02156	-0.01501	0.00289	-0.00329	0.02643	0.00139
20	-0.01347	-0.00961	-0.07348	0.01867	-0.08393	-0.00008
21	0.02259	-0.01474	-0.00612	-0.00095	0.01492	-0.00126
22	0.06542	-0.02409	0.09174	-0.01083	0.11783	-0.00119
23	0.03136	-0.01635	0.01225	-0.00423	0.03736	-0.00139
24	0.06670	0.34038	0.18809	-0.00415	-0.24698	-0.00147

Load condition 2+8 and 12, 14, 16, 18, 20, 22 are for a wind speed of 150 Km/h.
 Load condition are explained in table 2.2/2 and 2.2/3.

- TABLE 2.5/1 -

SUPPORTS REACTIONS AT RECEIVER/TOWER CONNECTION

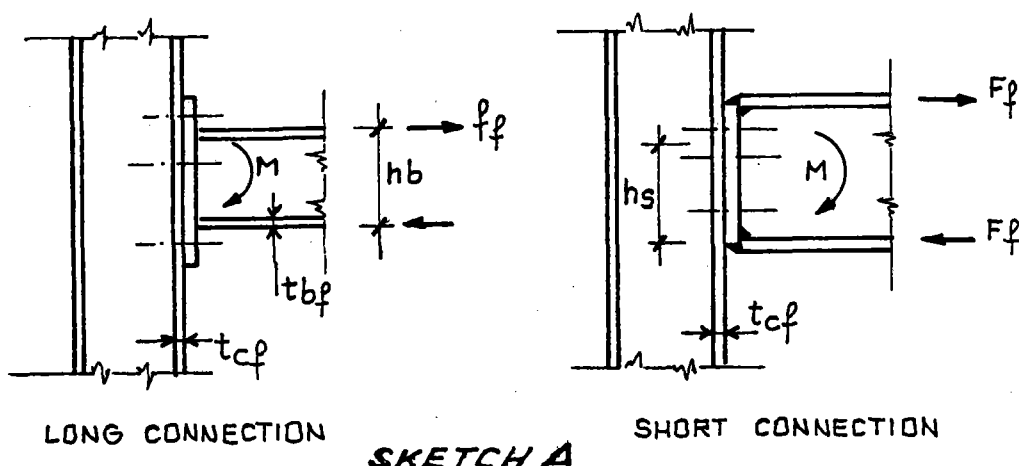
Node	Force (Kg)			Moment (Kg cm)		
	X	Y	Z	X	Y	Z
1	1521	1314	37	0	2198	0
2	-258	5422	-385	0	-18097	0
3	54	3062	496	0	23842	0
4	846	5762	-8	0	-794	0

- TABLE 2.5/2 -

Structural Standards. The methodology used is reported in tables 2.6/1 + 2.6/4 for different analysis in the bolts and in the beams.

All the nodes of the frame have been analyzed following the aforementioned procedures; as example two meaningful connections are reported in detail in table 2.6/5 for node B and in table 2.6/6 for node C (see fig. 2.1/1).

PLASTIC BUCKLING OF THE COLUMN WEB ANALYSIS



With reference to sketch A above:

- . limit moment for long connections $M_{vu} = F_f \times (h_b - T_{bf})$
- . limit moment for short connections $M_{vu} = F_f \times h_s$

where

- h_b = beam high
- h_c = column high
- t_{bf} = beam flange thickness
- t_{cf} = column thickness
- h_s = level arm of the force

$$F_f = \frac{\sigma_y \times t_{cw} \times S_c \times (h_c - 2t_{cf})}{\sqrt{(h_c - 2t_{cf})^2 + 3m^2 \times S_c^2}}$$

- σ_y = column yield stress
- t_{cw} = web column thickness
- S_c = distribution high stresses in the column high
- m = asymmetric load coefficient

COLUMN FLANGE ANALYSIS

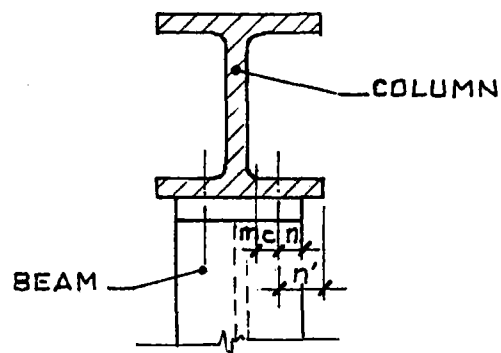
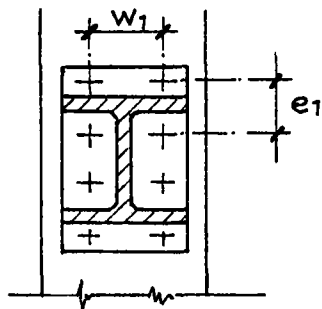
$$F_f = \frac{4 \cdot b_m \cdot m_{pl}}{m_c}$$

b_m = Luder line in the column flange

$$b_m = e_1 + 4 \cdot m_c + 1.25 \cdot n'$$

$$m_{pl} = \frac{1}{4} \cdot t_{cf}^2 \cdot \sigma_y$$

Distance between bolts and column start connector



- TABLE 2.6/2 -

BOLTS ANALYSIS

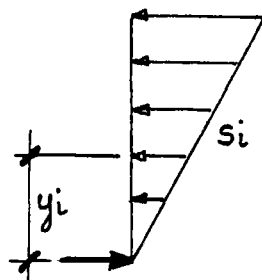
- a) According to EKS Recommendation for flanged connections the ultimate strength of the bolt is given by

$$F_f = \frac{2 \cdot b_m m_{pl} + n \sum F_{bu}}{m_c + n} \quad \text{if } \sum F_{bu} > F_f$$

$$F_f = \sum F_{bu} \quad \text{if } \sum F_{bu} \leq F_f$$

where: F_f ultimate strength of the bolt
 b_m Lüder line in the column flange
 $m_{pl} = 1/4 t_{cf}^2 \cdot \sigma_y$
 σ_1 yield strength of the column
 $\sum F_{bu}$ limit loads of the bolts
 m_c see sketch in table 2.6/2
 n see sketch in table 2.6/2
 ($n < 1.25 m_c$ and $n < n'$)

- b) According to Italian Standard for normal connections



$$\text{single bolt load } S_i = \frac{M y_i A_{ri}}{J_b}$$

$$\text{stress in the bolt } \sigma_b = \frac{S_i}{A_{ri}}$$

where: M applied moment
 y_i see sketch on side
 A_{ri} bolt cross sectional area
 J_b inertia moment of the bolt

COLUMN WEB ANALYSIS

$$F_f = \frac{\sigma_y \cdot t_{cw} \cdot S_t \cdot (h_c - 2 \cdot t_{cf})}{\sqrt{(h_c - 2 t_{cf})^2 + 3 \cdot m^2 \cdot S_t^2}}$$

where

$$S_t = e_1 + 4 \cdot m_c + 1.25 \cdot n' \quad (\text{see sketch in table 2.6/2})$$

t_{cw} = thickness web column

t_{cf} = thickness of column flange

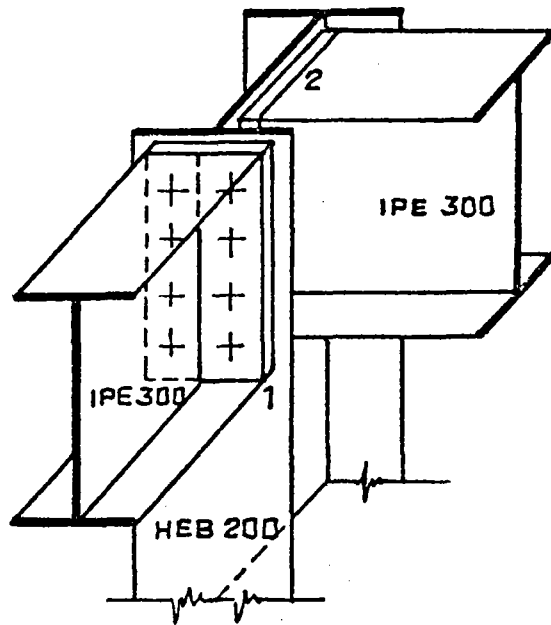
σ_1 = yield strength of the column

h_c = column high

m = asymmetric load coefficient

NODE CONNECTION "B"

CALCULATION (DW. E103007)

- NUMBER 1

- Plastic buckling of the column web

$$F_{u1} = \frac{2400 \times 0.9 \times 16.5 \times (20 - 2 \times 1.5)}{\sqrt{17^2 + 3 \times 16.5^2}} = 18248 \text{ Kg}$$

$$t_{ow} = 0.9 \text{ cm}$$

$$S_o = 5 \times (1.8 + 1.5) = 165$$

- Column flange analysis

$$F_f = \frac{4 \times b_m \times m_{pl}}{m_o} = \frac{4 \times 24.56 \times 1350}{3.61} = 36737 \text{ Kg}$$

$$b_m = 7 + 4 \times 3.61 + 1.25 \times 2.5 = 24.565 \text{ cm}$$

$$m_o = 32.5 + \frac{1}{5} \times 18 = 36.1 \text{ cm}$$

$$m_{pl} = \frac{1}{4} \times 1.5^2 \times 2400 = 1350 \text{ Kg}$$

- Column web analysis

$$F_f = \frac{2400 \times 0.9 \times 24.56 \times (20 - 2 \times 1.5)}{\sqrt{17^2 + 3 \times 24.56^2}} = 19686 \text{ Kg}$$

$$\bullet \text{ Limit moment: } 17740 \times 19.5 = 345930 \text{ Kg cm}$$

$$\bullet \text{ Principal moment: } 68617 \text{ Kg cm}$$

$$\bullet \text{ Safety factor: } 345930/68617 = 5 > 1.5$$

- NUMBER 2 (Italian standard)

- Bolts stress

$$M_z = 142073 \text{ Kg cm}$$

$$T_y = 1560 \text{ Kg}$$

$$S_{bott \text{ max}} = \frac{142073 \times 23 \times 1.15}{1918.2} = 1959 \text{ Kg}$$

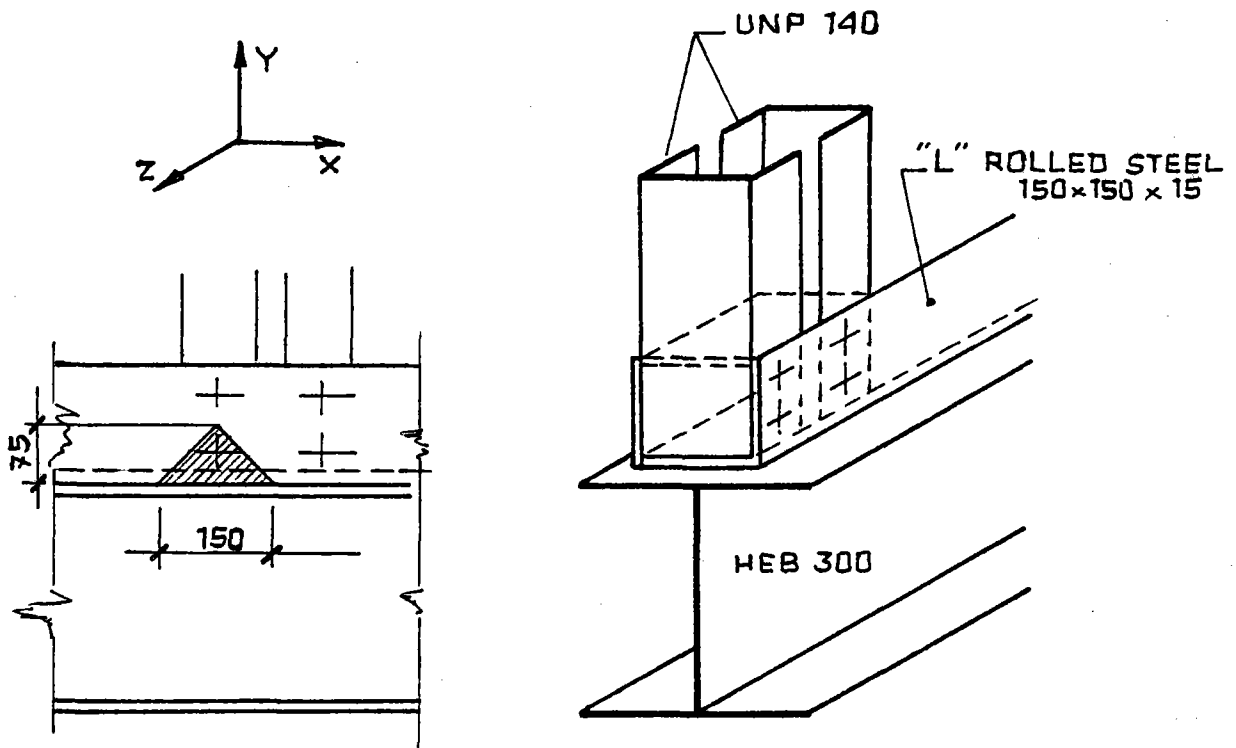
$$\sigma_{bott} = \frac{1959}{115} = 17 \text{ Kg/mm}^2$$

$$\tau_{bott} = 2.52 \text{ Kg/mm}^2 \text{ bolts type 80}$$

$$\left(\frac{17}{18}\right)^2 + \left(\frac{2.52}{19}\right)^2 = 0.38 < 1$$

NODE CONNECTION "C"

CALCULATION (DW D108366)



The analysis consists in the evaluation of the strength of the equal angle against bending.

The force acting on the UNP 140 at bolts location is $F_x = 100.66 \text{ Kg}$ and $F_y = 859 \text{ Kg}$ (see table 2.2/1).

A resisting cross section has been considered with the following characteristics:

$$A = 150 \times 15 = 2250 \text{ mm}^2$$

$$W = \frac{1}{6} b h^2 = \frac{1}{6} 150 \times 15^2 = 5625 \text{ mm}^3$$

$$\sigma_{\text{bending}} = \frac{F_x \times 75}{W} = \frac{100.66 \times 75}{5625} = 1.34 \text{ Kg/mm}^2$$

$$\sigma_{\text{compr}} = \frac{F_y}{A} = \frac{859}{2250} = 0.38 \text{ Kg/mm}^2$$

$$\sigma_{\text{tot}} = 1.34 + 0.38 = 1.72 \text{ Kg/mm}^2 < \sigma_{\text{all}} = 16 \text{ Kg/m}^2 \quad \text{accepted}$$

3. SLIDING DOORS CALCULATION

3.1. ANALYSIS LIMITS

The analysis regards sliding door subjected to dead weight and wind loads.

In fig. 3.1/1 the sliding door structural scheme is presented.

3.2. LOAD ANALYSIS

The sliding door is loaded by:

- . dead weight
- . wind at 50 Km/h (opened doors)
- . wind at 150 Km/h (closed doors).

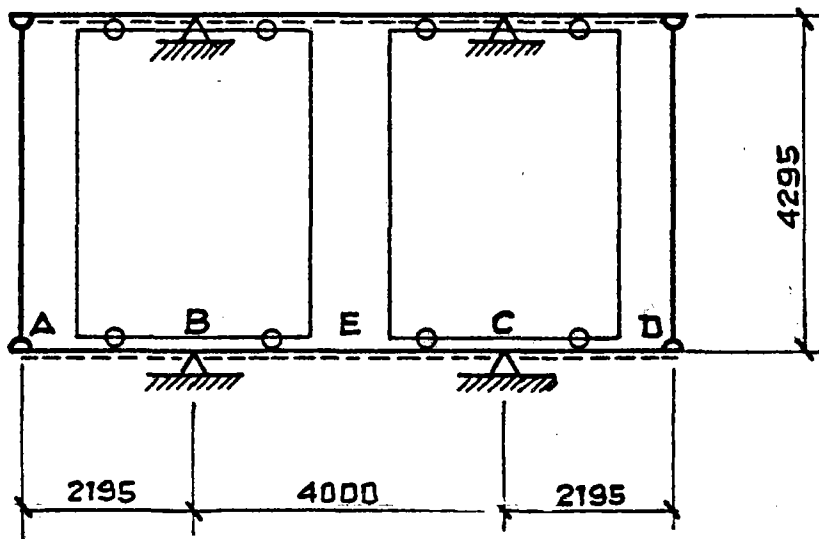
The earthquake loads have not been considered because they give negligible effects compared with wind effects taking into account that the two loads don't act contemporary.

It was also been considered the possibility of a failure of the door driving system with a different position of the doors.

The load values are reported in table 3.2/1.

SLIDING DOOR SYSTEM

STRUCTURAL SCHEME FOR VERTICAL LOADS



STRUCTURAL SCHEME FOR HORIZONTAL LOADS

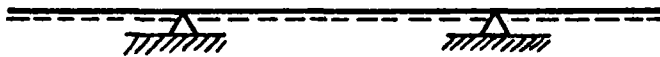


FIG. 3.1/1

DOOR SYSTEM LOAD TABLE

- DEAD LOAD

. Door weight	880 Kg
. Dead rolled steel weight	65 Kg/m

- WIND LOAD

	Wind speed (Km/h)	
	50	150
Pressure to 44 m (Kg/m ²)	18	166
Espositure coefficient	1.2	1.2

Surface: 2290 x 4495 \approx 10 m²

Wind force:

$$F_{50} = (10 \times 1.2 \times 18) / 4 = 54 \text{ Kg}$$

$$F_{150} = (10 \times 1.2 \times 166) / 4 = 498 \text{ Kg}$$

3.3. STRESS AND DISPLACEMENTS ANALYSIS

A calculation of the stresses and displacements in the sliding door system for different door positions has been performed.

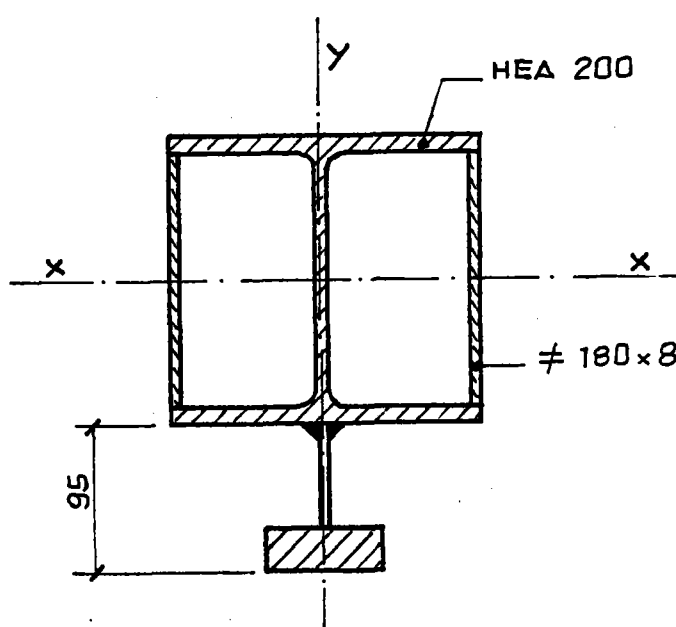
The section properties of the beams used in the doors supporting frame are reported in table 3.3/1; it has to be noted that the frame itself has a guide function.

In table 3.3/2 the maximum bending moments for different load conditions are presented; the corresponding bending stresses and displacements are collected in table 3.3/3.

The detailed analysis of the guides is reported in table 3.3/4.

GUIDES SECTION CHARACTERISTICS

A closed section made of a rolled steel HEA 200 and a couple of plates is considered



HEA 200 characteristics:

$$W_x \quad 389 \quad \text{cm}^3$$

$$W_y \quad 134 \quad \text{cm}^3$$

$$J_x \quad 3690 \quad \text{cm}^4$$

$$J_y \quad 1340 \quad \text{cm}^4$$

Total section characteristics:

$$J_x \quad 4470 \quad \text{cm}^4$$

$$J_y \quad 4451 \quad \text{cm}^4$$

$$W_x \quad 470 \quad \text{cm}^3$$

$$W_y \quad 412 \quad \text{cm}^3$$

MAXIMUM BENDING MOMENTS

a) DEAD LOAD

- . Opened doors

$$M_{\max} = -670000 \text{ Kg mm} \quad \text{at location B in fig. 3.1/1}$$

- . Closed doors

$$M_{\max} = 996665 \text{ Kg mm} \quad \text{at location E in fig. 3.1/1}$$

b) WIND LOAD

- . Wind 50 Km/h opened doors

$$M_{\max} = -107000 \text{ Kg mm} \quad \text{at location B in fig. 3.1/1}$$

- . Wind 150 Km/h closed doors

$$M_{\max} = 1098900 \text{ Kg mm} \quad \text{at location E in fig. 3.1/1}$$

MAXIMUM STRESSES AND DISPLACEMENTS

$$\sigma_{\max} \left(\begin{array}{l} \text{opened} \\ \text{doors} \end{array} \right) = \frac{107000}{412000} + \frac{670000}{470000} = 1.68 \text{ Kg/mm}^2$$

$$\sigma_{\max} \left(\begin{array}{l} \text{closed} \\ \text{doors} \end{array} \right) = \frac{1098900}{412000} + \frac{996000}{470000} = 4.78 \text{ Kg/mm}^2$$

The section characteristics W are reported in table 3.3/1.

$$\sigma = 4.78 < \sigma_{\text{allowable}} = 16 \text{ Kg/mm}^2$$

Displacements

f (opened doors, v= 50 Km/h) = 0.5 mm at location A

f (opened doors, v= 50 Km/h) = 0.2 mm at location E

f (closed doors, v=150 Km/h) = 1.3 mm at location E

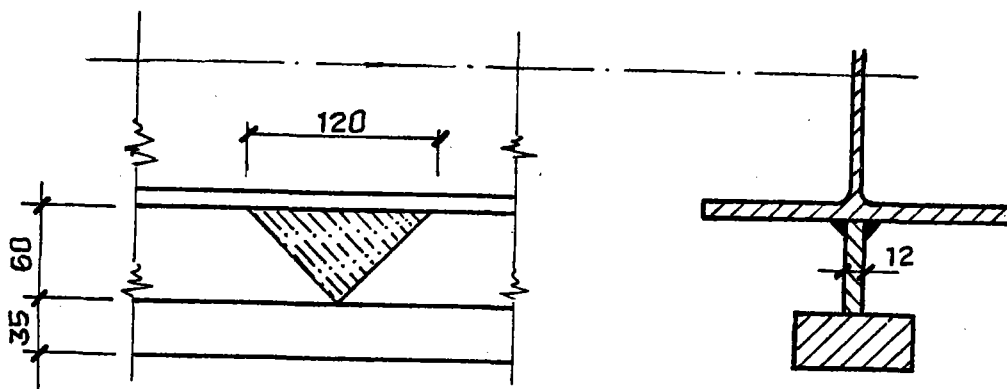
If we consider a speed wind of 150 Km/h with opened doors the results are:

$$\sigma_{\max} = 4.00 \text{ Kg/mm}^2$$

f = 4.64 mm at location A

GUIDES ANALYSIS

Calculation slide guide



Force ≈ 498 Kg (see table 3.2/1)

$$M = 498 \times 60 = 29880 \text{ Kg mm}$$

Considering a 45° force distribution

$$W = \frac{1}{6} 120 \times 12^2 = 2880 \text{ cm}^3$$

$$\sigma_{\text{bending}} = \frac{29880}{2880} = 10.35 \text{ Kg/mm}^2$$

$$\tau = \frac{498}{120 \times 12} = 0.34 \text{ Kg/mm}^2$$

$$\sigma_{\text{id}} = \sqrt{10.35^2 + 3 \times 0.34^2} = 10.36 \text{ Kg/mm}^2 < 16$$

4. CONCLUSION

A detailed stress analysis of the receiver frame has been carried out.

No particular problems have been found from stress point of view; the structure is as stiff as requested by the good operability of the panels and of the door system.

DDC FINAL CONFIGURATION
REFERENCE TRANSIENTS CALCULATION

TOPIC REPORT N. 11

Date: 25 January 1983

PREPARED BY: AGN
ENEL
FRANCO TOSI

INTRODUCTION

For ASR life time evaluation the following steps are foreseen:

- design conditions assesement and steady state computation (Topic Report n. 1, 2, Progres Report n. 8).
- statement of reference transients taking into account real situations and plant characteristics (Topic Report n. 6)
- evaluation of system behaviour (transient temperature distributions and thermal fields in the most critical sections) for every transient considered. (Topic Report n. 4, 5, Progress Report n. 11)
- stress analysis computation
- damage evaluation

The principal aim of this report is to collect the most meaningful transients obtained applying the final control system configuration and some results of the sensitivity analysis performed on critical parameters (sun presence sensor error, maximum sodium flow rate).

The final control configuration is similar to the one already presented, (T.R. n. 5) only showing some improvement in the sun presence sensor use (a derivative action in parallel with the proportional one is included). Referring to Topic Report n. 6, transients in ASR lifetime analysis are splitted into three categories:

- normal operation transients
- upset operation transients
- fault event transients

This subdivision is followed also in this report.

NORMAL OPERATION TRANSIENTS

Morning cold start-up, hot start-up and overnight shut-down are manually operated according to predetermined procedures. Only transients due to cloud passages are managed by control system and depend on weather conditions. Table 1 (from Topic Report n. 6) shows the different incident power behaviour as related to cloud velocity (wind) and dimension. For simulation purpose the worst case (maximum wind velocity and available power), is assumed.

Plots show:

- absorbed power (in a central section of panel 5) and sodium flow rate
- receiver outlet sodium temperature
- last radiated section sodium temperature and maximum radiated section sodium temperature
- receiver outlet support flange temperature
- panel 5 inlet sodium temperature

versus time in case of

- "V" transient
- short "U" transient
- long "U" transient.

In all the above mentioned cases the sun presence sensor signal has been assumed as affected by an error of 50% in defect.

In case of the worst foreseen "V type" transient, (fig. n. 1) the computed maximum outlet sodium temperature is 543 °C with an overshoot of 13 °C since the normal condition is 530 °C; maximum temperatures of sodium in correspondence of peak flux section and receiver outlet "flange" are 490 °C and 540 °C respectively. Maximum sodium temperature time gradients at the same points are 15 °C/sec, 6 °C, 15 °C/sec. Considering the very strong disturbance (100% sun power to 0 within 11 sec. and back to 100%) the overshoot is appreciably limited.

In case of short "U type" transient (from 100% to 0 within 22 sec and back to 100% after 30 sec.), which is again the worst case considered, the simulation results are presented in Fig. 2. It shows (referring always to receiver outlet, maximum incident flux position and receiver outlet "flange") sodium temperatures and maximum gradients of 545 °C, 490 °C, 545 °C and 16 °C/sec, 12,5 °C/sec, 23 °C/sec.

Considering long "U" type transients (Fig. 3), maximum temperatures (after a complete transient including 300 seconds of shading) are 540 °C, 490 °C and 540 °C; gradients are 12 °C/sec., 10 °C/sec, 10 °C/sec.

The results can be compared with data from Fig. 4 (250

sec. of shading and 10.9 kg/sec. of maximum flow rate available) from which it can be seen that peak temperatures and maximum time gradients are weakly dependent on these values of maximum sodium flow rate.

The receiver cools down completely within 350 seconds of shading roughly. For this reason the behaviour of the system at sun restarts after shading longer than 350 sec. is always the same and for this regard the restart transient from cold condition is representative of any case of prolonged shading.

Fig. 5 presents the behaviour after a 0 to 100% reinsolation in 11 seconds, starting from 270 °C (cold storage temperature). Also in this case temperatures and maximum time gradients are maintained within very acceptable bounds.

The Figures 6, 7 show a transient due to a reinsolation from 10% to 100% in 11 sec. starting from a steady-state condition of the receiver temperatures.

In Fig. 6 the sun presence sensor error is +50% and in Fig. 7 it is -50%.

In the latter case, due to the derivative action, the results are obviously quite good, but even in the first one, temperature variations and time gradients are acceptable.

This fact leads to the conclusion that control system can work satisfactorily with very large range of possible sun presence sensor error.

UPSET AND FAULT OPERATING CONDITIONS: LOSS OF CONTROL

Failures of control system are analyzed referring to system configuration. The control loop is subdivided into the following parts:

- 1 temperature sensors, instrumentation and connection wirings
- 2 input cards and channel scanning
- 3 microprocessor
- 4 D/A converter
- 5 Siemens PI controller and auto/manual station
- 6 Motor/pump
- 7 Power supply;

automatic actions to troubles in these subsystems are foreseen.

Out of range measurements from the field or wiring troubles (part 1) are recognized by the microprocessor which activate alarm signals. If the measurement is essential for regulation, a safety condition of the loop is forced (fast defocusing and high flow rate).

The same philosophy is followed in case of part 2 failure too.

Part 3 failure is managed by a watch-dog signal; also in this case a safety condition is foreseen.

Part 4-5-6 failures are automatically recognized both by large regulation errors or digital signal and by alarm or blocking signals.

Power supply troubles are avoided connecting the system to uninterruptible lines.

Owing to the low flow rate and the long time delays connected with, the worst situation happens in case of loss of control (point 4 or 5 failure) at minimum load at the same time of a sudden reinsolation.

For this event the computed results are presented in Fig. 8. Taking into account the time delays for defocusing and the slow dynamics of the system, tubes overpass 700 °C when the mirror field has been defocused and incident power already decreased to zero.

In this transient it was supposed that the field defocusing was started by the protection system when the temperature in the most radiated section exceeded the threshold of 530 °C.

A quick cooling starting from full load is presented in Fig. 9; the flow rate does not change owing to a control failure in case of sudden power decrease. Fig. 10 shows the behaviour as a consequence of a loss of power supply to the pump. In this case fast defocusing prevents from overtemperature.

 MG/mb1
 File: DDC

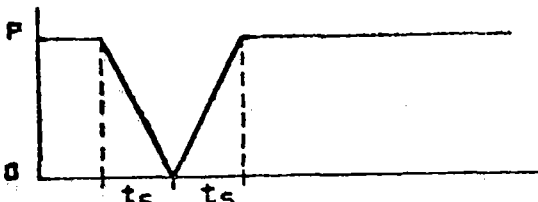
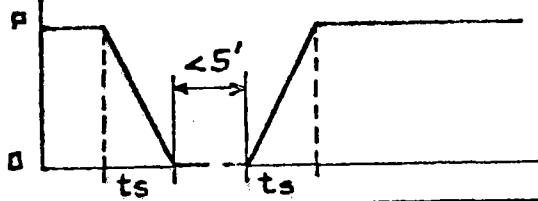
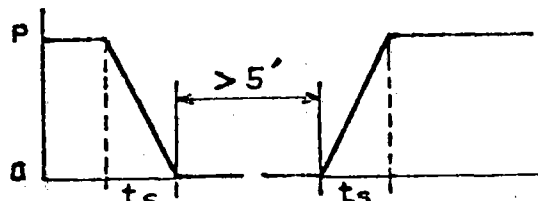
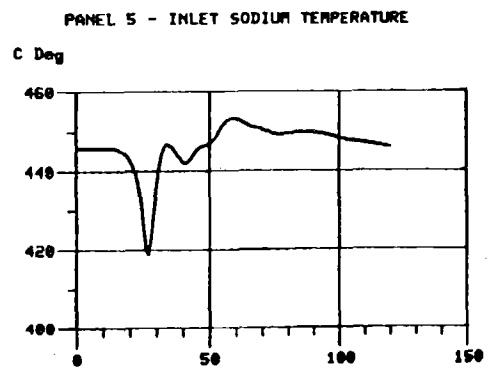
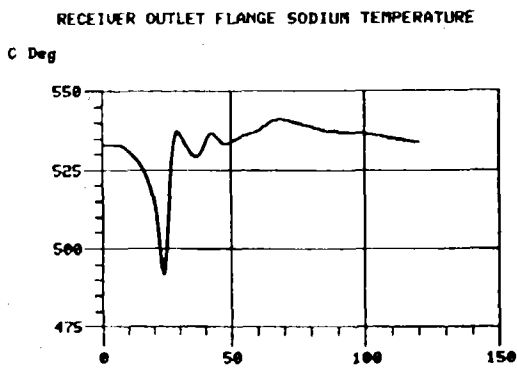
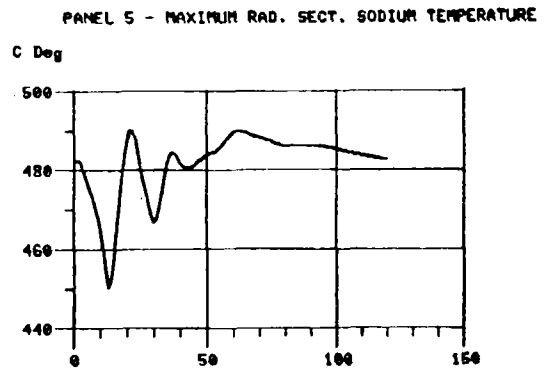
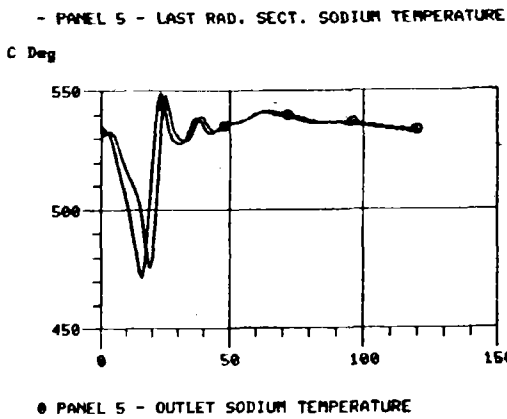
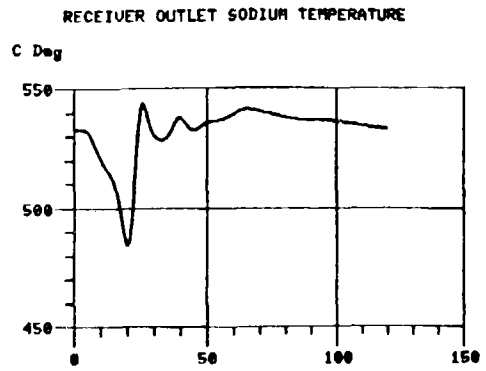
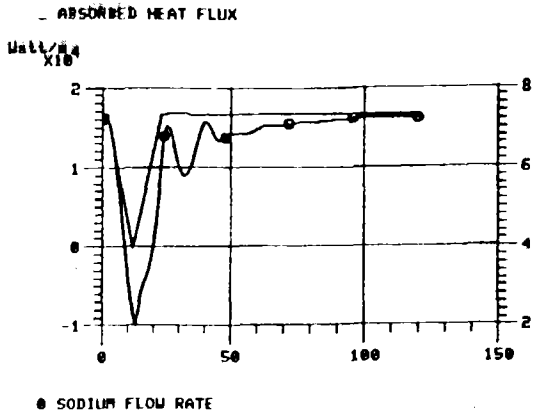
TYPE	CLOUD VELOCITY (Km/h)				
	10	23	50		
	t_s (sec)				
	54	24	11		
a)	1		1000	1000	1000
	2		1000	1000	1000
	3		150	150	25
		2150	2150	2025	

TABLE 1 CLOUD PASSAGE TRANSIENTS (PER YEAR)
(P = PEAK INCIDENT FLUX
 Σ EVENTS = 6050)

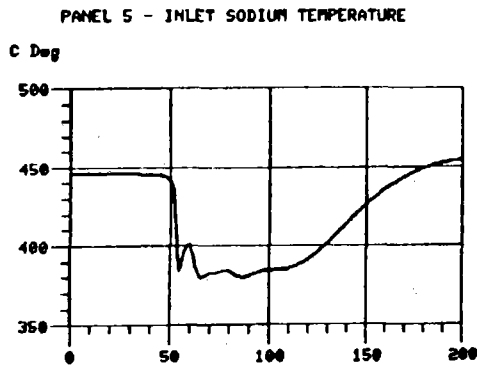
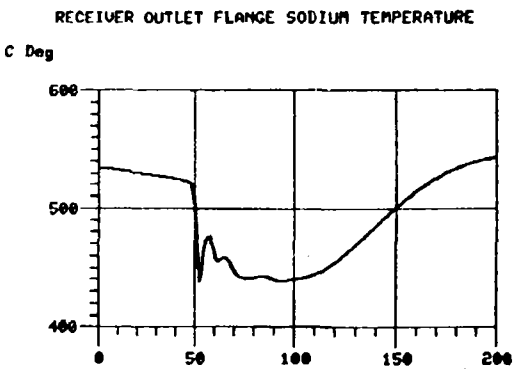
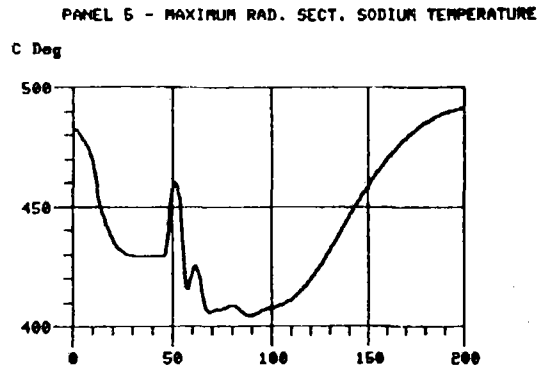
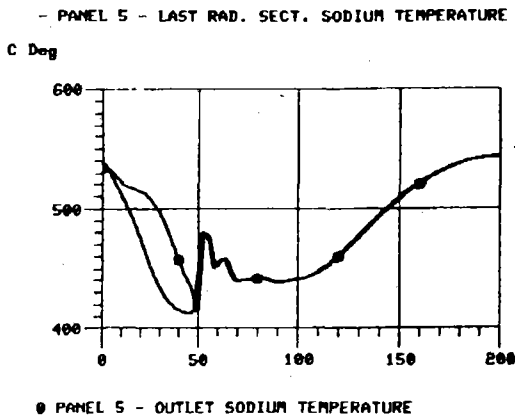
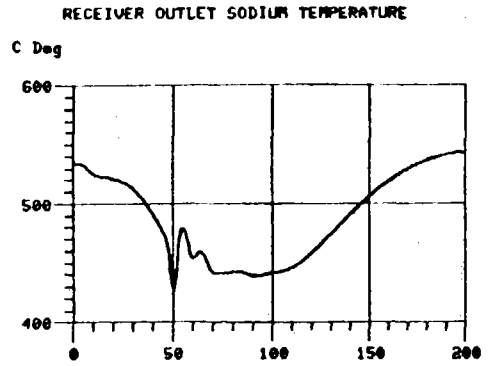
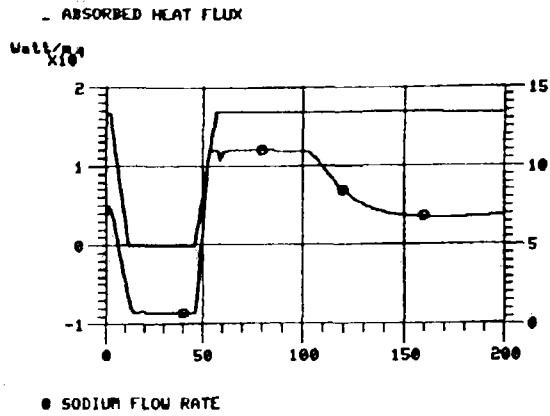


U-Type TRANSIENT - Max. Sodium Flow Rate 9.2 Kg/s

ENEL-CRA

19-NOV-82

Fig. 1

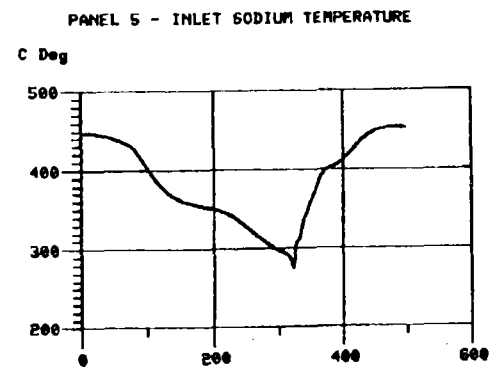
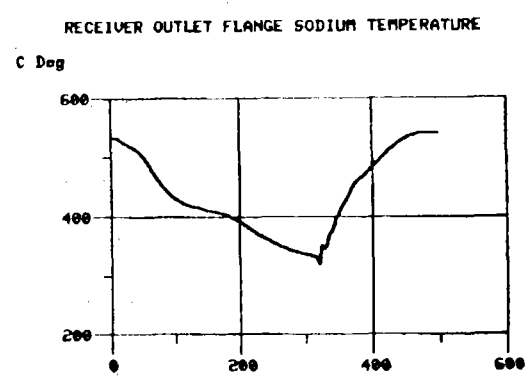
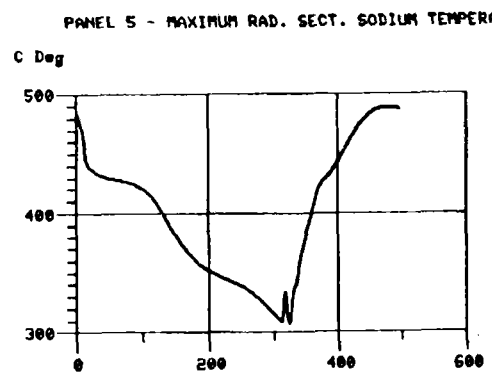
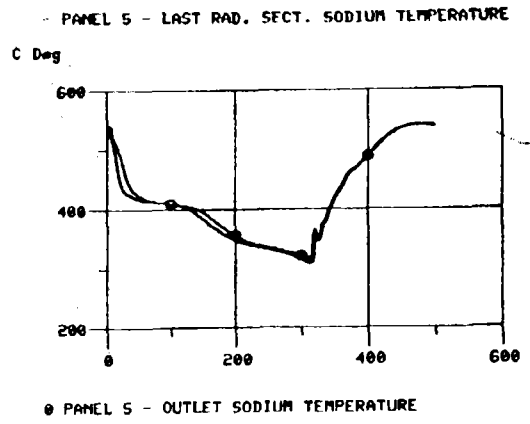
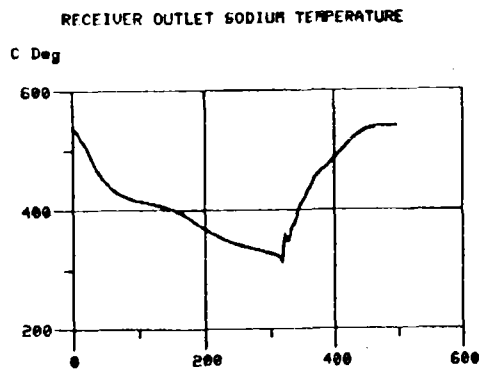
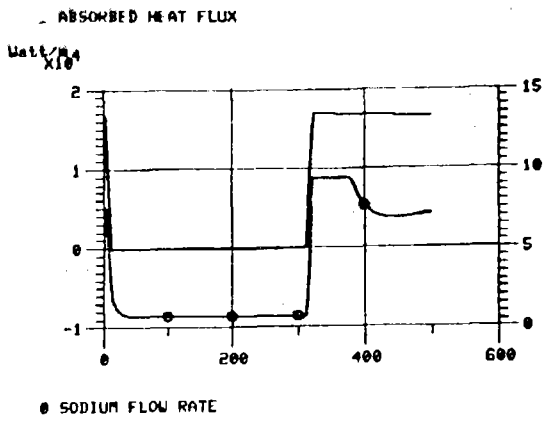


U-type TRANSIENT - Max. Sodium Flow Rate 10.9 Kg/s

ENEL-CRA

19-NOV-82

Fig. 2

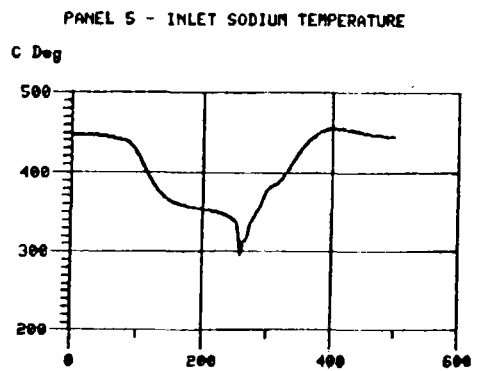
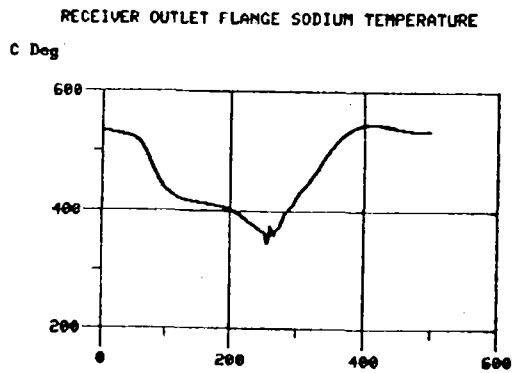
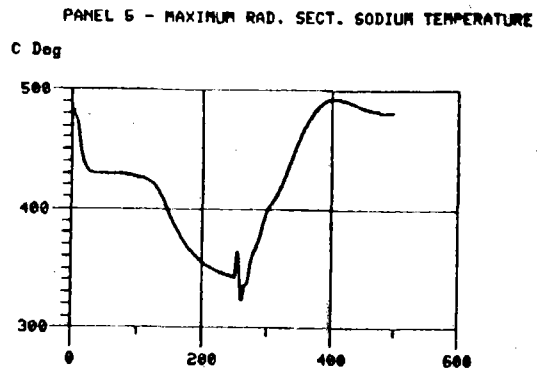
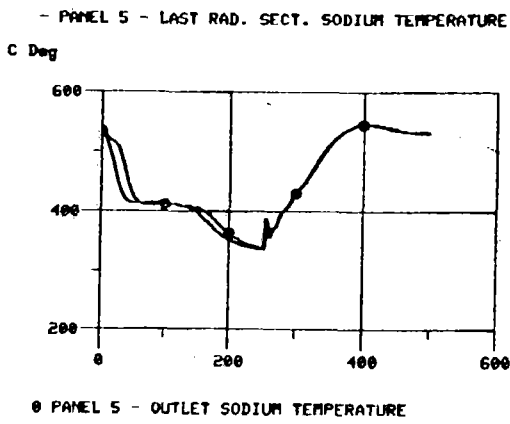
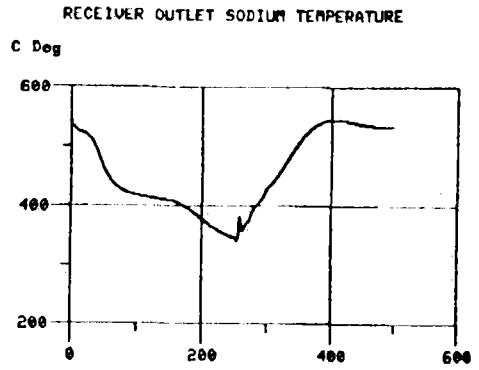
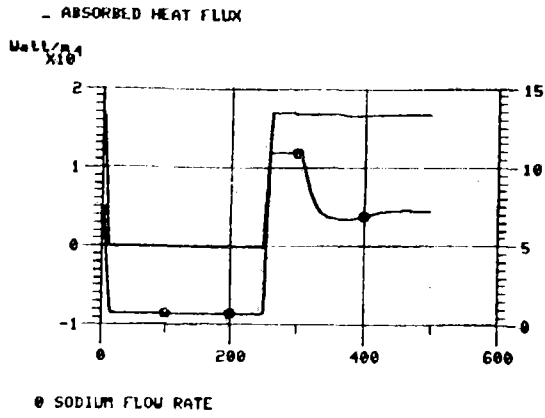


U-Type TRANSIENT - Max. Sodium Flow Rate 9.2 Kg/s

ENEL-CRA

19-NOV-82

Fig. 3

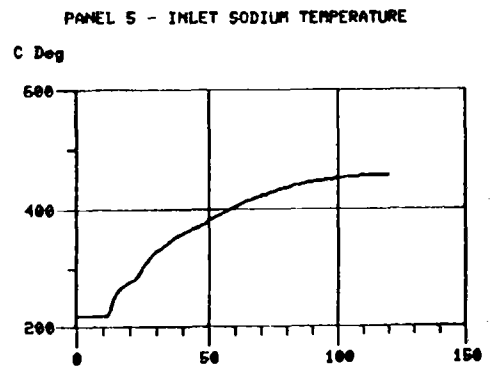
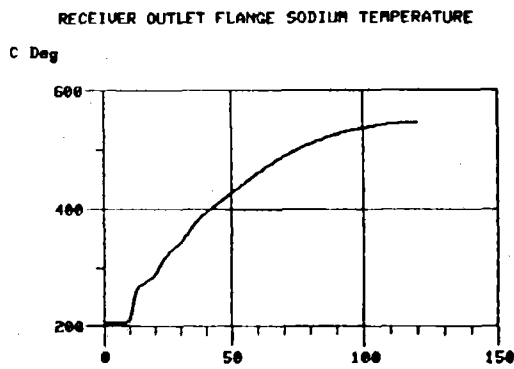
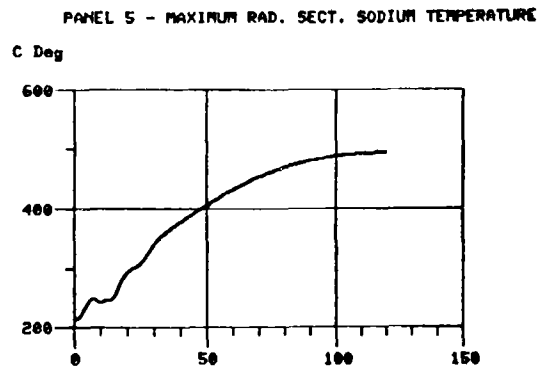
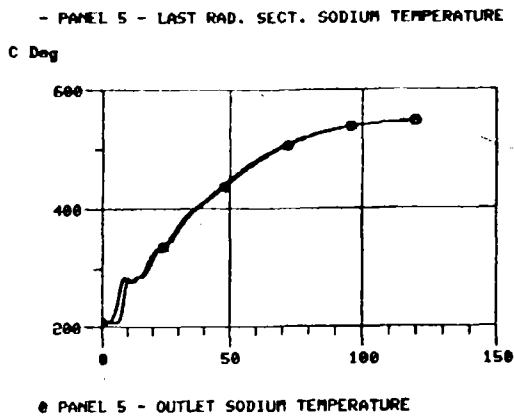
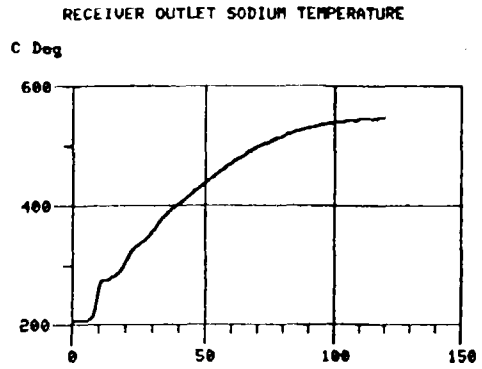
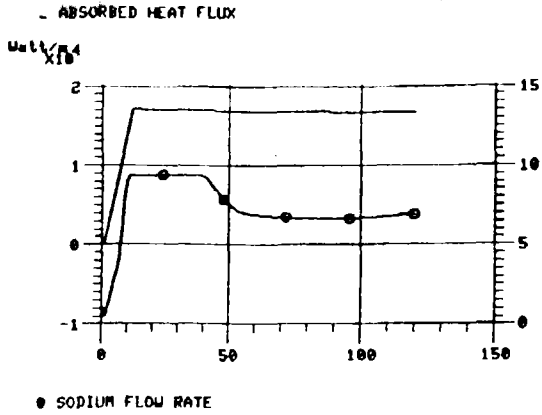


U-type TRANSIENT - Max. Sodium Flow Rate 10.9 Kg/s

ENEL-CRA

19-NOV-82

Fig. 4

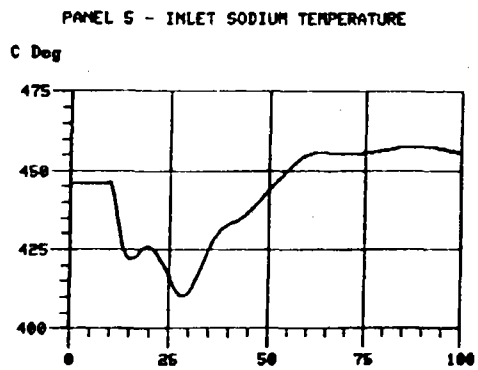
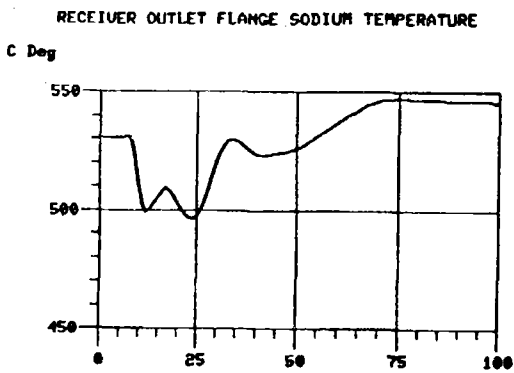
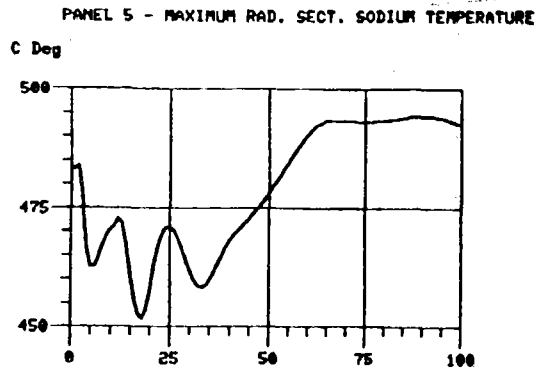
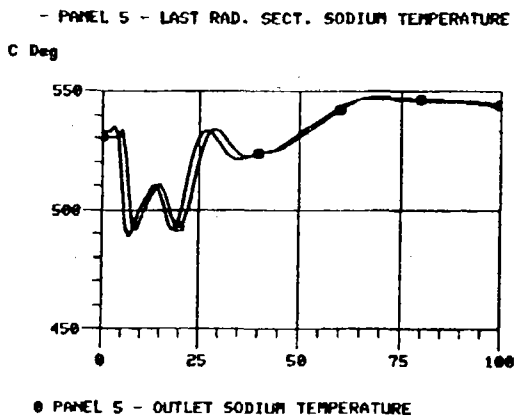
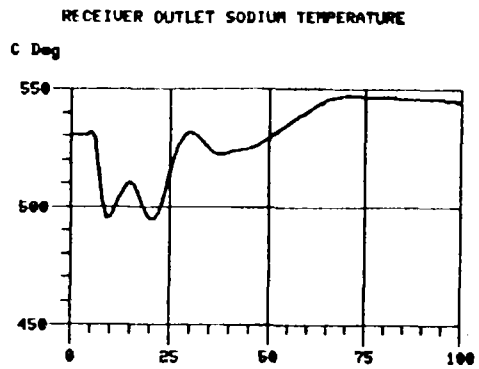
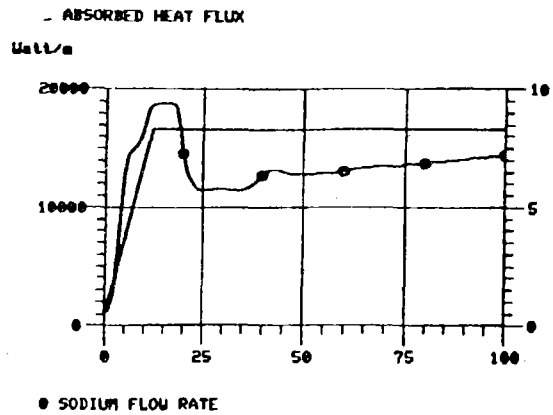


HEAT FLUX RAMP ON THE COLD RECEIVER

ENEL-CRA

19-NOV-82

Fig. 5

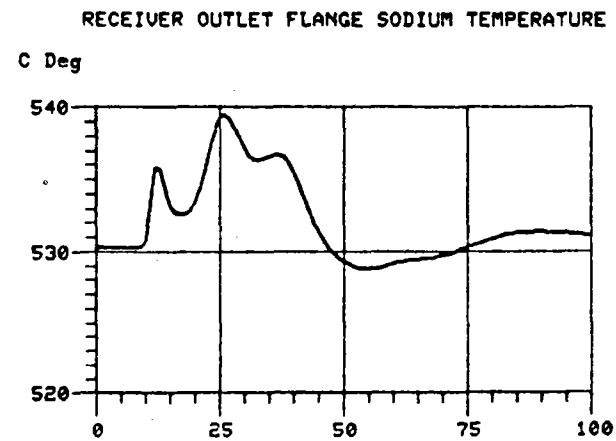
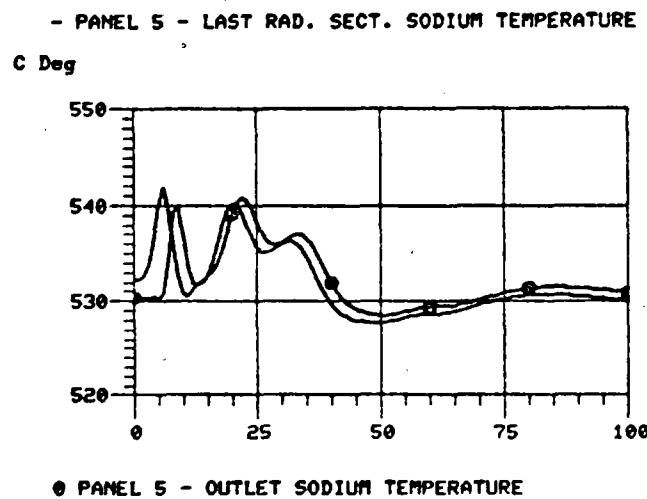
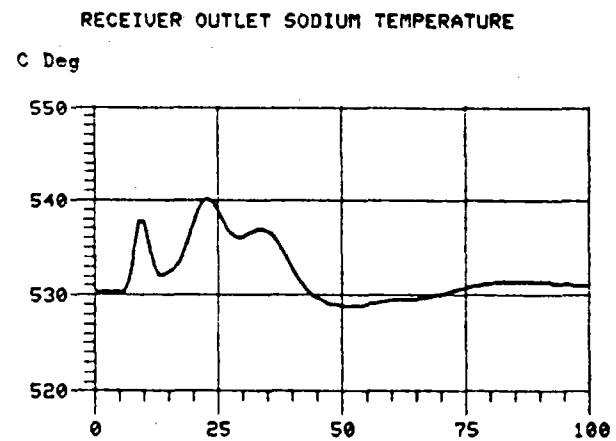
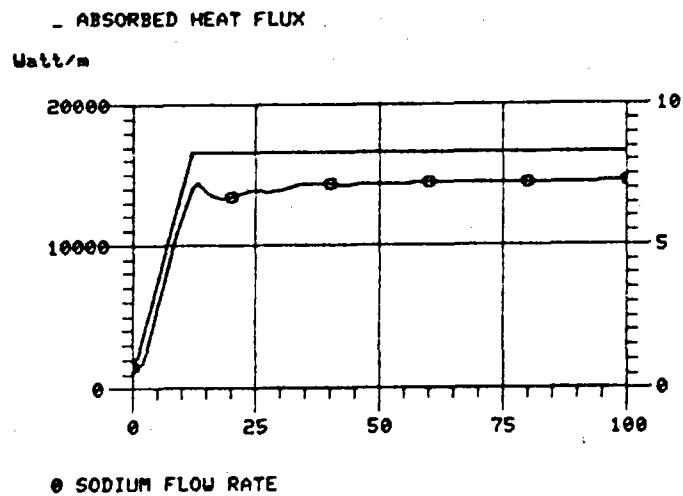


10% - 100% reinsolation from steady state

ENEL-CRA

22-NOV-82

Fig. 6

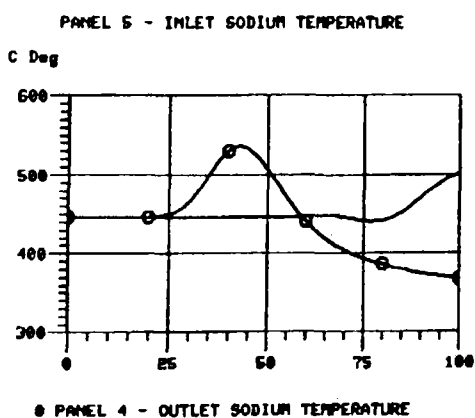
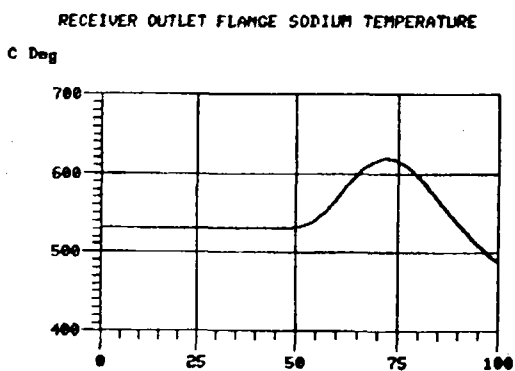
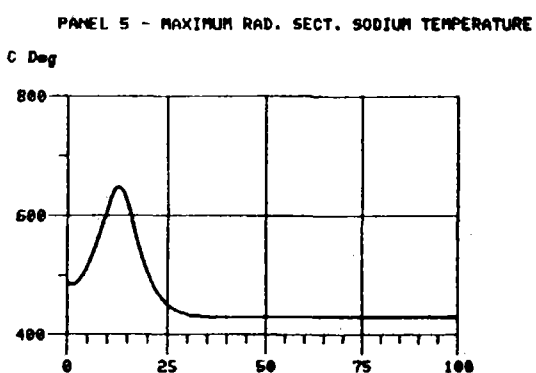
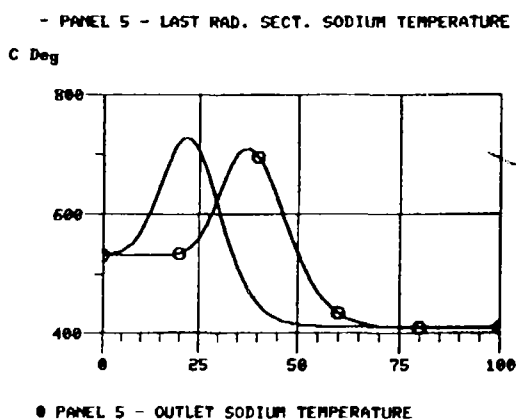
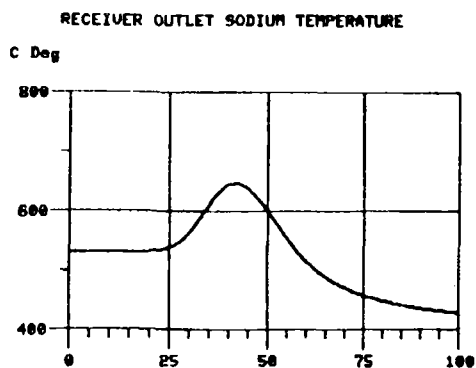
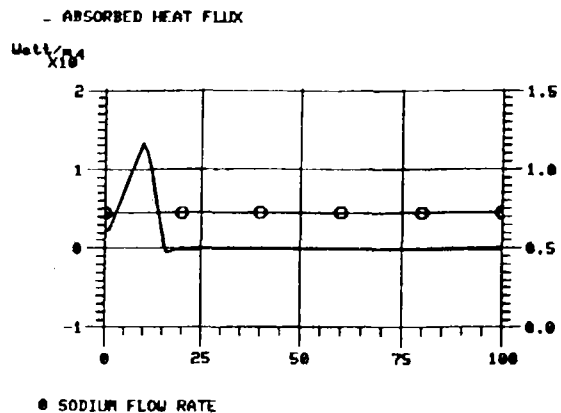


10% --> 100% Reinsolation from steady-state

ENEL-CRA

27-JAN-83

Fig. 7

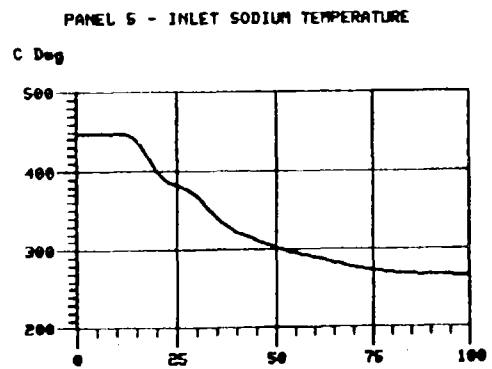
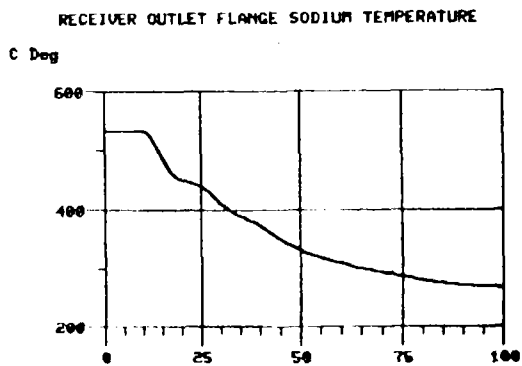
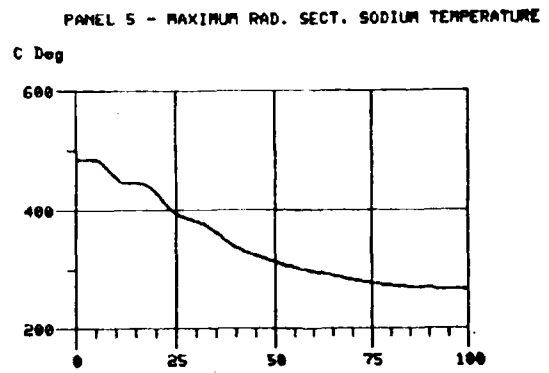
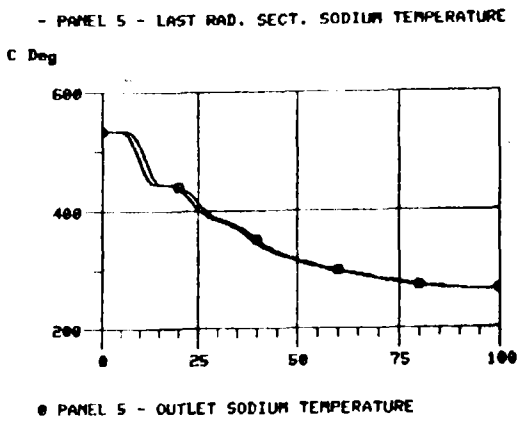
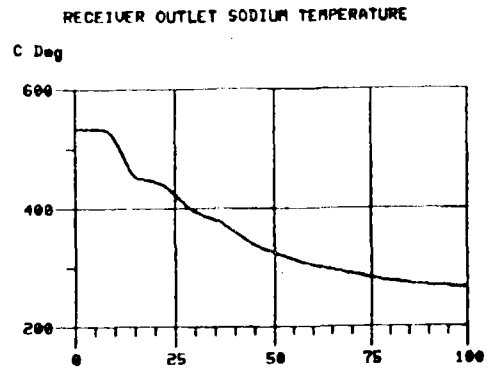
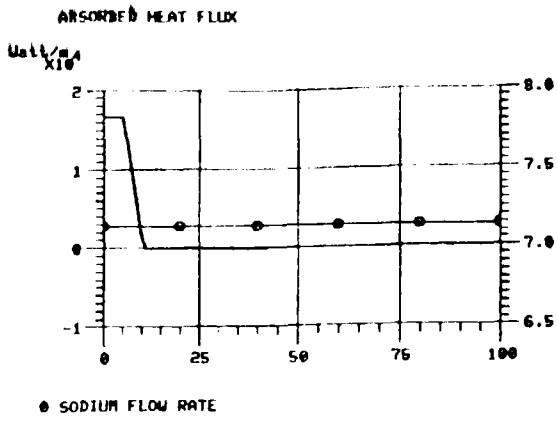


LOSS OF CONTROL AT MINIMUM LOAD

ENEL-CRA

24-NOV-82

Fig. 8

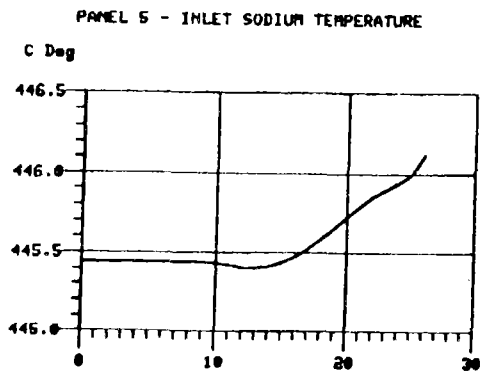
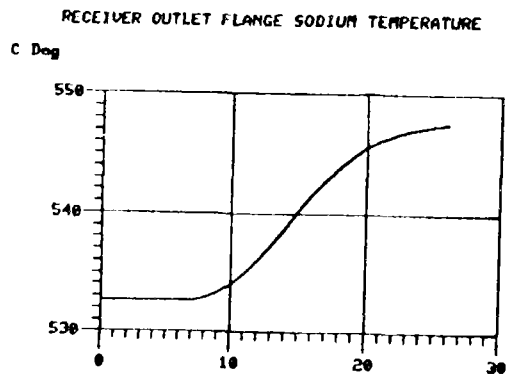
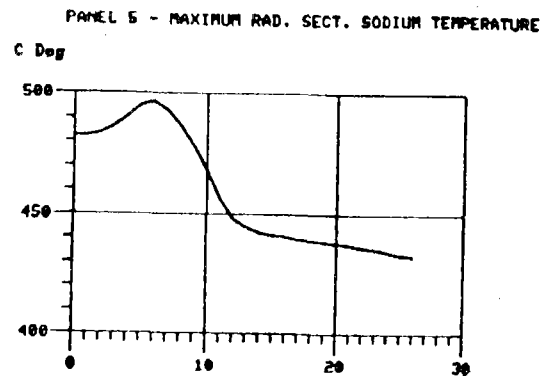
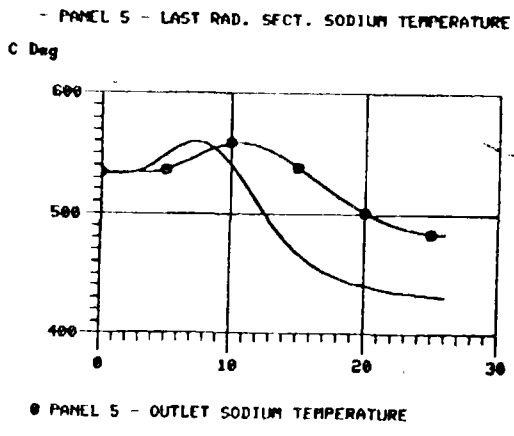
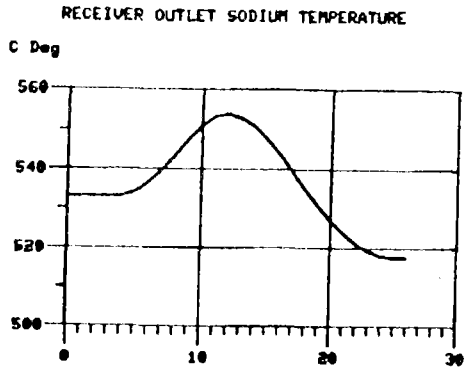
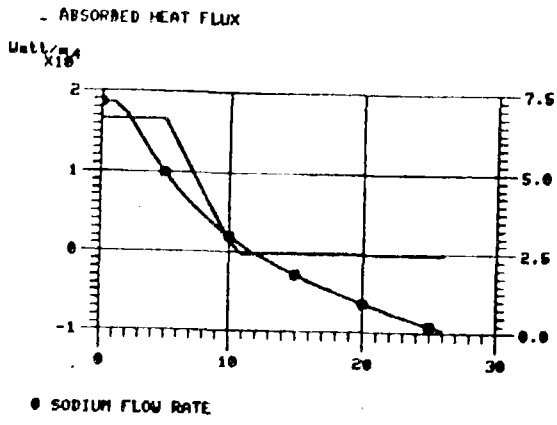


LOSS OF CONTROL STARTING FROM FULL LOAD

ENEL-CRA

19-NOV-82

Fig. 9



LOSS OF PUMP POWER SUPPLY

ENEL-CRA

19-NOV-82

Fig. 10

IEA ALMERIA PROJECT
ADVANCED SODIUM RECEIVER
ASR

Receiver headers stress analysis

Topic Report No. 12

Revision 0

January 1983

Prepared by: ENEL

FRANCO TOSI

AGIP NUCLEARE

CONTENTS

1. Forward
2. Code stress limits compliance
 - 2.1. Analysis limits
3. Material basic data
4. Thermal transient description
5. Calculation methodology
6. Lower header flange
 - 6.1. Analysis limits and description of the structure
 - 6.2. Temperature field evaluation
 - 6.3. Thermal stress evaluation
 - 6.4. Stress evaluation due to piping moments
 - 6.5. Stress table according to ASME criteria
 - 6.6. Design conditions analysis
 - 6.7. Operating conditions analysis
 - 6.8. Shake down analysis
 - 6.9. Ratcheting analysis
 - 6.10. Creep-fatigue analysis
 - 6.11. Flange bearing area analysis

7. Upper header nozzle

- 7.1. Analysis limits and description of structure
- 7.2. Temperature field evaluation
- 7.3. Thermal stress evaluation
- 7.4. Stress evaluation due to the panel tube flexibility
- 7.5. Stress table according to ASME criteria
- 7.6. Bursting analysis (Design conditions)
- 7.7. Operating conditions analysis
- 7.8. Shake down analysis
- 7.9. Ratcheting analysis
- 7.10. Creep-fatigue analysis

8. Flat head

- 8.1. Transient description and thermal stress evaluation
- 8.2. Stress evaluation due to mechanical loads
- 8.3. Stress table according to ASME criteria
- 8.4. Bursting analysis
- 8.5. Operating conditions analysis
- 8.6. Shake down analysis
- 8.7. Ratcheting analysis
- 8.8. Creep-fatigue analysis

9. Downcomer - Header connection

Appendix 1

Appendix 2

1. FORWARD

The object of this report is the description of the headers stress analysis based on the final receiver configuration and dimensions.

With reference to the receiver central panel (that works at the highest temperatures), the structure section hereafter analysed are the following:

- 1) lower header flange
- 2) tube-upper header connection
- 3) upper header flat heads
- 4) down comer-upper header connection.

The analysis at point 2 and 3 has been carried out only for the upper header because it has been considered the most stressed one working at the maximum temperature.

2. CODE STRESS LIMITS COMPLIANCE

2.1. ANALYSIS LIMITS

In compliance with contract section A-7.1 for a sodium containing component, the design has been carried out by means of the following criteria.

- a) Primary membrane stress is limited to prevent bursting according to par. UG-27 ASME Section VIII, Division 1.
- b) An extension of the shakedown limit is imposed on primary and secondary stresses, to prevent noticeable distortions, that is: $P_1 + P_b + Q \leq 3S_m$, according to par. 4-134, Appendix A, ASME Section VIII, Division 2.
- c) To satisfy the distortion limits by using an elastic analysis, and particularly to limit the inelastic strain amount that can occur during the service life of the component, Test No. 3, par. T-1324, Appendix T, Code Case N47-17 has been applied.

This analysis is not strictly required by the Contract, but is necessary in order to make possible the use of subsequent creep-fatigue analysis on elastic basis.

d) For component service life time evaluations, that is to evaluate creep-fatigue interaction effects, the limit by eq. (5) of the par. T-1411, Appendix T, Code Case N-47-17, for elastic analysis has been imposed.

Note

With reference to c) and d) above, some modifications have been assumed with respect to that requested by Code Case, provided that we deal with a solar receiver and not a nuclear component, as forecast by Contract.

3. MATERIAL BASIC DATA

The material used in the components hereafter analyzed, that in headers and downcomer, is AISI 316 L.

In Appendix 1 the material mechanical characteristics are completely specified; in Appendix 2 the physical characteristics are reported as well.

4. THERMAL TRANSIENT DESCRIPTION

In order to fulfill a complete lifetime analysis of the parts of the receiver hereafter considered, an extensive evaluation of all the transient conditions described in Topic Report No. 6 has been carried out by means of the simulation code for the receiver dynamic analysis described in Topic Report No. 4.

The behaviors of the temperatures for the different transients have been reported corresponding to the lower header flange and the upper header nozzles of the fifth panel (central one).

The transients considered in the ASR lifetime analysis are:

1) Normal operating conditions

3 types of shading-reinsolation sequences caused by a cloud passage are considered other than the normal daily cycling.

- a) Shading and prompt reinsolation.
- b) Shading over a period of 5 minutes and succeeding reinsolation.
- c) Shading for long time (>5 minutes) and succeeding reinsolation.

2) Upset conditions

- d) Failure of the control system of the pump in case of 100% reinsolation (flowrate at 10%).
- e) Failure of the control system of the pump in case of shading of the field.
- f) Loss of electrical power supply of the sodium pump.

The following conditions have been cautiously assumed in accordance to the Topic Report n° 6:

- "a" type transient
 - . cloud velocity of 50 Km/h;
 - . 3000 cloud passages per year;
 - . absorbed flux, flowrate and sodium temperature reported in figg. 4/1, 4/2, 4/3 (Transient T8 (see note 1));
 - . the level of the peak incident flux before cloud passage is the one corresponding to the design point (equinox noon).

Note 1: Actually a transient with a shading of 30 seconds has been considered instead of a shading/prompt insolation. The reason is connected to the existence of such a transient (analyzed for different purposes) very similar to the one in question in order to avoid a repetition of an analysis very time consuming.

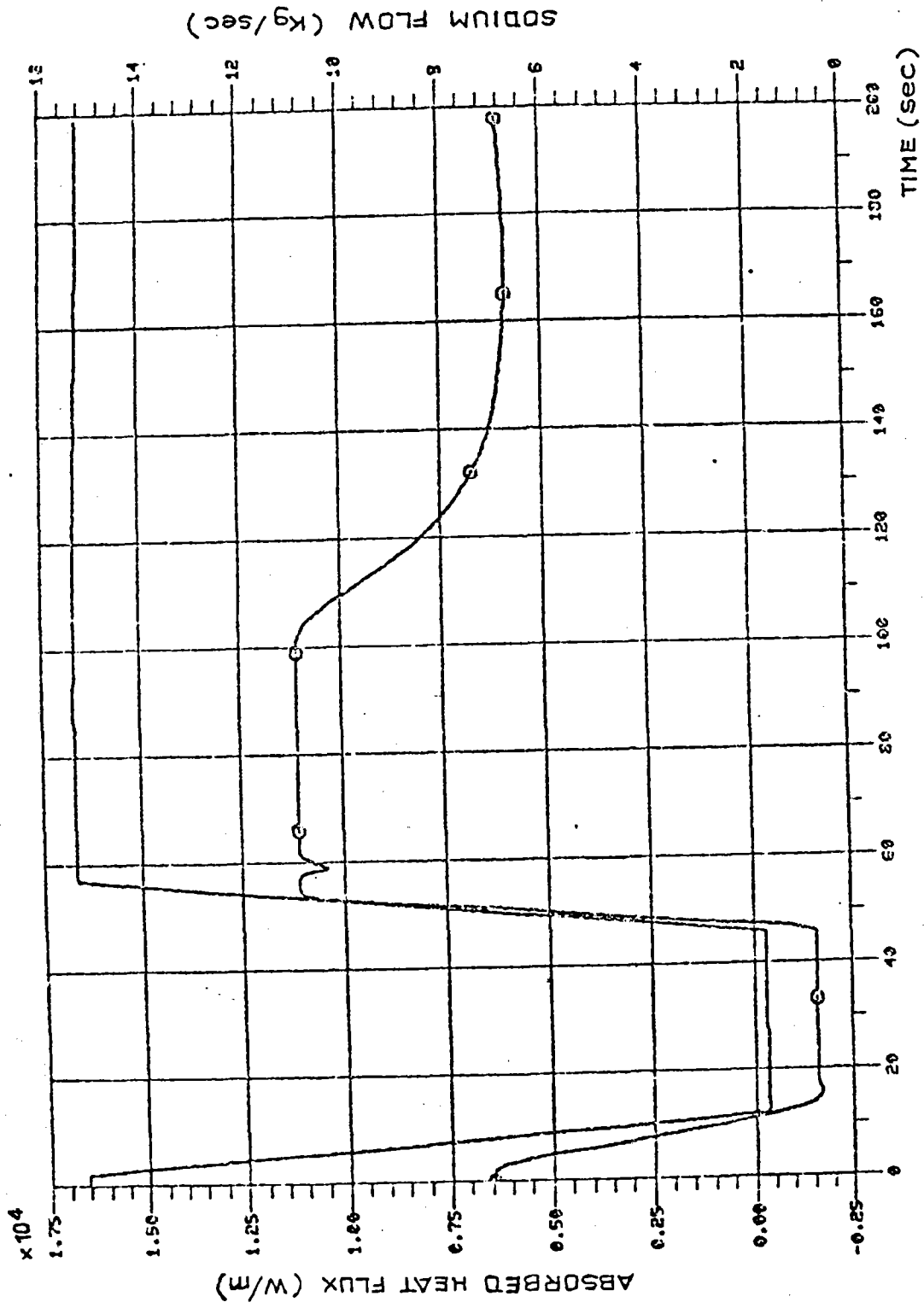


FIG. 4/1

SODIUM FLOW —○—

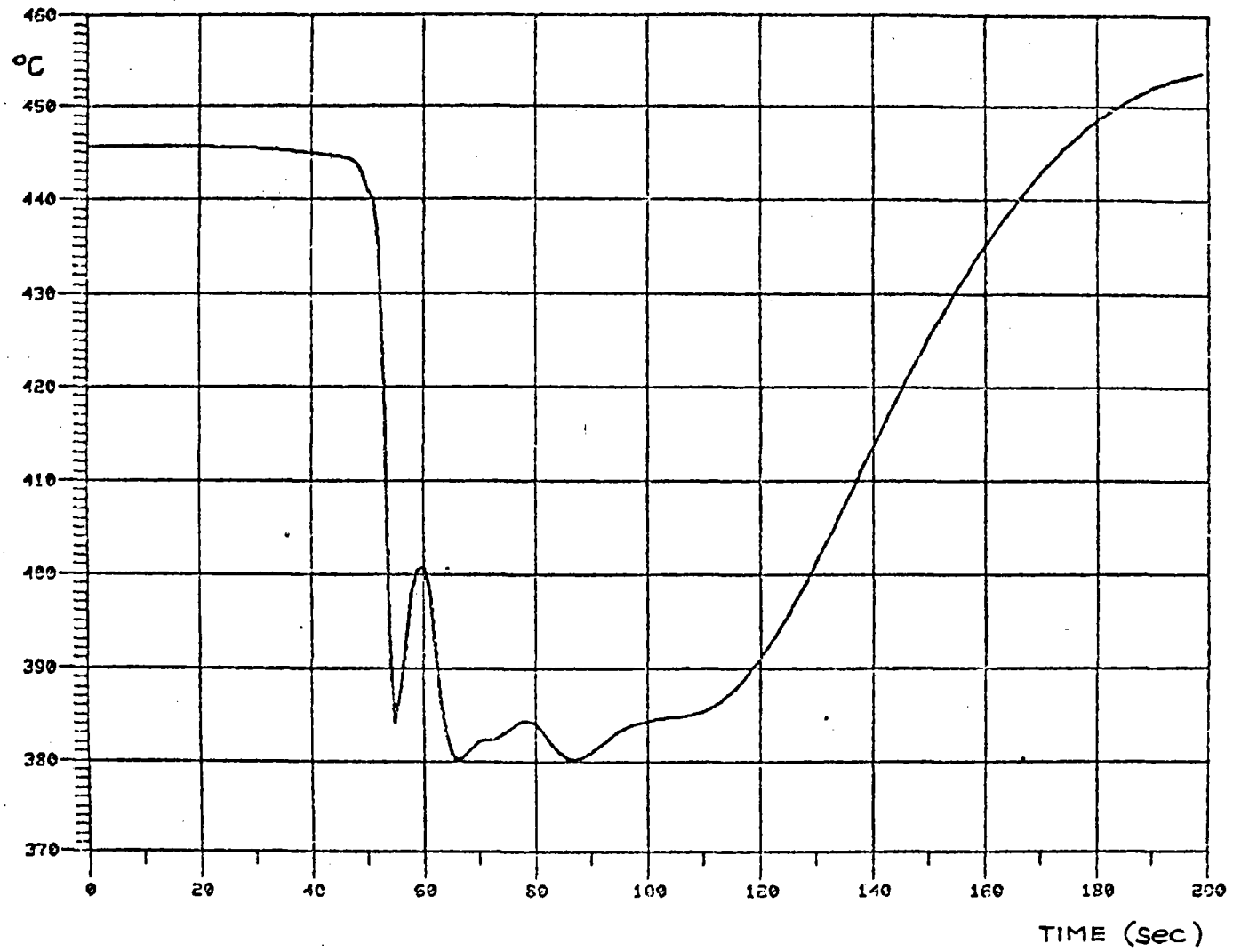


FIG. 4/2 - LOWER HEADER FLANGE

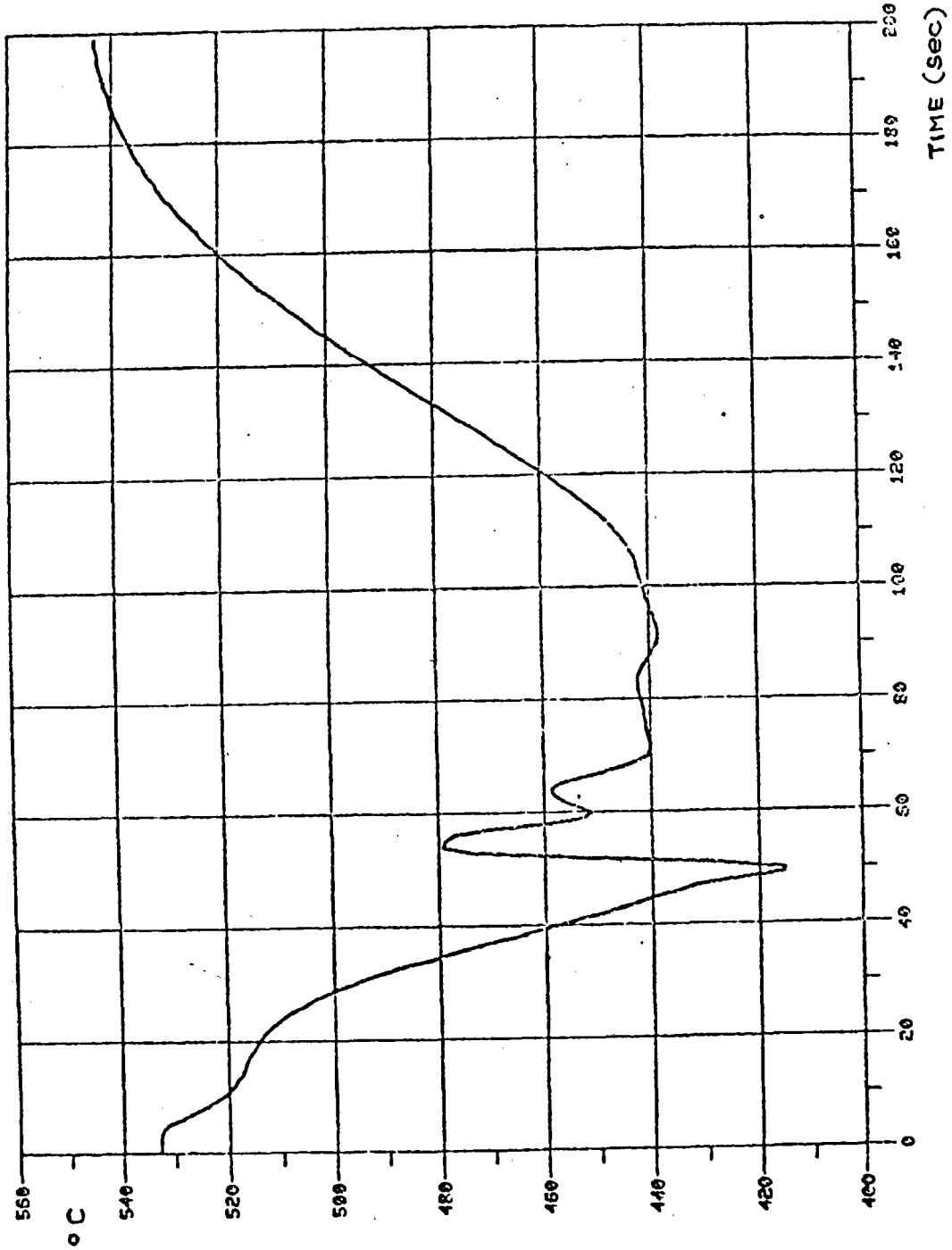


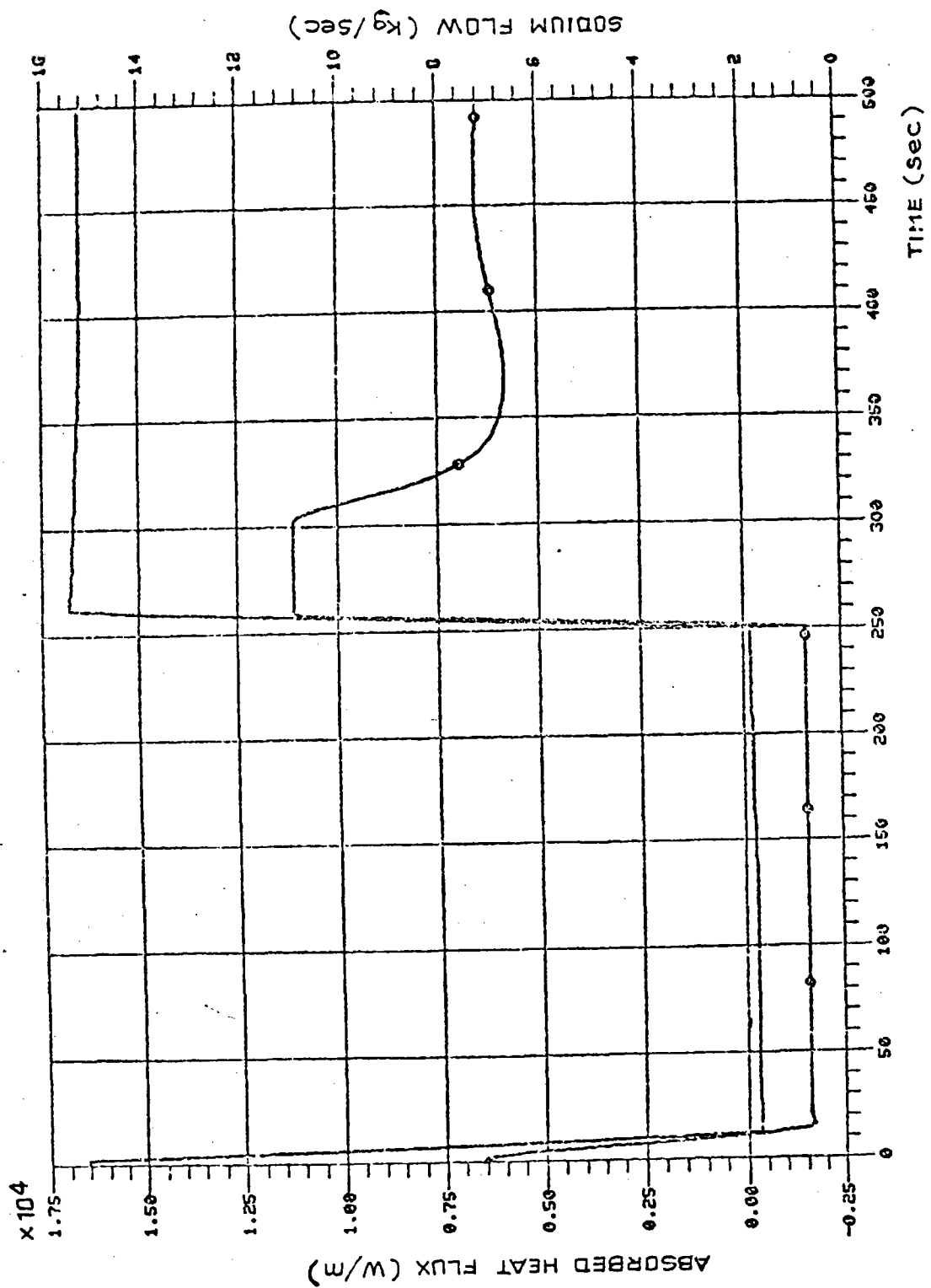
FIG. 4/3 - UPPER HEADER NOZZLE

- "b" type transient
 - . cloud velocity of 50 Km/h;
 - . 3000 cloud passage per year;
 - . absorbed flux, flowrate and sodium temperatures reported in figg. 4/4, 4/5, 4/6 (Transient T9);
 - . the level of the peak incident flux before cloud passage is the one corresponding to the design point (equinox noon).

- "c" type transient
 - . cloud velocity of 50 Km/h;
 - . 325 cloud passage per year;
 - . absorbed flux, flowrate and sodium temperature reported in fig. 4/7, 4/8, 4/9 (transient T11-T12 (see note 2));
 - . the level of the peak incident flux before cloud passage is the one corresponding to the design point (equinox noon).

- "d" type transient
 - . 6 events per year;
 - . the level of the peak incident flux is the one corresponding to the design point (equinox noon);

Note 2: The actual analysed transient has been considered as the combination of the transient T11 and T12: the shading part is the same as in T11 and the re-insolation is the same as in T12.



SODIUM FLOW —○—

FIG. 4/4

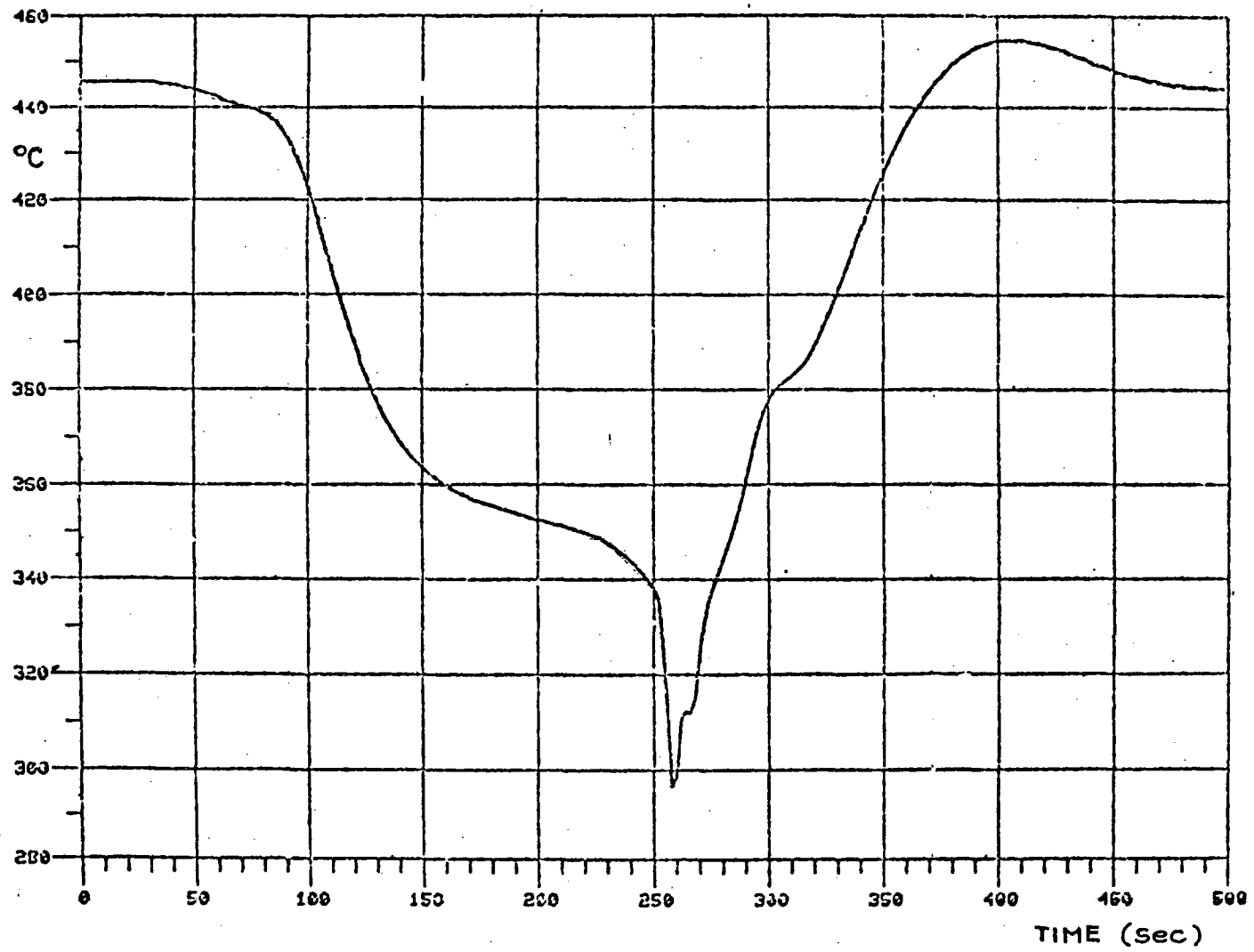


FIG. 4/5 - LOWER HEADER FLANGE

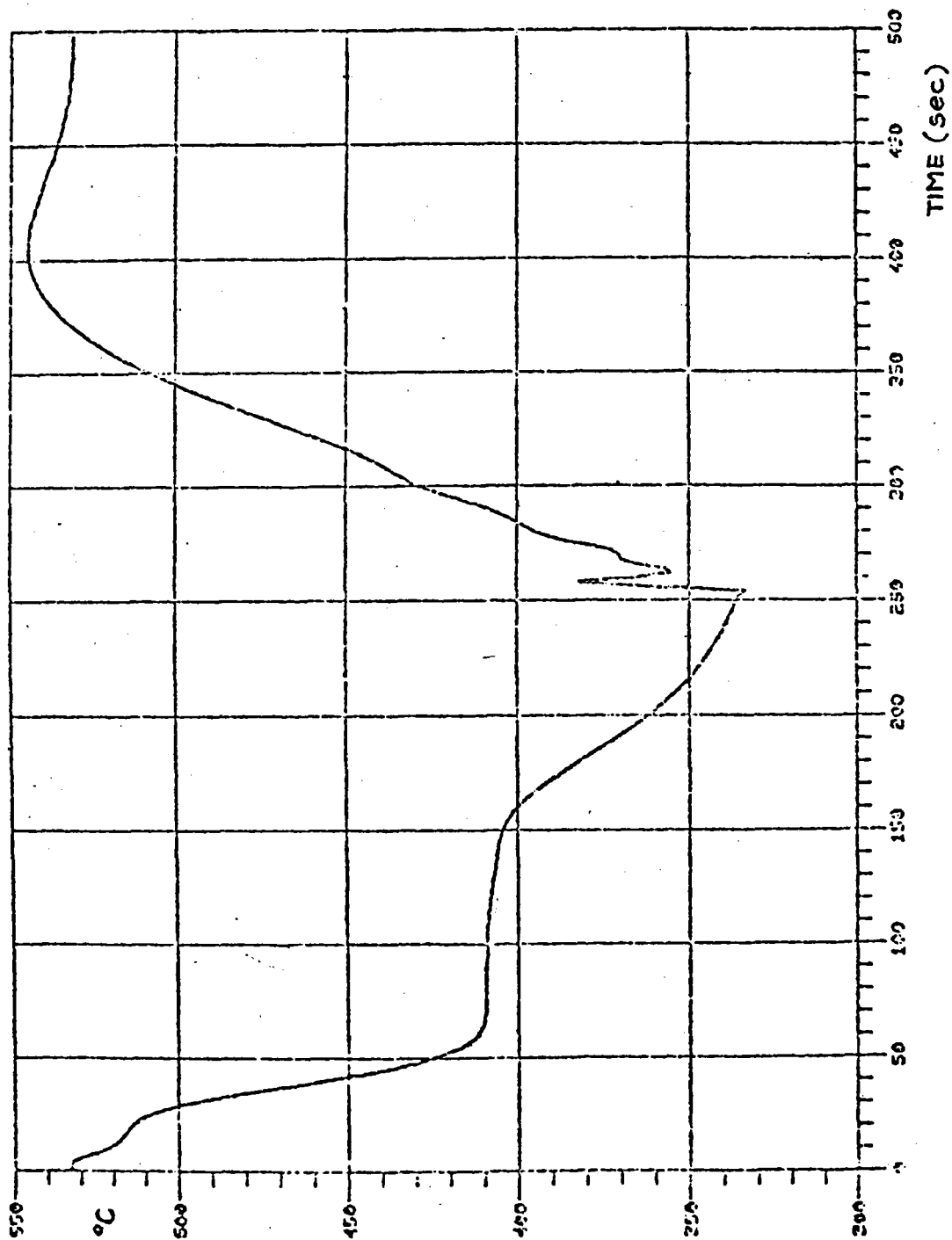
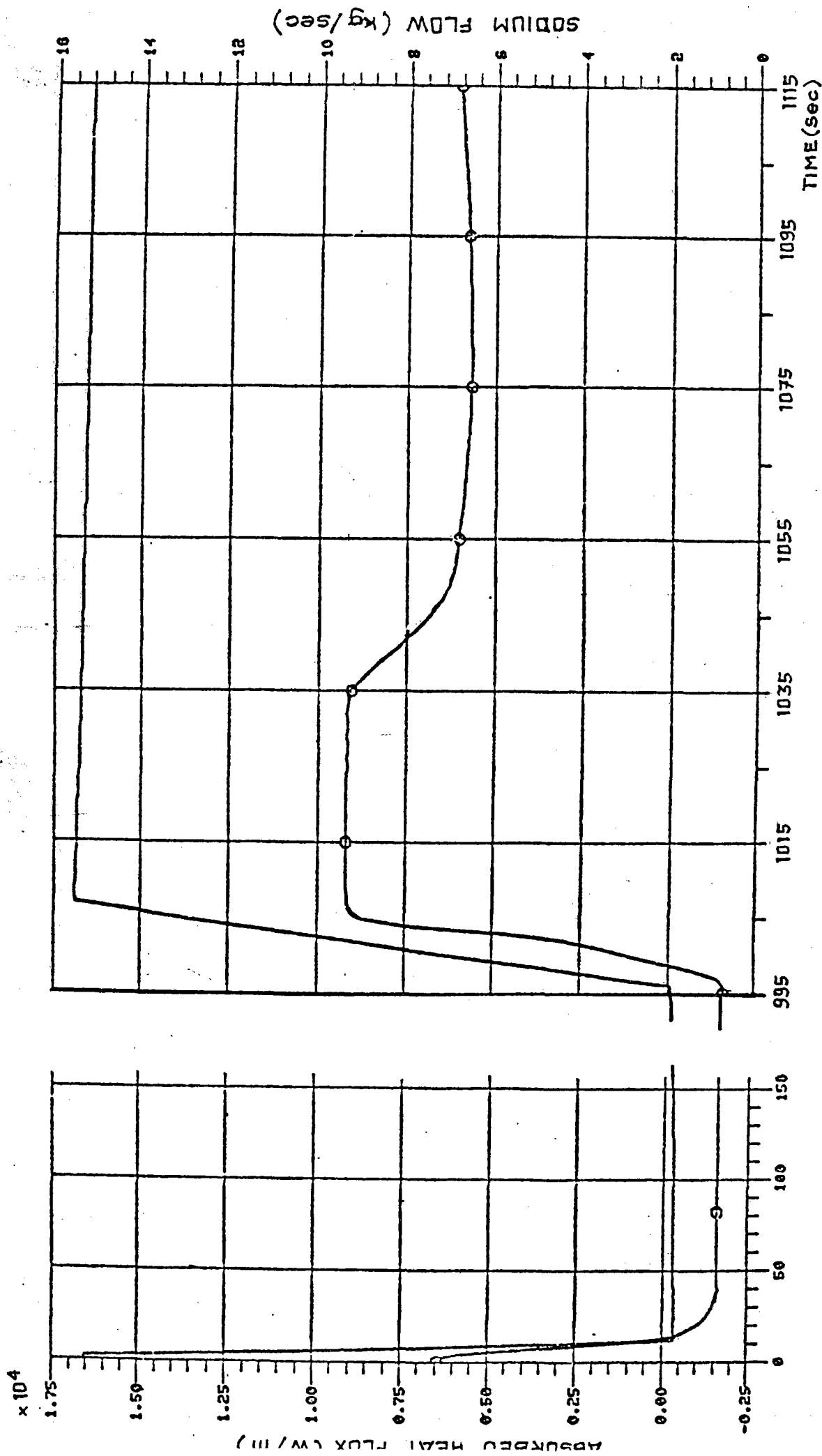


FIG. 4/6 - UPPER HEADER NOZZLE



SODIUM FLOW RATE —○—
FIG. 4/7

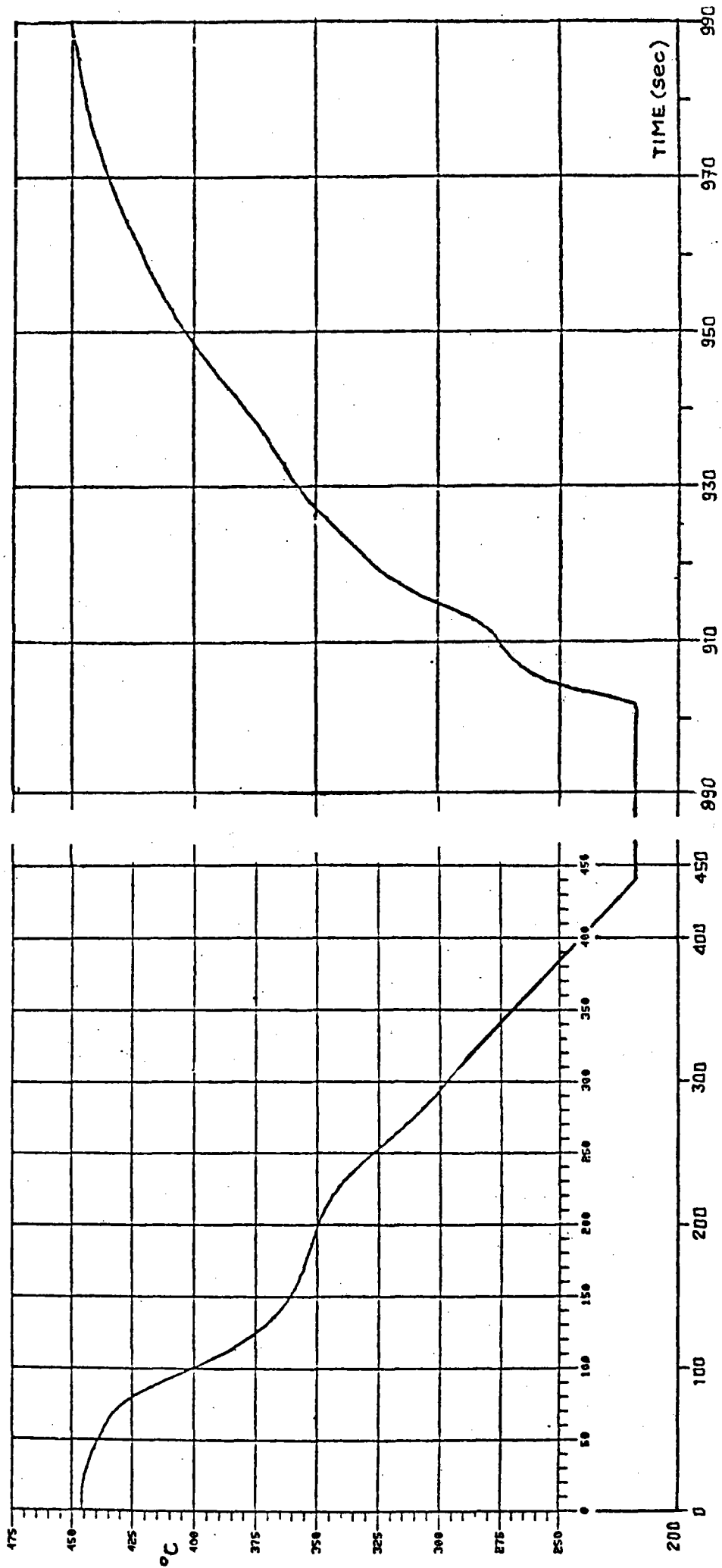


FIG. 4/8 - LOWER HEADER FLANGE

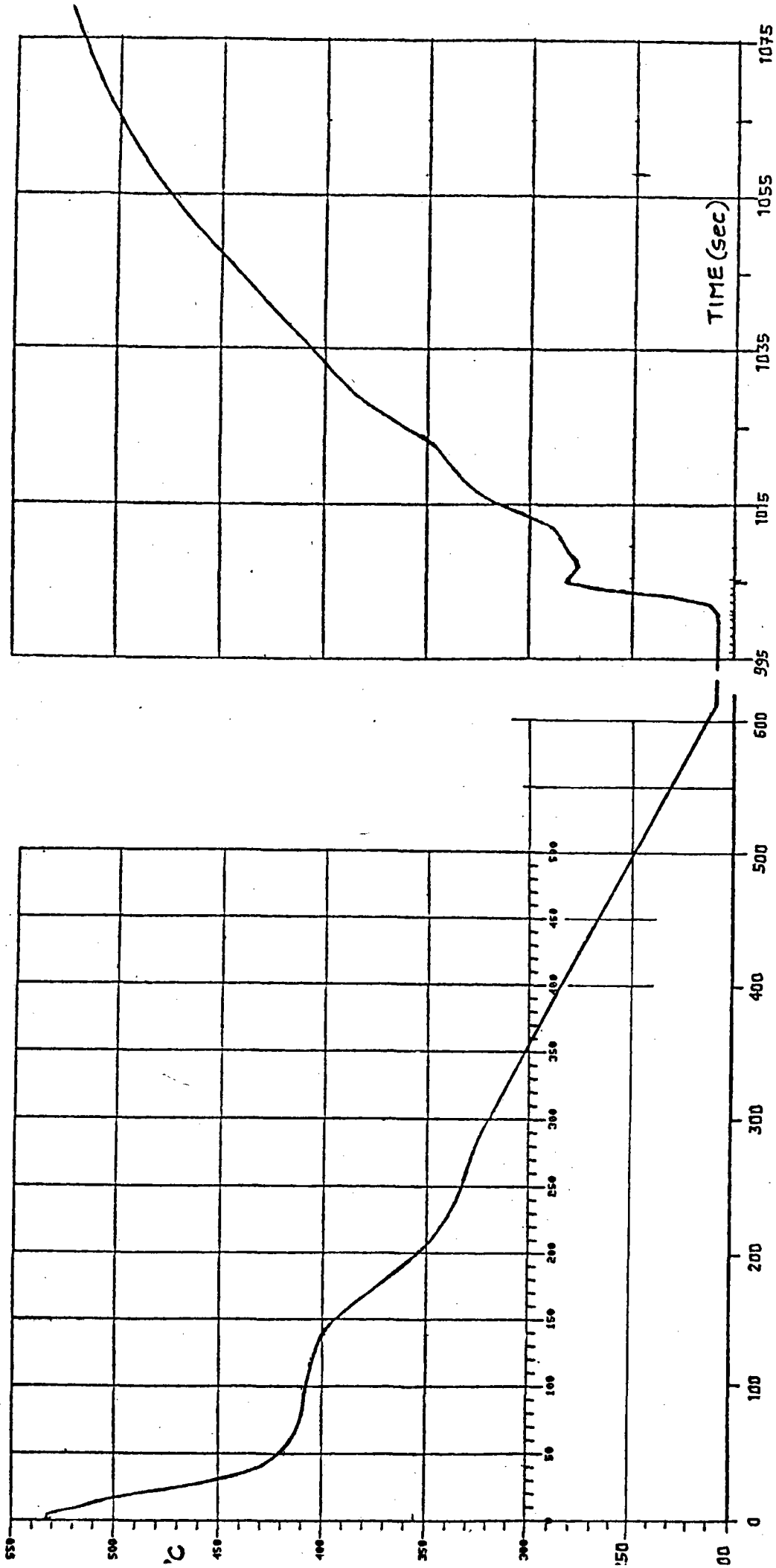


FIG. 4/9 - UPPER HEADER NOZZLE

- . absorbed flux, flowrate and sodium temperature reported in fig. 4/10, 4/11, 4/12 (transient T16).
- "e" type transient
 - . 6 events per year;
 - . the level of the peak incident flux is the one corresponding to the design point (equinox noon);
 - . absorbed flux, flowrate and sodium temperature reported in figg. 4/13, 4/14, 4/15 (transient T14).
- "f" type transient
 - . 6 events per year;
 - . the level of the peak incident flux is the one corresponding to the design point (equinox noon);
 - . absorbed flux, flowrate and sodium temperature reported in figg. 4/16, 4/17, 4/18 (transient T15).

The aforementioned transients have been calculated according to the conditions reported in the Topic Report No. 11.

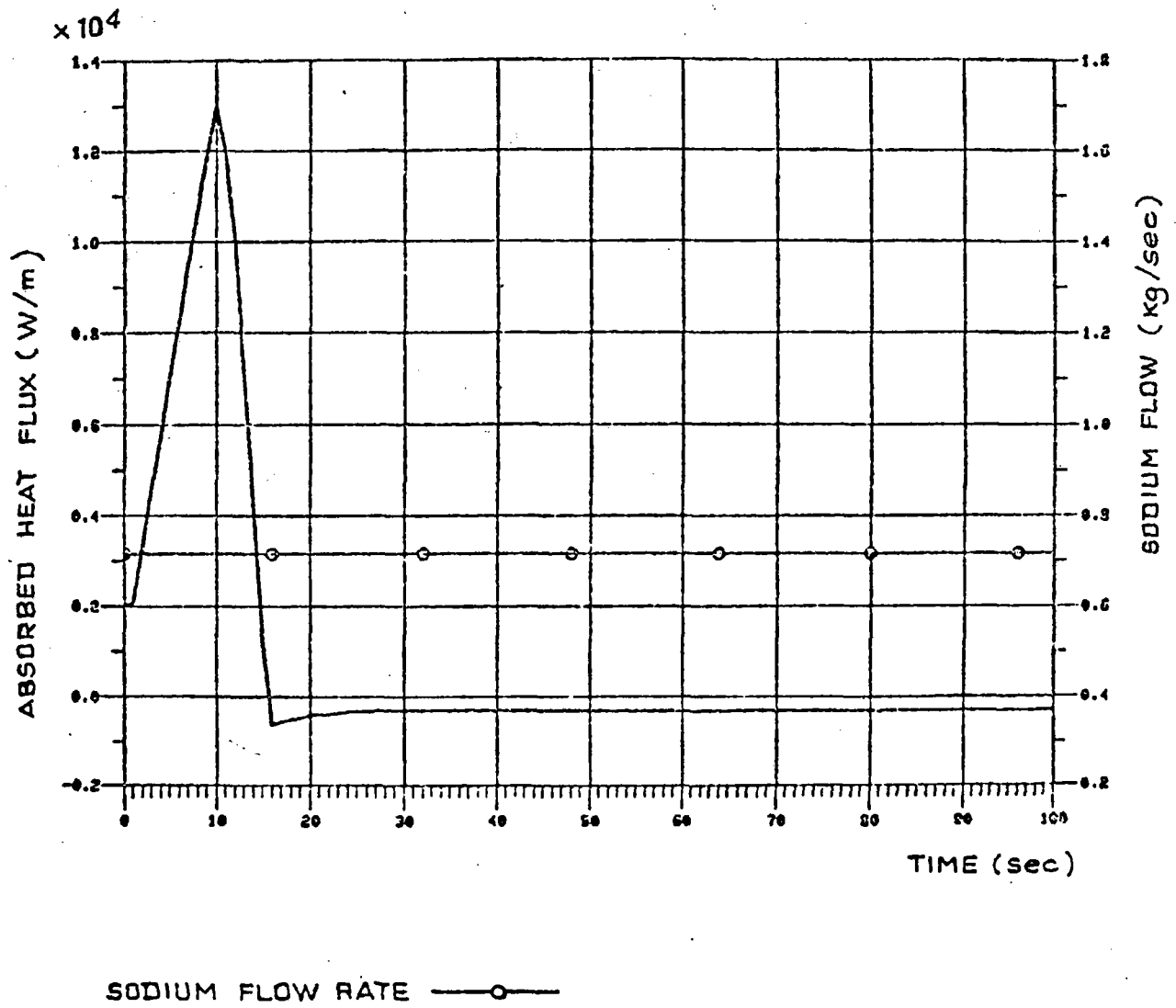


FIG. 4/10

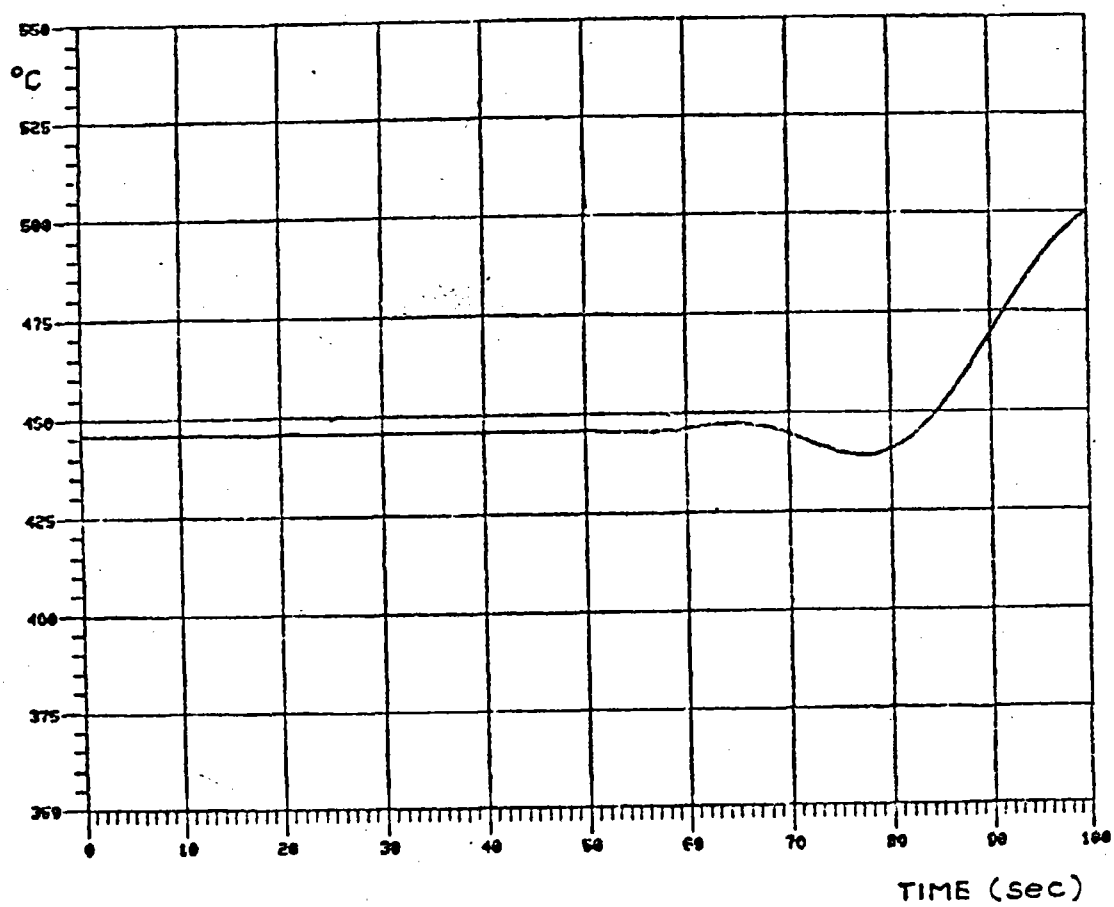


FIG. 4/11 - LOWER HEADER FLANGE

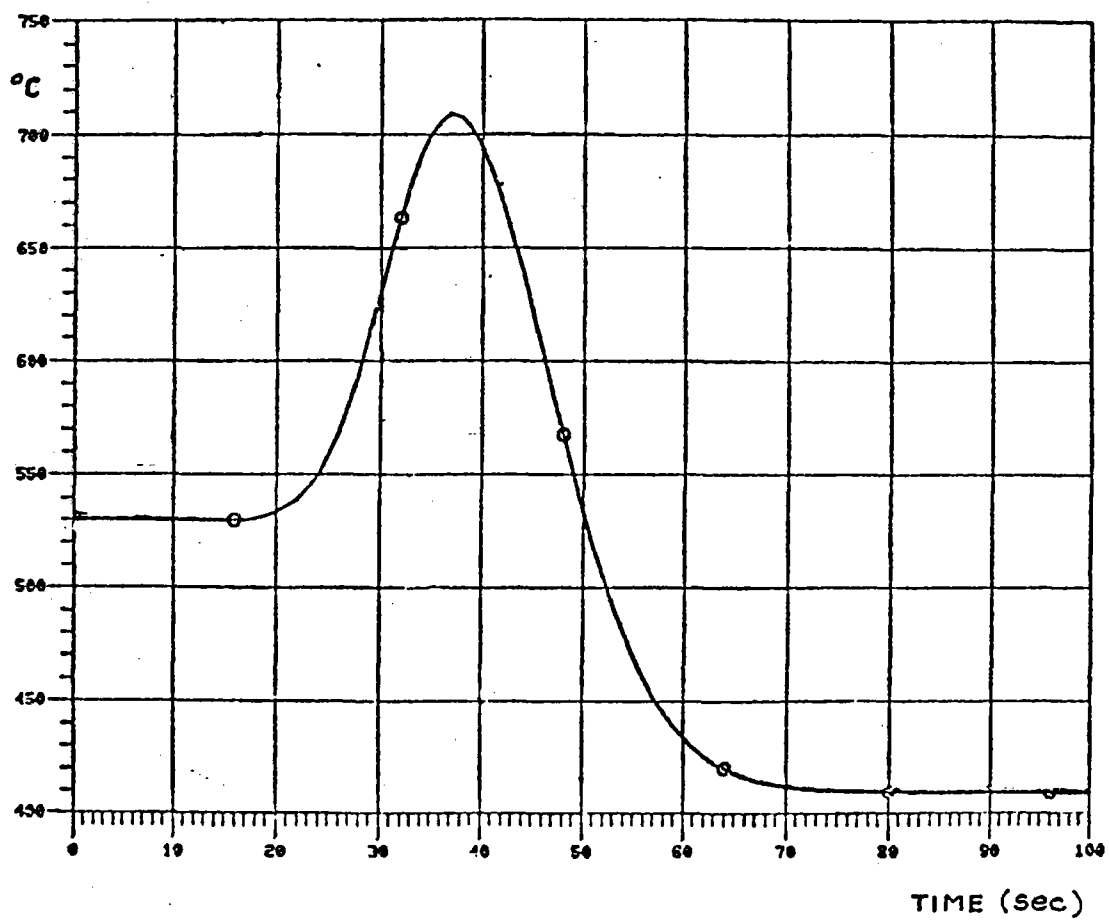


FIG. 4/12 - UPPER HEADER NOZZLE

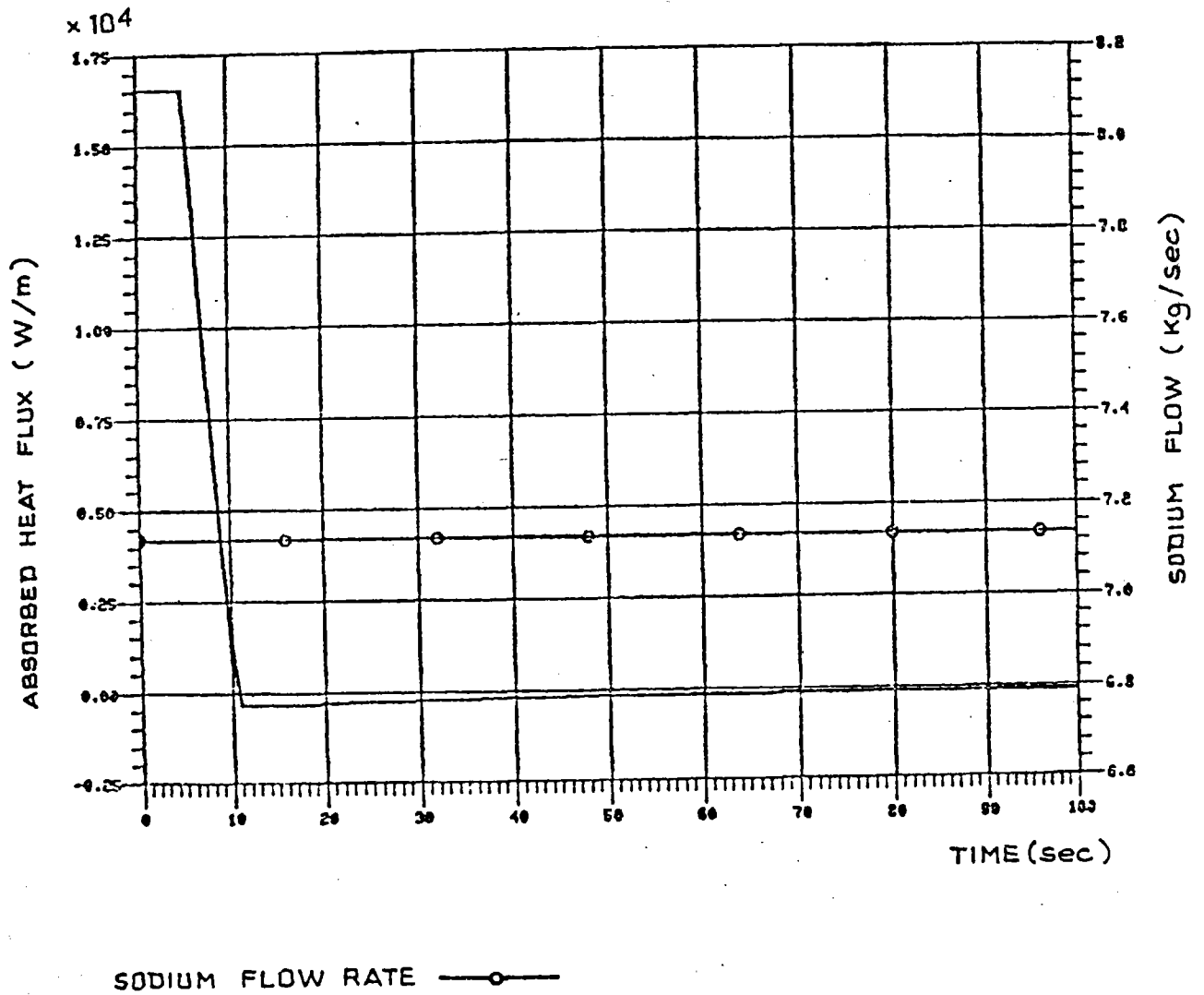


FIG. 4/13

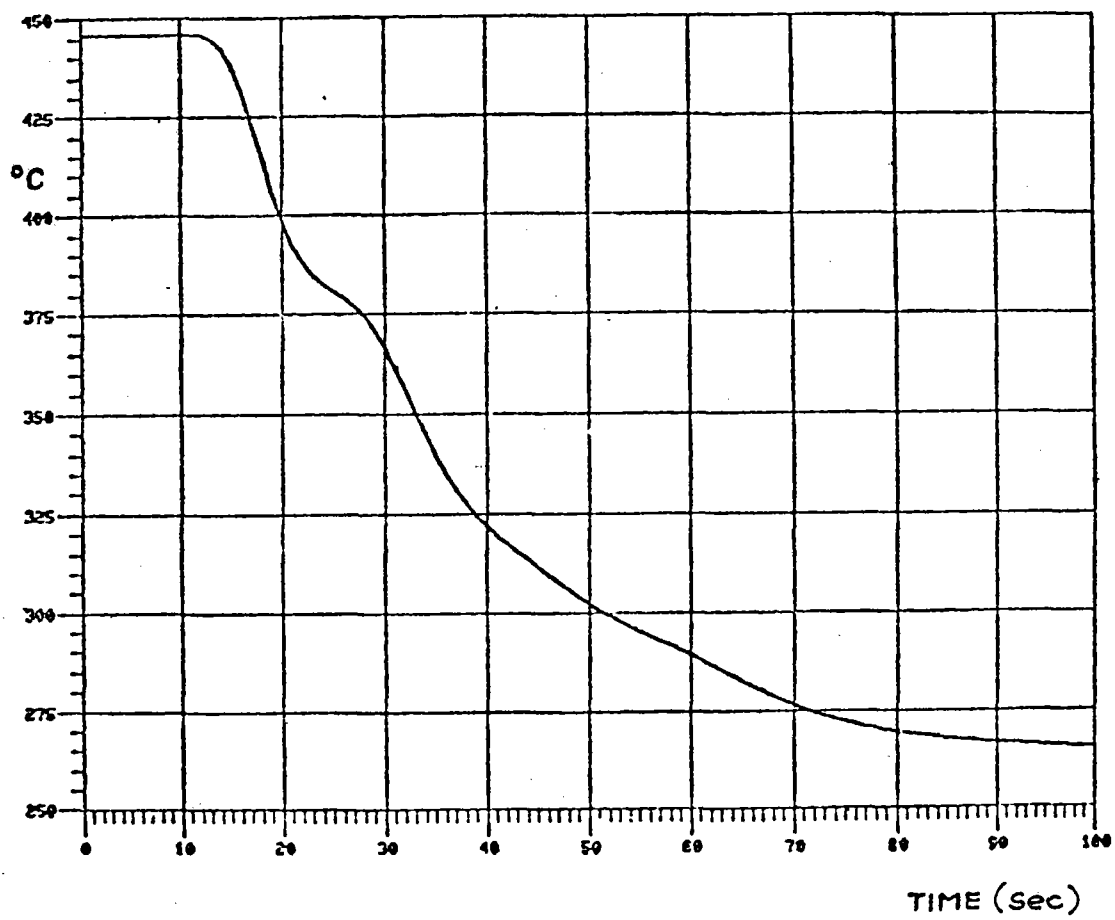


FIG. 4/14 - LOWER HEADER FLANGE

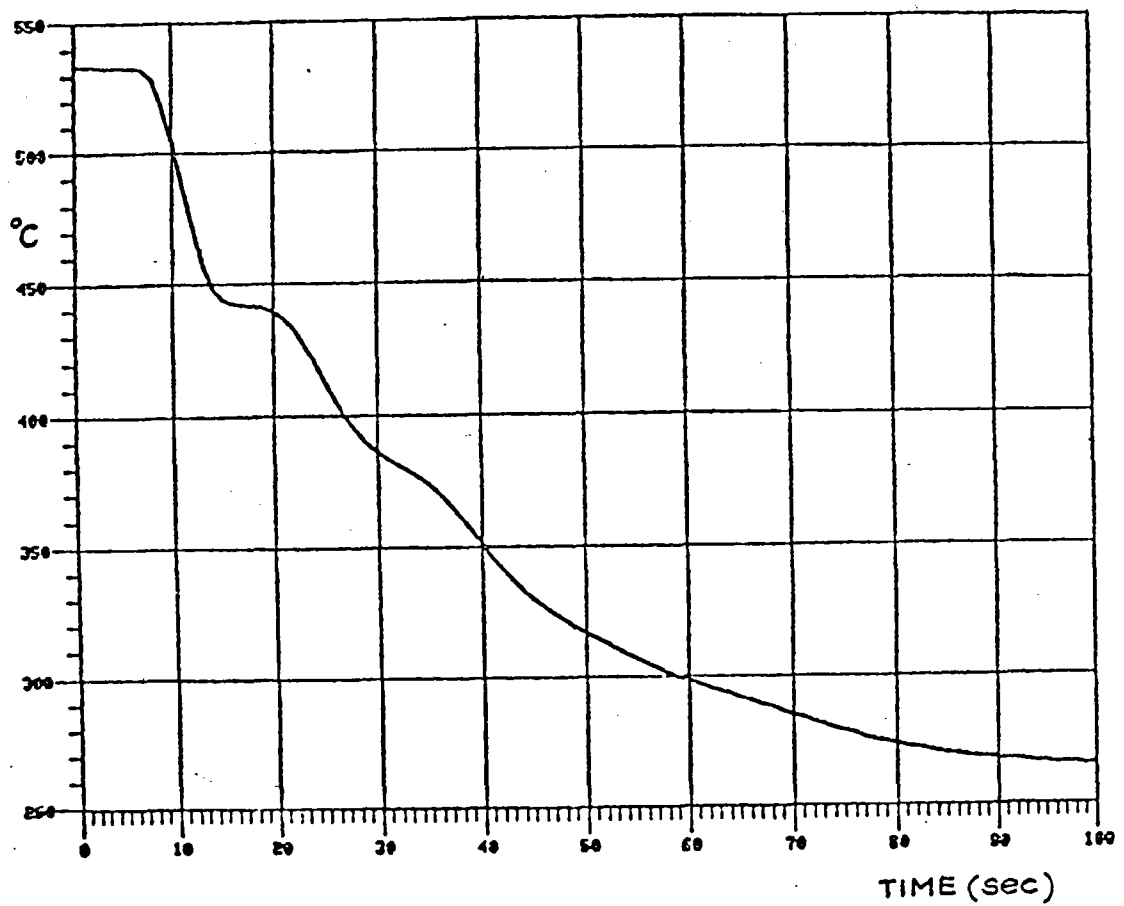
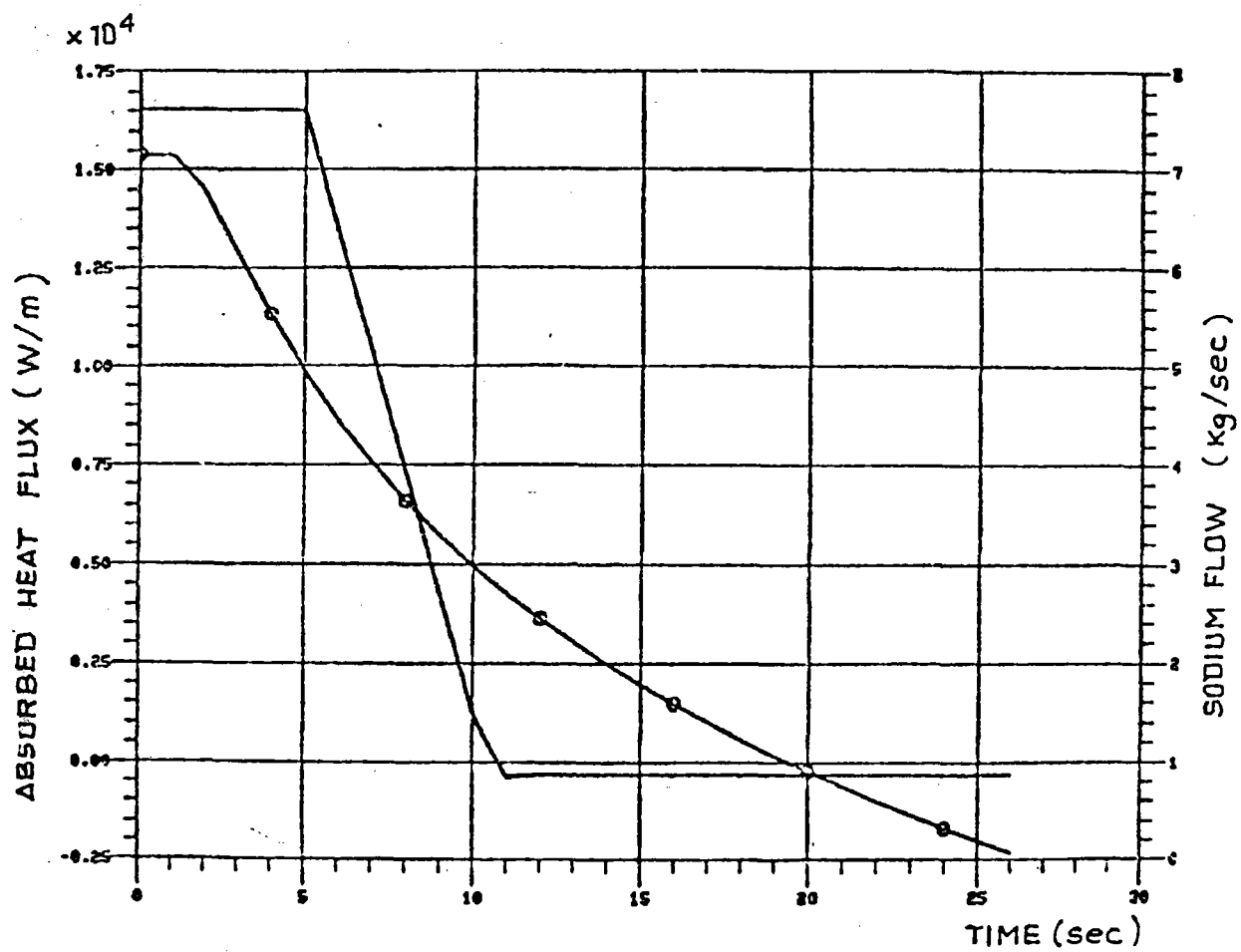


FIG. 4/15 - UPPER HEADER NOZZLE



SODIUM FLOW RATE —○—

FIG. 4/16

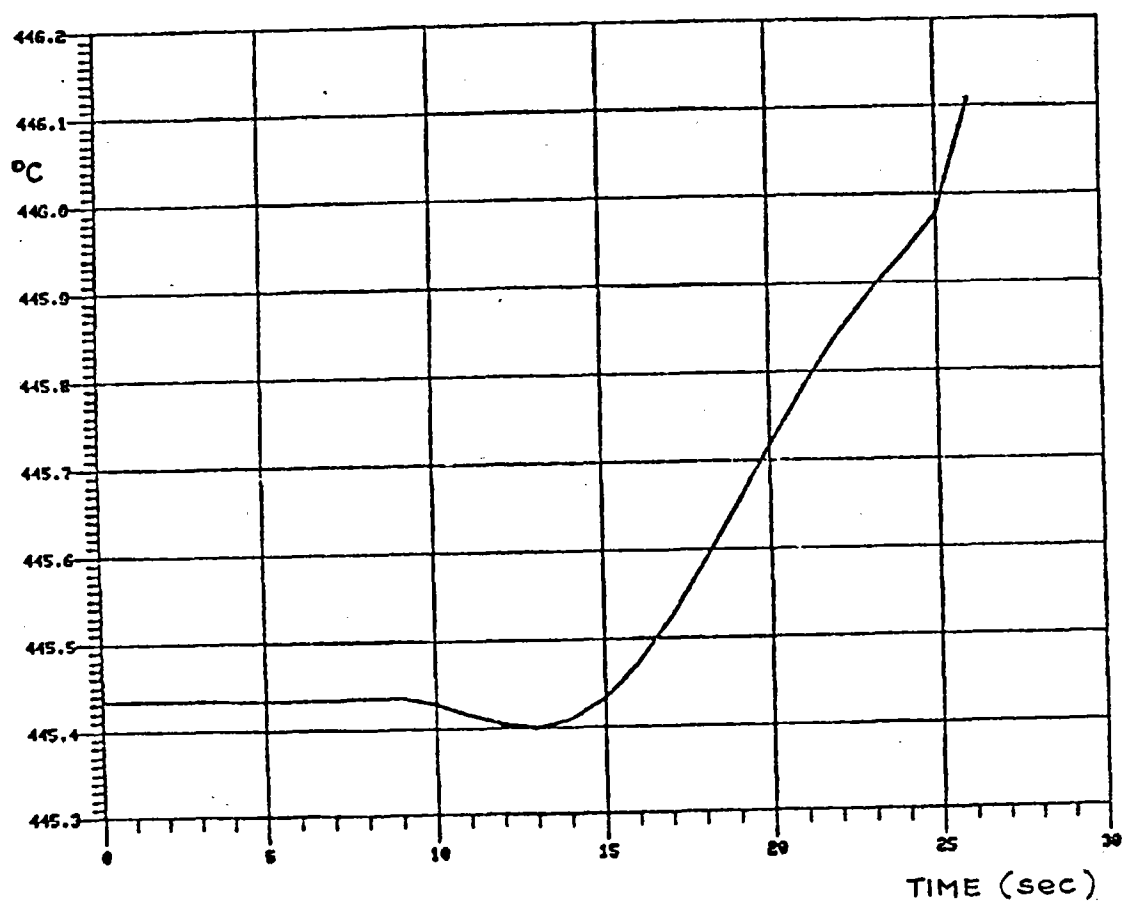


FIG. 4/17 - LOWER HEADER FLANGE

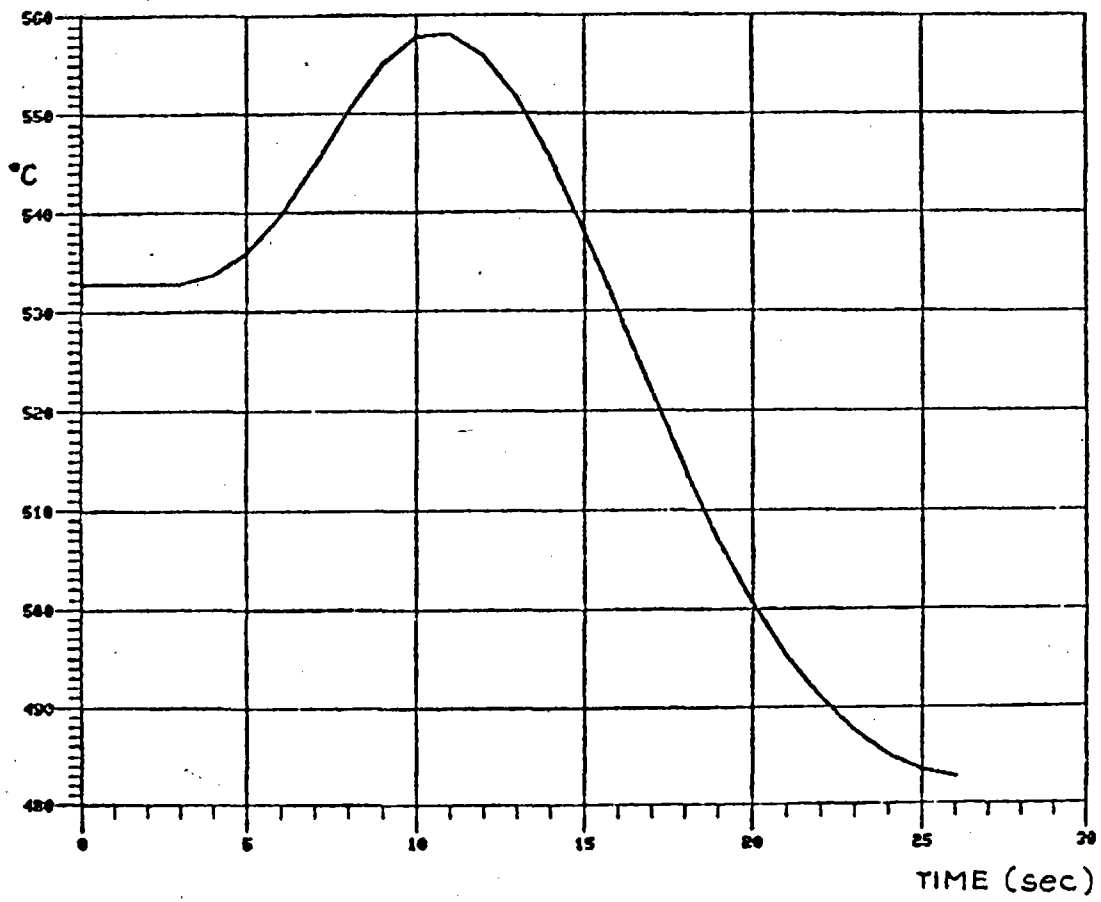


FIG. 4/18 _ UPPER HEADER NOZZLE

5. CALCULATION METHODOLOGY

In the assumption of linear elastic behaviour of the material, the stress conditions have been determined by means of the superimposition of the following effects:

- 1) Stresses due to internal pressure.
- 2) Self equilibrating stresses in every section, due to the non linear temperature distribution in the section.
- 3) Stresses due to piping moments.
- 4) Stresses due to earthquake.

Stresses at point 1) can easily be determined by formulas.

Stresses at point 2) can be found by finite element calculations imposing the non linear temperature field previously determined.

Stresses at point 3) are evaluated again by finite element calculations using axisymmetric (Fourier) elements allowing non-axisymmetric loads.

Stresses at point 4) are evaluated in the same way as point 3).

The stresses described at point 1) are to be considered constant in time.

The stresses of point 2) are time dependent following the thermal transients presented at chapter 4.

The stresses referred at point 3) and 4) are again time dependent following the sodium temperature in pipe.

6. LOWER HEADER FLANGE

6.1. ANALYSIS LIMITS AND DESCRIPTION OF THE STRUCTURE

The analysis refers to the hottest lower header flange, subjected to thermal transients and to stationary and variable mechanical loads.

The most important geometric characteristics of this part of the structure are represented in fig. 6.1/1.

All further considerations are related to the most stressed section "A-A" in the aforementioned figure for which a complete code compliance analysis has been carried out. Some considerations are reported for section "B-B" as well in which maximum mechanical loads have to be expected.

In this calculation only the transient type T8, T9, T12 (see chapter 2) are analysed.

The comparison between the rate of sodium temperature change for T16, T14 and T12 transient has permitted to assume the last one for the evaluation of the fatigue damage.

The fatigue damage due to T15 transient has been considered negligible.

LOWER HEADER FLANGE GEOMETRY

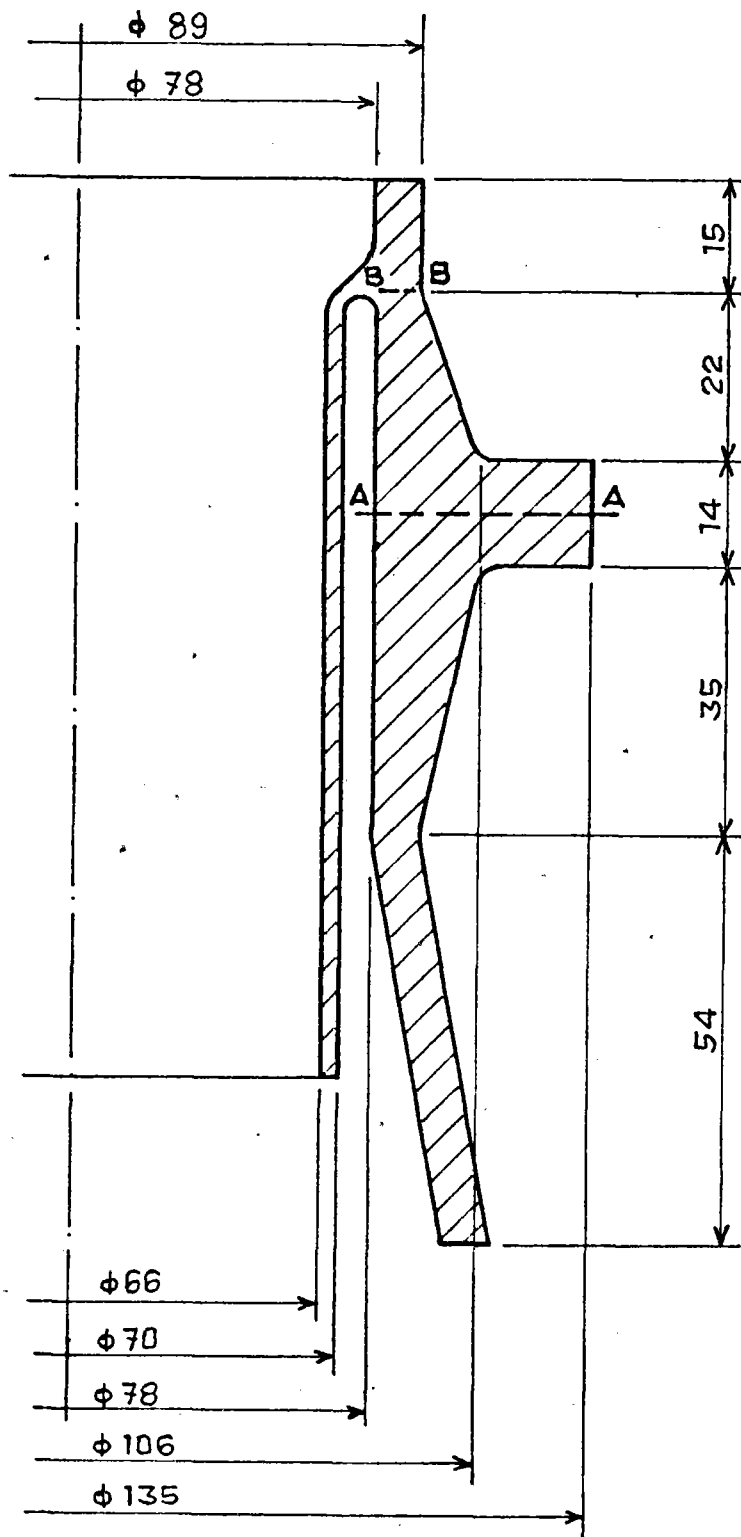


FIG. 6.1/1

6.2. TEMPERATURE FIELD EVALUATION

In tables 6.2/1 + 6.2/3 the discretization of the thermal transients considered for the "A-A" section are reported.

Every time interval is subdivided in 30 time-steps: at each time a forced convection must be applied to the sodium wetted surfaces.

The following assumptions are used in the temperature field calculation:

- the sodium layer between the tube and the thermal shield has been assumed stagnant (for sodium physical characteristics see Appendix 2);
- only the heat conduction in the radial direction has been considered;
- the external surface of the tube and the flange is assumed adiabatic.

By a finite element computer code (FLHE of BERSAFE series) the temperature field in every point of the section has been calculated at each time step.

In fig. 6.2/1 the axisymmetrical 2D mesh used is presented.

THERMAL TRANSIENT T8

TIME (sec)	TEMPERATURE (°C)	FLOW (Kg/sec)	DENSITY (Kg/m ³)	VELOCITY (m/sec)	HEAT COEFF. (W/m ² °C)
0.0	450	7.3	845.11	2.52	17772
14.0	448	0.7	845.58	0.24	6921
47.0	444	0.7	846.54	0.24	6965
52.0	435	11.5	848.68	3.96	23818
55.0	384	11.5	860.79	3.90	24248
60.0	402	11.5	856.53	3.92	24057
65.0	380	11.5	861.73	3.90	24313
102.0	384	11.5	860.79	3.90	24248
110.0	385	10.3	860.55	3.50	22622
130.0	402	7.3	856.53	2.49	18254
190.0	455	7.3	843.91	2.53	17888
250.0	450	7.3	845.11	2.52	17772
300.0	450	7.3	845.11	2.52	17772

- TABLE 6.2/1 -

THERMAL TRANSIENT T9

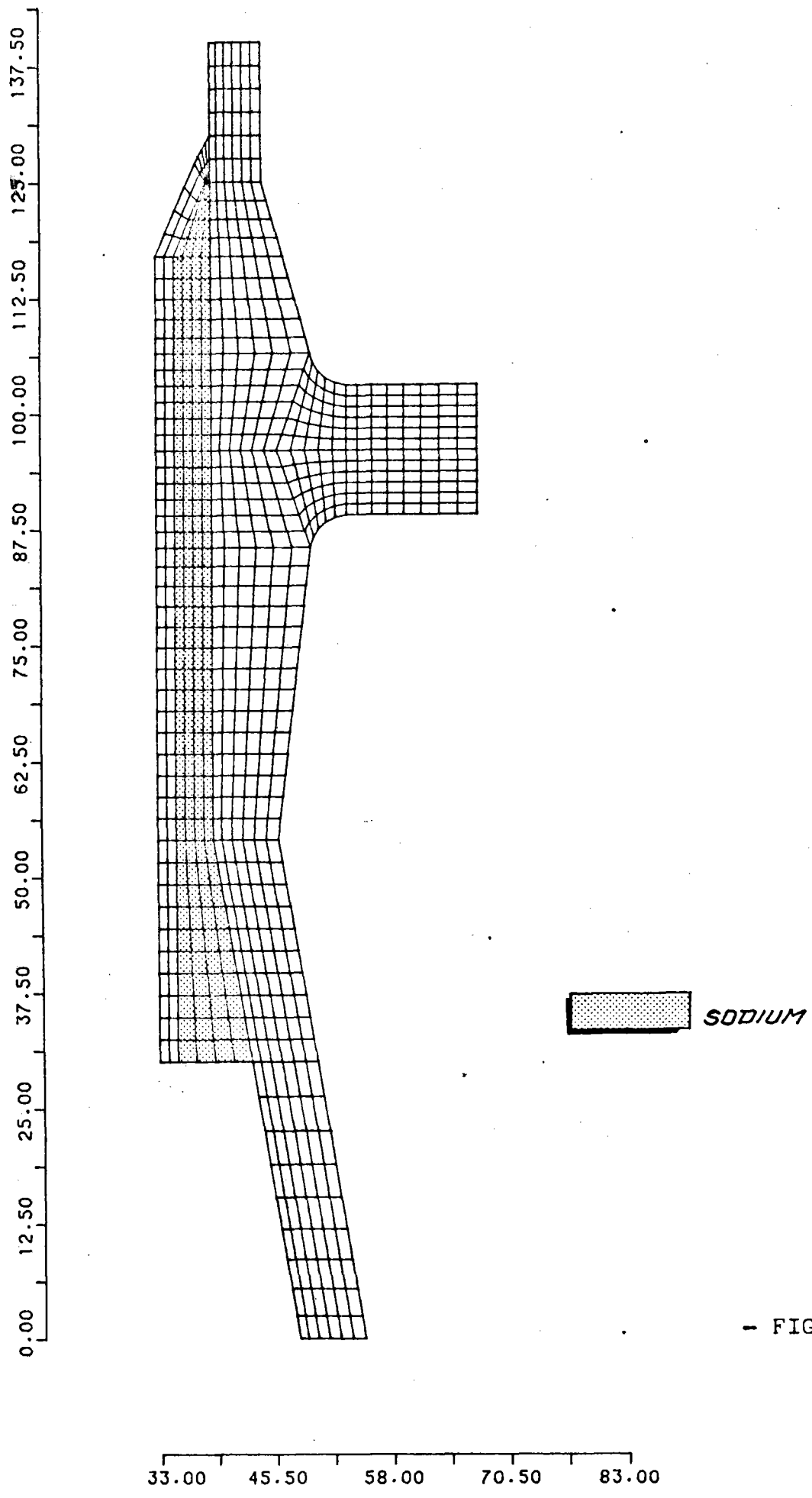
TIME (sec)	TEMPERATURE (°C)	FLOW (Kg/sec)	DENSITY (Kg/m ³)	VELOCITY (m/sec)	HEAT COEFF. (W/m ² °C)
0	450	7.3	845.1	2.52	17772
14	448	0.7	845.6	0.24	6921
90	437	0.7	848.2	0.24	6925
136	363	0.7	865.7	0.23	7294
230	348	0.7	869.3	0.23	7369
250	336	0.7	872.1	0.23	7415
252	335	3.5	872.3	1.17	12232
258	295	11.5	881.7	3.81	24962
262	310	11.5	878.2	3.83	25036
268	315	11.5	877.0	3.83	24900
307	370	11.5	864.1	3.89	24442
335	409	7.3	854.9	2.50	18156
370	458	7.3	843.2	2.53	17888
450	450	7.3	845.1	2.52	17772
550	450	7.3	845.1	2.52	17772

- TABLE 6.2/2 -

THERMAL TRANSIENT T12 + T11

TIME (sec)	TEMPERATURE (°C)	FLOW (Kg/sec)	DENSITY (Kg/m ³)	VELOCITY (m/sec)	HEAT COEFF. (W/m ² °C)
0	450	7.3	845.1	2.52	17772
14	447	0.7	845.8	0.24	6921
70	436	0.7	848.5	0.24	7440
130	370	0.7	864.1	0.24	7279
225	340	0.7	871.2	0.23	7415
440	220	0.7	899.1	0.23	7801
890	220	0.7	899.1	0.23	7801
900	220	9.4	899.1	3.06	22729
907	270	9.4	887.5	3.1	22322
926	350	9.4	868.8	3.16	21575
930	360	9.4	866.5	3.17	21459
944	388	7.3	859.8	2.48	18353
965	430	7.3	849.9	2.51	17963
990	450	7.3	845.1	2.52	17772
1100	450	7.3	845.1	2.52	17772

- TABLE 6.2/3 -



- FIG. 6.2/1 -

LOWER HEADER FLANGE
AXISYMMETRIC MESH

In figg. 6.2/2 + 6.2/4 the temperature trends in the considered "A-A" section are presented for two time instants giving the maximum range during the different transient conditions.

A post-processing program for plotting isolevel curves for any quantity whose value is defined at each node of a plane mesh or at the centroid of each element is available and allows to plot isothermal curves at any chosen time step.

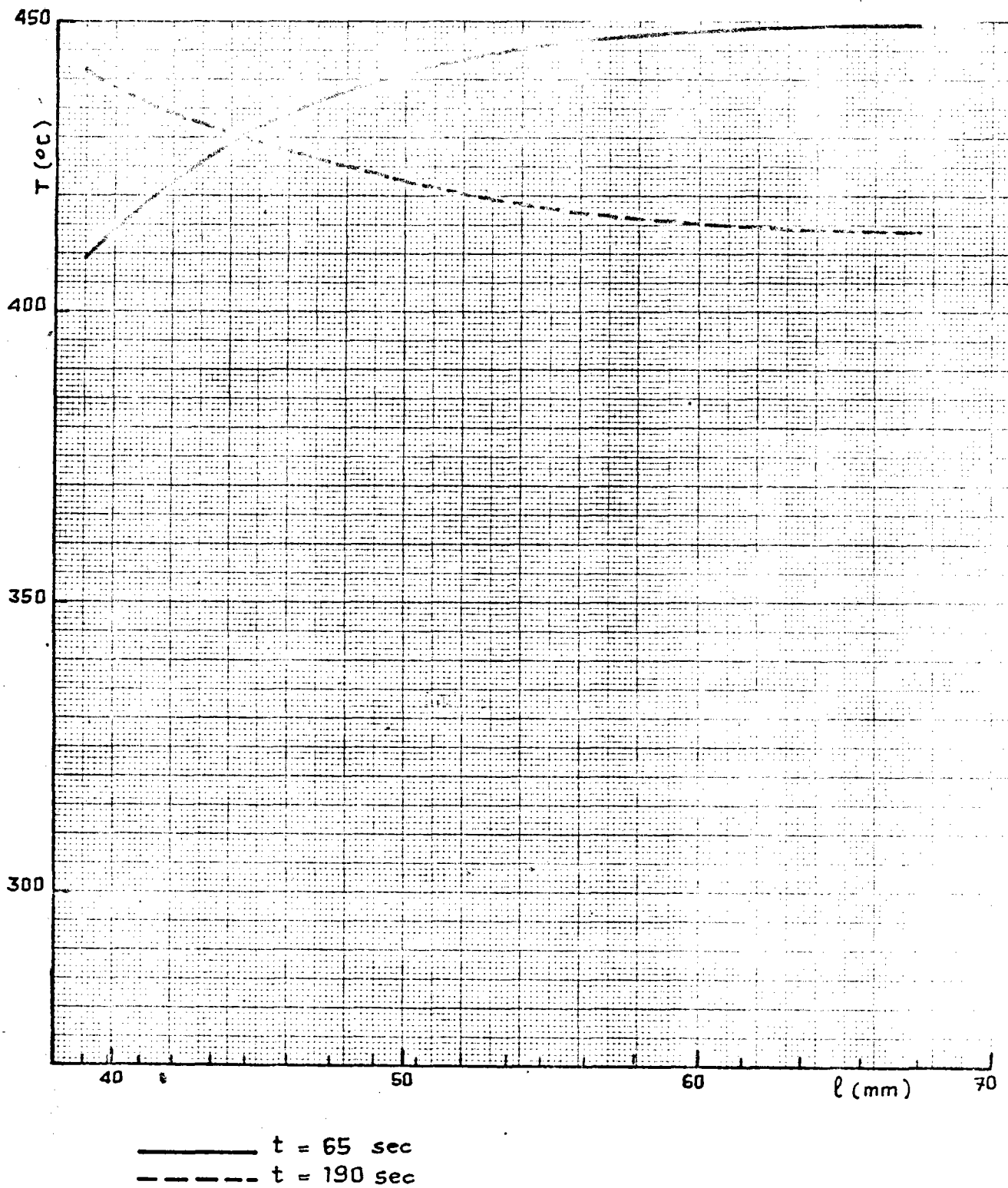
Figures 6.2/5 + 6.2/10 show, for the most dangerous time instants, isothermal curves for the analysed thermal transients.

6.3. THERMAL STRESS EVALUATION

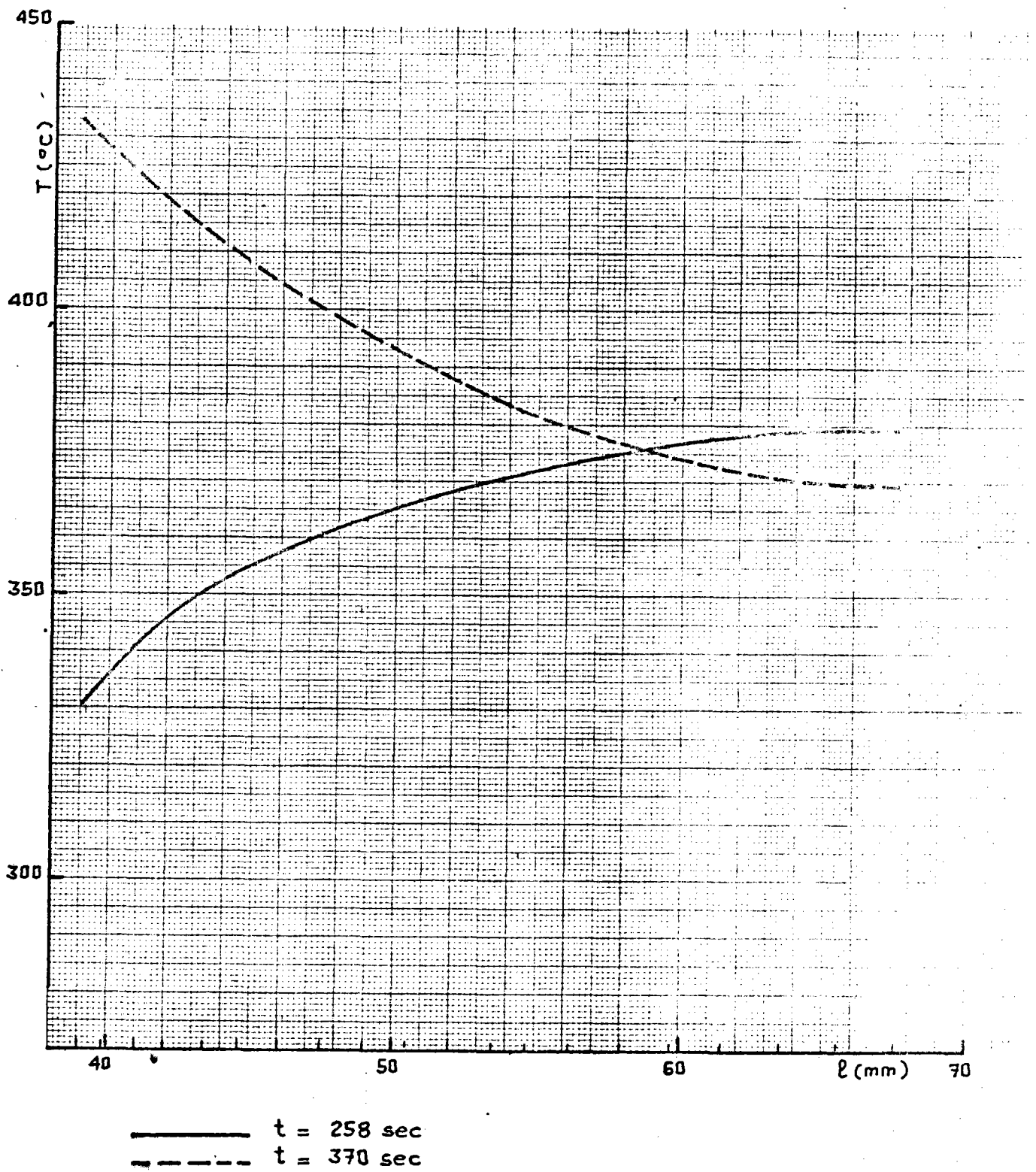
With loading conditions given by the nodal temperature obtained with the FLHE code, stress analysis in some time instants has been performed by means of the finite element program SAP V.

In fig. 6.3/1 the 2D mesh used in this analysis is presented.

The σ_r stress behaviors through the radial section A-A in the most dangerous time step for each transient are shown in figg. 6.3/2 + 6.3/4.



TRANSIENT T8



TRANSIENT T9

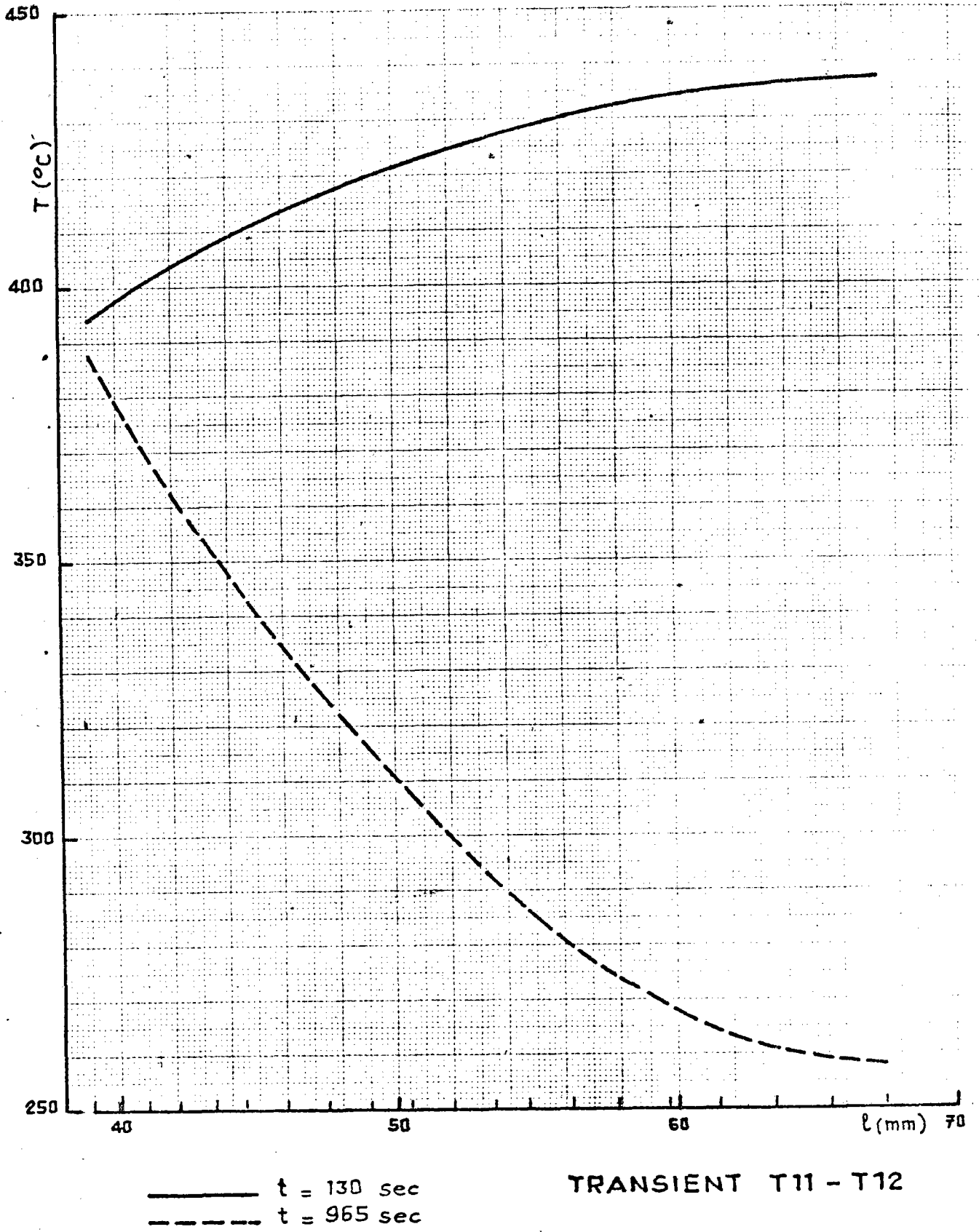
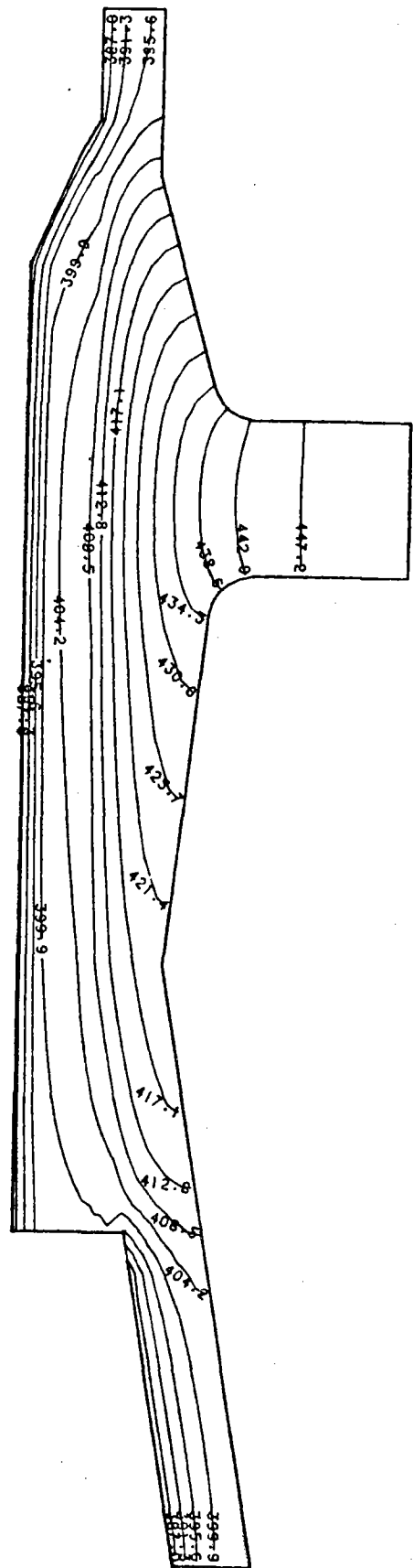
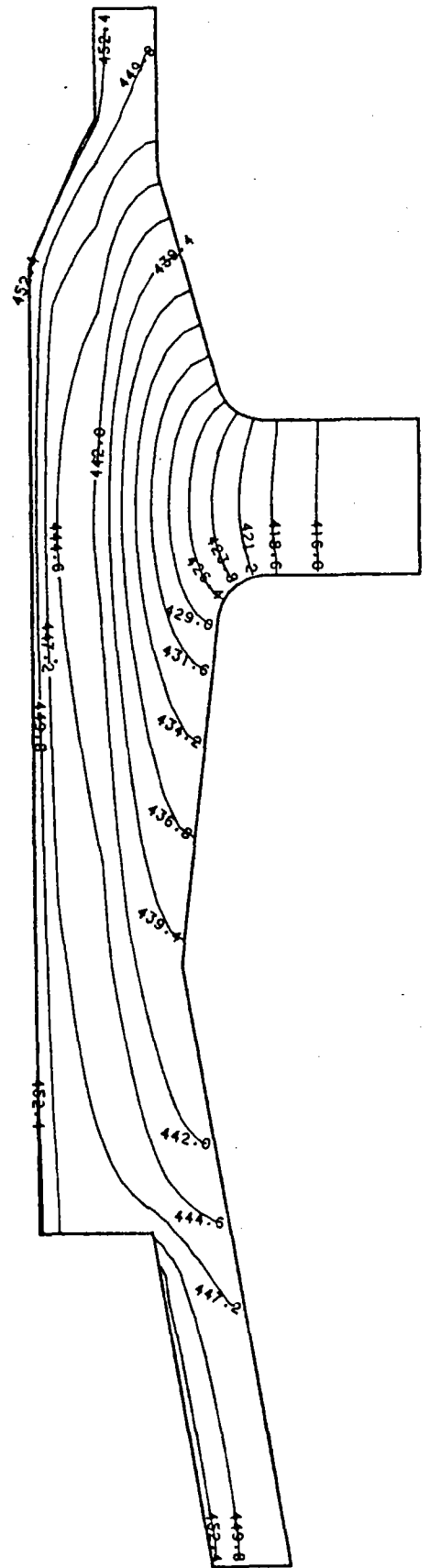


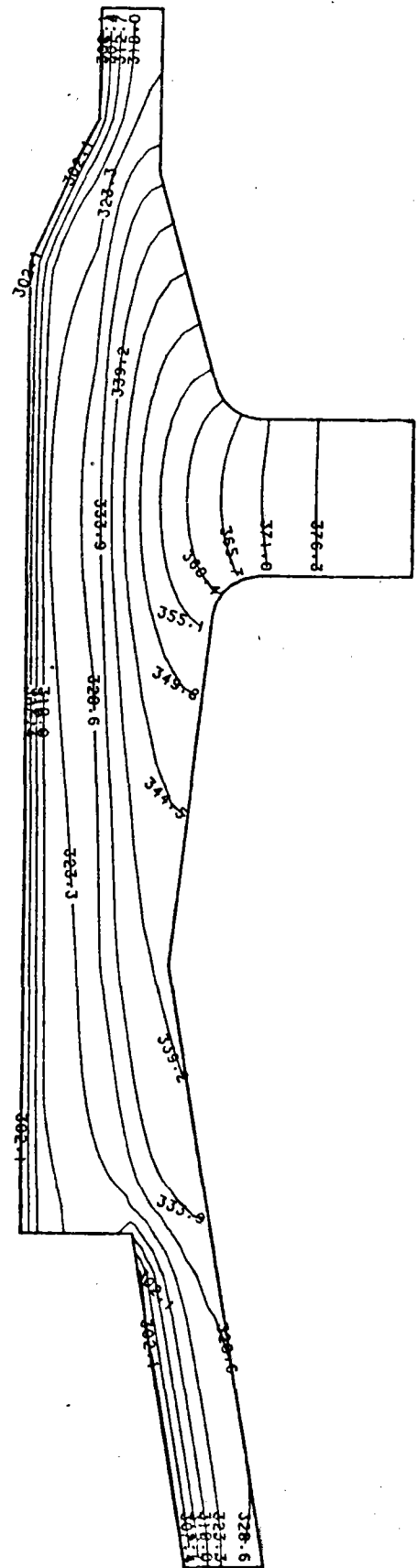
FIG. 6.2/4





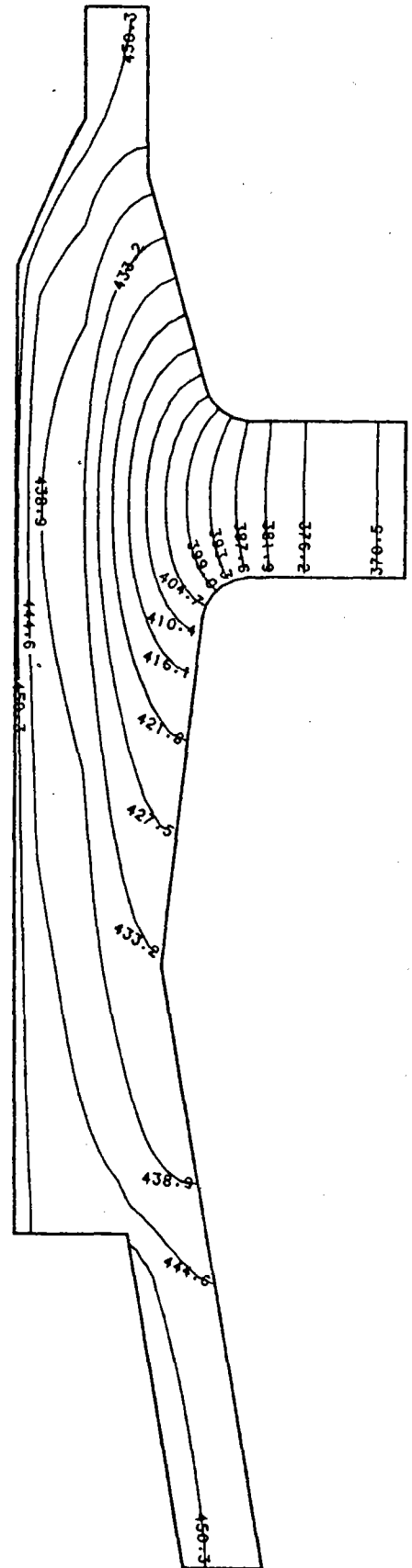
THERMAL TRANSIENT T8
ISOTHERM - TIME T=190 SEC.

- FIG. 6.2/6 -



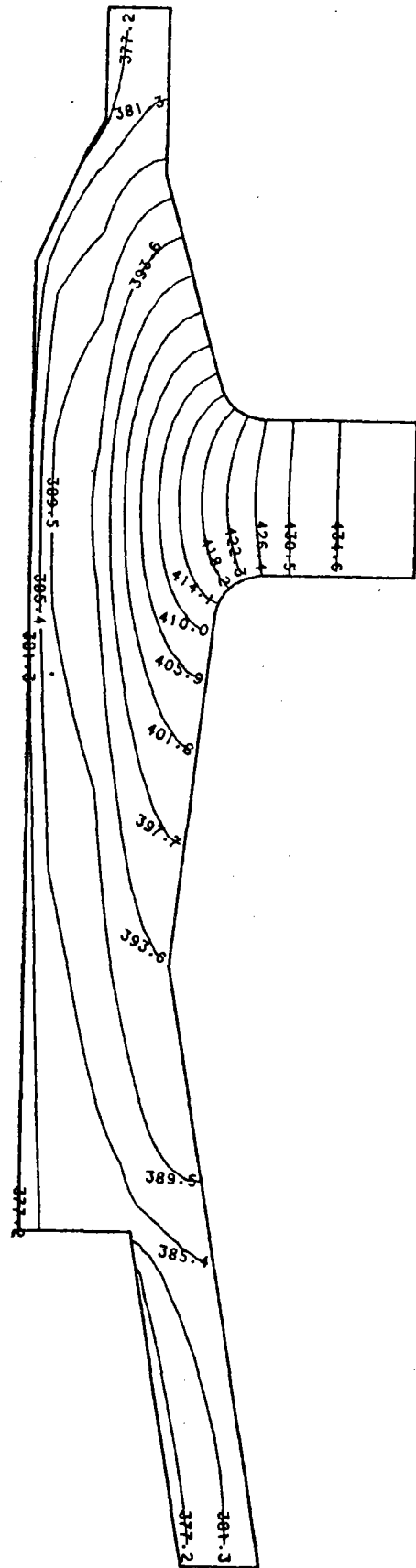
THERMAL TRANSIENT T9
ISOTHERM - TIME T=258 SEC

- FIG. 6.2/7 -



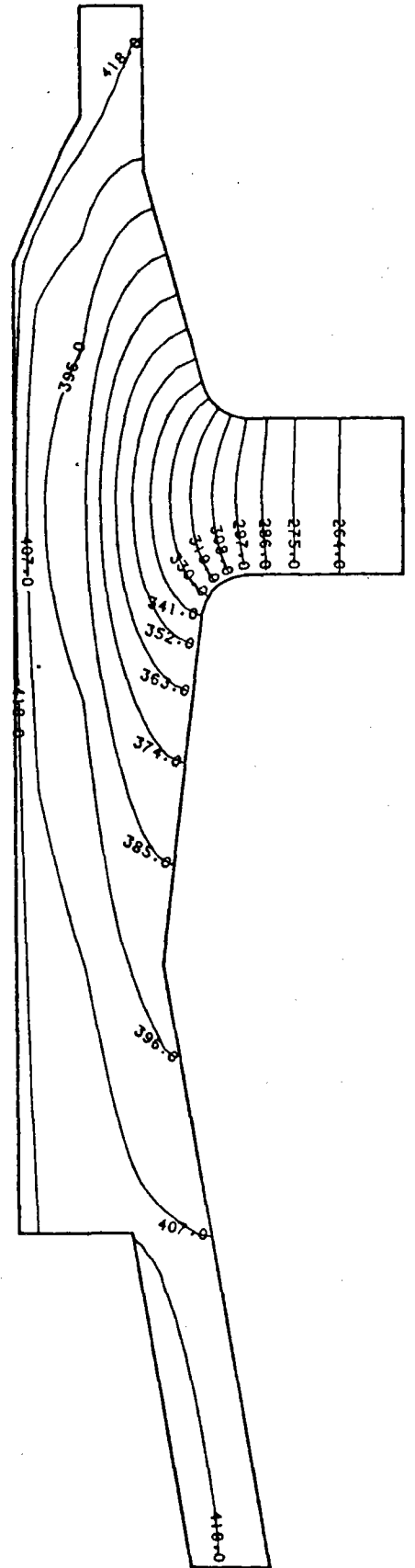
THERMAL TRANSIENT T9
ISOTHERM - TIME T=370 SEC.

- FIG. 6.2/8 -



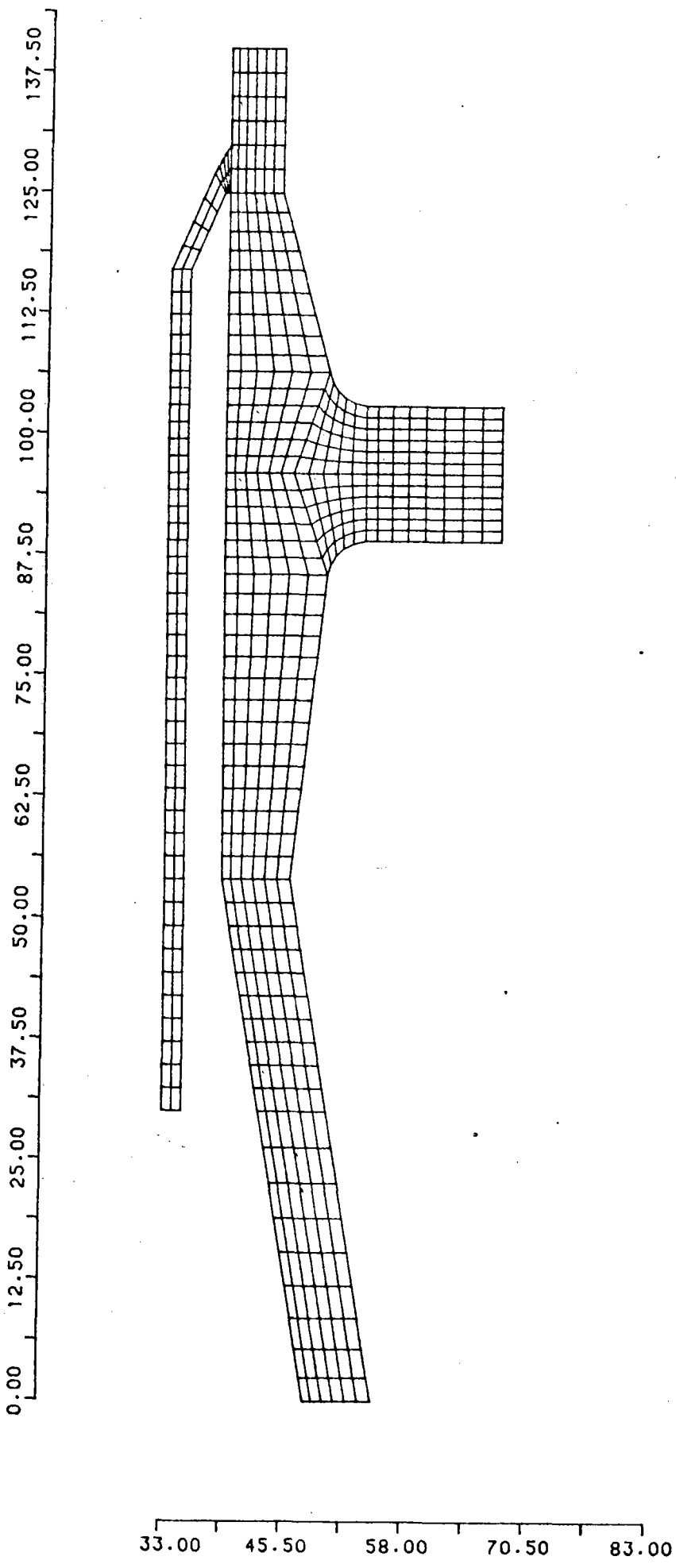
THERMAL TRANSIENT T12
ISOTHERM - TIME T=130 SEC

- FIG. 6.2/9 -



THERMAL TRANSIENT T12
ISOTHERM - TIME T=965 SEC.

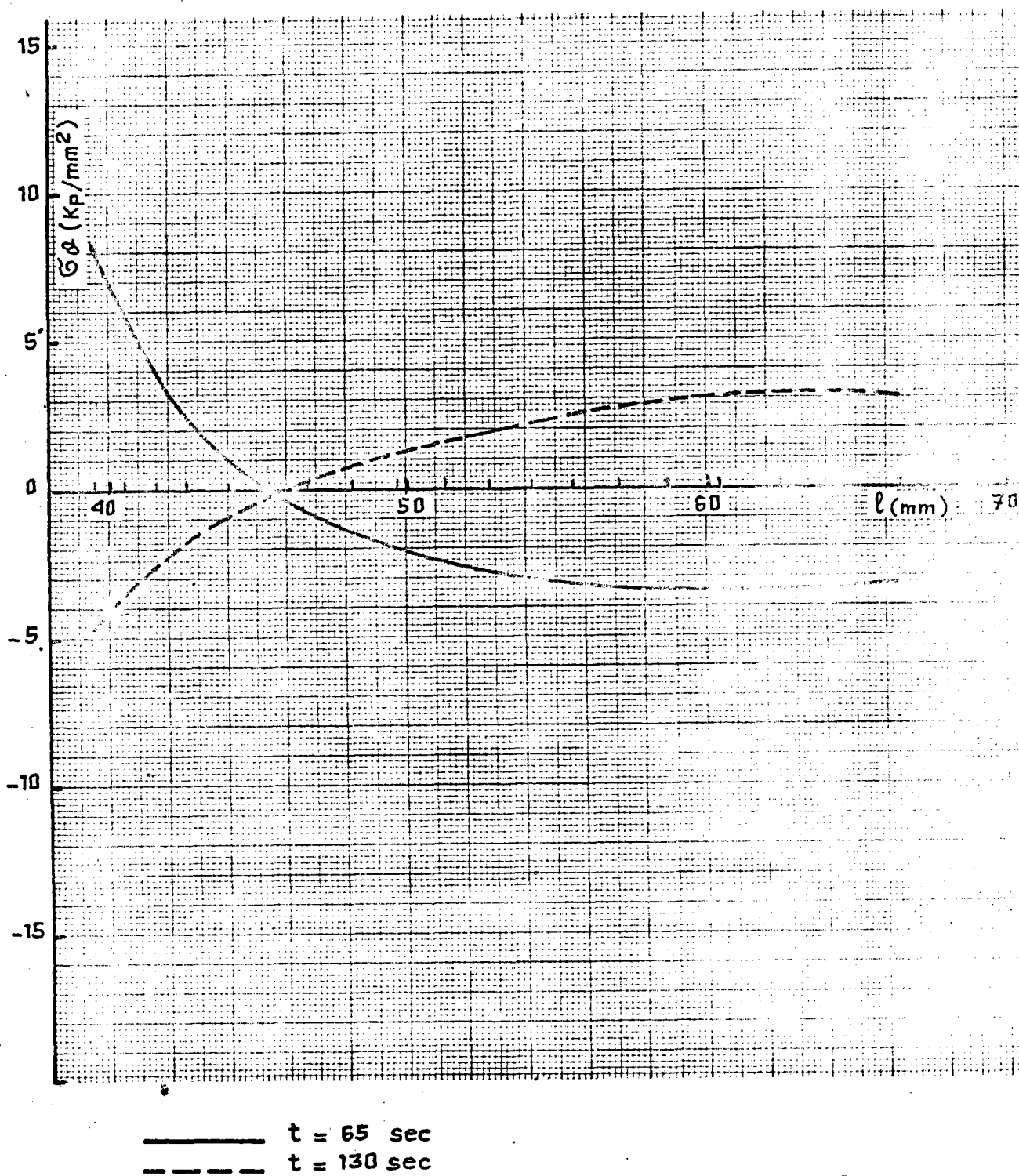
- FIG. 6.2/10 -



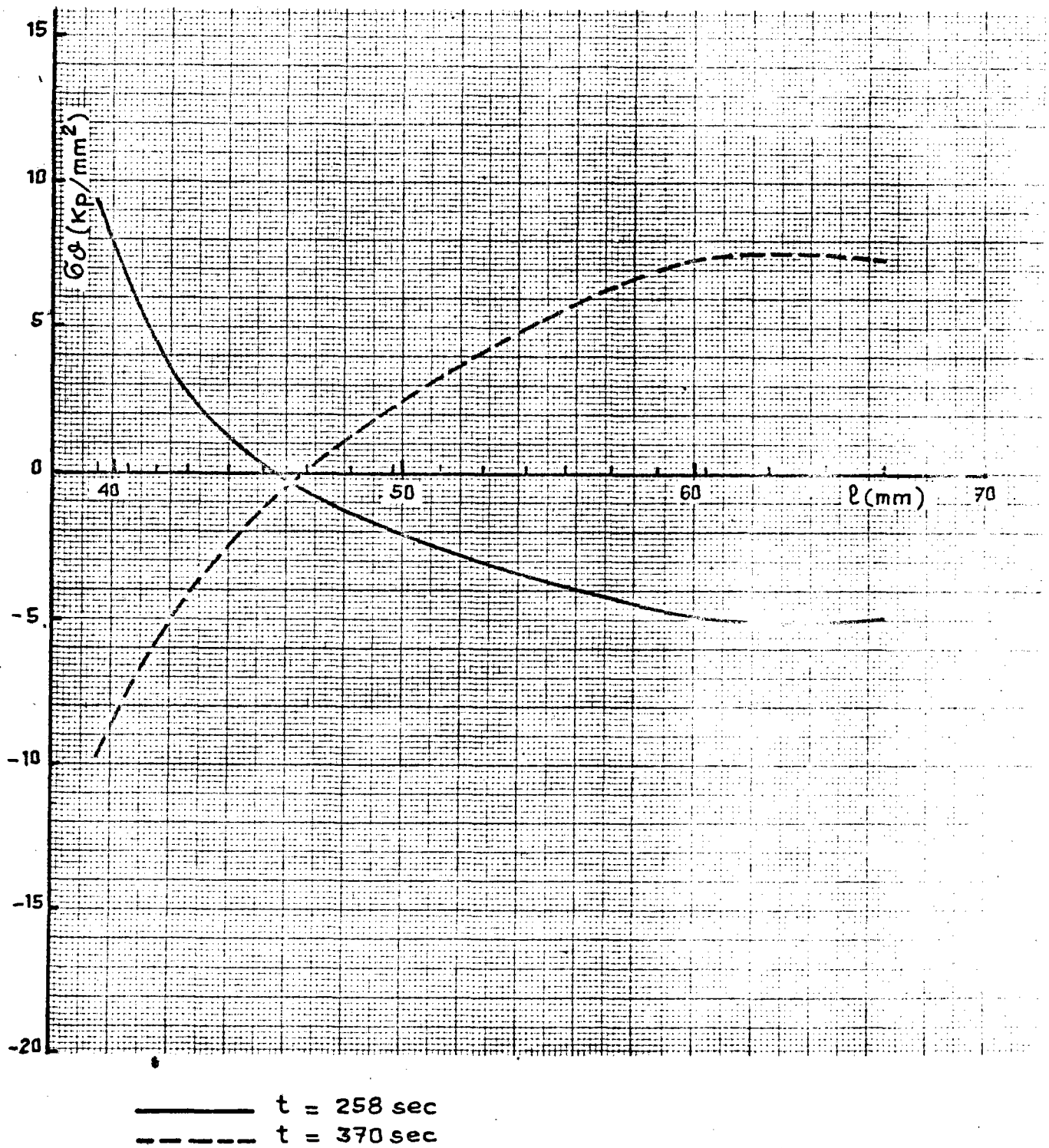
- FIG. 6.3/1 -

LOWER HEADER. FLANGE

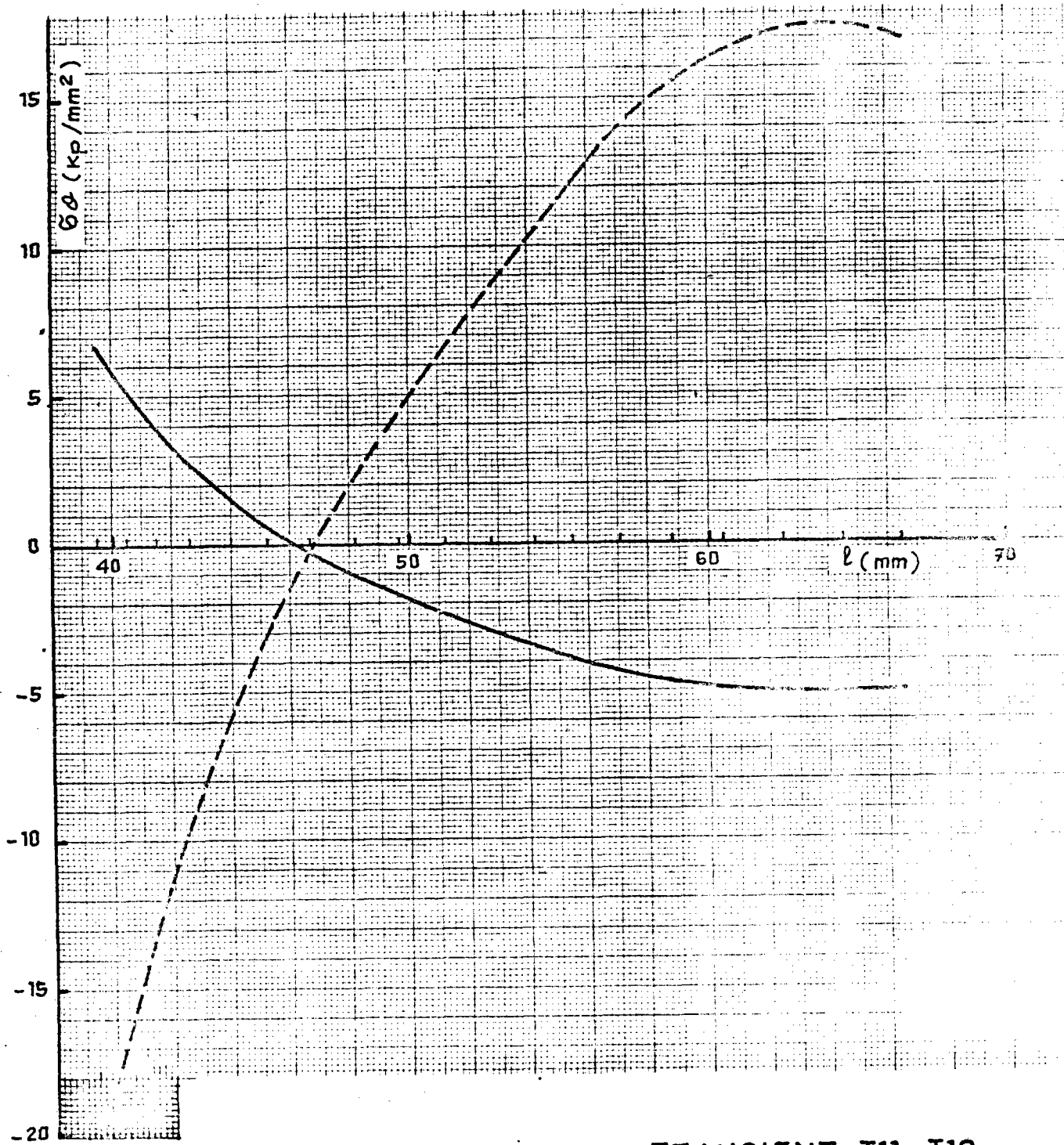
AXISYMMETRIC MESH.



TRANSIENT T8



TRANSIENT T9



TRANSIENT T11-T12

— $t = 130 \text{ sec}$
 - - - $t = 965 \text{ sec}$

By means of a postprocessor computer code based on the definition of the stress components (membrane, bending and peak) given in Code Case N-47-17, point 3215, for axisymmetric structures, the stress classification has been carried out.

Another post-processing program allows to plot the σ_{GUEST} curves at the chosen time steps (see figg. 6.3/5 + 6.3/10).

6.4. STRESS EVALUATION DUE TO PIPING MOMENTS

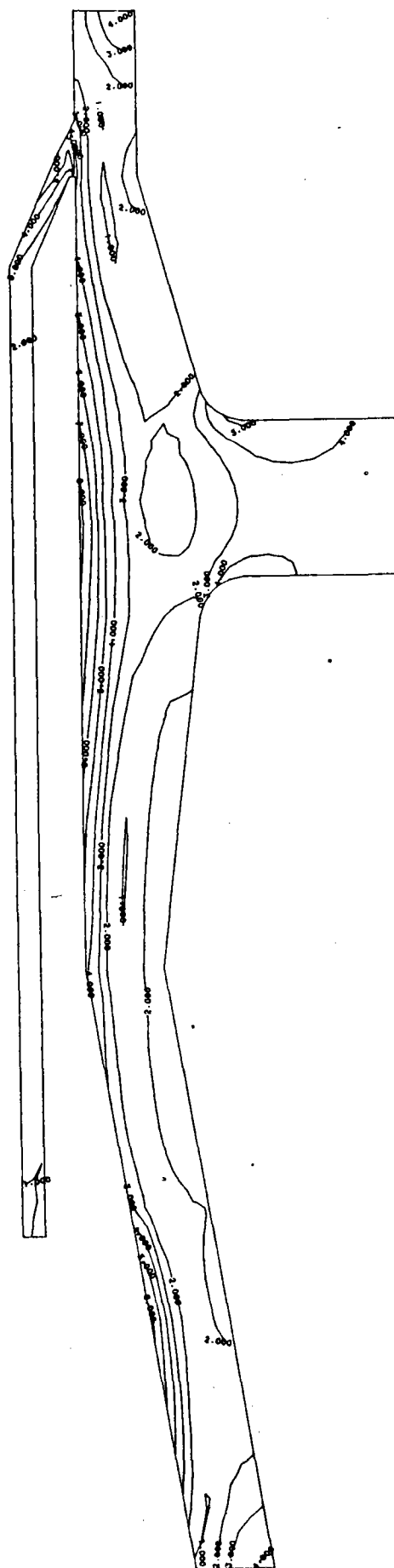
The stresses, due to the piping moment, are calculated by the finite element BERSAFE computer code using axisymmetric Fourier elements.

For an axisymmetric body subjected to non-axisymmetric loads, these elements allow a solution using a two dimensional mesh.

The loads on the body are expanded in a Fourier series.

An important point for stress analysis calculation are the boundary condition of the structure.

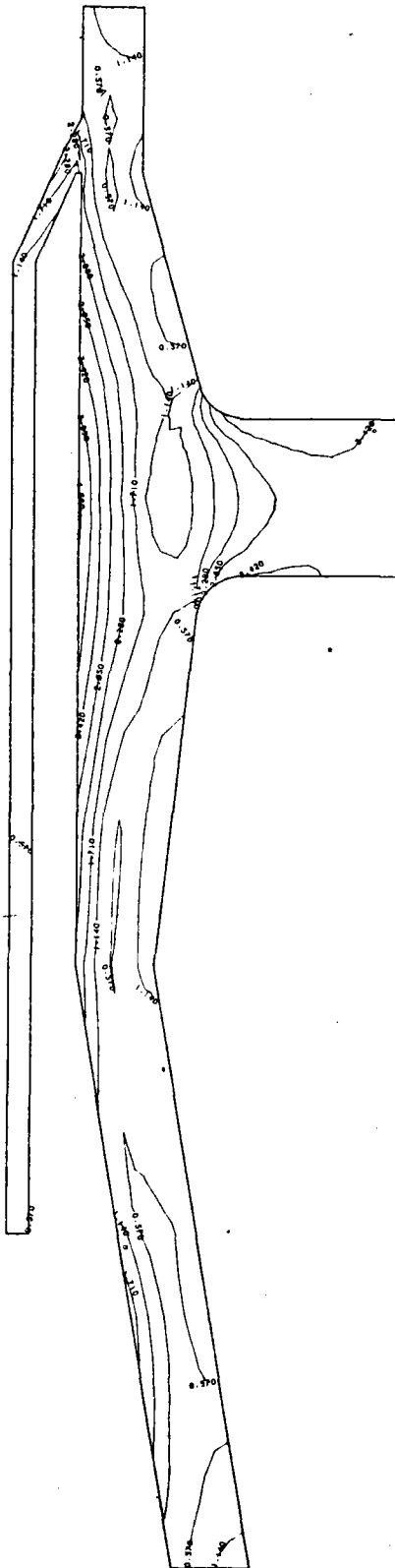
Considering code limits and in the hypothesis of small clearance in the coupling between flange and frame, clamps on the upper and lower planes of the flange have been assumed.



THERMAL TRANSIENT T8
TIME T = 65 SEC.

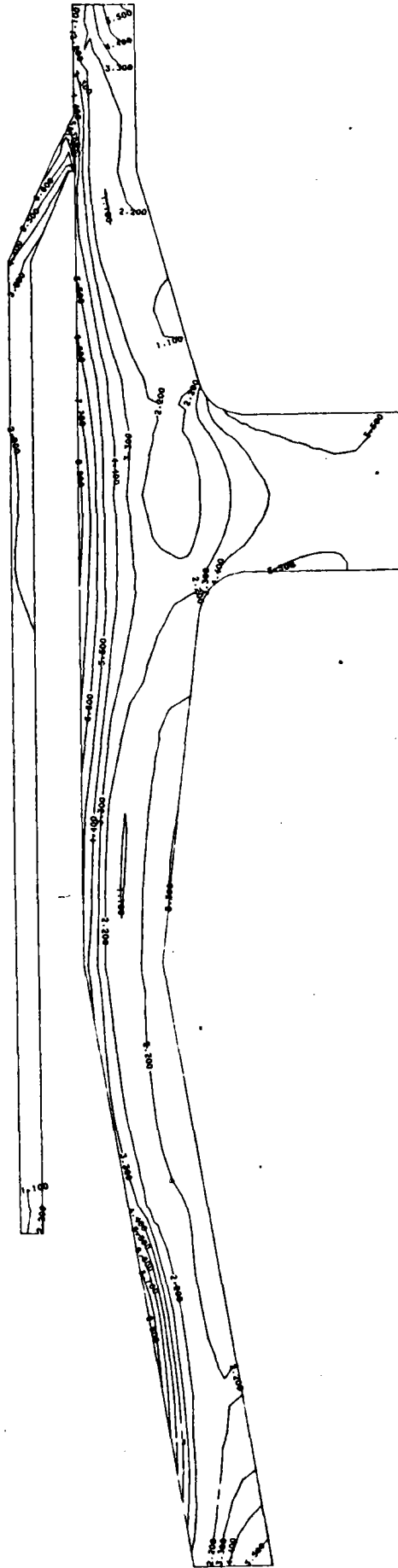
GUEST (KP/MM²)

- FIG. 6.3/5 -



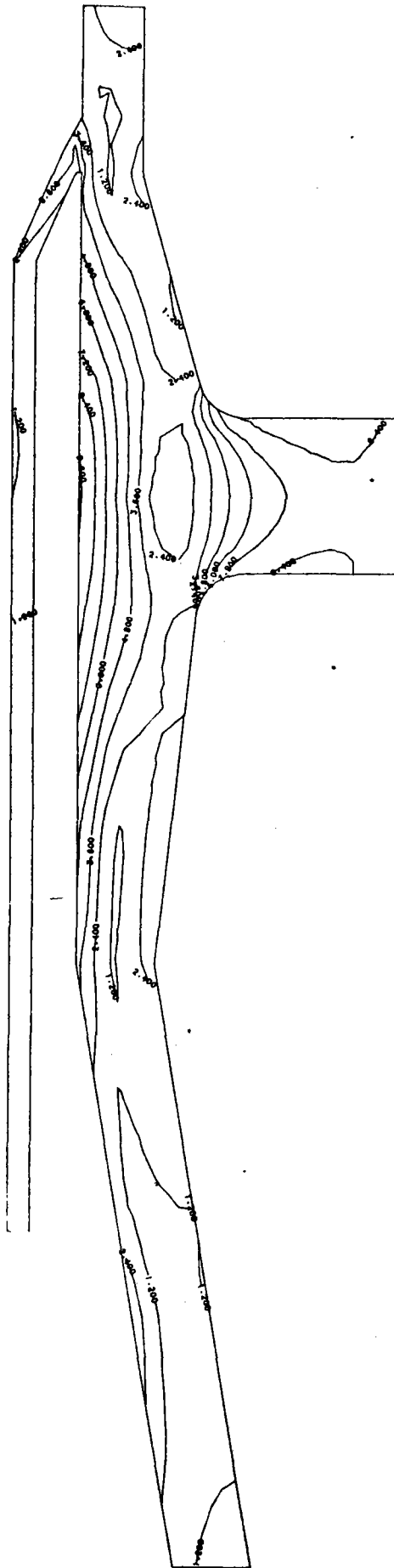
THERMAL TRANSIENT T8
TIME T = 100 SEC.
QUEST (KP/MM²)

- FIG. 6.3/6 -



THERMAL TRANSIENT T9
TIME T = 258 SEC.
GUEST (KP/MM**2)

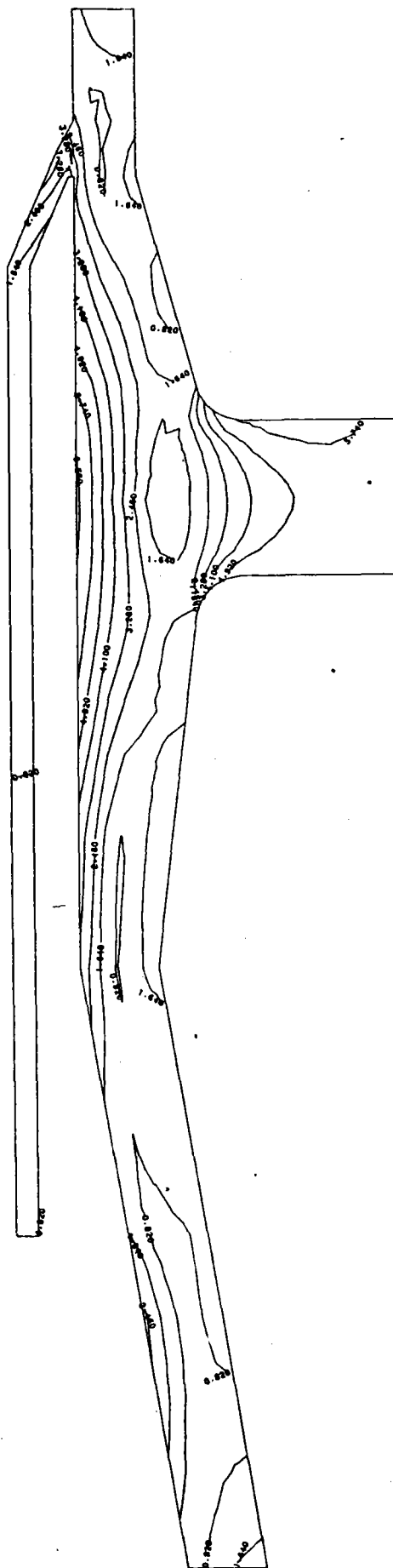
- FIG. 6.3/7 -



THERMAL TRANSIENT T9
TIME T = 370 SEC.

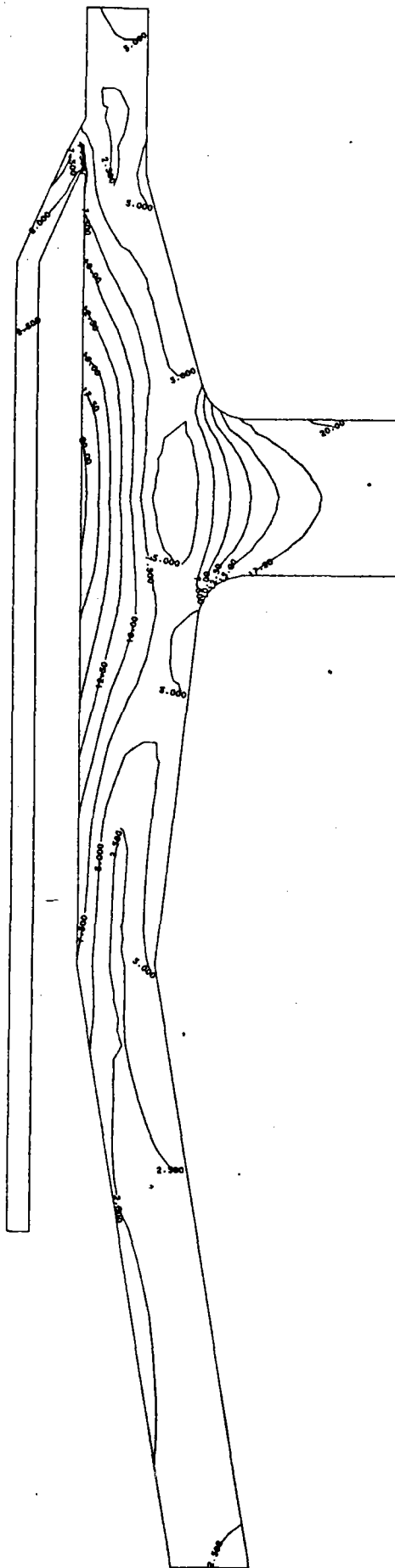
GUEST (KP/MM**2)

- FIG. 6.3/8 -



THERMAL TRANSIENT T12
TIME T = 130 SEC.
GUEST (KP/MM²)

- FIG. 6.3/9 -



THERMAL TRANSIENT T12
TIME T = 965 SEC.

GUEST (KP/MM**2)

- FIG. 6.3/10 -

The maximum moment value obtained by pipe flexibility analysis is 100000 Kp mm.

This moment value is time dependent following the sodium temperature between ≈ 100000 Kp mm and ≈ 48000 Kp mm. Cautiously the fatigue analysis has been carried out with a cycle 100000 Kp mm - 0 Kp mm.

6.5. STRESS TABLE ACCORDING TO ASME CRITERIA

In the following analysis, only the inner point (labeled P) of section A-A is considered, which is the most stressed one.

For all the compliance analysis other than creep - fatigue interaction, the thermal transient T12 has been assumed as the most dangerous one; the analyzed time step corresponds to $t = 965$ sec.

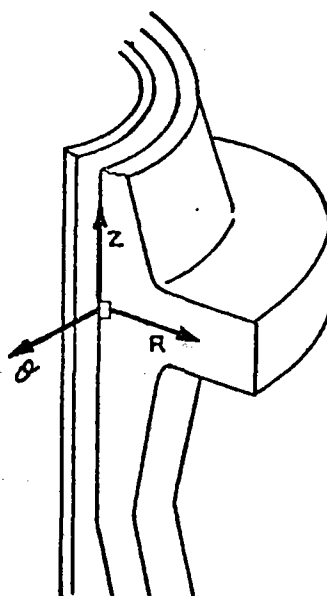
In table 6.5/1 the stresses with their classification according ASME criteria as presented.

With a large conservatism the effects of loads due to piping have been classified as primary membrane stresses P_m .

STRESS TABLE AT POINT "P" FOLLOWING ASME CRITERIA,
AT TIME t = 965 sec OF TRANSIENT T12

Origin	$\bar{\sigma}_R$ (Kp/mm ²)	$\bar{\sigma}_\theta$ (Kp/mm ²)	$\bar{\sigma}_z$ (Kp/mm ²)	Class
Pressure	0.0	0.084*	0.0	P _m
Mechanical loads	0.0	0.0	1.13	P _m
Earthquake	0.0	0.0	±0.23	P _m
Thermal transient	0.0	-12.385	1.677	Q
Thermal transient	0.0	-8.853	-0.925	F

$$(*) \bar{\sigma}_\theta = \frac{PR}{t}$$



6.6. DESIGN CONDITIONS ANALYSIS

The stresses in the point under analysis are taken from table 6.5/1. The design temperature is 450 °C corresponding conservatively to the maximum metal temperature.

In table 6.6/1 the compliance analysis is presented.

6.7. OPERATING CONDITIONS ANALYSIS

The allowable stress values S_{mt} and S_t are determined for 30000 Hrs working time at the maximum metal temperature on the hottest radial section.

The analysis is carried out in table 6.7/1. The earthquake effects, considered as level C operating conditions, are presented in table 6.7/2.

6.8. SHAKE DOWN ANALYSIS

The S_m value is taken as average of the two S_m values at maximum and minimum cycle temperature, according to Note (1), fig. 4-130.1, Appendix 4, ASME Section VIII, Division 2, because all the secondary stresses

DESIGN CONDITIONS ANALYSIS

Design temperature $T = 450 \text{ }^\circ\text{C}$
Allowable stress $S_o = 8.46 \text{ Kp/mm}^2$
Stress due to pressure and mechanical
loads (see also table 6.5/1) $P_m = 1.13 \text{ Kp/mm}^2$

$$P_m = 1.13 \text{ Kp/mm}^2 < S_o = 8.46 \text{ Kp/mm}^2$$

OPERATING CONDITIONS ANALYSIS

Highest metal temperature in a point of the radial section	$T_{\max} = 458 \text{ }^{\circ}\text{C}$
Allowable value for general primary membrane stress at T_{\max}	$S_{mt} = 8.46 \text{ Kp/mm}^2$
Allowable stress at T_{\max}	$S_m = 8.4 \text{ Kp/mm}^2$
Time dependent stress at T_{\max}	$S_t = 11.6 \text{ Kp/mm}^2$

$$P_m \leq S_{mt}$$

$$1.13 \text{ Kp/mm}^2 \leq 8.46 \text{ Kp/mm}^2$$

$$P_l + P_b \leq \begin{cases} 1.5 S_m \\ K_t S_t \end{cases}$$

$$K_t = 1 + K_s \left(1 - \frac{PL}{S_t}\right) \cong 1 + K_s \quad K_s = \alpha (K - 1)$$

$$K = 1.5 \quad (\text{from ASME Section III, App. A Table A-9221(a)-1})$$

$$\alpha = 0.5$$

$$K_t = 1.25$$

$$P_l + P_b = 1.13 \text{ Kp/mm}^2 \leq \begin{cases} 1.5 \times 8.4 = 12.6 \text{ Kp/mm}^2 \\ 1.25 \times 11.6 = 14.5 \text{ Kp/mm}^2 \end{cases}$$

OPERATING CONDITIONS ANALYSIS

Highest metal temperature in a
point of the radial section $T_{\max} = 458 \text{ }^{\circ}\text{C}$

Allowable stress at T_{\max} $S_m = 8.4 \text{ Kp/mm}^2$

Maximum time dependent stress at
 T_{\max} $S_t = 11.6 \text{ Kp/mm}^2$

$$P_m \leq \begin{cases} 1.2 S_m \\ 1.0 S_t \end{cases}$$

$$1.36 \text{ Kp/mm}^2 \leq \begin{cases} 1.2 \cdot 8.4 = 10.08 \text{ Kp/mm}^2 \\ 11.6 \text{ Kp/mm}^2 \end{cases}$$

considered are thermal originated. The analysis is presented in table 6.8/1.

6.9. RATCHETING ANALYSIS

The presence of "Elastic follow-up" is reasonably excluded in the following analysis. In table 6.9/1 the stress values in two different instants are presented in order to determine the maximum stress range.

The step by step procedure proposed by T-1324 in the Appendix T of Code Case N-47-17 has been applied and the results are shown in table 6.9/2.

Non axisymmetric loads have been included as axisymmetric ones, and the curves of fig. T-1324-1 have been used, according to T-1324(a), Appendix T, Code Case N-47-17.

6.10. CREEP-FATIGUE ANALYSIS

The following assumption have been held:

- Allowable number of cycles to use in equation (5), T-1411, is taken from curves of fig. T-1420-1B, Code Case N-47-17, with a reduction factor of 5 in the cycles number.

SHAKE DOWN ANALYSIS

Highest metal temperature in a point of the radial section	$T_{max} = 458 \text{ }^{\circ}\text{C}$
Lowest metal temperature in a point of the radial section	$T_{min} = 220 \text{ }^{\circ}\text{C}$
Allowable stress a T_{max}	$S_m(T_{max}) = 8.4 \text{ Kp/mm}^2$
Allowable stress a T_{min}	$S_m(T_{min}) = 10.6 \text{ Kp/mm}^2$
Allowable stress for Test B	$S_m = 9.5 \text{ Kp/mm}^2$

$$P_1 + P_b + Q \leq 3 S_m$$

$$\begin{aligned}
 P_1 + P_b + Q &= \left| (0.084 - 12.385) - (1.13 + 1.677) \right| = \\
 &= 14.808 \text{ Kp/mm}^2 \leq 3 S_m = 28.5 \text{ Kp/mm}^2
 \end{aligned}$$

RATCHETING ANALYSIS

(Test 3)

STRESSES DURING TRANSIENT T11 + T12

	TIME t = 130 sec				TIME t = 965 sec			
	σ_R (Kp/mm ²)	σ_θ (Kp/mm ²)	σ_Z (Kp/mm ²)	CL.	σ_R (Kp/mm ²)	σ_θ (Kp/mm ²)	σ_Z (Kp/mm ²)	CL.
Pressure	0.0	0.084	0.0	P _m	0.0	0.084	0.0	P _m
Mechanical loads	0.0	0.0	1.13	P _m	0.0	0.0	1.13	P _m
Earthquake	0.0	0.0	<u>+0.23</u>	P _m	0.0	0.0	<u>+0.23</u>	P _m
Thermal transient	0.0	3.7	-0.48	Q	0.0	-12.385	1.677	Q
Thermal transient	0.0	3.768	0.855	F	0.0	-8.853	-0.925	F

- TABLE 6.9/1 -

RATCHETING ANALYSIS

(TEST 3)

Maximum metal temperature $T_{\max} = 458 \text{ }^\circ\text{C}$
 Minimum metal temperature $T_{\min} = 220 \text{ }^\circ\text{C}$
 Yield strength at T_{\min} $S_y = 11.85 \text{ Kp/mm}^2$

$$X = \left(P_1 + \frac{P_b}{K_t} \right) / S_y$$

$$Y = \frac{(Q_R)_{\max}}{S_y}$$

$$K_t = 1 + K_s \left(1 - \frac{P_1}{S_t} \right) \cong 1 + K_s$$

$$K_s = \alpha (K - 1)$$

$K = 1.5$ (from ASME Section III App. A Table A-9221(a)-1)

$$\alpha = 0.5$$

$$K_s = 0.25$$

$$K_t = 1.25$$

P_1 (Kp/mm ²)	P_b (Kp/mm ²)	Q_R (Kp/mm ²)	K_t	X	Y	Z	σ_c^* (Kp/mm ²)
1.36	0.0	18.242	1.25	0.115	1.539	0.1766	2.62

$$(*) \sigma_c = 1.25 S_y Z$$

Entering the isochronous stress-strain curves at temperature $458 \text{ }^\circ\text{C}$ ($850 \text{ }^\circ\text{F}$) and for any time, by σ_c , we read no significant strain, % due to creep.

- The step by step procedure suggest in T-1410 in the Appendix T of Code Case N-47-17 has been carried out and the results are described in table 6.10/1.
- The creep damage calculation is omitted because the maximum temperature is 458 °C (850 °F).
- The total fatigue damage is given by adding the fatigue damages due to:
 - 30000 transient T8 cycles (see table 6.10/1);
 - 30000 transient T9 cycles (see table 6.10/2);
 - 3360 transient T11+T12 cycles (see table 6.10/3);^(*)
 - 10 earthquake cycles connected with (T11 + T12) type transients (see table 6.10/4) (very conservative assumption);
 - 3270 overnight shutdown (see table 6.10/5).

From this analysis the following damage has been obtained:

$$D_T = D_1 + D_2 + D_3 + D_4 + D_5$$

$$D_T = 0.013 + 0.15 + 0.11 + 0.0004 + 0.0 = 0.28$$

NOTE: The elastic analysis rules applied in this note may be used because elastic ratcheting rules have been satisfied.

(*) The number has been obtained by the sum of 3240 (T11+T12) type cycles, 60 T14 type cycles and 60 T16 type cycles.

FATIGUE ANALYSIS

TRANSIENT T8	TIME t = 65 sec			TIME t = 190 sec		
	σ_R (Kp/mm ²)	σ_θ (Kp/mm ²)	σ_Z (Kp/mm ²)	σ_R (Kp/mm ²)	σ_θ (Kp/mm ²)	σ_Z (Kp/mm ²)
Load contr.	0.0	0.084	1.13	0.0	0.084	1.13
Strain contr.	0.0	3.312	-0.039	0.0	-2.412	0.229
Peak	0.0	6.131	3.082	0.0	-2.765	-0.891

$$\sigma_{VLC} = 0.0 \text{ Kp/mm}^2$$

$$\sigma_{VSC} = 5.992 \text{ Kp/mm}^2$$

$$\sigma_{VF} = 8.896 \text{ Kp/mm}^2$$

Calculation of ϵ_t , D

$$\epsilon_t = \left(\frac{S^*}{S}\right) K^2 \epsilon_n + K \epsilon_c + K_T \epsilon_F \quad E = 16500 \text{ Kp/mm}^2$$

$$\text{with } \epsilon_n = \epsilon_{LC} + \frac{1}{E} \sigma_{VSC}$$

$$\frac{S^*}{S} = 1; \quad K = 1; \quad K_T = 1; \quad \epsilon_c = 0$$

$$\epsilon_t = \frac{\sigma_{VLC}}{E} + \frac{\sigma_{VSC}}{E} + \frac{\sigma_{VF}}{E} = 0.0009023$$

Entering the fatigue curves we read

$$N_d = 11.8 \times 10^6 / 5 \text{ cycles}; \quad n = 30000 \text{ operating cycles}$$

$$D_1 = \frac{n}{N_d} = 0.013$$

FATIGUE ANALYSIS

TRANSIENT T9	TIME t = 258 sec			TIME t = 370 sec		
	$\bar{\sigma}_R$ (Kp/mm ²)	$\bar{\sigma}_\theta$ (Kp/mm ²)	$\bar{\sigma}_Z$ (Kp/mm ²)	$\bar{\sigma}_R$ (Kp/mm ²)	$\bar{\sigma}_\theta$ (Kp/mm ²)	$\bar{\sigma}_Z$ (Kp/mm ²)
Load contr.	0.0	0.084	1.13	0.0	0.084	1.13
Strain contr.	0.0	4.207	-0.212	0.0	-5.723	0.696
Peak	0.0	6.412	3.284	0.0	-4.929	-0.989

$$\sigma_{VLC} = 0.0 \text{ Kp/mm}^2$$

$$\sigma_{VSC} = 10.838 \text{ Kp/mm}^2$$

$$\sigma_{VF} = 11.341 \text{ Kp/mm}^2$$

Calculation of ϵ_t , D

$$\epsilon_t = \left(\frac{S^*}{S}\right) K^2 \epsilon_n + K \epsilon_c + K_T \epsilon_F \quad E = 16500 \text{ Kp/mm}^2$$

$$\text{with } \epsilon_n = \epsilon_{LC} + \frac{1}{E} \sigma_{VSC}$$

$$\frac{S^*}{S} = 1 ; K = 1 ; K_T = 1 ; \epsilon_c = 0$$

$$\epsilon_t = \frac{\sigma_{VLC}}{E} + \frac{\sigma_{VSC}}{E} + \frac{\sigma_{VF}}{E} = 0.001344$$

Entering the fatigue curves we read

$$N_d = 1 \times 10^6 / 5 \text{ cycles}; n = 30000 \text{ operating cycles}$$

$$D_2 = \frac{n}{N_d} = 0.15$$

FATIGUE ANALYSIS

TRANSIENT T11 - T12	TIME t = 130 sec			TIME t = 965 sec		
	σ_R (Kp/mm ²)	σ_θ (Kp/mm ²)	σ_Z (Kp/mm ²)	σ_R (Kp/mm ²)	σ_θ (Kp/mm ²)	σ_Z (Kp/mm ²)
Load contr.	0.0	0.084	1.13	0.0	0.084	1.13
Strain contr.	0.0	3.700	-0.480	0.0	-12.385	1.677
Peak	0.0	3.768	0.855	0.0	-8.853	-0.925

$$\sigma_{VLC} = 0.0 \text{ Kp/mm}^2$$

$$\sigma_{VSC} = 18.242 \text{ Kp/mm}^2$$

$$\sigma_{VF} = 12.621 \text{ Kp/mm}^2$$

Calculation of ϵ_t , D

$$\epsilon_t = \left(\frac{S^*}{S}\right) K^2 \epsilon_n + K \epsilon_c + K_T \epsilon_F \quad E = 16500 \text{ Kp/mm}^2$$

$$\text{with } \epsilon_n = \epsilon_{LC} + \frac{1}{E} \sigma_{VSC}$$

$$\frac{S^*}{S} = 1; \quad K = 1; \quad K_T = 1; \quad \epsilon_c = 0$$

$$\epsilon_t = \frac{\sigma_{VLC}}{E} + \frac{\sigma_{VSC}}{E} + \frac{\sigma_{VF}}{E} = 0.001870$$

Entering the fatigue curves we read

$$N_d = 1.54 \times 10^5 / 5 \text{ cycles}; \quad n = 3360 \text{ operating cycles}$$

$$D_3 = \frac{n}{N_d} = 0.11$$

FATIGUE ANALYSIS

EARTHQUAKE + TRANSIENT T11 - T12	TIME t = 130 sec			TIME t = 965 sec		
	$\bar{\sigma}_R$ (Kp/mm ²)	$\bar{\sigma}_\varphi$ (Kp/mm ²)	$\bar{\sigma}_Z$ (Kp/mm ²)	$\bar{\sigma}_R$ (Kp/mm ²)	$\bar{\sigma}_\varphi$ (Kp/mm ²)	$\bar{\sigma}_Z$ (Kp/mm ²)
Load contr.	0.0	0.084	1.13	0.0	0.084	1.13
Earthquake	0.0	0.0	± 0.23	0.0	0.0	± 0.23
Strain contr.	0.0	3.7	-0.48	0.0	-12.385	1.677
Peak	0.0	3.768	0.855	0.0	-8.853	-0.925

$$\sigma_{VLC} = 0.43 \text{ Kp/mm}^2$$

$$\sigma_{VSC} = 18.242 \text{ Kp/mm}^2$$

$$\sigma_{VF} = 12.621 \text{ Kp/mm}^2$$

Calculation of ϵ_t , D

$$\epsilon_t = \left(\frac{S^*}{S}\right) K^2 \epsilon_n + K \epsilon_c + K_T \epsilon_F \quad E = 16500 \text{ Kp/mm}^2$$

$$\text{with } \epsilon_n = \epsilon_{LC} + \frac{1}{E} \sigma_{VSC}$$

$$\frac{S^*}{S} = 1; \quad K = 1; \quad K_T = 1; \quad \epsilon_c = 0$$

$$\epsilon_t = \frac{\sigma_{VLC}}{E} + \frac{\sigma_{VSC}}{E} + \frac{\sigma_{VF}}{E} = 0.001897$$

Entering the fatigue curves we read

$$N_d = 1.4 \times 10^5 / 5 \text{ cycles}; \quad n = 10 \text{ operating cycles}$$

$$D_4 = \frac{n}{N_d} = 0.0004$$

FATIGUE ANALYSIS

Loads: overnight shutdown transient	$\tilde{\sigma}_R$ (Kp/mm ²)	$\tilde{\sigma}_\varphi$ (Kp/mm ²)	$\tilde{\sigma}_Z$ (Kp/mm ²)	$\tilde{\sigma}_R$ (Kp/mm ²)	$\tilde{\sigma}_\varphi$ (Kp/mm ²)	$\tilde{\sigma}_Z$ (Kp/mm ²)
Load contr.	0.0	0.0	1.13	0.0	0.0	0.0

$$\tilde{\sigma}_{VLC} = 1.13 \text{ Kp/mm}^2$$

Calculation of ϵ_t , D

$$\epsilon_t = \left(\frac{S^*}{S}\right) K^2 \epsilon_n + K \epsilon_c + K_T \epsilon_F \quad E = 16500 \text{ Kp/mm}^2$$

$$\text{with } \epsilon_n = \epsilon_{LC} + \frac{1}{E} \tilde{\sigma}_{VSC}$$

$$\frac{S^*}{S} = 1; \quad K = 1; \quad K_T = 1; \quad \epsilon_c = 0$$

$$\epsilon_t = \frac{\tilde{\sigma}_{VLC}}{E} + \frac{\tilde{\sigma}_{VSC}}{E} + \frac{\tilde{\sigma}_{VF}}{E} = 0.00007$$

Entering the fatigue curves we read

$$D_5 \cong 0.$$

6.11. FLANGE BEARING AREA ANALYSIS

The object of this calculation is the determination of the portion of area which plasticizes in the contact zone (AB in fig. 6.11/1) between the flange and the bearing surface because of the applied bending moment.

The following hypothesis have been held:

- The material is considered perfectly elastic-plastic (see fig. 6.11/2).
- The stresses distribution is variable according to the behavior reported in fig. 6.11/3.
- In this calculation only the plastic stress is considered (see fig. 6.11/4) acting on GLHE area; this is a conservative assumption.

With this hypothesis we have (see fig. 6.11/4):

$$M/2 = \sigma_y \cdot A(\text{GLHE}) \cdot b_0$$

with

$$A(\text{GLHE}) = \frac{1}{2} r^2 (2\vartheta_0 - \text{sen } 2\vartheta_0)$$

$$b_0 = \frac{4}{3} \frac{r \text{sen}^3 \vartheta_0}{2\vartheta_0 - \text{sen } 2\vartheta_0}$$

Therefore we have

$$M/2 = \sigma_y \frac{1}{2} r^2 (2\mathcal{J}_0 - \text{sen } 2\mathcal{J}_0) \frac{4}{3} \frac{r \text{sen}^3 \mathcal{J}_0}{2\mathcal{J}_0 - \text{sen } 2\mathcal{J}_0}$$

Hence

$$\mathcal{J}_0 = 17^\circ + 18^\circ$$

$$f \cong 3 \text{ mm} < 5 \text{ allowed}$$

Therefore (see fig. 6.11/1) the bearing area is considered adequate.

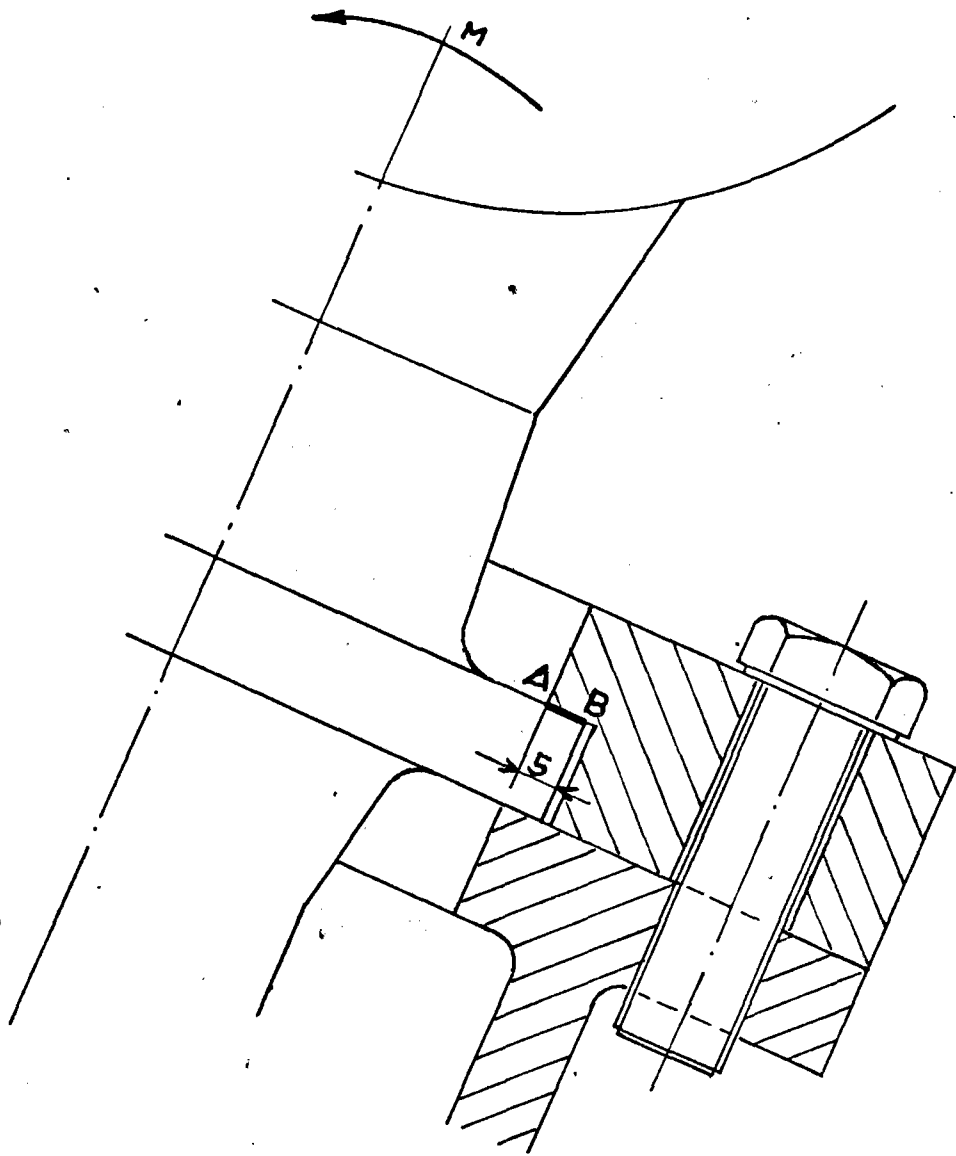


FIG. 6.11/1

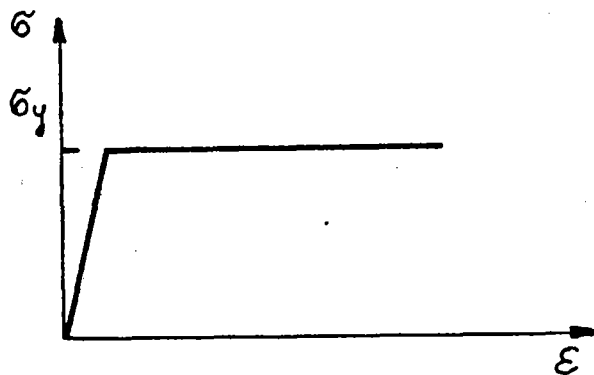
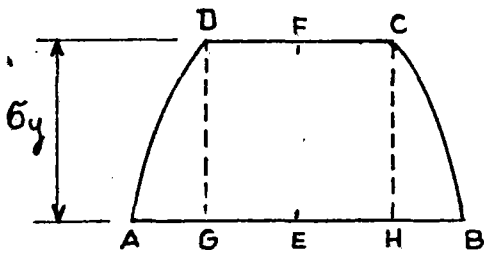
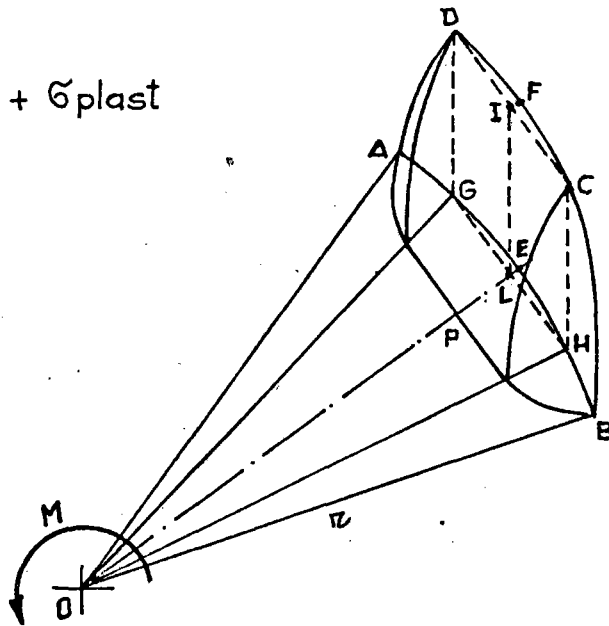
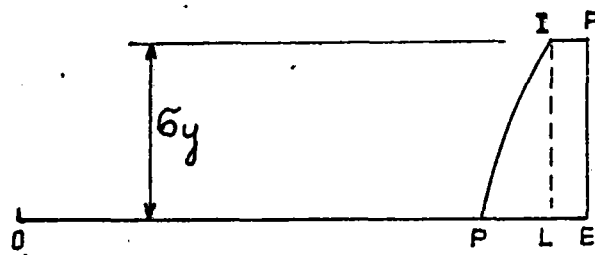


FIG. 6.11/2

$\sigma_{elast} + \sigma_{plast}$

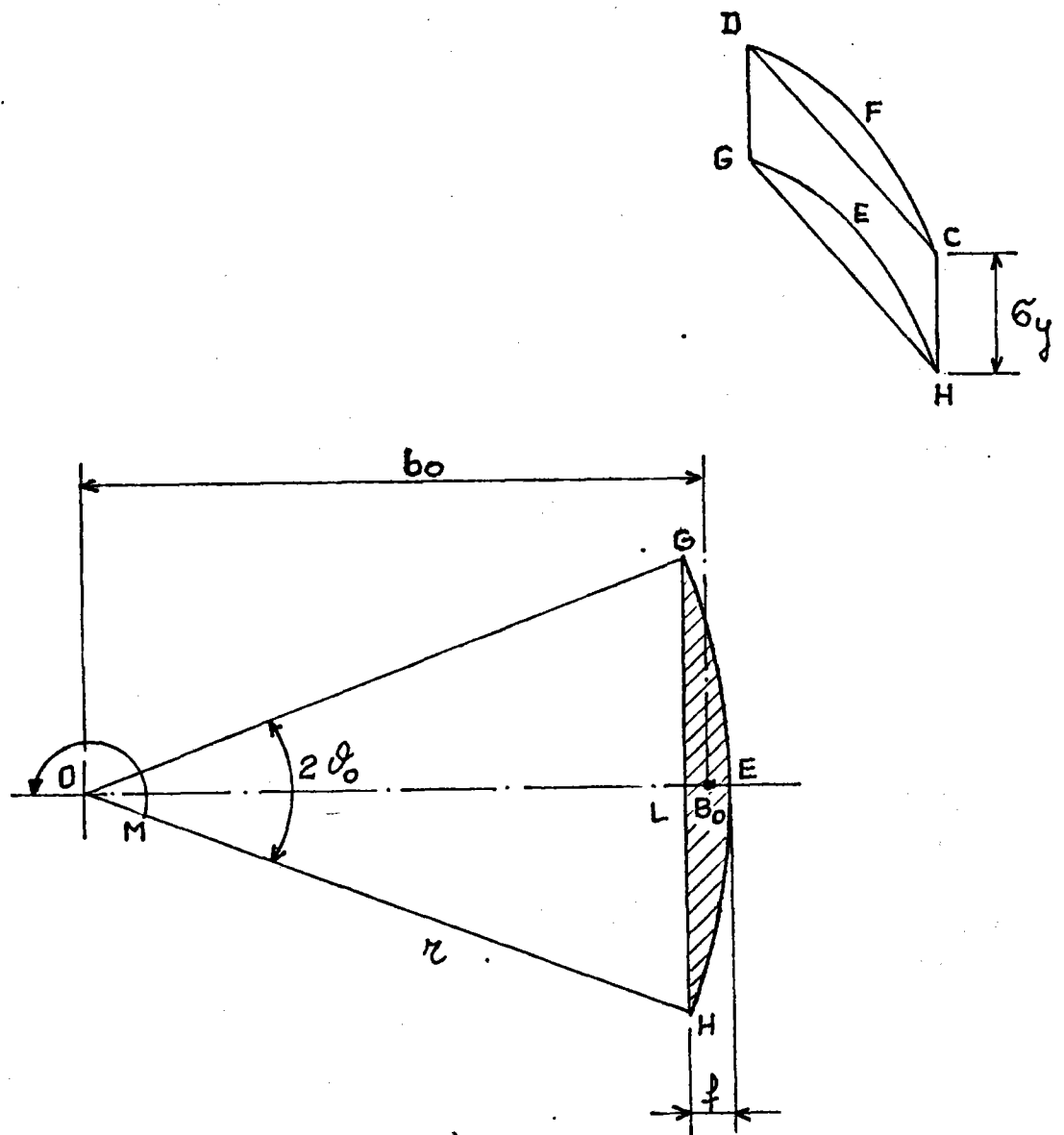


CIRCUMFERENTIAL



RADIAL

FIG. 6.11/3



σ_y = yield strength = 8.8 Kg/mm²
 r = flange radius = 67.5 mm
 M = moment max due to tube
 flexibility (see point 6.4) = 100000 Kgmm

FIG. 6.11/4

7. UPPER HEADER NOZZLE

7.1. ANALYSIS LIMITS AND DESCRIPTION OF STRUCTURE

The structure under consideration is the receiver tube-header connection, subjected to thermal transients and mechanical loads.

In fig. 7.1/1 the geometric characteristics are shown.

Only the transient type T8, T12 (see chapter 2) are analyzed.

The analysis of the rate of sodium temperature change allows to consider, for stresses calculations, transient T8 and T12 more dangerous than transients T9-T15-T16 and T14 respectively.

7.2. TEMPERATURE FIELD EVALUATION

The transient analysis has been carried out considering a forced convection applied to the sodium wetted surface.

The sodium temperature is considered variable following a given loading law.

UPPER HEADER
NOZZLE

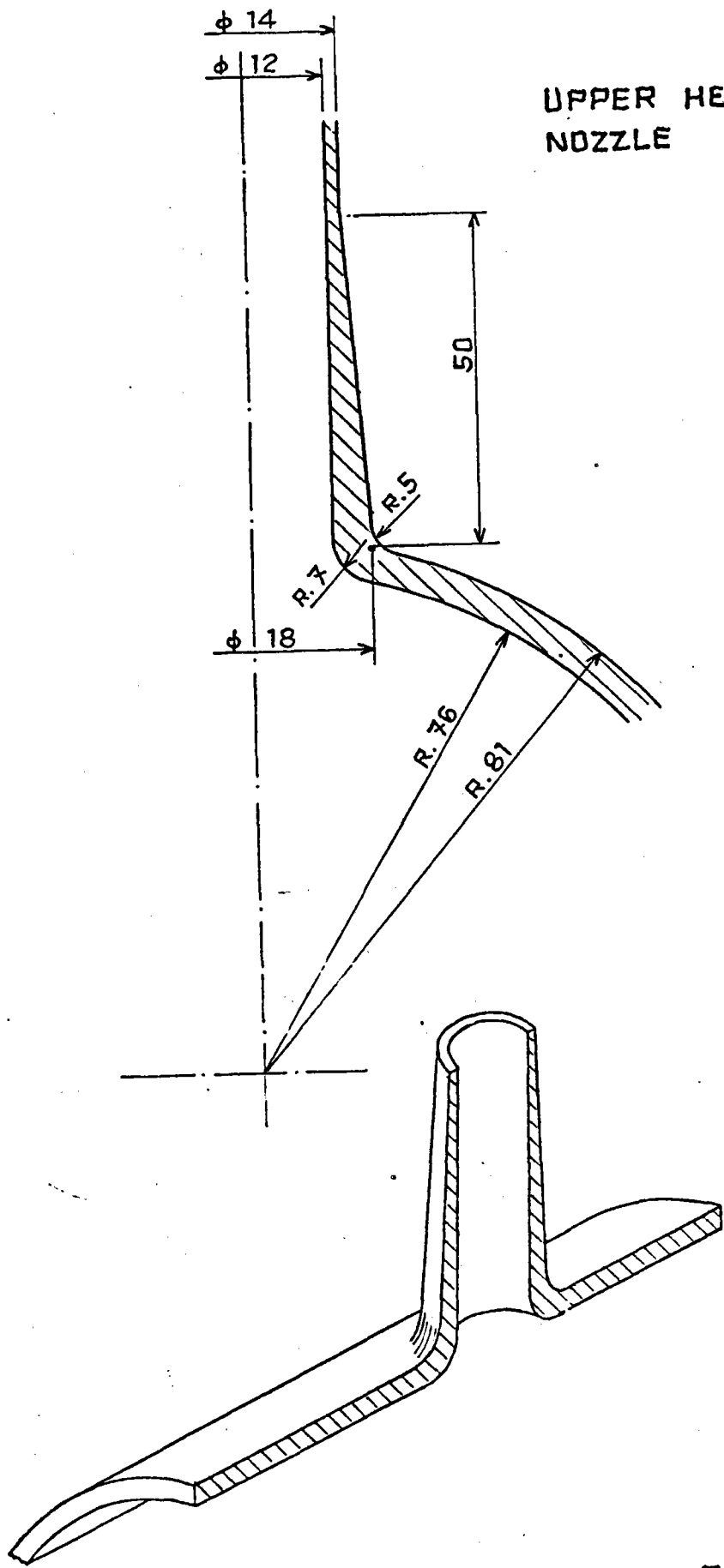


FIG. 7.1/1

The thermal transients analysed are discretized in tables 7.2/1, 7.2/2. Every time interval is subdivided in 30 time steps.

The external surface of the tube and the header is assumed to be adiabatic. At each time step the temperature field in every point has been determined by a finite element computer code (FLHE).

In fig. 7.2/1 the axisymmetrical 2D mesh used, is shown.

In fig. 7.2/2 + 7.2/4 the temperature trends in 3 considered section are presented for two time instants giving the most dangerous time-step.

A post processing program allows to plot isothermal curves at any chosen time-step.

Figures 7.2/5 + 7.2/8 show, for the most dangerous time instants, isothermal curves for the analysed thermal transients.

7.3. THERMAL STRESS EVALUATION

Considering the difference between the diameters of receiver tube and header an axisymmetric scheme with the axis coincident with the tube axis has been reasonably assumed.

THERMAL TRANSIENT T8

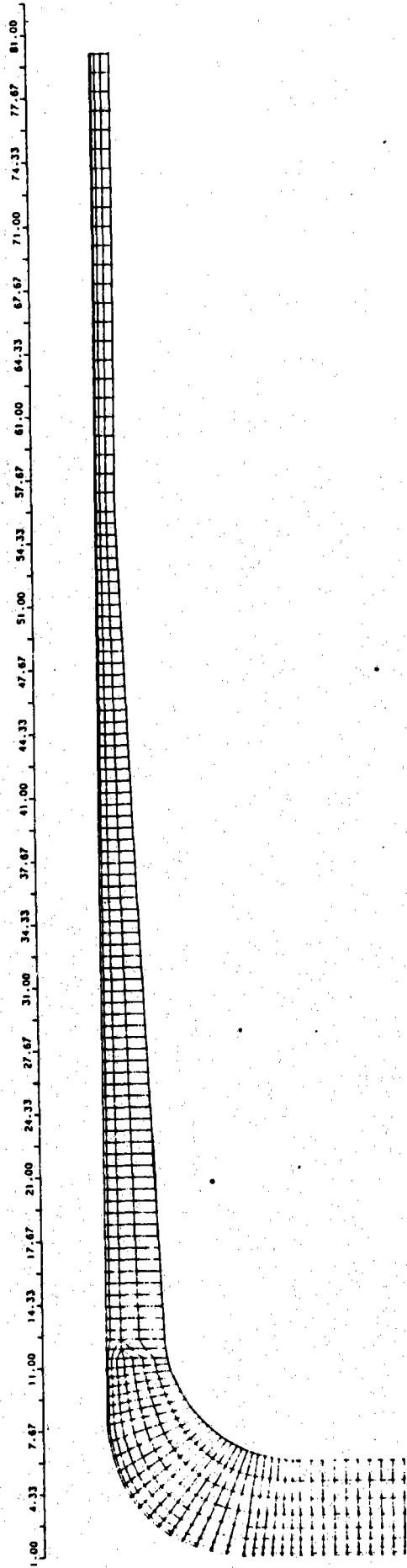
TIME (sec)	TEMPERATURE (°C)	FLOW (Kg/sec)	DENSITY (Kg/m ³)	VELOCITY (m/sec)	HEAT COEFF. (W/m ² °C)
0	530	7.3	825.9	2.00	39801
14	517	0.7	829.0	0.19	28313
28	505	0.7	831.9	0.19	28600
47	431	0.7	849.6	0.18	30152
49	415	4.0	853.4	1.06	36800
50	414	5.5	853.7	1.46	39400
54	481	11.5	837.7	3.11	47216
60	452	11.5	844.6	3.09	48080
64	460	11.5	842.7	3.09	47791
70	440	11.5	847.5	3.08	48370
102	440	11.5	847.5	3.08	48370
130	479	7.3	838.1	1.97	40790
167	530	7.3	825.9	2.00	39801
250	530	7.3	825.9	2.00	39801

- TABLE 7.2/1 -

THERMAL TRANSIENT T11+ 12

TIME (sec)	TEMPERATURE (°C)	FLOW (Kg/sec)	DENSITY (Kg/m ³)	VELOCITY (m/sec)	HEAT COEFF. (W/m ² °C)
0	530	7.3	825.9	2.00	39801
14	490	0.7	835.5	0.19	28925
40	420	0.7	852.3	0.19	30357
140	405	0.7	855.8	0.19	30660
200	355	0.7	867.6	0.18	31690
610	210	0.7	901.4	0.18	34696
995	210	0.7	901.4	0.18	34696
1000	210	5.0	901.4	1.26	43209
1005	275	9.4	886.4	2.40	49100
1011	280	9.4	885.2	2.41	48949
1035	405	9.4	855.8	2.49	46000
1049	450	7.3	845.1	1.96	41565
1065	500	7.3	833.1	1.99	40567
1085	530	7.3	825.9	2.00	39801
1200	530	7.3	825.9	2.00	39801

- TABLE 7.2/2 -



- FIG. 7.2/1 -

6.00 9.33 12.67 16.00 19.33 22.67
• PLOTMESH-2D • T6/2 • STRUTTURA INDEFORMATA
TUBE-HEADER CONNECTION
AXISYMMETRIC MESH

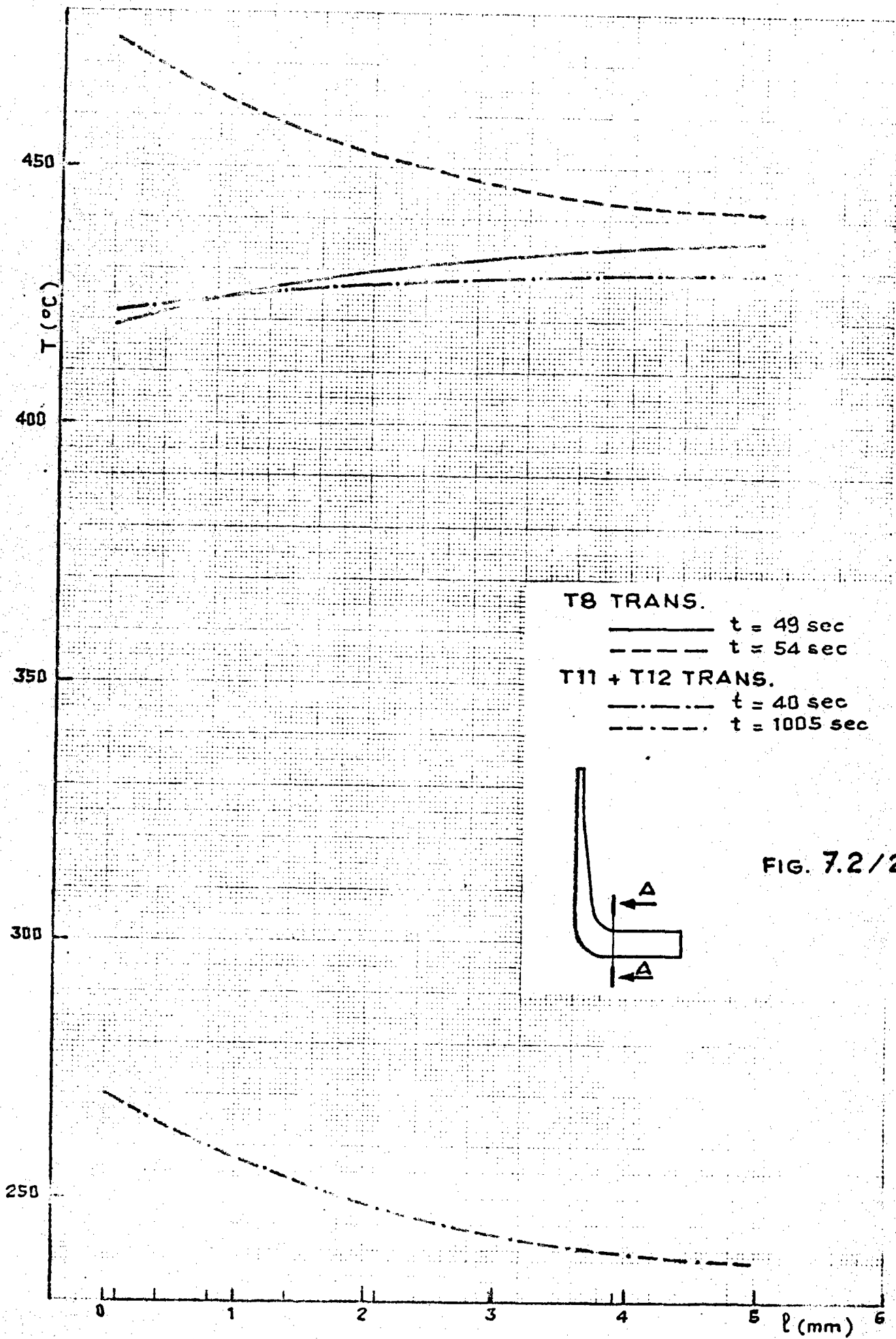


FIG. 7.2/2

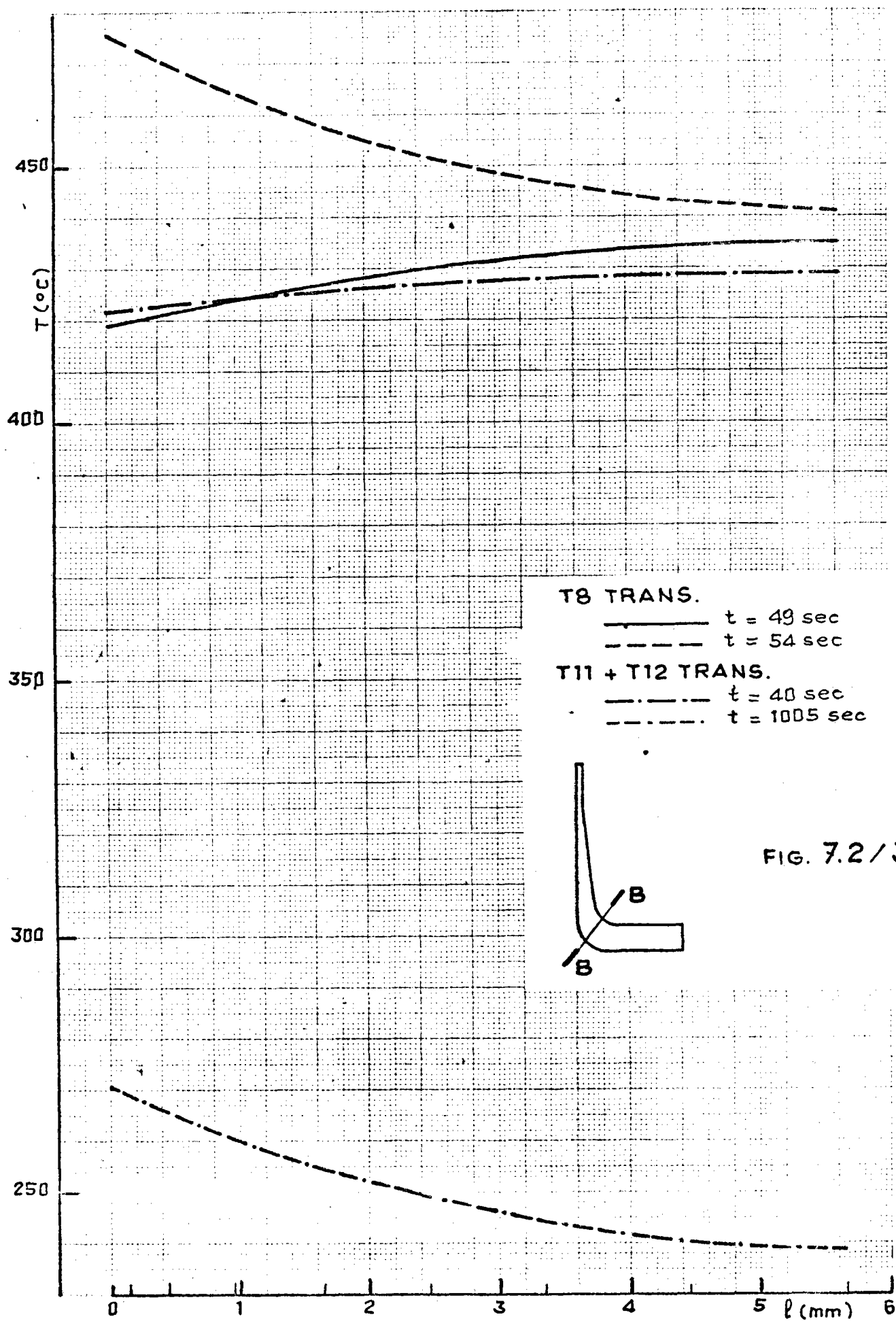
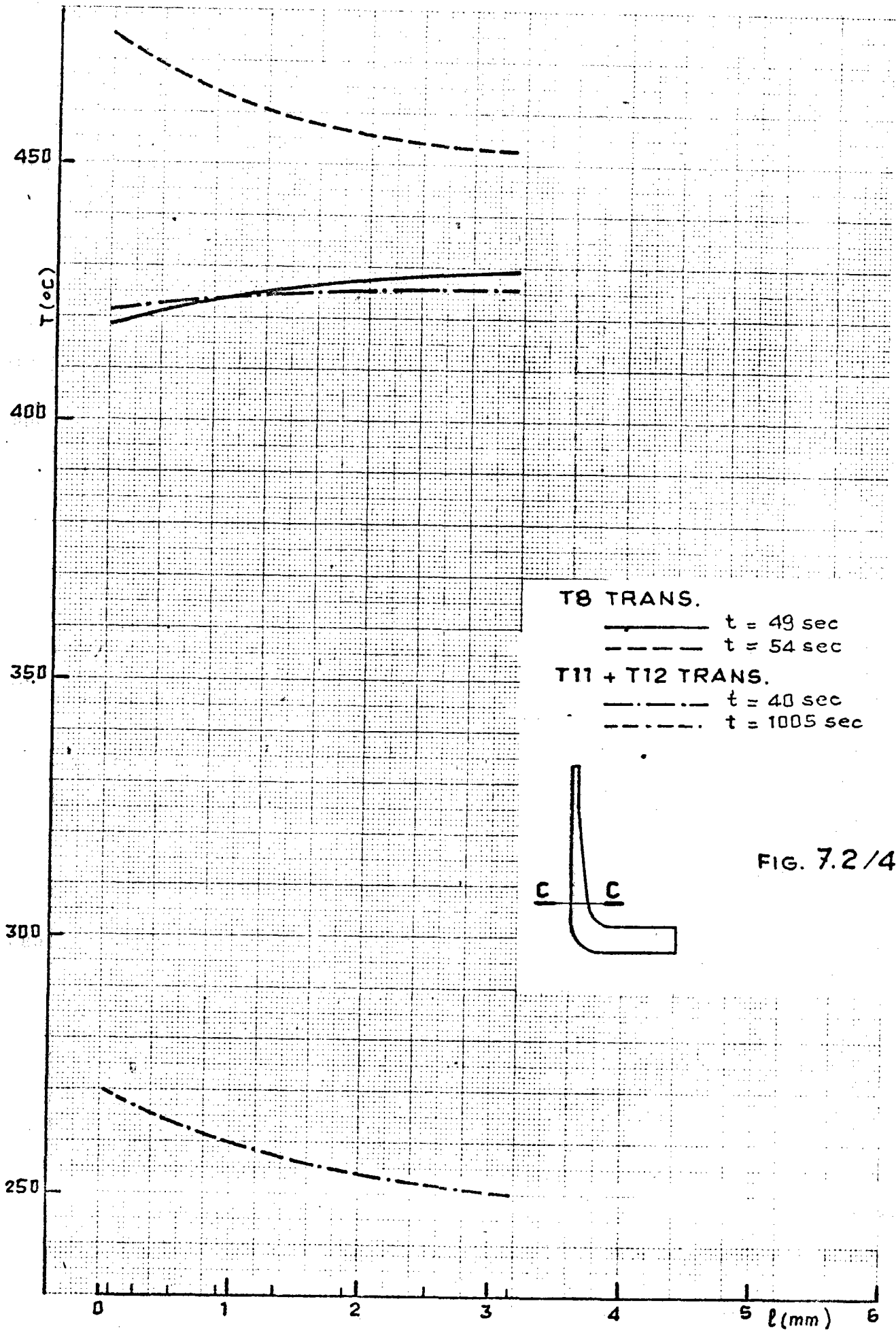
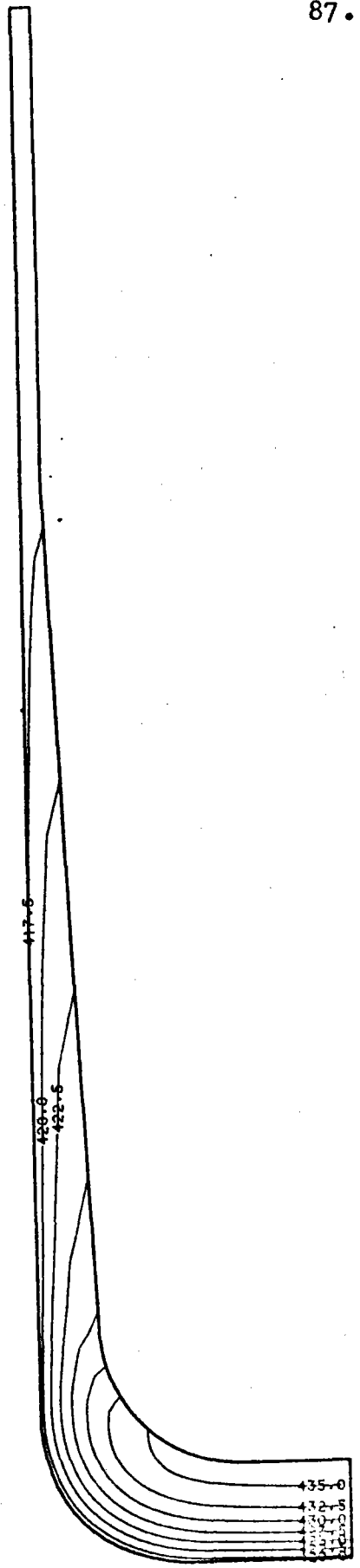


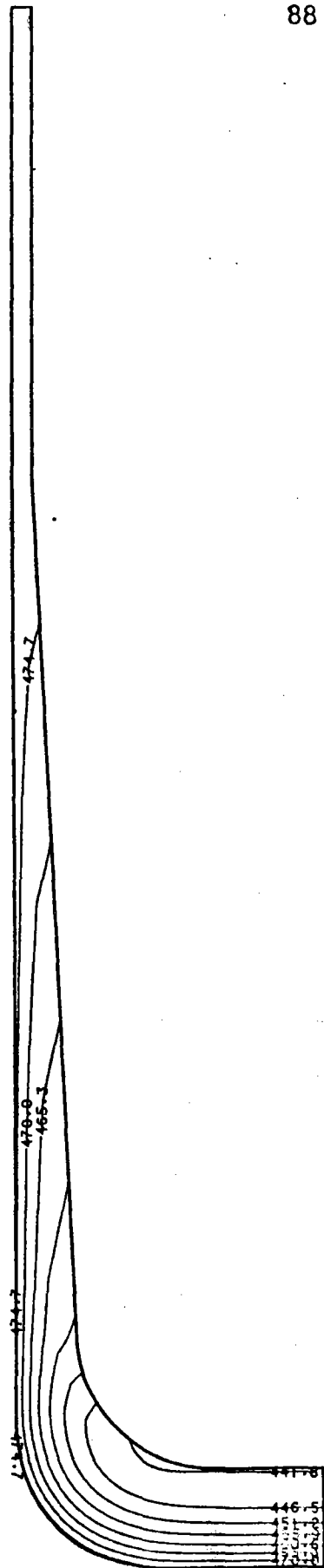
FIG. 7.2/3





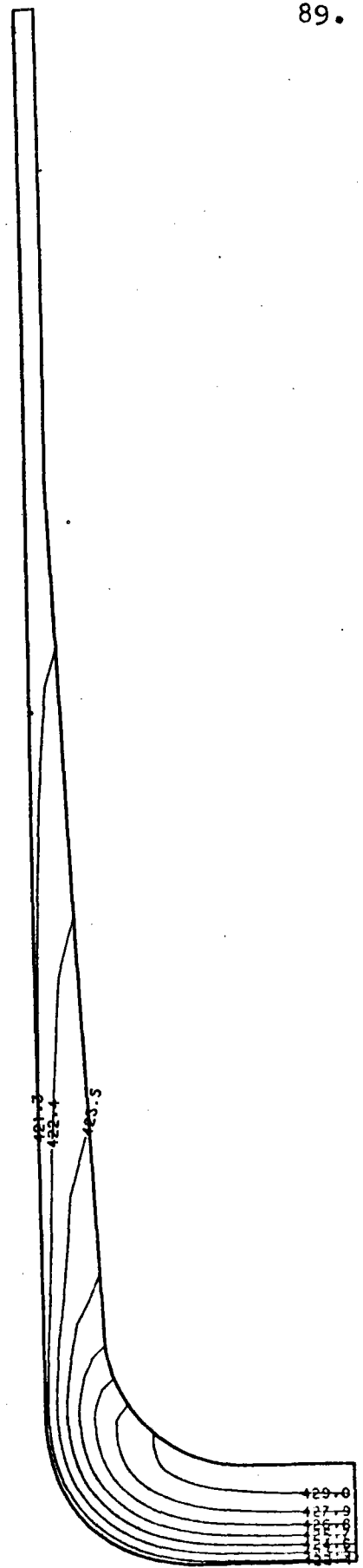
THERMAL TRANSIENT T8
ISOTHERM - TIME T=49 SEC

- FIG. 7.2/5 -



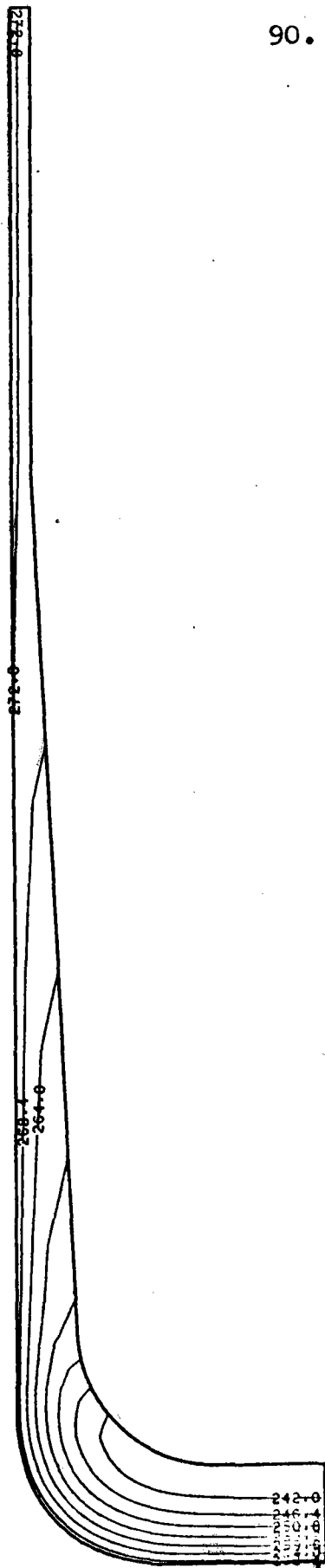
THERMAL TRANSIENT T8
ISOTHERM - TIME T=54 SEC.

- FIG. 7.2/6 -



THERMAL TRANSIENT T12
ISOTHERM - TIME T=40 SEC

- FIG. 7.2/7 -



THERMAL TRANSIENT T12
ISOTHERM - TIME T=1005 SEC.

- FIG. 7.2/8 -

The mesh used is presented in fig. 7.2/1.

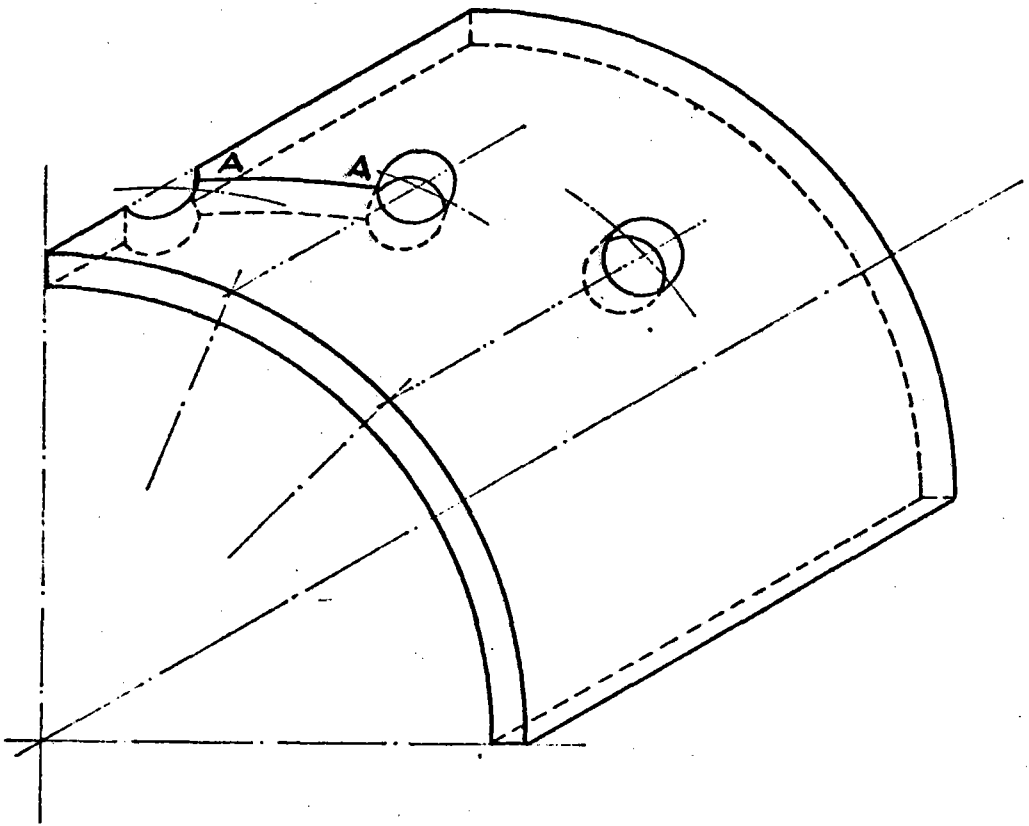
Stress and strain analysis in some time instants has been performed through structural analysis finite element program SAP V, with loading conditions given by the sets of nodal temperatures supplied by FLHE.

A very important point for stress and strain analysis calculation are the boundary conditions of the structure.

Fig. 7.3/1 shows the hole pattern in the header: the plane of the mesh has been assumed as the one identified by "A-A", so that at the middle of A-A there is a symmetry section which does not rotate; this section is the outermost section of the mesh, which is therefore free to translate, keeping parallel to itself.

The σ_y stress behavior through the "A-A", "B-B", "C-C", sections at the most dangerous time step for each transient are shown in figg. 7.3/2 + 7.3/4.

Two post processor computer codes allow to carry out the stress classification (membrane, bending and peak) and to plot the σ_{GUEST} curves at any chosen time step (see figg. 7.3/5 + 7.3/8).



POSITION OF TUBES CONNECTIONS WITH THE HEADER

FIG. 7.3/1

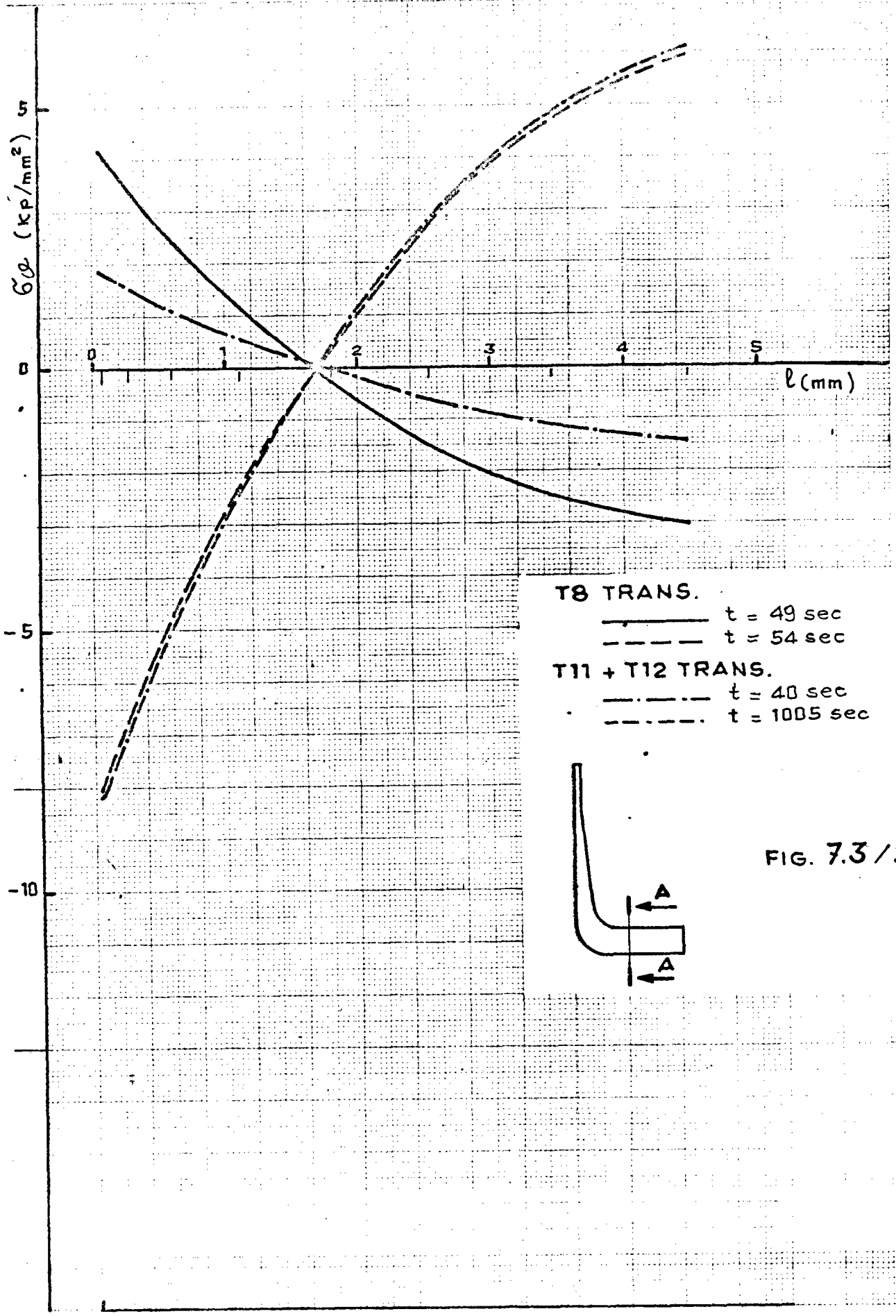


FIG. 7.3/2

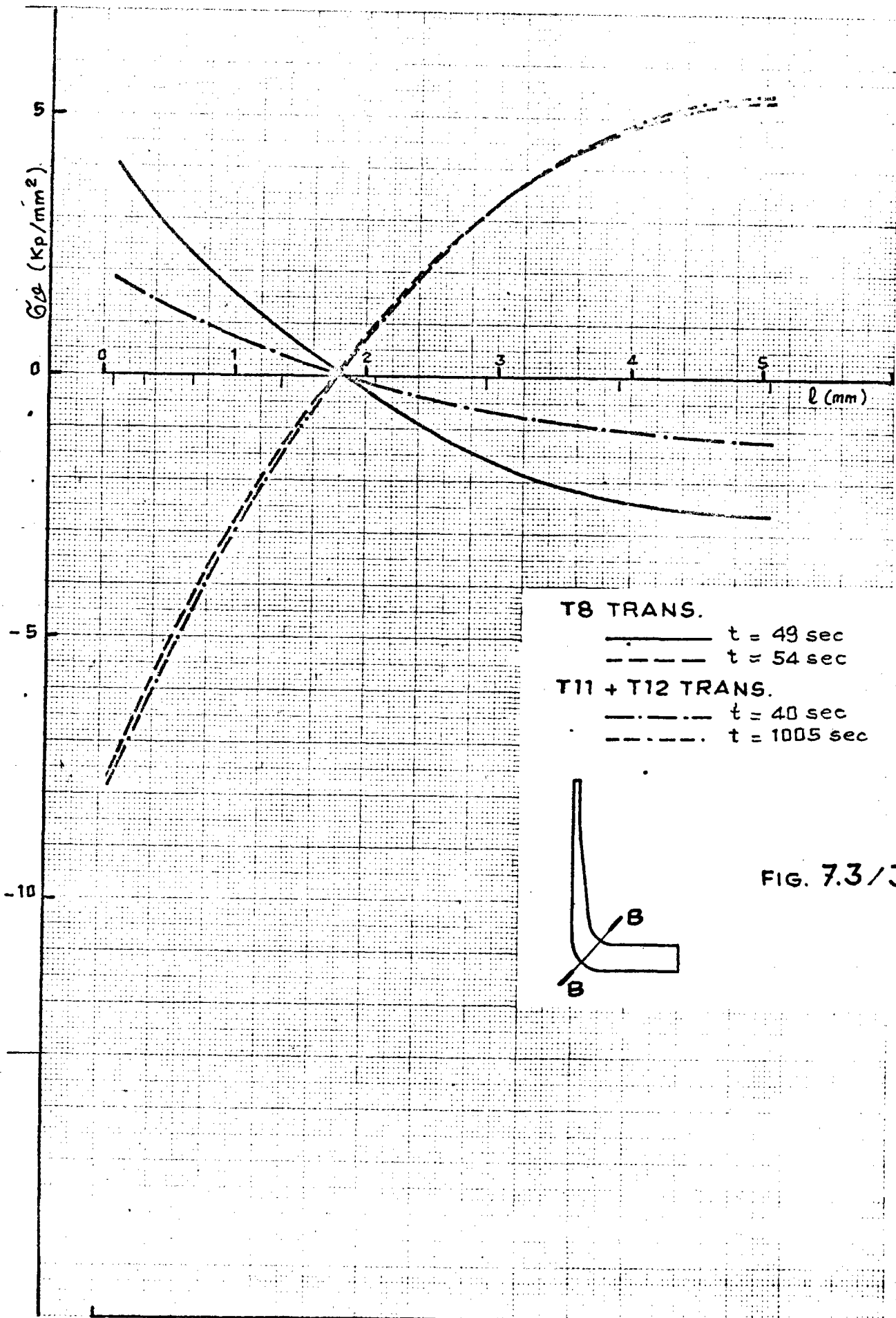
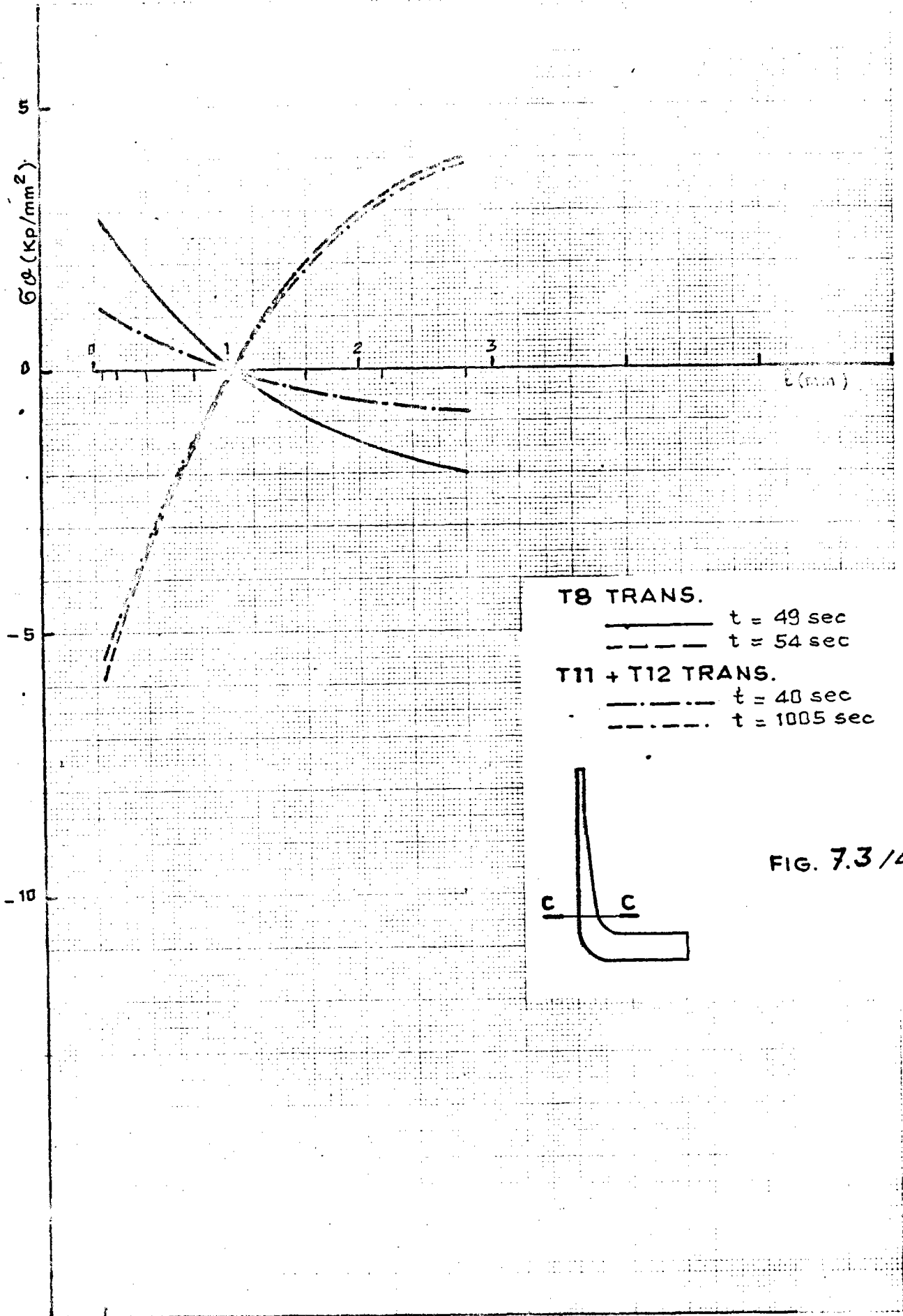
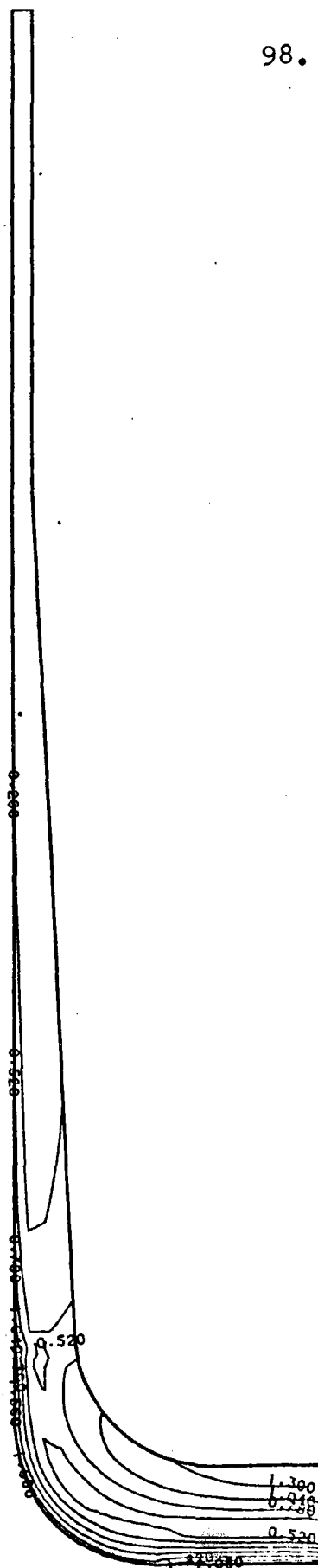


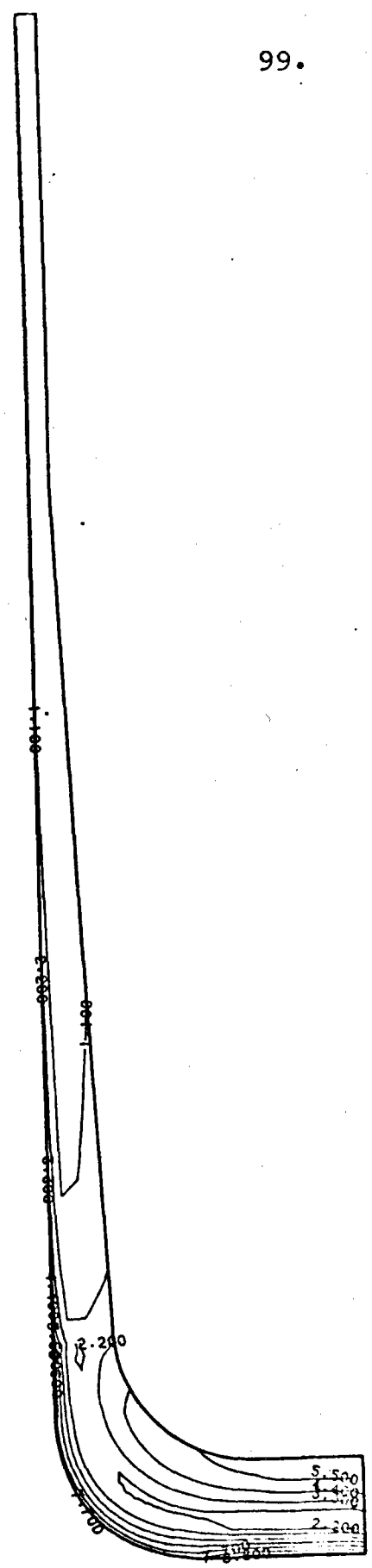
FIG. 7.3/3





THERMAL TRANSIENT T12
TIME T = 40 SEC.

- FIG. 7.3/7 -



THERMAL TRANSIENT T12
TIME T = 1005 SEC.

- FIG. 7.3/8 -

7.4. STRESS EVALUATION DUE TO THE PANEL TUBE FLEXIBILITY

In the considered sections, the loads due to weight, moments and forces on the tube, earthquake, are very low and therefore the induced stresses are negligible.

7.5. STRESS TABLE ACCORDING TO ASME CRITERIA

In the following analysis, except for creep-fatigue analysis, the thermal transient T8 has been assumed as the most dangerous one.

The analyzed time step corresponds to $t = 54$ sec.

Only the inner part of section A-A is considered, which has got the most stressed point. In table 7.5/1 the stresses with their classification, by definitions in 3213, Code Case N47, are shown.

7.6. BURSTING ANALYSIS (Design conditions)

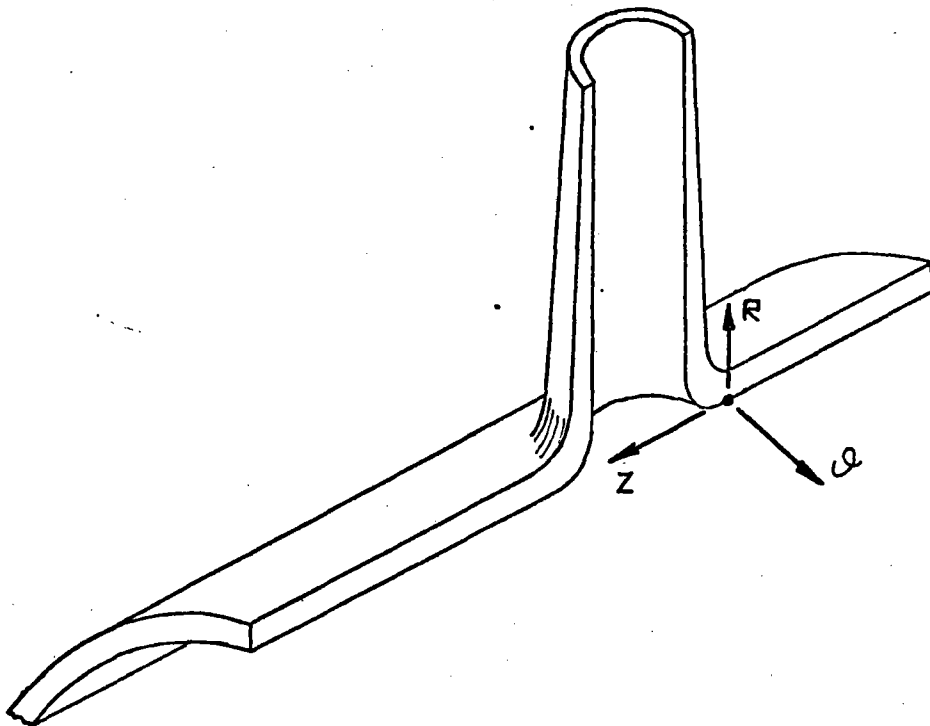
The header efficiency E , requested in UG-27, ASME Section VIII, Division 1, is calculated. The stresses in the point under analysis are taken from table 7.5/1.

The allowable stress value S_m is determined conservatively corresponding to the maximum metal temperature at the hottest cross section.

STRESS TABLE AT POINT "P" FOLLOWING ASME CRITERIA,
AT TIME t = 54 sec OF TRANSIENT T8

Origin	R (Kp/mm ²)	(Kp/mm ²)	Z (Kp/mm ²)	Class
Pressure	0.0	1.48*	0.0	P _m
Thermal transient	0.0	-5.803	-7.209	Q
Thermal transient	0.0	-2.532	-2.493	F

(*) calculated as $\frac{PR}{Et}$



In table 7.6/1 and fig. 7.6/1 the analysis is presented.

7.7. OPERATING CONDITIONS ANALYSIS

The same procedure used at point 6.7. has been used; the results are collected in table 7.7/1.

7.8. SHAKE DOWN ANALYSIS

See for that analysis point 6.8. and table 7.8/1.

7.9. RATCHETING ANALYSIS

The same procedure used at point 6.9. has been applied; the results are collected at tables 7.9/1 and 7.9/2.

7.10. CREEP-FATIGUE ANALYSIS

The following assumptions have been held:

- Allowable number of cycles to use in equation (5) T-1411, is taken from curves of fig. T-1420-1B, Code Case N-47-17 with a reduction factor of 5 in the cycles number.

BURSTING ANALYSIS
(ASME VIII Div. 1 par. UG-27)

Design temperature: 550 °C

$$P = 0.061 \text{ Kp/mm}^2$$

$$R = 81. \text{ mm}$$

$$S = S_m = 7.7 \text{ Kp/mm}^2$$

$$t_{\min} = \frac{PR}{S \cdot E - 0.6 P}$$

E = eff. legament calculated from UG-53 point(d)

$$\text{Longitudinal efficiency} = \frac{42 - 14}{42} = 66.6\%$$

$$P'/P_1 = 99\%$$

From fig. UG-53.5:

$$\text{Diagonal efficiency} = 91.9\%$$

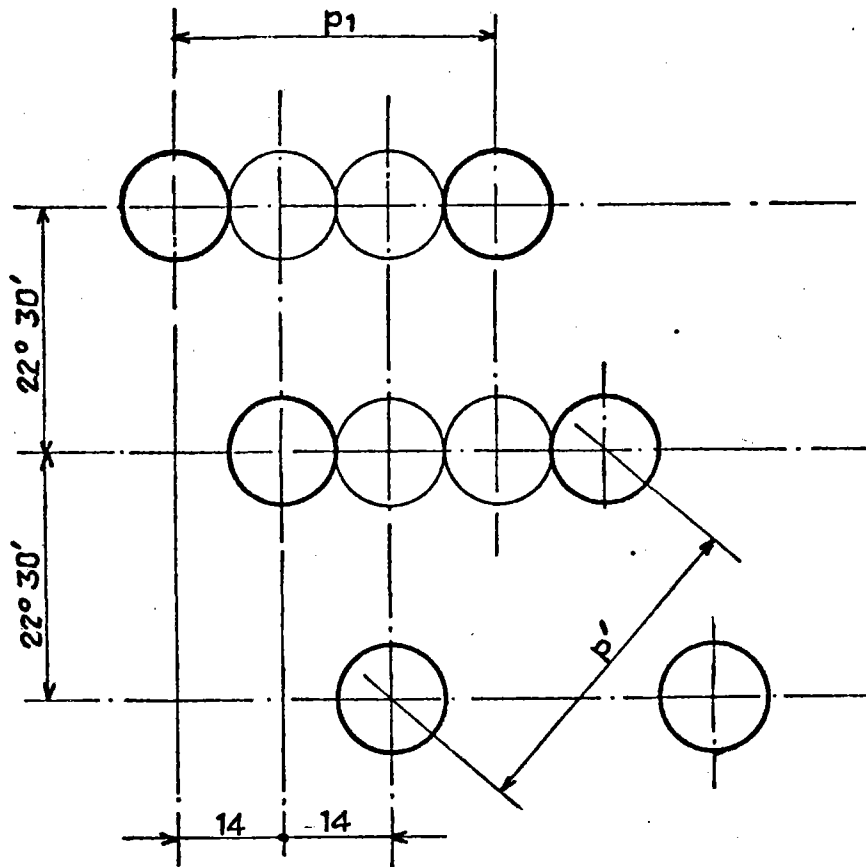
E is lower from

longitudinal efficiency

diagonal efficiency

$$E = 66.6\%$$

$$t_{\min} = 0.97 \text{ mm} < 5 \text{ mm}$$



$$p_1 = 42 \text{ mm}$$

$$\text{medium header diam,} = 162 - 5 = 157 \text{ mm}$$

$$p' \approx \sqrt{28^2 + \left(\pi 157 \times \frac{22^\circ 30'}{360} \right)^2} = 41.64 \text{ mm}$$

FIG. 7.6/1

OPERATING CONDITIONS ANALYSIS

Highest metal temperature in a point of the radial section	$T_{max} = 550 \text{ } ^\circ\text{C}$
Allowable value for general primary membrane stress at T_{max}	$S_{mt} = 7.75 \text{ Kp/mm}^2$
Allowable stress at T_{max}	$S_m = 7.7 \text{ Kp/mm}^2$
Time dependent stress at T_{max}	$S_t = 8.4 \text{ Kp/mm}^2$

$$P_m \leq S_{mt}$$

$$1.48 \text{ Kp/mm}^2 \leq 7.75 \text{ Kp/mm}^2$$

$$P_l + P_b \leq \begin{cases} 1.5 S_m \\ K_t S_t \end{cases}$$

$$K_t = 1 + K_s \left(1 - \frac{PL}{S_t}\right) \approx 1 + K_s \quad K_s = \alpha (K - 1)$$

$$K = 1.27 \quad (\text{from ASME Section III, App. A Table A-9221(a)-1})$$

$$\alpha = 0.5 \quad K_t \approx 1.14$$

$$P_l + P_b = 1.48 \text{ Kp/mm}^2 \leq \begin{cases} 1.5 \times 7.7 = 11.6 \text{ Kp/mm}^2 \\ 1.14 \times 8.4 = 9.6 \text{ Kp/mm}^2 \end{cases}$$

SHAKE DOWN ANALYSIS

Highest metal temperature in a point of the radial section	$T_{\max} = 550 \text{ }^{\circ}\text{C}$
Lowest metal temperature in a point of the radial section	$T_{\min} = 210 \text{ }^{\circ}\text{C}$
Allowable stress at T_{\max}	$S_m(T_{\max}) = 7.7 \text{ Kp/mm}^2$
Allowable stress at T_{\min}	$S_m(T_{\min}) = 10.6 \text{ Kp/mm}^2$
Allowable stress for Test B	$S_m = 9.1 \text{ Kp/mm}^2$

$$P_1 + P_b + Q \leq 3 S_m$$

$$\begin{aligned}
 P_1 + P_b + Q &= \left| ((-7.209) - (0.0)) \right| = \\
 &= 7.209 \text{ Kp/mm}^2 \leq 3 S_m = 23.1 \text{ Kp/mm}^2
 \end{aligned}$$

RATCHETING ANALYSIS

(Test 3)

STRESSES DURING TRANSIENT T8

	TIME t = 54 sec				TIME t = 49 sec			
	σ_R (Kp/mm ²)	σ_θ (Kp/mm ²)	σ_Z (Kp/mm ²)	CL.	σ_R (Kp/mm ²)	σ_θ (Kp/mm ²)	σ_Z (Kp/mm ²)	CL.
Pressure	0.0	1.48	0.0	P _m	0.0	1.48	0.0	P _m
Thermal transient	0.0	-5.803	-7.209	Q	0.0	2.989	3.682	Q
Thermal transient	0.0	-2.532	-2.493	F	0.0	1.352	1.347	F

- TABLE 7.9/1 -

RATCHETING ANALYSIS

(TEST 3)

Maximum metal temperature $T_{\max} = 550 \text{ }^\circ\text{C}$ Minimum metal temperature $T_{\min} = 210 \text{ }^\circ\text{C}$ Yield strength at T_{\min} $S_y = 11.85 \text{ Kp/mm}^2$

$$X = \frac{P_1 + \frac{P_b}{K_t}}{S_y}$$

$$Y = \frac{(Q_R)_{\max}}{S_y}$$

$$K_t = 1 + K_s \left(1 - \frac{P_1}{S_t}\right) \cong 1 + K_s$$

$$K_s = \alpha (K - 1)$$

 $K = 1.27$ (from ASME Section III App. A Table A-9221(a)-1)

$$\alpha = 0.5$$

$$K_s = 0.14$$

$$K_t = 1.14$$

P_1 (Kp/mm ²)	P_b (Kp/mm ²)	Q_R (Kp/mm ²)	K_t	X	Y	Z	σ_c^* (Kp/mm ²)
1.48	0.0	10.891	1.14	0.125	0.919	0.115	1.7

$$(*) \sigma_c = 1.25 S_y Z$$

Entering the isochronous stress-strain curves at temperature $550 \text{ }^\circ\text{C}$ ($\cong 1000 \text{ }^\circ\text{F}$) and for any time, by σ_c , we read no significant strain, % due to creep.

- The step by step procedure suggested in T-1410 in the Appendix T of Code Case N-47-17 has been carried out and the results are described in table 6.10/1.
- Considering the actual operating conditions, no modifications have been applied to the Poisson ratio as requested by T-1431 Code Case N47-17; the reasons are contained in Franco Tosi Short Notice 16/4/82.
- The total fatigue damage is given by adding the fatigue damages due to:
 - 60120 transient T8 cycles (see table 7.10/1). The number has been obtained by the sum of 30000 T8 type cycles, 30000 T9 type cycles, 60 T15 type cycles and 60 T16 type cycles.
 - 3250 transient T11+T12 cycles (see table 7.10/2).

From this analysis the following damage has been obtained

$$D_T = D_1 + D_2 = 0.25$$

It has to be noted that the creep damage has been neglected because is very small: in fact the thermal stresses are very short in time during cloud passage and, on the contrary, the stresses extended in time are the mechanical ones (overnight transients) that are low (see table 7.5/1).

FATIGUE ANALYSIS

TRANSIENT T8	TIME t = 49 sec			TIME t = 54 sec		
	$\bar{\sigma}_R$ (Kp/mm ²)	$\bar{\sigma}_\theta$ (Kp/mm ²)	$\bar{\sigma}_Z$ (Kp/mm ²)	$\bar{\sigma}_R$ (Kp/mm ²)	$\bar{\sigma}_\theta$ (Kp/mm ²)	$\bar{\sigma}_Z$ (Kp/mm ²)
Load contr.	0.0	1.48	0.0	0.0	1.48	0.0
Strain contr.	0.0	2.989	3.682	0.0	-5.603	-7.209
Peak	0.0	1.352	1.347	0.0	-2.532	-2.492

$$\sigma_{VLC} = 0.0 \text{ Kp/mm}^2$$

$$\sigma_{VSC} = 10.891 \text{ Kp/mm}^2$$

$$\sigma_{VF} = 3.884 \text{ Kp/mm}^2$$

Calculation of ϵ_t , D

$$\epsilon_t = \left(\frac{S^*}{S}\right) K^2 \epsilon_n + K \epsilon_c + K_T \epsilon_F \quad E = 15700 \text{ Kp/mm}^2$$

$$\text{with } \epsilon_n = \epsilon_{LC} + \frac{1}{E} \sigma_{VSC}$$

$$\frac{S^*}{S} = 1; \quad K = 1; \quad K_T = 1; \quad \epsilon_c = 0$$

$$\epsilon_t = \frac{\sigma_{VLC}}{E} + \frac{\sigma_{VSC}}{E} + \frac{\sigma_{VF}}{E} = 0.000941$$

Entering the fatigue curves we read

$$N_d = 1.19 \times 10^6 / 5 \text{ cycles}; \quad n = 60120 \text{ operating cycles}$$

$$D_1 = \frac{n}{N_d} = 0.25$$

FATIGUE ANALYSIS

TRANSIENT T11 + T12	TIME t = 40 sec			TIME t = 1005 sec		
	$\bar{\sigma}_R$ (Kp/mm ²)	$\bar{\sigma}_\theta$ (Kp/mm ²)	$\bar{\sigma}_Z$ (Kp/mm ²)	$\bar{\sigma}_R$ (Kp/mm ²)	$\bar{\sigma}_\theta$ (Kp/mm ²)	$\bar{\sigma}_Z$ (Kp/mm ²)
Load contr.	0.0	1.48	0.0	0.0	1.48	0.0
Strain contr.	0.0	1.352	1.651	0.0	-5.969	-7.312
Peak	0.0	0.546	0.548	0.0	-2.464	-2.436

$$\sigma_{VLC} = 0.0 \text{ Kp/mm}^2$$

$$\sigma_{VSC} = 8.963 \text{ Kp/mm}^2$$

$$\sigma_{VF} = 3.01 \text{ Kp/mm}^2$$

Calculation of ϵ_t, D

$$\epsilon_t = \left(\frac{S^*}{S}\right)^2 \epsilon_n + K \epsilon_c + K_T \epsilon_F \quad E = 15700 \text{ Kp/mm}^2$$

$$\text{with } \epsilon_n = \epsilon_{LC} + \frac{1}{E} \sigma_{VSC}$$

$$\frac{S^*}{S} = 1; \quad K = 1; \quad K_T = 1; \quad \epsilon_c = 0$$

$$\epsilon_t = \frac{\sigma_{VLC}}{E} + \frac{\sigma_{VSC}}{E} + \frac{\sigma_{VF}}{E} = 0.000763$$

Entering the fatigue curves we read

$$N_d = 5.6 \times 10^6 / 5 \text{ cycles}; \quad n = 3250 \text{ operating cycles}$$

$$D_2 \cong 0$$

NOTE: The elastic analysis rules applied in this note may be used because elastic ratcheting rules have been satisfied.

8. FLAT HEAD

The flat head geometry is shown in fig. 8/1.

8.1. TRANSIENT DESCRIPTION AND THERMAL STRESS EVALUATION

The thermal transients considered are the same adopted at point 7.1.

The thermal stresses are assumed similar to those in tube-header connection section A-A (see point 7.3.) although the flat head had a greater thickness because in the flat head the analysed transients have effects damped by the header sodium thermal inertia.

8.2. STRESS EVALUATION DUE TO MECHANICAL LOADS

In the considered section, the main mechanical load is the pressure.

The pressure stresses has been easily determined by ASME Section VIII, Division 1, UG34 formulas.

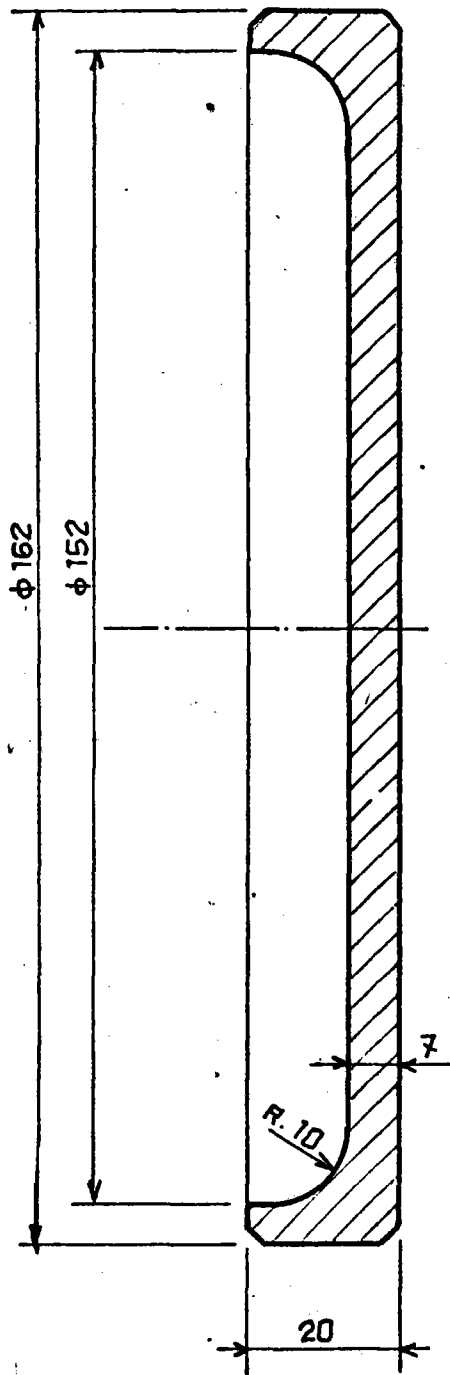


FIG. 8./1

8.3. STRESS TABLE ACCORDING TO ASME CRITERIA

In table 8.3/1 the stresses with their classification by definitions in 3213, Code Case N47, are shown.

8.4. BURSTING ANALYSIS

The t_{min} and r_{min} , requested in UG34, ASME Section VIII are calculated.

The allowable stress value S_m is determined conservatively corresponding with the maximum metal temperature at the hottest cross section.

In table 8.4/1 these calculations are carried out.

8.5. OPERATING CONDITIONS ANALYSIS

See for that analysis the methodology used at point 6.7.; the results are collected in table 8.5/1.

8.6. SHAKE DOWN ANALYSIS

See for that analysis point 6.8. and table 7.8/1.

STRESS TABLE AT MOST STRESS POINT FOLLOWING
ASME CRITERIA

Origin	σ_R (Kp/mm ²)	σ_θ (Kp/mm ²)	σ_z (Kp/mm ²)	Class
Pressure	0.0	2.1*	0.0	P _m
Thermal transient	0.0	-5.803	-7.209	Q
Thermal transient	0.0	-2.532	-2.493	F

(*) calculated as $d^2 \frac{CP}{t^2 E}$

BURSTING ANALYSIS

Header inside diameter

$$d = 152 \text{ mm}$$

Required thickness of header for
pressure (see table 7.6/1)

$$t_r = 0.97 \text{ mm}$$

Actual thickness of header

$$t_s = 5 \text{ mm}$$

Allowable stress value at T_{max}

$$S = S_m = 7.7 \text{ Kp/mm}^2$$

Design pressure

$$p = 0.061 \text{ Kp/mm}^2$$

Joint efficiency (from table UW-12
for type No. 2)

$$E = 0.9$$

$$t_{min} = d \sqrt{CP/SE}$$

with $C = 0.33 \text{ m}$ (from fig. UG-34 for type b-2)

$$m = \frac{t_r}{t_s}$$

$$t_{min} = 3.61 \text{ mm} < 7 \text{ mm}$$

$$T_{min} = 0.375 \text{ in} \approx 9.53 \text{ mm} < r = 10 \text{ mm}$$

OPERATING CONDITIONS ANALYSIS

Highest metal temperature in a point of the radial section	$T_{\max} = 550 \text{ }^{\circ}\text{C}$
Allowable value for general primary membrane stress at T_{\max}	$S_{mt} = 7.75 \text{ Kp/mm}^2$
Allowable stress at T_{\max}	$S_m = 7.7 \text{ Kp/mm}^2$
Time dependent stress a T_{\max}	$S_t = 8.4 \text{ Kp/mm}^2$

$$P_m \leq S_{mt}$$

$$2.1 \text{ Kp/mm}^2 \leq 7.75 \text{ Kp/mm}^2$$

$$P_l + P_b \leq \begin{cases} 1.5 S_m \\ K_t S_t \end{cases}$$

$$K_t = 1 + K_s \left(1 - \frac{PL}{S_t}\right) \cong 1 + K_s \quad K_s = \alpha (K - 1)$$

$$K = 1.5 \quad (\text{from ASME Section III, App. A Table A-9221(a)-1})$$

$$\alpha = 0.5$$

$$K_t = 1.25$$

$$P_l + P_b = 2.1 \text{ Kp/mm}^2 \leq \begin{cases} 1.5 \times 7.7 = 11.6 \text{ Kp/mm}^2 \\ 1.25 \times 8.4 = 10.5 \text{ Kp/mm}^2 \end{cases}$$

8.7. RATCHETING ANALYSIS

See for that analysis point 6.9. and tables 8.7/1 and 8.7/2.

8.8. CREEP-FATIGUE ANALYSIS

See for that analysis point 7.10, and tables 7.10/1 and 7.10/2.

RATCHETING ANALYSIS

(Test 3)

	TIME t = 54 sec				TIME t = 49 sec			
	$\bar{\sigma}_R$ (Kp/mm ²)	$\bar{\sigma}_\theta$ (Kp/mm ²)	$\bar{\sigma}_Z$ (Kp/mm ²)	CL.	$\bar{\sigma}_R$ (Kp/mm ²)	$\bar{\sigma}_\theta$ (Kp/mm ²)	$\bar{\sigma}_Z$ (Kp/mm ²)	CL.
Pressure	0.0	2.1	0.0	P _m	0.0	2.1	0.0	P _m
Thermal transient	0.0	-5.803	-7.209	Q	0.0	2.989	3.682	Q
Thermal transient	0.0	-2.532	-2.493	F	0.0	1.352	1.347	F

- TABLE 8.7/1 -

RATCHETING ANALYSIS

(TEST 3)

Maximum metal temperature $T_{\max} = 550 \text{ }^{\circ}\text{C}$
 Minimum metal temperature $T_{\min} = 210 \text{ }^{\circ}\text{C}$
 Yield strength at T_{\min} $S_y = 11.85 \text{ Kp/mm}^2$

$$X = \left(P_1 + \frac{P_b}{K_t} \right) / S_y$$

$$Y = \frac{(QR)_{\max}}{S_y}$$

$$K_t = 1 + K_s \left(1 - \frac{P_1}{S_t} \right) \cong 1 + K_s$$

$$K_s = \alpha (K - 1)$$

$K = 1.5$ (from ASME Section III App. A Table A-9221(a)-1)

$$\alpha = 0.5$$

$$K_t = 1.25$$

P_1 (Kp/mm ²)	P_b (Kp/mm ²)	QR (Kp/mm ²)	K_t	X	Y	Z	σ_c^* (Kp/mm ²)
2.1	0.0	10.891	1.25	0.177	0.919	0.163	2.4

$$(*) \sigma_c = 1.25 S_y Z$$

Entering the isochronous stress-strain curves at temperature $550 \text{ }^{\circ}\text{C}$ ($\cong 1000 \text{ }^{\circ}\text{F}$) and for any time, by σ_c , we read no significant strain, % due to creep.

9. DOWNCOMER - HEADER CONNECTION

In fig. 9/1 the downcomer - header connection is shown. This section is stressed by the following loads:

- 1) thermal stresses due to transients;
- 2) stresses due to downcomer flexibility including the maximum earthquake.

Stresses at point 1) have been reasonably considered similar to those determined at point 7.3.

Stresses at point 2) have been determined by Bijlaard formulas.

In table 9/1 the stress in the most representative point are reported. In table 9/2 and 9/3 the operating conditions analysis and the reatcheting analysis are carried out respectively.

The fatigue damage is evaluated adding to the damage calculated at point 7.10. the damage due to 10 earthquake cycles connected with T8 type transient. In table 9/4 this analysis is reported.

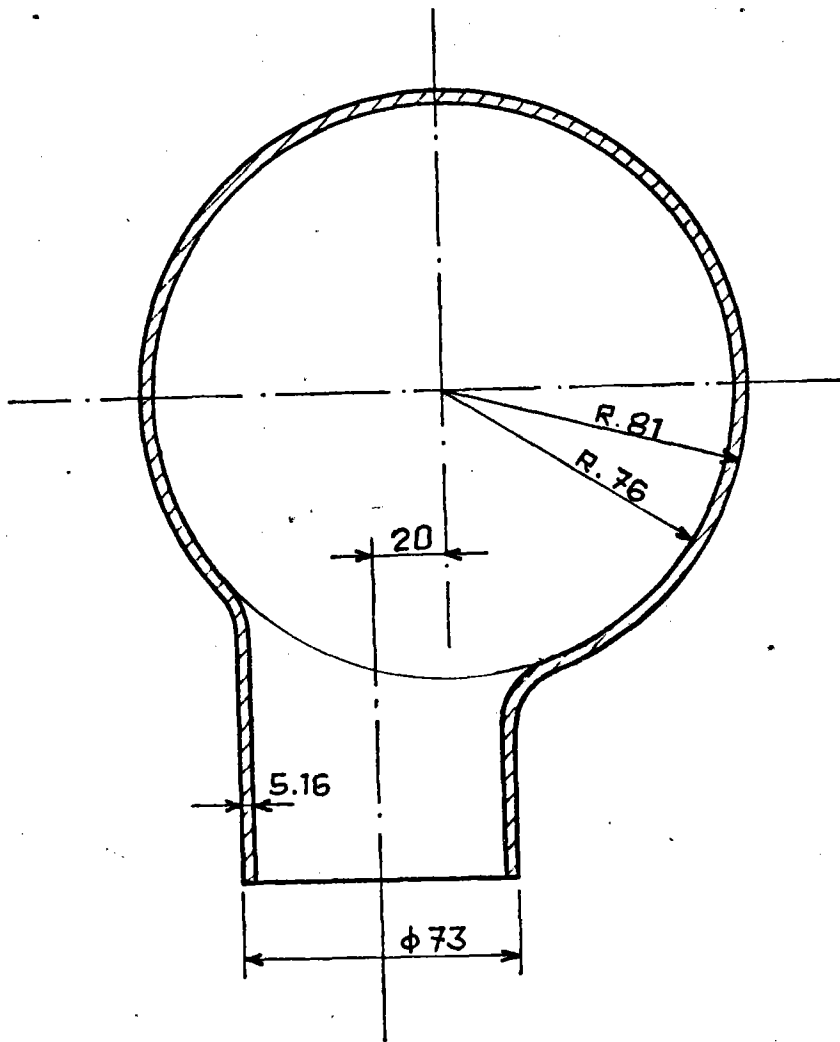
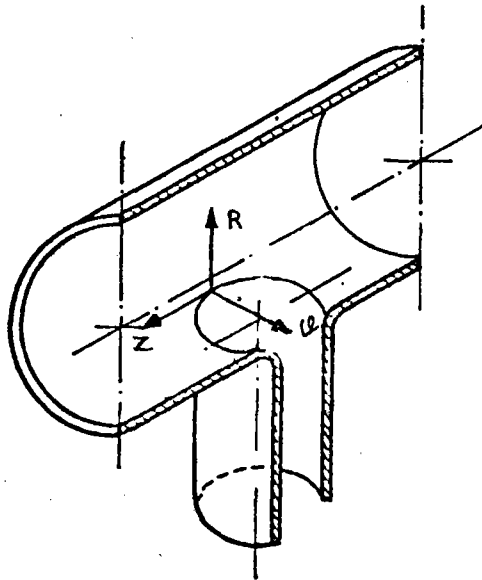


FIG. 9/1

STRESSES AT POINT "A"

	TIME t = 54 sec				TIME t = 49 sec			
	σ_R (Kp/mm ²)	σ_θ (Kp/mm ²)	σ_Z (Kp/mm ²)	CL.	σ_R (Kp/mm ²)	σ_θ (Kp/mm ²)	σ_Z (Kp/mm ²)	CL.
Pressure	0.0	1.48	0.0	P _m	0.0	1.48	0.0	P _m
Thermal transient	0.0	-5.803	-7.209	Q	0.0	2.989	3.682	Q
Thermal transient	0.0	-2.532	-2.493	F	0.0	1.352	1.347	F
Earthquake	0.0	± 0.72	± 1.75	P _m	0.0	± 0.72	± 1.75	P _m
Earthquake	0.0	± 7.0	± 3.32	P _b	0.0	± 7.0	± 3.32	P _b



OPERATING CONDITIONS ANALYSIS

Highest metal temperature in a point of the radial section	$T_{\max} = 550 \text{ }^{\circ}\text{C}$
Allowable value for general primary membrane stress at T_{\max}	$S_{mt} = 7.75 \text{ Kp/mm}^2$
Allowable stress at T_{\max}	$S_m = 7.7 \text{ Kp/mm}^2$
Time dependent stress a T_{\max}	$S_t = 8.4 \text{ Kp/mm}^2$

$$P_m \leq S_{mt}$$

$$2.20 \text{ Kp/mm}^2 \leq 7.75 \text{ Kp/mm}^2$$

$$P_1 + P_b \leq \begin{cases} 1.5 S_m \\ K_t S_t \end{cases}$$

$$K_t = 1 + K_s \left(1 - \frac{PL}{S_t}\right) \approx 1 + K_s \quad K_s = \alpha (K - 1)$$

$$K = 1.27 \quad (\text{from ASME Section III, App. A Table A-9221(a)-1})$$

$$\alpha = 0.5$$

$$K_t = 1.14$$

$$P_1 + P_b = 9.2 \text{ Kp/mm}^2 \leq \begin{cases} 1.5 \times 7.7 = 11.6 \text{ Kp/mm}^2 \\ 1.14 \times 8.4 = 9.6 \text{ Kp/mm}^2 \end{cases}$$

RATCHETING ANALYSIS

(TEST 3)

Maximum metal temperature $T_{\max} = 550 \text{ }^\circ\text{C}$ Minimum metal temperature $T_{\min} = 210 \text{ }^\circ\text{C}$ Yield strength at T_{\min} $S_y = 11.85 \text{ Kp/mm}^2$

$$X = \left(P_1 + \frac{P_b}{K_t} \right) / S_y$$

$$Y = \frac{(Q_R)_{\max}}{S_y}$$

$$K_t = 1 + K_s \left(1 - \frac{P_1}{S_t} \right) \cong 1 + K_s$$

$$K_s = \alpha (K - 1)$$

 $K = 1.27$ (from ASME Section III App. A Table A-9221(a)-1)

$$\alpha = 0.5$$

$$K_t = 1.14$$

P_1 (Kp/mm ²)	P_b (Kp/mm ²)	Q_R (Kp/mm ²)	K_t	X	Y	Z	σ_c^* (Kp/mm ²)
2.2	7.0	8.792	1.14	0.704	0.742	0.8047	11.92

$$(*) \sigma_c = 1.25 S_y Z$$

Entering the isochronous stress-strain curves at temperature $550 \text{ }^\circ\text{C}$ ($\cong 1000 \text{ }^\circ\text{F}$) and for a time of 30000 h (very conservative), an acceptable strain of 0.22% is found.

FATIGUE ANALYSIS

Calculation of D_1

$$D_1 \cong 0.25 \quad (\text{see table 7.10/1})$$

Calculation of D_2

$$D_2 \cong 0.0 \quad (\text{see table 7.10/2})$$

Calculation of D_3

(see table 9/1)

$$\sigma_{VLC} = 15.44 \text{ Kp/mm}^2$$

$$\sigma_{VSC} = 10.891 \text{ Kp/mm}^2$$

$$\sigma_{VF} = 3.884 \text{ Kp/mm}^2$$

Hence

$$\epsilon_t = 0.001925$$

Entering the fatigue curves we read

$$N_d = 10^4 / 5 \text{ cycles}; \quad n = 10 \text{ operating cycles}$$

$$D_3 = \frac{n}{N_d} = 0.005$$

From this analysis the following damage has been obtained

$$D_T = D_1 + D_2 + D_3 = 0.25 + 0.0 + 0.005 \cong 0.26$$

A P P E N D I X 1

APPENDIX 11. ALLOWABLE STRESS LIMITS FOR AISI 316 L

The following tables contain, as a function of the temperature, the values of allowable stresses that are used by Franco Tosi in design of stainless steel sodium component working of high temperature.

The definition of the term used is assumed according Code Case N47-17 sub. 3221.

1.1 Maximum allowable design stress intensity S_o

T (°C)	S_o (N/mm ²)
20	107
100	105
200	96
300	95
400	86
500	80
600	72

1.2 Maximum time independent stress intensity S_m

T (°C)	S_m (N/mm ²)
20	115
100	115
200	107
300	94
400	85
500	80
600	72

1.3 Maximum temperature dependent stress intensity.

The value is tabulated for a working time of 30000 hours.

T (°C)	S_t (N/mm ²)
450	114
500	100
550	83
600	53

1.4 Maximum allowable value for general primary membrane stress intensity S_{mt}

The value is tabulated for a working time of 30000 h

T (°C)	S_{mt} (N/mm ²)
450	83
500	80
550	76
600	53

1.5 Yeld strenght S_y

T (°C)	S_y (N/mm ²)
20	172
100	143
200	119
300	105
400	95
500	89
600	80

APPENDIX 2

1. PHYSICAL PROPERTIES

The following tables contain, as a function of the temperature, the value of physical properties used by Franco Tosi in design of stainless steel sodium component working at high temperature.

1.1. PHYSICAL PROPERTIES FOR AISI 316L1.1.1. Thermal expansion

Temperature (°C)	$\alpha \cdot 10^{-6}$
20 - 100	16
20 - 200	17
20 - 300	17.5
20 - 400	17.8
20 - 500	18.0
20 - 600	18.2

1.1.2. Specific heat capacity

Temp. (°C)	CP (J/Kg °C)
100	500
300	552
400	578
500	604
600	630

1.1.3. Thermal conductivity

Temp. (°C)	W/m °C
100	16
300	19
400	20
500	21
600	22

1.1.4. Density

$$\rho = 8. \text{ Kg} / \text{ dm}^3$$

1.2. PHYSICAL PROPERTIES FOR SODIUM

1.2.1. Density

Temp. (°C)	Kg / m ³
100	926.
300	880.
400	857.
500	833.
600	809.

1.2.2. Specific heat capacity

Temp. (°C)	J/Kg °C
100	1383
300	1304
400	1278
500	1262
600	1254

1.2.3. Thermal conductivity

Temp. (°C)	W/m °C
100	86
300	76
400	71
500	66
600	61

IEA ALMERIA PROJECT
ADVANCED SODIUM RECEIVER
ASR

Tube-stirrup supporting plate connection
analysis

Topic Report No. 13

Revision 0

January 1983

Prepared by: ENEL

FRANCO TOSI

AGIP NUCLEARE

CONTENTS

1. Abstract
 2. Analysis limits and structure description
 3. Material basic data
 4. Thermal transient description
 5. Loads analysis
 6. Tube-supporting plate analysis
 - 6.1. Analysis methodology
 - 6.2. Temperature field evaluation
 - 6.3. Thermal stresses evaluation
 - 6.4. Stress table following ASME criteria
 - 6.5. Section "A-A" analysis
 - 6.6. Section "B-B" analysis
 7. Conclusion
- Appendix 1
- Appendix 2

1. ABSTRACT

The main object of this report is the analysis of the plate connecting the three tubes assembly in the stirrup supporting system.

The main stress status in the plate is related to the different thermal inertia during transient between the plate itself and the tubes: therefore a shrink effect has to be expected in the tube zone and a compression (traction) in the plate zone.

The effects of all the transients considered in Topic Report No. 6 are analyzed including the earthquake effects.

2. ANALYSIS LIMITS AND STRUCTURE DESCRIPTION

The analysis refers to the tube supporting plate subjected to stationary mechanical loads and thermal transients originated by direct heat flux and by time dependent sodium temperature and flowrate.

The considered part consists of a slice of the three tubes assembly and of the connecting plate.

The most important geometric characteristics of the structure are represented in fig. 2/1.

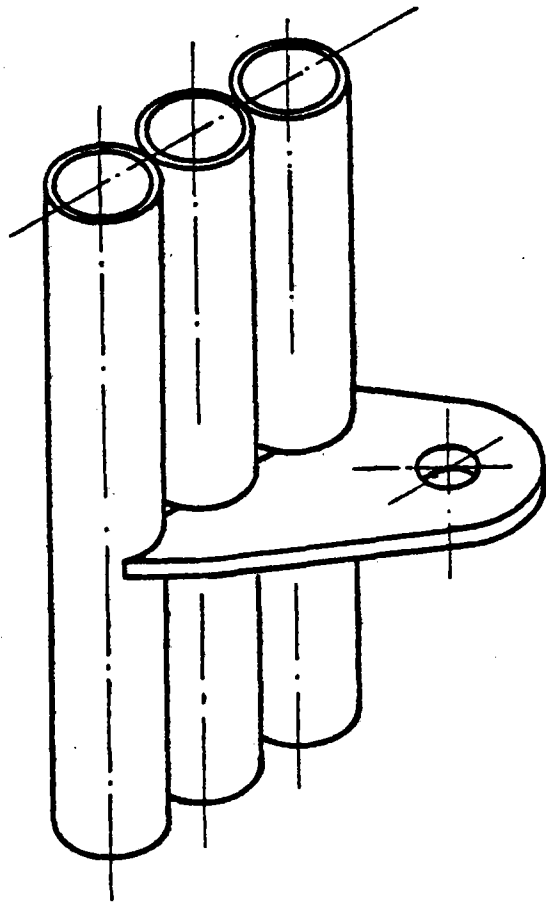
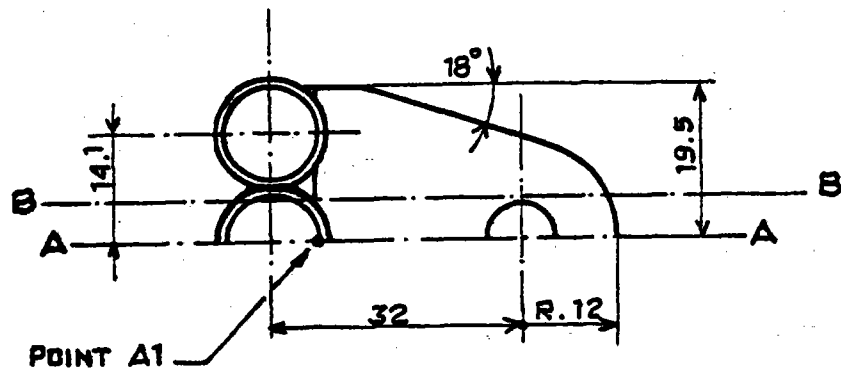


FIG. 2/1

3. MATERIAL BASIC DATA

The receiver tube material is SANDVIK Alloy 3R60 corresponding to the ASTM 316L type.

The stirrup plate is ASTM 316L type.

The material mechanical properties are reported in Appendix 1.

The thermal properties of the alloy and of the sodium are collected in Appendix 2.

4. THERMAL TRANSIENT DESCRIPTION

In order to have a complete lifetime analysis of the parts of the receiver hereafter considered an extensive evaluation of all the transient conditions described in Topic Report No. 6 has been carried out by means of the simulation code for the receiver dynamic analysis described in Topic Report No. 4.

The behavior of the temperatures for the different transients have been reported corresponding to the last irradiated section of the fifth panel. The chosen section gives the most unfavorable situation in the considered element.

The following transients in the ASR lifetime analysis are examined:

1) Normal operating conditions

Three types of shading-reinsolation sequences caused by a cloud passage are considered other than the normal daily cycling:

- a) shading and prompt reinsolation;
- b) shading over a period of 5 minutes and succeeding reinsolation;
- c) shading for long time (>5 minutes) and succeeding reinsolation.

2) Upset conditions

- d) Failure of the control system of the pump in case of 100% reinsolation (flow rate at 10%).
- e) Failure of the control system of the pump in case of shading of the field.
- f) Loss of electrical power supply of the sodium pump.

3) Emergency conditions

The earthquake effects of 1 event per year has been considered; cautiously to the earthquake the "e" transient has been associated.

The following conditions have been cautiously assumed in accordance to the Topic Report No. 6:

- "a" type cloud passage transient
 - . cloud velocity of 50 Km/h;
 - . 3000 cloud passages per year;
 - . sodium temperature behavior as reported in fig. 4/1 (transient T8);
 - . the level of the peak incident flux before the cloud passage is that corresponding to the design point.

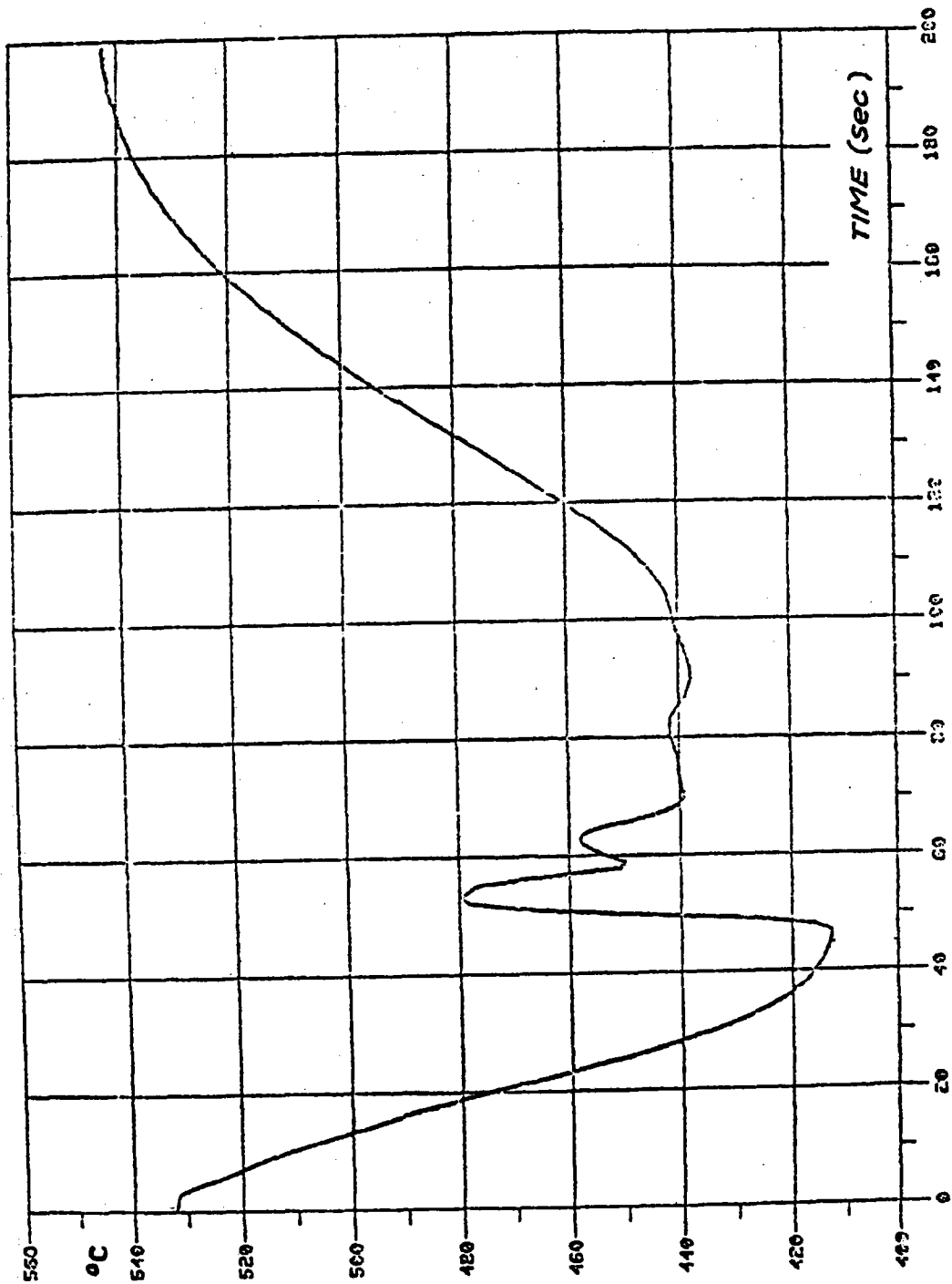


FIG. 4/1

- "b" type cloud passage

- . cloud velocity of 50 Km/h;
- . 3000 cloud passage per year;
- . sodium temperature as reported in fig. 4/2 (transient T9).

In order to simplifying the analysis, a comparison between transient T8 and T9 has permitted the assumption of the former as the most representative one; therefore the damage of "b" transients is evaluated on "a" transient basis.

- "c" type cloud passage transient

- . cloud velocity of 50 Km/h;
- . 325 cloud passage per year;
- . the sodium temperature behavior has been assumed as the combination of transients T11 and T12 (fig. 4/3);
- . the level of the peak incident flux before cloud passage is corresponding to the design point (equinox noon).

- "d" type transient

- . 6 events per year;
- . the level of the peak incident flux is corresponding to the design point (equinox noon);

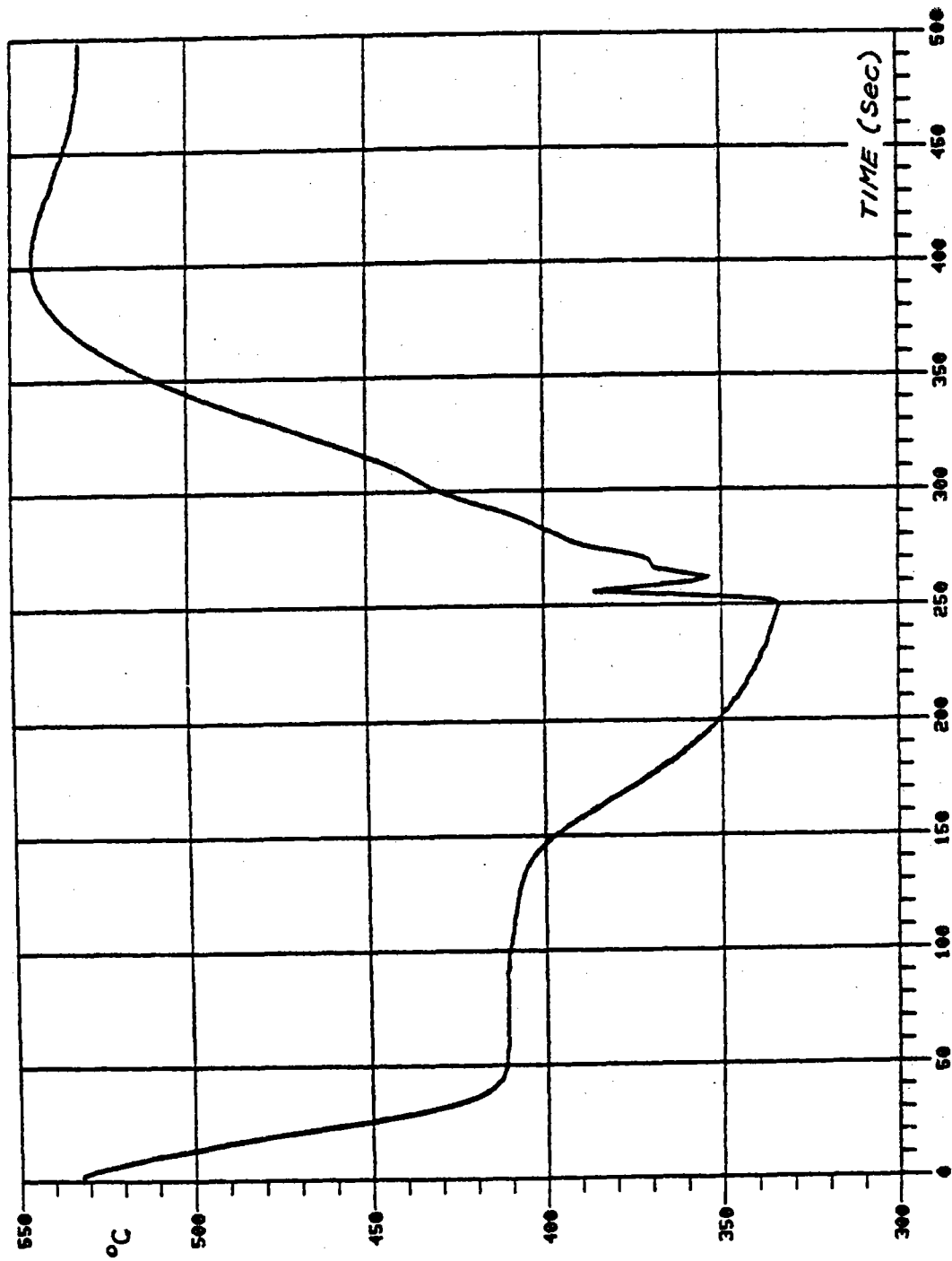


FIG. 4/2

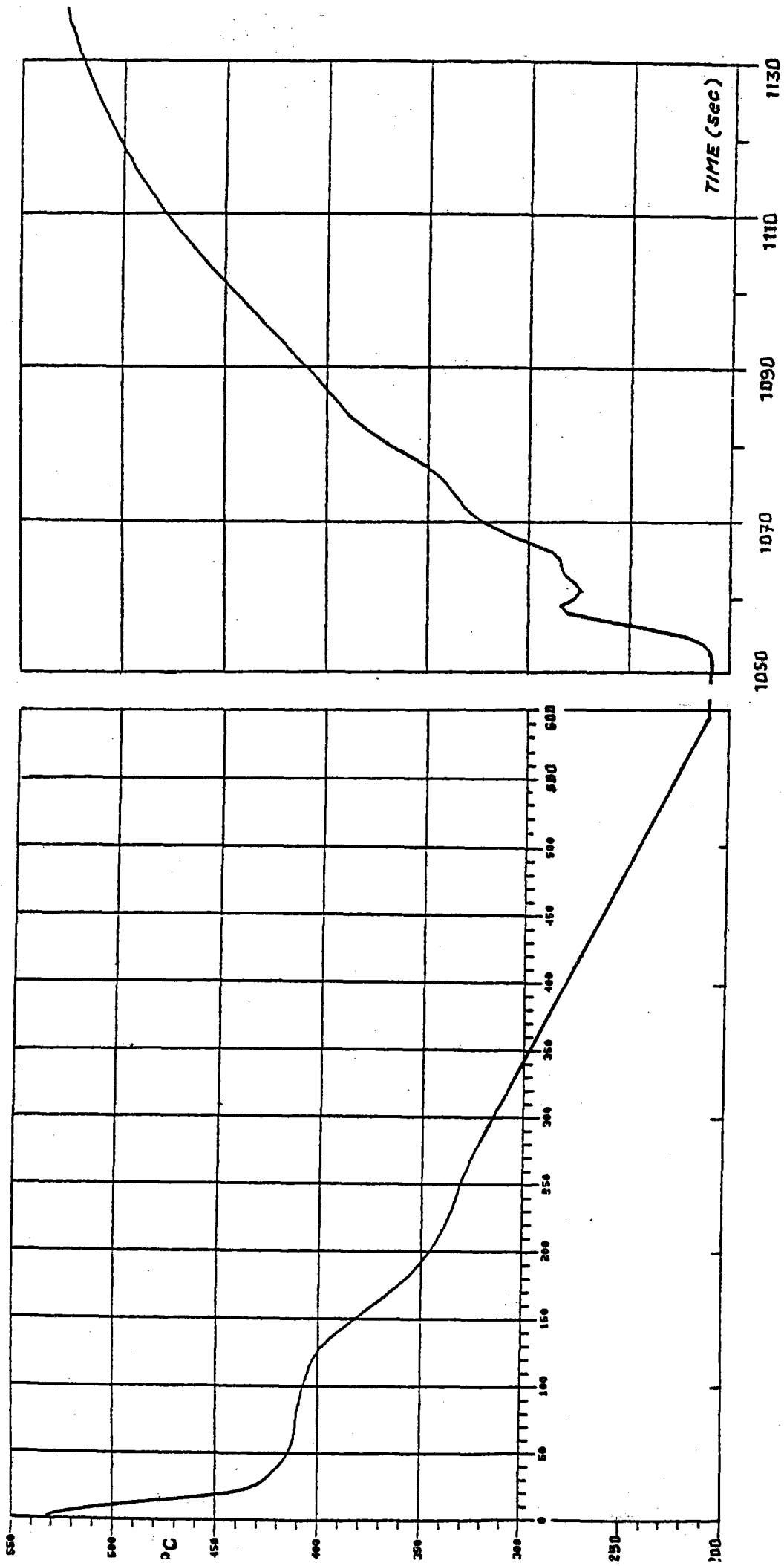


FIG. 4/3

- . sodium temperature reported in fig. 4/4 (transient T16).

In order to simplifying the analysis, a comparison between transient T12 and T16 has permitted the assumption of the former as the most dangerous one; therefore in the lifetime analysis the strain range of T12 has been assumed representative for T16 as well.

- "e" type transient

- . 6 events per year;
- . the level of the peak incident flux is corresponding to the design point (equinox noon);
- . temperature behavior is reported in fig. 4/5 (transient T14).

Again for simplification purpose a comparison between the sodium temperature ramps and flowrate of transient T14 and of transient T12 in the decreasing sense, has permitted the assumption of transient T12 as more dangerous than.

- "f" type transient

- . 6 events per year;
- . the level of the peak incident flux is that corresponding to the design point (equinox noon);

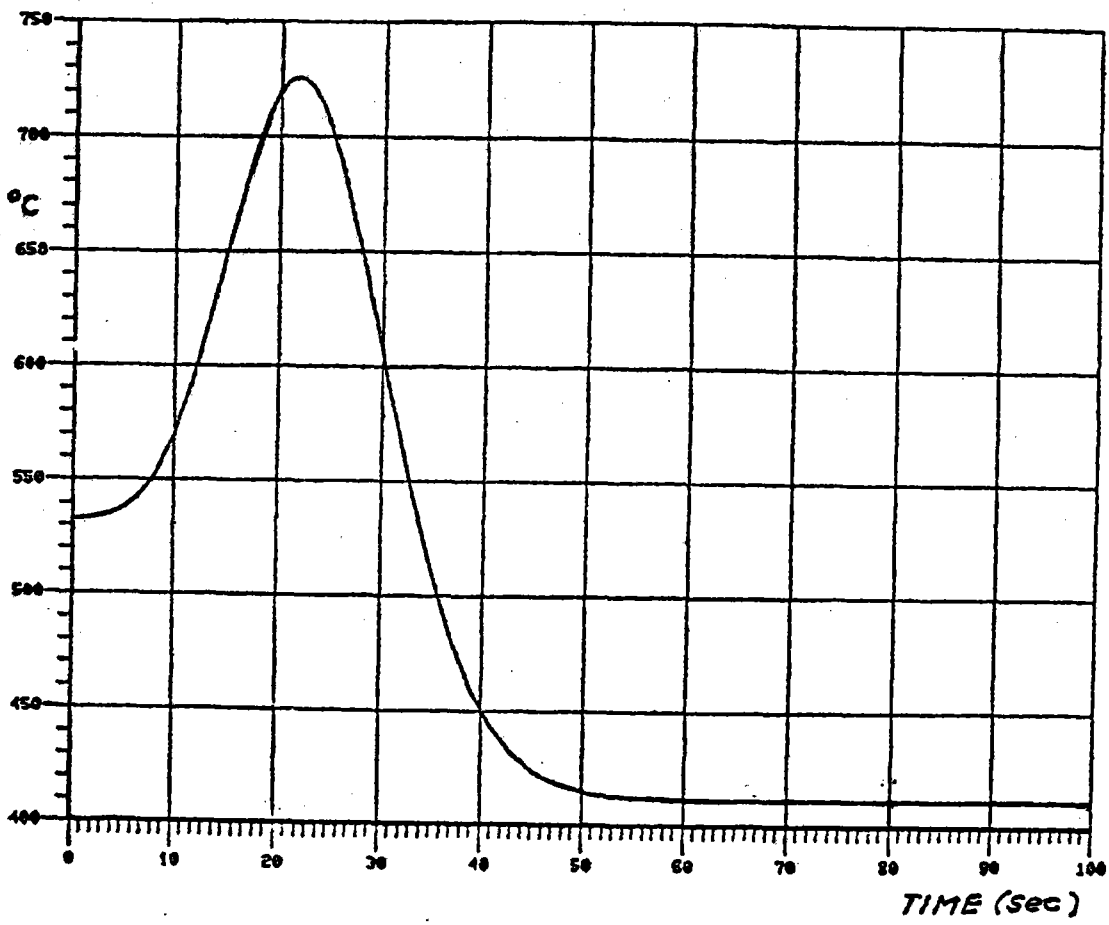


FIG. 4/4

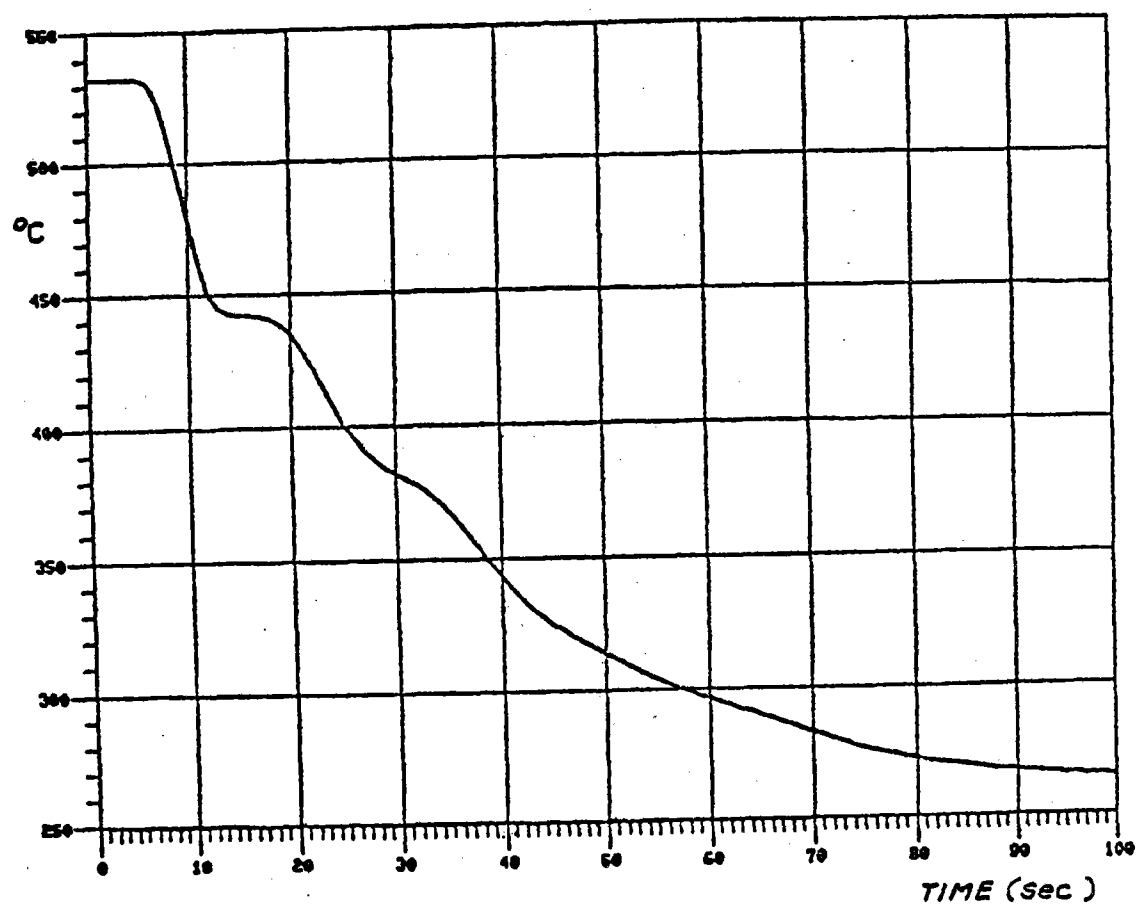


FIG. 4/5

sodium temperature behavior is reported in fig. 4/6 (transient T15).

Again a comparison between the sodium temperature ramps and flowrate of transient T15 and of transient T8 in the decreasing temperature zone has permitted to assume T8 as upper bound between the two transients with a simplification of the analysis.

All the aforementioned transients have been calculated according to the conditions reported in the Topic Report No. 11.

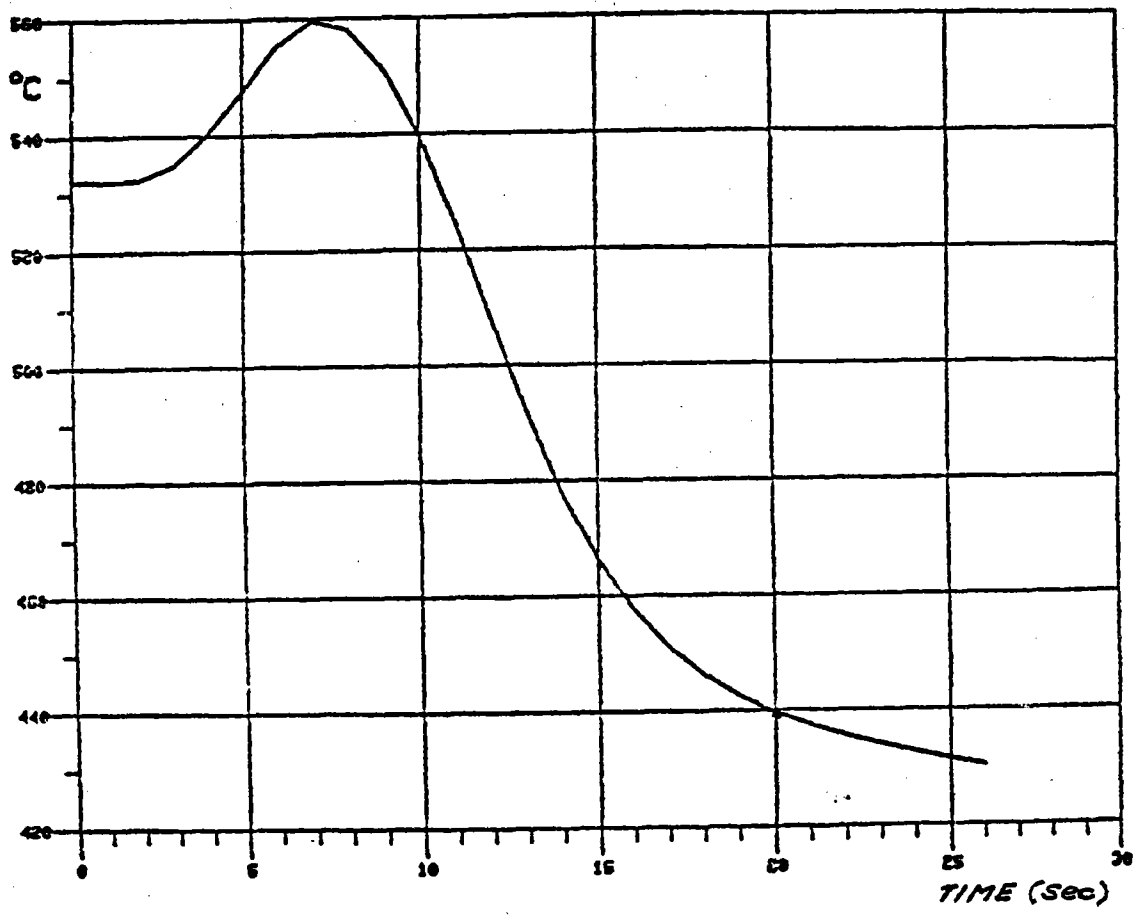


FIG. 4/6

5. LOADS ANALYSIS

In the assumption of linear elastic behavior of the material, the stress conditions have been determined by means of the superimposition of the following effects.

- 1) Stationary stresses due to internal pressure (in the tube sections).
- 2) Self equilibrating time dependent stresses due to the linear and nonlinear parts of the temperature distribution in the tube sections.
- 3) Stationary stresses due to the weight (in the tube sections).
- 4) Self equilibrating time dependent stressed due to the linear and nonlinear parts of the temperature distribution in the plate sections.

Stresses at point 1) can be easily determined by formulas.

Stresses at point 2) can be found by finite element calculations for the nonlinear temperature distribution and by a flexibility analysis using beam element discretization for the linear temperature distribution; the latter procedure (flexibility analysis) is used for the calculation of the stresses due to the weight (point 3) as well.

Stresses at point 4 are carried out by 3D finite element analysis starting from the time dependent temperature field evaluated from the heat flux and sodium flow rate boundary conditions.

6. TUBE-SUPPORTING PLATE ANALYSIS

6.1. ANALYSIS METHODOLOGY

The analysis consists in the evaluation, for each of the transients presented at point 4, of the thermal field in the structure. In order to carry out the life time calculations, the most representative time instants are selected that give the maximum strain range.

A detailed description of the methodology is reported in Progress Report No. 9.

6.2. TEMPERATURE FIELD EVALUATION

A group of three tubes connected by plate of the stirrup style supporting system is considered; the internal surface of the tubes is wetted by sodium with a time variable temperature.

The structure under analysis has two symmetry planes: the part actually considered is shown in fig.6.2/1.

All further considerations are related to the sections labelled "AA" and "BB". The section "BB" is the most stressed plate section, section "AA" is the most tube stressed section.

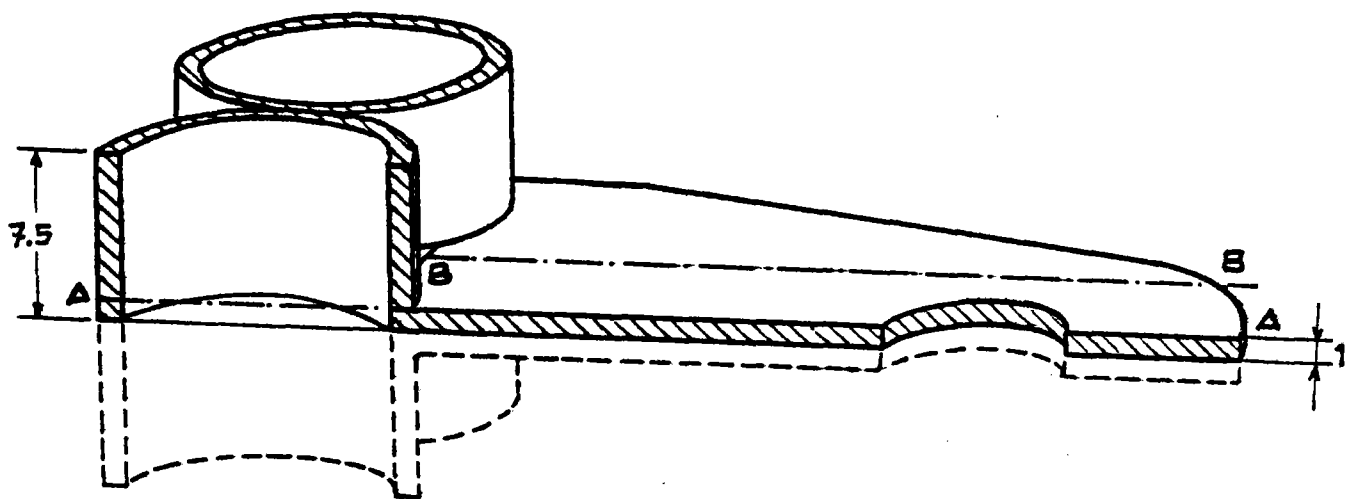


FIG. 6.2/1

In fig. 6.2/2 the 3D mesh is shown with "20 nodes brick" finite elements: the mesh is used both for the thermal calculation (FLHE code) and for mechanical calculations (BERSAFE code).

In tables 6.2/1 - 6.2/2 the discretizations of the thermal transients considered are reported.

Every time interval is subdivided in 5 time steps: at each time a forced convection must be applied to the sodium wetted surfaces; the external surfaces of the tube and the plate are assumed to be adiabatic.

For sodium physical characteristics see Appendix 2.

In fig. 6.2/3 - 6.2/4 the temperature behavior in the considered "A-A" section are presented for two time instants giving the maximum range during the different transient conditions.

6.3. THERMAL STRESSES EVALUATION

With the loading conditions given by the nodal temperature obtained by the FLHE code, stress analysis in the most representative time instants has been performed by means of the finite elements programm BERSAFE.

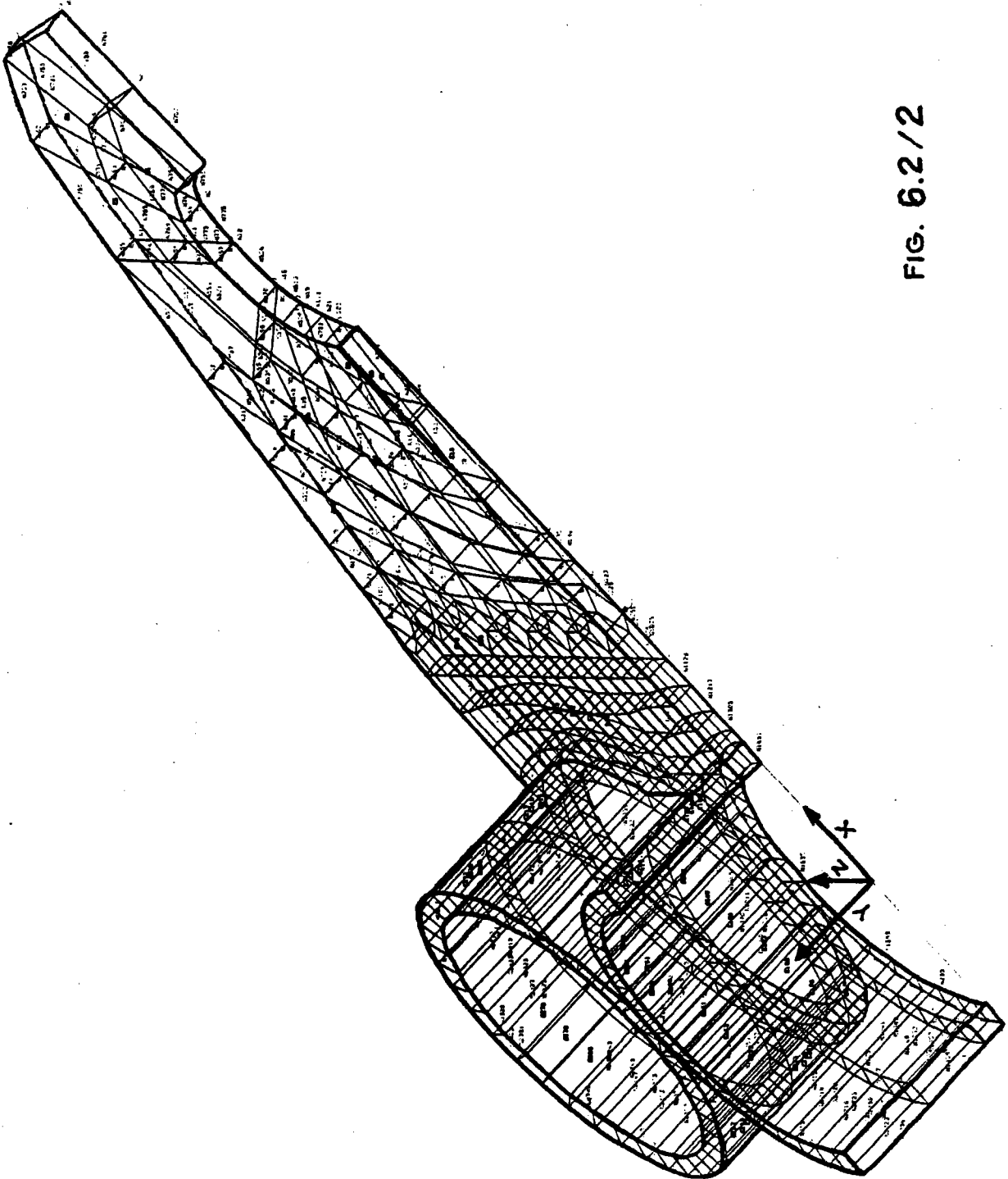


FIG. 6.2/2

UNDEFORMED SCALE = 1.0000

-300.0 -300.0 1000.0 CART 0.0 0.0 0.0 CART

PLOT OF COMPONENT 1 - MESH PLOT

THERMAL TRANSIENT T8

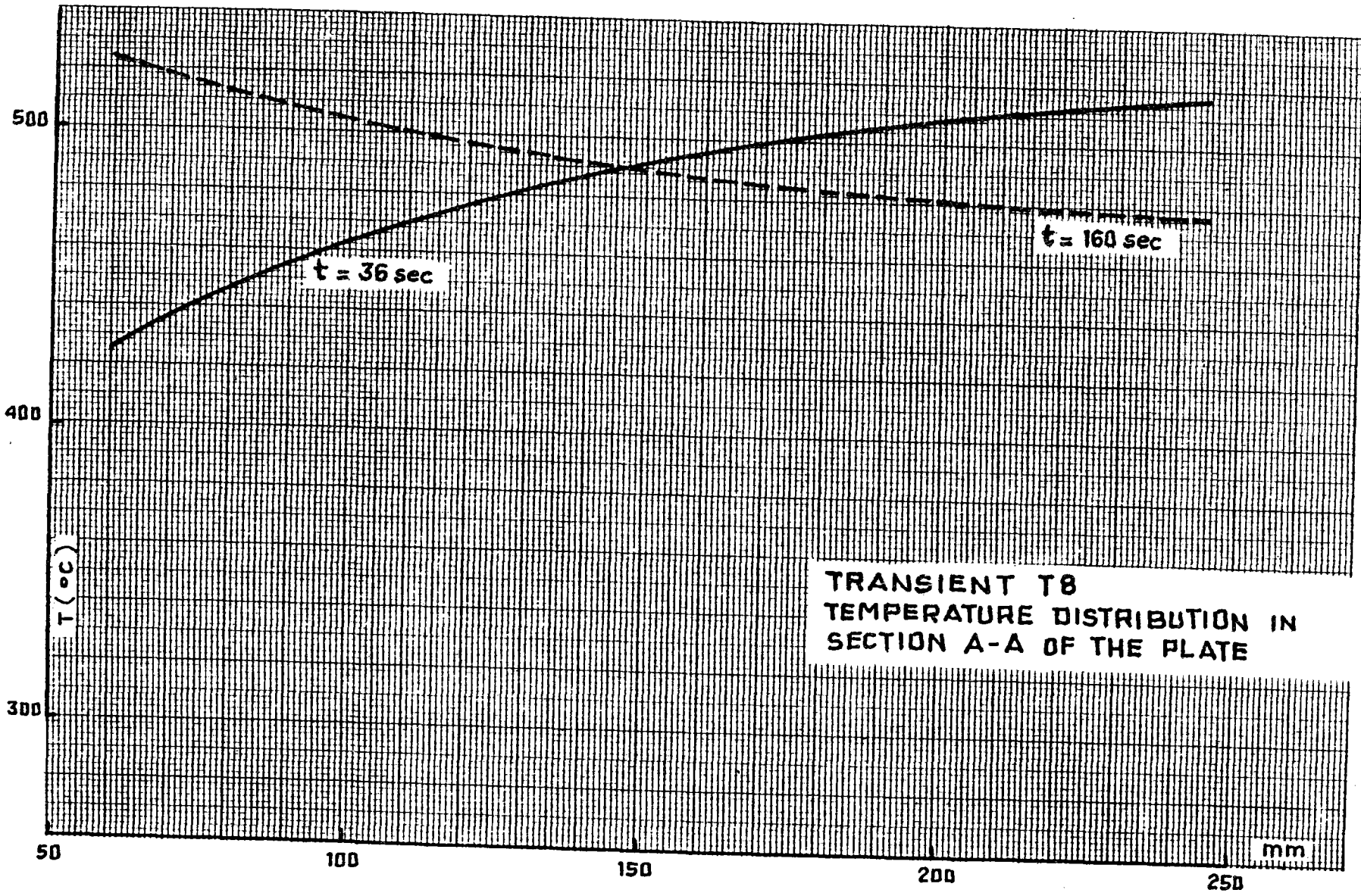
TIME (sec)	TEMPERATURE (°C)	FLOW (Kg/sec)	DENSITY (Kg/m ³)	VELOCITY (m/sec)	HEAT COEFF. (W/m ² °C)
0	532	7.3	825.41	2.00	39801
2	532	6.4	825.41	1.75	38365
14	492	0.7	835.05	0.19	28925
36	420	0.7	852.25	0.19	30357
45	413	0.7	853.92	0.19	30562
47	412	3.69	854.15	0.98	36580
52	468	11.	840.80	2.96	46688
53	479	11.	838.17	2.98	46677
59	450	11.	845.11	2.95	47257
62	458	11.	843.19	2.96	46972
70	440	11.	847.49	2.94	47544
102	440	11.	847.49	2.94	47544
107	440	10.33	847.49	2.76	46431
130	477	7.3	838.65	1.97	40790
160	526	7.3	826.86	2.00	39801
200	543	7.3	822.75	2.01	39547
300	532	7.3	825.41	2.00	39801

- TABLE 6.2/1 -

THERMAL TRANSIENT T11-T12

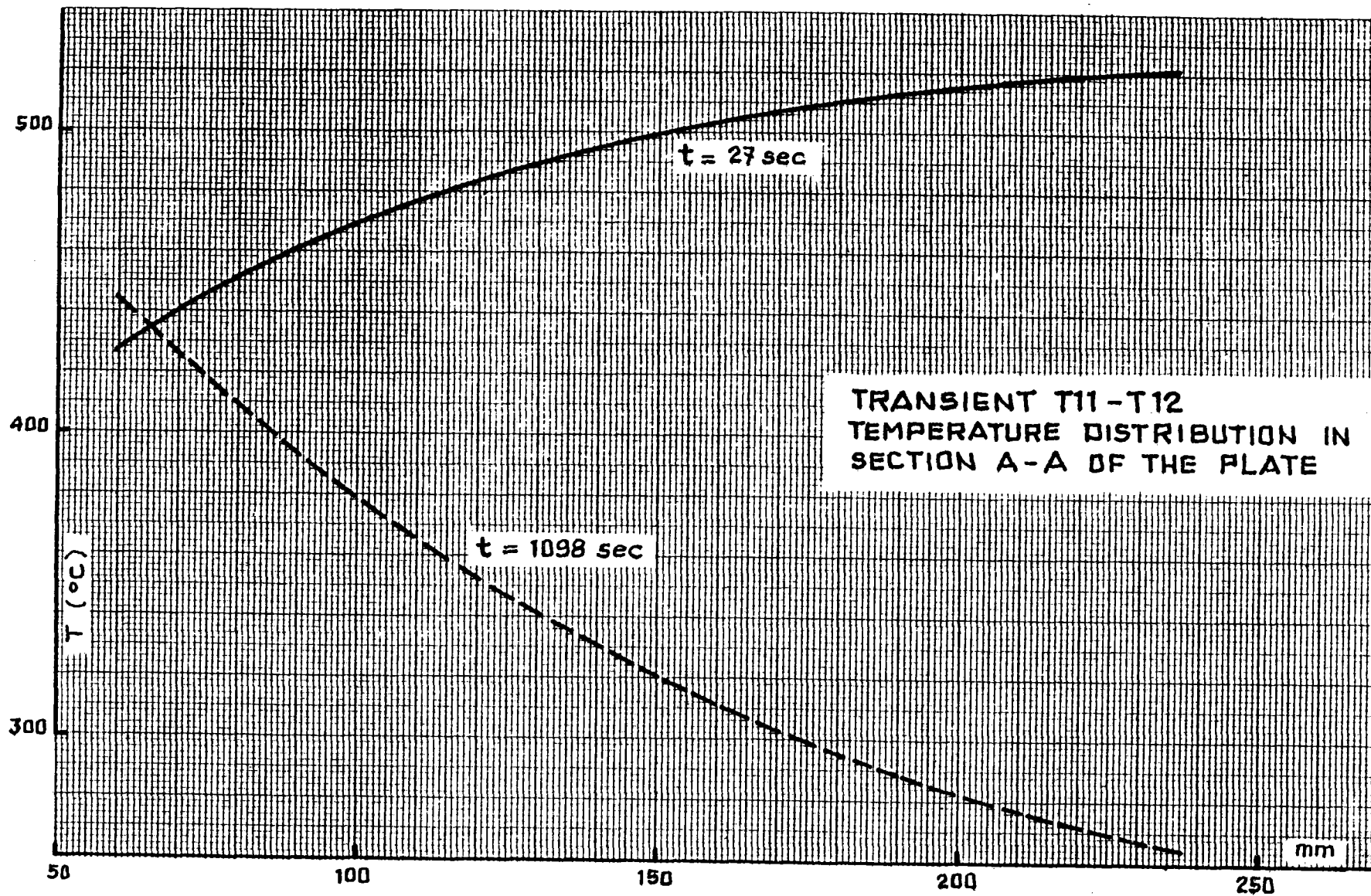
TIME (sec)	TEMPERATURE (°C)	FLOW (Kg/sec)	DENSITY (Kg/m ³)	VELOCITY (m/sec)	HEAT COEFF. (W/m ² °C)
0	532	7.20	825.41	1.98	39801
14	479	1.61	838.17	0.43	31128
27	421	1.11	852.02	0.30	31214
38	419	0.70	852.49	0.19	30357
130	398	0.70	857.47	0.19	30768
190	350	0.70	868.81	0.18	31796
312	308	0.70	878.66	0.18	32622
597	210	0.70	878.66	0.18	34696
1050	210	0.70	878.66	0.18	34696
1052	210	2.4	878.66	0.60	38245
1055	270	4.4	887.51	1.12	40630
1056	283	6	884.49	1.53	43483
1058	277	9.4	885.89	2.41	48949
1059	274	9.4	886.58	2.40	49239
1088	406	9.4	855.58	2.50	45851
1098	450	7.6	845.11	2.04	42154
1103	465	6.8	841.52	1.83	40459
1126	525	6.8	827.10	1.86	38943
1168	545	6.8	822.27	1.87	38444
1250	545	6.8	822.27	1.87	38444

- TABLE 6.2/2 -



TRANSIENT T8
TEMPERATURE DISTRIBUTION IN
SECTION A-A OF THE PLATE

FIG. 6.2/3



TRANSIENT T11-T12
TEMPERATURE DISTRIBUTION IN
SECTION A-A OF THE PLATE

FIG. 6.2/4

The maximum principal stresses for transients T8 and T11-12 related to sections "AA" and "BB" are presented in tables 6.3/1 - 6.3/2.

6.4. STRESS TABLE FOLLOWING ASME CRITERIA

In table 6.4/1 the stress classification, valid, if applicable, both for point A1 and B1, is reported. For simplicity and with a great conservatism the effects of the nonlinear part of the temperature distribution has been classified as secondary stress (actually a large part is F).

The values of the stresses due to internal pressure, weight, tube assemblies restraints and direct heat flux are taken from Topic Report No. 7.

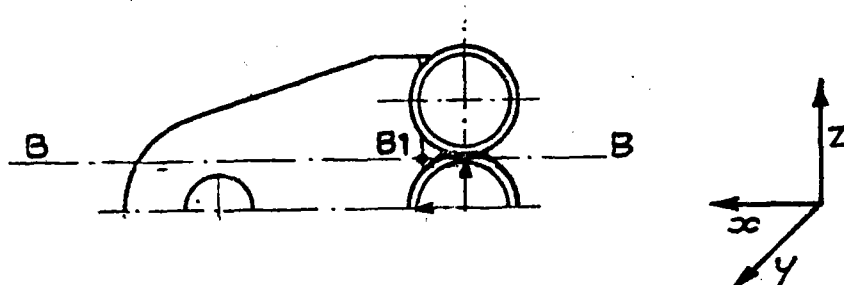
6.5. SECTION "A-A" ANALYSIS

The analysis is carried out at point A1 (see table 6.3/2).

The maximum stress values corresponding to time $t = 1098$ sec during transient T12 are reported in table 6.5/1.

SECTION B - B

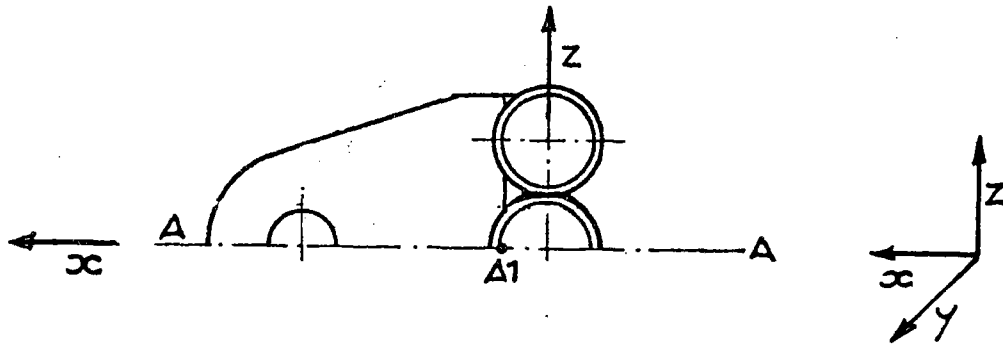
Point B1



	Time instant (sec.)	σ_x (Kg/mm ²)	σ_y (Kg/mm ²)	σ_z (Kg/mm ²)
TRANSIENT T11-T12:	27	0.11	0.81	11.43
	1098	0.07	-0.99	-15.19
TRANSIENT T8 :	36	0.048	0.66	9.66
	160	-0.4	-0.67	-8.23

SECTION A - A

Point A1



	Time instant (sec.)	σ_x (Kg/mm ²)	σ_y (Kg/mm ²)	σ_z (Kg/mm ²)
TRANSIENT T11-T12:	27	-0.41	-2.60	5.51
	1098	0.69	3.75	-7.43
TRANSIENT T8 :	36	-0.37	-2.32	4.60
	160	-0.0039	0.81	-4.16

STRESS CLASSIFICATION ACCORDING TO
ASME CRITERIA

Load origin	Point A1	Point B1
Weight	P_M	
Pressure	P_M	
Tube assembly restraints	Q	
Direct heat flux: effect in the tube	Q	
Direct heat flux: effect in the plate	Q	Q
Earthquake	P_M	

- TABLE 6.4/1 -

STRESS TABLE - POINT A1 SECTION "A-A"

TRANSIENT T12

LOAD	σ_y (Kg/mm ²)	σ_z (Kg/mm ²)	σ_x (Kg/mm ²)	TIME (sec.)
Weight	-0.09	0.	0.	
Pressure	0.17	0.34	0.	
Restraints	10.64	0.	0.	
Thermal due to direct heat flux	-3.2	-0.55	0.	
Thermal due to plate restraint effect	3.75	-7.43	0.69	1098
Earthquake	± 0.23	0.	0.	

6.5.1. Design condition analysis

The stresses for the design analysis are taken from table 6.5/1; the design temperature is assumed as 530 °C.

In table 6.5.1/1 the detailed compliance analysis is presented.

6.5.2. Operating conditions analysis

The allowable stress values S_{mt} and S_t are determined for a working time of 30000 h at the maximum metal temperature on the hottest radial section.

The analysis is carried out in table 6.5.2/1.

The earthquake effects, considered as level C operating conditions, are presented in table 6.5.2/2.

6.5.3. Shake down analysis

The S_m value is taken as the average of the two S_m value at maximum and minimum cycle temperature, according to Note (1), fig. 4-130.1, Appendix 4, ASME Section VIII, Division 2 because all the considered secondary stresses are thermal ones.

The analysis is presented in table 6.5.3/1.

DESIGN LIMITS

(ASME Section III, Division I, Subsection NA)

Design temperature $T = 530 \text{ }^\circ\text{C}$
Allowable stress $S_o = 7.82 \text{ Kg/mm}^2$
Stress due to pressure and mechanical
loads (see also table 6.4/1) $P_m = 0.34 \text{ Kg/mm}^2$

$$P_m = 0.34 \text{ Kg/mm}^2 < S_o = 7.82 \text{ Kg/mm}^2$$

OPERATING CONDITIONS ANALYSIS

(Normal + Upset)

Highest metal temperature in a point of the radial section	$T_{\max} = 545 \text{ }^{\circ}\text{C}$
Allowable value for general primary membrane stress at T_{\max}	$S_{mt} = 7.64 \text{ Kg/mm}^2$
Allowable stress at T_{\max}	$S_m = 7.64 \text{ Kg/mm}^2$
Time dependent stress at T_{\max}	$S_t = 8.47 \text{ Kg/mm}^2$

$$P_m \leq S_{mt}$$

$$0.34 \text{ Kg/mm}^2 \leq 7.64 \text{ Kg/mm}^2$$

$$P_1 + P_b \leq \begin{cases} 1.5 S_m \\ K_t S_t \end{cases}$$

$$K_t = 1 + K_s \left(1 - \frac{PL}{S_t}\right) = 1.13$$

$$K_s = \alpha (K - 1)$$

$$K = 1.27$$

$$K_s = 0.135$$

$$P_1 + P_b = 0.34 \text{ Kg/mm}^2 \leq \begin{cases} 1.27 \times 7.64 = 9.70 \text{ Kg/mm}^2 \\ 1.13 \times 8.47 = 9.57 \text{ Kg/mm}^2 \end{cases}$$

OPERATING CONDITIONS ANALYSIS

(Level C)

Highest metal temperature in a
point of the radial section $T_{\max} = 545 \text{ }^{\circ}\text{C}$

Allowable stress at T_{\max} $S_m = 7.64 \text{ Kg/mm}^2$

Time dependent allowable stress at
 T_{\max} $S_{mt} = 8.47 \text{ Kg/mm}^2$

$$P_m \leq \begin{cases} 1.2 S_m \\ 1.0 S_t \end{cases}$$

$$0.87 \text{ Kg/mm}^2 \leq \begin{cases} 9.17 \text{ Kg/mm}^2 \\ 8.47 \text{ Kg/mm}^2 \end{cases}$$

SHAKE DOWN ANALYSIS

Highest metal temperature in a point of the radial section	$T_{\max} = 545 \text{ }^{\circ}\text{C}$
Lowest metal temperature in a point of the radial section	$T_{\min} = 210 \text{ }^{\circ}\text{C}$
Allowable stress at T_{\max}	$S_m(T_{\max}) = 7.64 \text{ Kg/mm}^2$
Allowable stress at T_{\min}	$S_m(T_{\min}) = 10.57 \text{ Kg/mm}^2$
Allowable stress for Test B	$S_m = 9.105 \text{ Kg/mm}^2$

$$P_1 + P_b + Q \leq 3 S_m$$

$$\left| (-0.09 + 0.17 + 10.64 - 3.2 + 3.75) - (0.34 - 0.55 - 7.32) \right| \leq 3 S_m$$

$$18.91 \leq 27.31 \text{ Kg/mm}^2$$

6.5.4. Ratcheting analysis

The presence of "Elastic follow-up" is reasonably excluded in the following analysis.

In table 6.5.4/1 the stress values in two different instants are presented in order to determine the maximum stress range during the T11-T12 transient that is the most dangerous.

The step by step procedure proposed by T 1324 in the Appendix T of Code Case N-47-17 has been applied and the results are shown in table 6.5.4/2.

6.5.5. Creep-fatigue analysis

The total fatigue damage has been evaluated according to the following assumptions:

- . Allowable number of cycles to use in equation (5), T-1411, is taken from curves of fig. T-1420-1B, Code Case N-47-17 with a reduction factor of 5 in the allowable cycles number.
- . The step by step procedure suggest in T 1410 in the Appendix T of Code Case N-47-17 has been assumed and the results are described in tables 6.5.5/1 + 6.5.5/3.

RATCHETING ANALYSIS

Stresses during transient T11-T12

LOAD	TIME t = 27 sec			TIME t = 1098 sec		
	σ_y (Kg/mm ²)	σ_z (Kg/mm ²)	σ_x (Kg/mm ²)	σ_y (Kg/mm ²)	σ_z (Kg/mm ²)	σ_x (Kg/mm ²)
Weight	-0.09	0.	0.	-0.09	0.	0.
Pressure	0.17	0.34	0.	0.17	0.34	0.
Restraints	10.64	0.	0.	10.69	0.	0.
Thermal due to direct heat flux	-3.2	-0.55	0.	-3.2	-0.55	0.
Thermal due to plate restraint effect	-2.60	5.51	-0.41	3.75	-7.43	0.69
Earthquake	<u>+0.23</u>	0.	0.	<u>+0.23</u>	0.	0.

- TABLE 6.5.4/1 -

RATCHETING ANALYSIS

(TEST 3)

Maximum metal temperature $T_{\max} = 545 \text{ }^{\circ}\text{C}$ Minimum metal temperature $T_{\min} = 220 \text{ }^{\circ}\text{C}$ Yield strength at T_{\min} $S_y = 11.42 \text{ Kg/mm}^2$

$$X = (P_1 + \frac{P_b}{K_t}) / S_y$$

$$Y = \frac{(Q_R)_{\max}}{S_y}$$

$$K_t = 1 + K_s \left(1 - \frac{P_1}{S_t}\right)$$

$$K_s = \alpha (K - 1)$$

$$K = 1.27$$

$$K_s = 0.135$$

$$K_t = 1.13$$

P_1 (Kg/mm ²)	P_b (Kg/mm ²)	Q_R (Kg/mm ²)	K_t	K	Y	Z	σ_c (Kg/mm ²)
0.40	0.0	19.29	1.13	0.03	1.60	0.05	0.75

$$(*) \sigma_c = 1.25 \times Z \times S_y$$

Entering the isochronous stress-strain curves at temperature 545 °C and for any time, by σ_c , we read no significant strain, % due to creep.

FATIGUE ANALYSIS

TRANSIENT T8	TIME t = 36 sec			TIME t = 160 sec		
	$\bar{\sigma}_R$ (Kg/mm ²)	$\bar{\sigma}_\varphi$ (Kg/mm ²)	$\bar{\sigma}_Z$ (Kg/mm ²)	$\bar{\sigma}_R$ (Kg/mm ²)	$\bar{\sigma}_\varphi$ (Kg/mm ²)	$\bar{\sigma}_Z$ (Kg/mm ²)
Load controlled	0.0	0.34	0.08	0.0	0.34	0.08
Strain controlled	-0.37	4.05	5.12	0.0	-4.71	8.25

$$\sigma_{LC} = 0.0 \text{ Kg/mm}^2$$

$$\sigma_{VSC} = 5.992 \text{ Kg/mm}^2$$

Calculation of ϵ_t , D

$$\epsilon_t = \left(\frac{S^*}{S}\right) K^2 \epsilon_n + K \epsilon_c + K_T \epsilon_F$$

$$\text{with } \epsilon_n = \epsilon_{LC} + \frac{1}{E} \sigma_{VSC}$$

$$\frac{S^*}{S} = 1 ; K = 1 ; K_T = 1 ; \epsilon_c = 0$$

$$\epsilon_t = 0.0007646 = 0.76 \text{ E-3}$$

Entering the fatigue curves we read

$$N_d = (5.75 \times 10^6) / 5 = 1.15 \times 10^6 \text{ cycles ; } n_d = 60060 \text{ cycles}$$

$$D_1 = \frac{n_d}{N_d} = 0.0522$$

FATIGUE ANALYSIS

TRANSIENT T11 - T12	TIME t = 27 sec			TIME t = 1098 sec		
	σ_R (Kg/mm ²)	σ_φ (Kg/mm ²)	σ_Z (Kg/mm ²)	σ_R (Kg/mm ²)	σ_φ (Kg/mm ²)	σ_Z (Kg/mm ²)
Load controlled	0.0	0.34	0.08	0.0	0.34	0.08
Strain controlled	-0.41	4.96	4.84	0.69	-7.98	11.19

$$\sigma_{VSC} = 19.29 \text{ Kg/mm}^2$$

Calculation of ϵ_t , D

$$\epsilon_t = \left(\frac{S^*}{S}\right) K^2 \epsilon_n + K \epsilon_c + K_T \epsilon_F$$

$$\text{with } \epsilon_n = \epsilon_{LC} + \frac{1}{E} \sigma_{VSC}$$

$$\frac{S^*}{S} = 1; K = 1; K_T = 1; \epsilon_c = 0$$

$$\epsilon_t = 0.00124$$

Entering the fatigue curves we read

$$N_d = 1.7 \times 10^5 / 5 = 3.4 \times 10^4 \text{ cycles}; n_d = 3370 \text{ cycles}$$

$$D_2 = \frac{n_d}{N_d} = 0.0991$$

FATIGUE ANALYSIS

EARTHQUAKE + TRANSIENT T11 - T12	TIME t = 27 sec			TIME t = 1098 sec		
	σ_R (Kg/mm ²)	σ_θ (Kg/mm ²)	σ_Z (Kg/mm ²)	σ_R (Kg/mm ²)	σ_θ (Kg/mm ²)	σ_Z (Kg/mm ²)
Load controlled	0.0	0.34	0.08	0.0	0.34	0.08
Earthquake	0.0	0.0	± 0.23	0.0	0.0	± 0.23
Strain controlled	-0.41	4.96	4.84	0.69	-7.98	11.19

$$\sigma_{VLC} = 0.46 \text{ Kg/mm}^2$$

$$\sigma_{VSC} = 19.29 \text{ Kg/mm}^2$$

Calculation of ϵ_t , D

$$\epsilon_t = \left(\frac{S^*}{S}\right) K^2 \epsilon_n + K \epsilon_c + K_T \epsilon_T$$

$$\text{with } \epsilon_n = \epsilon_{LC} + \frac{1}{E} \sigma_{VSC}$$

$$\frac{S^*}{S} = 1; K = 1; K_T = 1; \epsilon_c = 0$$

$$\epsilon_t = 0.00127$$

Entering the fatigue curves we read

$$N_d = 1.54 \times 10^5 / 5 \text{ cycles}; n_d = 10 \text{ cycles}$$

$$D_3 = \frac{n_d}{N_d} = 0.0003$$

Considering the actual operating conditions, no modifications have been applied to the Poisson ratio as requested by T 1431 Code Case N-47-17; the reasons are contained in Franco Tosi Short Notice 16/4/1982.

The total fatigue damage is given by adding the damage due to:

- 60060 T8 cycles (see table 6.5.5/1 and considerations at point 4.) as representative of type transients "a", "b" and "f".
- 3370 T11-T12 cycles (see table 6.5.5/2 and again considerations at point 4.) as representative of type transients "c", "d" and "e".
- 10 earthquake cycles connected with (T11-T12) type transient (see table 6.5.5/3). (Very conservative assumption.)
- 3270 overnight shutdown transients (daily cycling) approximately assumed from Topic Report No. 7, Table 9 as $D_4 = 0.032$

From the aforementioned detailed analysis, the following total fatigue damage has been obtained.

$$D_{\text{fatigue}} = D_1 + D_2 + D_3 + D_4 = 0.1836$$

The total creep damage is given by adding the creep damages due to the same loading cycles examined during the fatigue damage analysis.

According to the step by step procedure suggested by Code Case N-47-17 T1433 without considering the factor $K = 0.9$ the following damages have been carried out.

- . DC1 Damage due to T8 transient; see table 6.5.5/4;
- . DC2 Damage due to T11-T12 transient; see table 6.5.5/5.
- . DC3 No creep damage has to be expected from earthquake loads.
- . DC4 Damage due to overnight shutdown transients approximately assumed from Topic Report No. 7 as $DC4 = 0.0508$

The total creep damage is therefore:

$$D_{\text{creep}} = DC1 + DC2 + DC3 + DC4 = 0.058$$

The total creep-fatigue damage is:

$$D_{\text{TOT}} = D_{\text{fatigue}} + D_{\text{creep}} = 0.1852 + 0.0508 = 0.236 < 1$$

CREEP DAMAGE CALCULATION

TRANSIENT T8

$$S_{ym} = 10.38 \text{ Kg/mm}^2$$

$$S_k = 12.79 \text{ Kg/mm}^2$$

$$T \text{ allowable} > 3 \times 10^5$$

The creep damage for transient T8 is negligible.

CREEP DAMAGE CALCULATION

TRANSIENT T11-T12

$$S_{ym} = 10.38 \text{ Kg/mm}^2$$

$$S_k = 12.97 \text{ Kg/mm}^2$$

$$T \text{ allowable} > 3 \times 10^5$$

The creep damage for transient T11-T12 is negligible.

6.6. SECTION "B-B" ANALYSIS

The analysis is carried out at point B1.

In the section BB there are no relevant primary stresses therefore only shake down, ratcheting and creep-fatigue analysis are carried out.

The stress values are taken from table 6.3/1 and are referred to the T11-T12 transient that results as the most dangerous.

6.6.1. Shake down analysis

The shake down analysis is presented in table 6.6.1/1 according to the procedure already described at point 6.5.3.

6.6.2. Ratcheting analysis

All the consideration carried out at point 6.5.4. are still valid; the stresses contained in table 6.3/1 are used in the analysis whose results are presented in table 6.6.2/1.

SHAKE DOWN ANALYSIS

Highest metal temperature in a point of the radial section	$T_{\max} = 545 \text{ }^{\circ}\text{C}$
Lowest metal temperature in a point of the radial section	$T_{\min} = 210 \text{ }^{\circ}\text{C}$
Allowable stress at T_{\max}	$S_m(T_{\max}) = 7.64 \text{ Kg/mm}^2$
Allowable stress at T_{\min}	$S_m(T_{\min}) = 10.57 \text{ Kg/mm}^2$
Allowable stress for Test B	$S_m = 9.105 \text{ Kg/mm}^2$

$$P_1 + P_b + Q \leq 3 S_m$$

$$15.26 \leq 3 \times 9.105 \leq 27.31 \text{ Kg/mm}^2$$

RATCHETING ANALYSIS

(TEST 3)

Maximum metal temperature $T_{\max} = 545 \text{ }^{\circ}\text{C}$
 Minimum metal temperature $T_{\min} = 220 \text{ }^{\circ}\text{C}$
 Yield strength at T_{\min} $S_y = 11.42 \text{ Kg/mm}^2$

$$K = 1.5$$

$$K_t = 1 + K_s = 1.25$$

P_1 (Kg/mm ²)	P_b (Kg/mm ²)	Q_R (Kg/mm ²)	K_t	X	Y	Z	σ_c (Kg/mm ²)
0	0	26.62	1.25	0	2.20	0	0

$$Z = X \cdot Y = 0 ; \quad \sigma_c = \epsilon_c = 0$$

There are not significant strain at the analyzed point.

6.6.3. Creep-fatigue analysis

The same assumptions and procedures used for the "A-A" section are held; the earthquake and the daily cycling loads have negligible effects in the considered section.

Therefore:

$$D_{\text{fatigue}} = D_1 + D_2 = 0.9276$$

where:

D_1 Fatigue damage for T8 transient; see table 6.6.3/1.

D_2 Fatigue damage for T11-T12 transient; see table 6.6.3/2.

$$D_{\text{creep total}} = DC_1 + DC_2 \cong 0$$

where:

DC_1 Damage due to T8 transient; see table 6.6.3/3.

DC_2 Damage due to T11-T12 transient; see table 6.6.3/3.

$$D_{\text{TOTAL}} = 0.9276 < 1$$

FATIGUE ANALYSIS

Transient T8

TIME t = 27 sec			TIME t = 1098 sec		
σ_x (Kg/mm ²)	σ_y (Kg/mm ²)	σ_z (Kg/mm ²)	σ_x (Kg/mm ²)	σ_y (Kg/mm ²)	σ_z (Kg/mm ²)
0.048	0.66	9.66	-0.4	-0.67	-0.23

$$\sigma_{VSC} = 17.44 \text{ Kg/mm}^2$$

Calculation of ϵ_t , D

$$\epsilon_t = \left(\frac{S^*}{S}\right) K^2 \epsilon_n + K \epsilon_c + K_T \epsilon_F$$

$$\text{with } \epsilon_n = \epsilon_{LC} + \frac{1}{E} \sigma_{VSC}$$

$$\frac{S^*}{S} = 1; K = 1; K_T = 1; \epsilon_c = 0$$

$$\epsilon_t = 0.001038$$

Entering the fatigue curves we read

$$N_d = (5.74 \times 10^5) / 5 = 11.4 \times 10^4 \text{ cycles}; n_d = 60060 \text{ cycles}$$

$$D_1 = \frac{n_d}{N_d} = 0.526$$

FATIGUE ANALYSIS

Transient T11 - T12

TIME t = 27 sec			TIME t = 1098 sec		
σ_x (Kg/mm ²)	σ_y (Kg/mm ²)	σ_z (Kg/mm ²)	σ_x (Kg/mm ²)	σ_y (Kg/mm ²)	σ_z (Kg/mm ²)
0.11	0.81	11.43	0.07	-0.99	-15.19

$$\sigma_{VSC} = 26.58 \text{ Kg/mm}^2$$

Calculation of ϵ_t , D

$$\epsilon_t = \left(\frac{S^*}{S}\right) K^2 \epsilon_n + K \epsilon_c + K_T \epsilon_F$$

$$\text{with } \epsilon_n = \epsilon_{LC} + \frac{1}{E} \sigma_{VSC}$$

$$\frac{S^*}{S} = 1; K = 1; K_T = 1; \epsilon_c = 0$$

$$\epsilon_t = 0.001596$$

Entering the fatigue curves we read

$$N_d = (4.19 \times 10^4) / 5 = 8.39 \times 10^3 \text{ cycles}; n_d = 3370 \text{ cycles}$$

$$D_2 = \frac{n_d}{N_d} = 0.4016$$

CREEP DAMAGE

TRANSIENT T8

$$s_{ym} = 10.38 \text{ Kg/mm}^2$$

$$s_k = 9.60 \text{ Kg/mm}^2$$

$$T \text{ allowable} > 3 \times 10^5$$

The creep damage for transient T8 is negligible.

TRANSIENT T11-T12

$$s_{ym} = 10.38 \text{ Kg/mm}^2$$

$$s_k = 12.97 \text{ Kg/mm}^2$$

$$T \text{ allowable} > 3 \times 10^5$$

The creep damage for transient T11-T12 is negligible.

7. CONCLUSION

A detailed stress analysis of the tube-plate assembly has been carried out during all the envisaged operating conditions undertaken by the receiver.

No particular problems have been recognized therefore a good operability of the system has to be expected from the stress analysis point of view.

A P P E N D I X 1

APPENDIX 11. ALLOWABLE STRESS LIMITS FOR AISI 316 L

The following tables contain, as a function of the temperature, the values of allowable stresses that are used by Franco Tosi in design of stainless steel sodium component working of high temperature.

The definition of the term used is assumed according Code Case N47-17 sub. 3221.

1.1 Maximum allowable design stress intensity S_0

T (°C)	S_0 (N/mm ²)
20	107
100	105
200	96
300	95
400	86
500	80
600	72

1.2 Maximum time independent stress intensity S_m

T (°C)	S_m (N/mm ²)
20	115
100	115
200	107
300	94
400	85
500	80
600	72

1.3 Maximum temperature dependent stress intensity.

The value is tabulated for a working time of 30000 hours.

T (°C)	S_t (N/mm ²)
450	114
500	100
550	83
600	53

1.4 Maximum allowable value for general primary membrane stress intensity S_{mt}

The value is tabulated for a working time of 30000 h

T (°C)	S_{mt} (N/mm ²)
450	83
500	80
550	76
600	53

1.5 Yield strenght S_y

T (°C)	S_y (N/mm ²)
20	172
100	143
200	119
300	105
400	95
500	89
600	80

A P P E N D I X 2

1. PHYSICAL PROPERTIES

The following tables contain, as a function of the temperature, the value of physical properties used by Franco Tosi in design of stainless steel sodium component working at high temperature.

1.1. PHYSICAL PROPERTIES FOR AISI 316L

1.1.1. Thermal expansion

Temperature (°C)	$\alpha \cdot 10^{-6}$
20 - 100	16
20 - 200	17
20 - 300	17.5
20 - 400	17.8
20 - 500	18.0
20 - 600	18.2

1.1.2. Specific heat capacity

Temp. (°C)	CP (J/kg °C)
100	500
300	552
400	578
500	604
600	630

1.1.3. Thermal conductivity

Temp. (°C)	W/m °C
100	16
300	19
400	20
500	21
600	22

1.1.4. Density

$$\rho = 8. \text{ Kg} / \text{dm}^3$$

1.2. PHYSICAL PROPERTIES FOR SODIUM

1.2.1. Density

Temp. (°C)	Kg / m ³
100	926.
300	880.
400	857.
500	833.
600	809.

1.2.2. Specific heat capacity

Temp. (°C)	J/Kg °C
100	1383
300	1304
400	1278
500	1262
600	1254

1.2.3. Thermal conductivity

Temp. (°C)	W/m °C
100	86
300	76
400	71
500	66
600	61

ASR

ADVANCED SODIUM RECEIVER

FINAL WORKSHOP ACCEPTANCE PROCEDURE

Topic Report. n.14

Revision 0

February 83

Prepared by AGIP NUCLEARE

FRANCO TOSI

ENEL

Contents List

1. Examination of Quality System of Manufacturer
2. Examination of Manufacturing Documentation
3. Final Workshop Inspections

1. Examination of Quality Control System of Manufacturer

The following examinations concerning the quality control system of the manufacturer shall be performed prior to the workshop acceptance of the ASR:

- Check of the independency of the quality control department of the manufacturer
- Examination of the quality control manual of the manufacturer and its application for the ASR fabrication
- Check of completeness of the inspection plan for the ASR fabrication
- Examination of workshop drawings and other documents with respect to actual status, applied revision system and internal/external approval
- Control of the identification system for parts/items
- Examination of the quality control equipment with respect to quality standart and adjustment procedures
- Examination of the official description of quality control procedures which are applied on ASR fabrication (see inspection plan)
- Examination of special procedure specifications (e. g. packing and trasport)

2. Examination of Manufacturing Documentation

Prior to final workshop acceptance the following documents which are part of the final documentation have to be checked on completeness and conformity with the applicable contractual specifications:

- Inspection Plan
- Non-destructive Examination Certificates
- Final Workshop Inspection Certificates
- Welding Procedure Records Qualification
- Welding Plan and Weld Location Plan (weld list) with respect to film identification
- Welders certificates
- Non conformity reports.

3. Final Workshop Inspections

At the end of the workshop manufacturing the following inspections have to be performed (in accordance to the ASR-inspection plan) and passed without any objections as prerequisite of final workshop acceptance:

- Pressure test of the complete tube bundles of the receiver incl. headers and connecting piping in accordance with the test procedure
- Helium leak test of the complete receiver (pressure loaded parts) in accordance with the test procedure
- Visual Control of the assembled receiver visual and spot check on prefabricated parts of piping
- Dimensioning Control of the tube bundles, supporting structure, interface related connection points (piping, structure etc.)

SSPS TECHNICAL REPORTS

1/79	HELIOSTAT FIELD AND DATA ACQUISITION SUBSYSTEM FOR CRS (BY MARTIN MARIETTA)	DECEMBER 1979
2/79	CRS-HELIOSTAT FIELD, INTERFACE CONTROL AND DATA ACQUISITION SYSTEM (BY MCDONNELL DOUGLAS)	DECEMBER 1979
1/80	COLLECTOR QUALIFICATION TESTS FOR THE IEA 500 KWE DISTRIBUTED COLLECTOR SYSTEM (BY SANDIA AND DFVLR)	JULY 1980
2/80	ANALYSIS OF SPECIAL HYDRAULICAL EFFECTS IN THE SHTS PIPING SYSTEM (BY BELGONUCLEAIRE)	NOVEMBER 1980
3/80	REDESIGN OF THE CRS - ALMERIA RECEIVER APERTURE AND COMPARISON OF INTERATOM AND MMC REFERENCE HELIOSTAT FIELD PERFORMANCE CALCULATIONS (BY INTERATOM)	NOVEMBER 1980
1/81	TABERNAS METEO DATA ANALYSIS BASED ON EVALUATED DATA PREPARED BY THE SSPS-O.A. (BY BELGONUCLEAIRE)	JUNE 1981
2/81	DCS INSTRUMENTATION REVIEW (BY BELGONUCLEAIRE)	JUNE 1981
3/81	CRS INSTRUMENTATION REVIEW (BY BELGONUCLEAIRE)	JUNE 1981
4/81	INTERNATIONAL ENERGY AGENCY SMALL SOLAR POWER SYSTEMS (SSPS) PROJECT REVIEW (JANUARY 1981) (BY A.F.BAKER, SANDIA)	JULY 1981
5/81	DEVICE FOR THE MEASUREMENT OF HEAT FLUX DISTRIBUTIONS (HFD) NEAR THE RECEIVER APERTURE PLANE OF THE ALMERIA CRS SOLAR POWER STATION (BY DFVLR)	NOVEMBER 1981
6/81	DETERMINATION OF THE SPECTRAL REFLECTIVITY AND THE BIDIRECTIONAL REFLECTANCE CHARACTERISTICS OF SOME WHITE SURFACES (BY DFVLR)	DECEMBER 1981

SSPS TECHNICAL REPORTS CONTD.

- | | | |
|------|--|----------------|
| 1/82 | SSPS WORKSHOP ON FUNCTIONAL AND PERFORMANCE CHARACTERISTICS OF SOLAR THERMAL PILOT PLANTS.
PART I. RESULTS OF THE DCS-PLANT SESSION.
(BY A. KALT, DFVLR) | APRIL 1982 |
| | PART II. RESULTS OF THE TOWER FACILITIES SESSION
(BY M. BECKER, DFVLR) | JULY 1982 |
| 2/82 | CONCENTRATED SOLAR FLUX MEASUREMENTS AT THE
IEA SSPS SOLAR CENTRAL RECEIVER POWER PLANT
TABERNAS - ALMERIA (SPAIN)
(BY G. VON TOBEL, CH. SCHELDERS, M. REAL, EIR) | APRIL 1982 |
| 3/82 | EFFECT OF SUNSHAPE ON FLUX DISTRIBUTION AND INTERCEPT FACTOR OF THE SOLAR TOWER POWER PLANT AT
ALMERIA
(BY G. LEMPERLE, DFVLR) | SEPTEMBER 1982 |
| 1/83 | DCS-MIDTERM-WORKSHOP PROCEEDINGS
(EDITED BY A. KALT, J. MARTIN) | FEBRUARY 1983 |
| 2/83 | FH-PTL WEDEL REFLECTOMETER, TYPE 02-1 NO.3 FINAL REPORT
AND REPORT ON THE TEST PROGRAM
(BY G. LENSCH, K. BRUDI, P. LIPPERT, FACHHOCHSCHULE WEDEL) | MARCH 1983 |
| 3/83 | THE ADVANCED SODIUM RECEIVER (ASR) - TOPIC REPORTS -
(AGIP NUCLEARE AND FRANCO TOSI) | MAY 1983 |

DISTRIBUTION LIST

- 1) SSPS-MEMBER COUNTRY REPRESENTATIVES
(EXECUTIVE COMMITTEE AND T+O ADVISORY BOARD)

L. REY (EC CHAIRMAN)
G. FANINGER (A)
H. KLEINRATH (A)
J. DELCROIX (B)
A. MICHEL (B)
P. KESSELRING (CH)
C.J. WINTER (D)
M. FISCHER (D)
W. HOFMANN (D)
A. MUNOZ TORRALBO (E)
C. ORTIZ (E)
E. CARABATEAS (GR)
F. REALE (I)
G. BEER (I)
L. BRANDELS (S)
J. HOLMBERG (S)
L. GUTIERREZ (USA)

- 2) IEA - SECRETERIAT

L. BOXER

- 3) B M F T

H. KLEIN

- 4) C E E

I. MARTIN

- 5) SANDIA LABORATORIES

A. BAKER (3 x)

- 6) D F V L R

R. KÖHNE (3 x)

- 7) OPERATING AGENT

M. BECKER
W. BUCHER
H. ELLGERING
W. GRASSE
P. HEINTZELMANN
A. KALT
W. VON KRIES

- 8) INTERNATIONAL TEST & EVALUATION TEAM

C. SELVAGE (20 x)

- 9) SEVILLANA

F. RUIZ (3 x)

- 10) ACUREX CORP.

A.F. SCHRAUB

- 11) BELGONUCLEAIRE

G. DEBIER

- 12) INTERATOM

B. FLOSS

- 13) MAN - NEUE TECHNOLOGIE

J. FEUSTEL

- 14) MARTIN MARIETTA CORP.

C. WROTON

- 15) SAIT

B. LORENT

- 16) AGIP NUCLEARE

G.C. SCARPI

- 17) FRANCO TOSI

V. BEDOGNI